Investigation of biomass gasification processes for the production of high quality syngas

A thesis submitted in fulfilment of the requirements for the Degree of Doctor of Philosophy (PhD)

By

Ahmed Morsy Mostafa Salem

B.Sc., M. Sc.

Systems, Power & Energy Research Division
James Watt School of Engineering
College of Science and Engineering
University of Glasgow
Glasgow UK

August 2019

Declaration

This dissertation is the result of my own work. Any published ideas, results or techniques from other works are fully acknowledged in accordance with the standard referencing practices.

……..

Ahmed Salem

August, 2019

Dedication

This work is dedicated
to my dear dad and my great mom,
all my teachers,
my beautiful wife and my lovely children

Abstract

The gradual increase of fossil fuel depletion, as well as the harmful emissions associated with the increased global energy demand, has led to an increased effort to find new alternatives for energy production. Great attention has been placed on using renewable sources, which are clean and sustainable. Biomass, being one of the main sources for renewable energy, is a promising alternative to fossil fuels and can be converted to solid, liquid, and gaseous fuels using different technologies. As a result, many research works are being focused on the energy production from biomass. The most common use of biomass for energy is direct combustion, followed by gasification, carbonisation, and pyrolysis. Biomass gasification is preferred for energy production for many reasons; its availability everywhere and all over the year, the technology is simple to operate and maintain, and the valuable gaseous with by-products produced using gasification.

A biomass gasifier must be designed based on experimentally or numerically trusted data for optimum energy production. Although experimental work is preferable, it is not always available; and undoubtedly, it is a cost and time intensive process. On the other hand, modelling can help in building up and designing biomass gasifiers and predicting the process of gasification based on a well-known validated dataset. Modelling can afford and study the gasification process considering the effect of varying working parameters, design, and fuel variations. Additionally, it is a cost-effective method that can be carried out in less time compared to experiments. However, the key challenges in economic and efficient design of a biomass gasifier often link with the biomass feedstock variety and hence their suitability for gasification. The wide variety of materials that can be used for gasification makes the design process complicated, because it depends on the feedstock type and required thermal power. Additionally, a biomass gasifier design has to deliver the highest possible production rate of syngas with its optimum gasification efficiency. These challenges are addressed in this thesis through an integrated research programme coupling novel modelling techniques with experiments.

A detailed kinetic model is initially built to simulate and subsequently optimise the downdraft gasification process for typical biomass. However, it is found that the model is sensitive to the chemical contents of biomass feedstock. While particularly testing the model with agricultural waste feedstocks, it fails to predict the producer gas composition. Thus, more focus is given to improve the model's capability to accommodate and investigate the gasification process of Scottish agricultural feedstocks. The model is set through a series of chemical kinetic reactions at each zone of gasifier. The model is iterative and uses the

previous zone's output as an input to the next zone to achieve higher accuracy compared to equilibrium and previous kinetic models. Further, a new approach for optimising the reduction zone length is developed in the model. The novel technique assumes all char to be consumed in the reduction zone. Gasifier design limitations and challenges are discussed, along with the identification of optimum process and design of a gasifier able to operate efficiently under numerous biomass materials.

Tar content in producer gas limits its direct use and thus requires additional removal techniques. The modelling of tar formation, conversion and destruction along a gasifier could give a wider understanding of the process and help in tar elimination and reduction. Hence, more focus is applied to tar formation modelling inside the gasifier. A detailed kinetic model for the evolution and formation of tar from downdraft gasifiers, for the first-time, is built. The model incorporates four main tar species (benzene, naphthalene, toluene, and phenol), with a total of 20 different kinetic reactions implemented in the code for every zone, leading to greater accuracy and prediction of tar evolution, formation and cracking throughout the different zones of downdraft gasifiers compared to experiments. Experimental work is carried out to initially validate the results of the kinetic model and found a good agreement for wood biomass materials. Experiments are carried out at KTH Royal Institute of Technology, Sweden, and further used to validate the results from modelling process. The four main tar species are found to be a good representative for tar evolution in downdraft wood gasifiers, and in most cases, they form 50-90 % of the total tar produced.

The producer gas predictions of the model are also found to be in good agreement over a wide range of feedstocks when comparing with various experimental data from literature for different moisture and equivalence ratios. Additionally, sensitivity analysis has been carried out to study the effect of varying moisture content and air equivalence ratio on the producer gas composition, tar content, and higher heating value. Furthermore, different gas and tar species distribution along the gasifier are discussed, along with the effect of changing working parameters. The input data to the model are the ultimate compositions of feedstock (CHNO), working conditions (e.g. moisture content and air equivalence ratio), and thermal power required. The model is built from scratch using MATLAB coding.

A 2D computational fluid dynamics (CFD) model for downdraft biomass gasifiers is built using ANSYS software. The dimensions of the 2D model of a 20-kW downdraft gasifier and its design are based on the kinetic model results. The current model is tested against two different feedstocks and found a good agreement. One of the research aims is to validate the CFD model to cover a wide range of materials; biomass, waste, and agricultural residues

such as wood, livestock beddings, and barley screenings. The novelty of the CFD model also includes the study of the formation and evolution of the four main tar species identified by the kinetic code. Mesh independency test is carried out using five different grids to choose the best grid for the simulations. The results of the tar species formation are validated against the kinetic and experimental data. Further novelty of the current CFD model is demonstrated through the prediction of gasification using different biomass, waste, and agricultural materials. Also, the model presents the tar species formation along the gasifier, which has not been discussed in any previously published works. The model also considers different tar and gas species formation along the gasifier centreline in both steady and unsteady states. Finally, the results obtained from the model conclude with the new findings of designing/optimising downdraft air-blown gasifiers including the production of high-quality syngas with low tar amounts.

Acknowledgement

In the Name of Allah, the Most Beneficent, the Most Merciful. All the praises and thanks to Allah who gave me strength, health, and patience to complete this work. During the course of my PhD, there are so many people who deserve a thank you for their deep insight and encouragement.

I owe a sincere gratitude to my principal supervisor, Dr Manosh C. Paul, for his great endless effort, support, scientific guidance, and wise criticism that improved my PhD thesis. A grateful thank to my second supervisor, Dr Ian Watson, for his support as well. I would like to thank Dr Weihong Yang and Ilman Zaini for their help and guidance during my mobility scholarship in KTH Institute, Sweden. A warm thank to the University of Glasgow for offering me this mobility scholarship. I can never forget the endless support of Prof. Ali Alzahaby, and Prof. Yasser Elsamadony for their guidance and support all times. I also would like to thank all the members of academic staff, IT staff, technical staff and administrative staff of the James Watt School of Engineering at the University of Glasgow, who have helped during the course of this work.

I must acknowledge the Egyptian Cultural Affairs and Missions Sector in Egypt, the British Embassy in Egypt, as long as the Egyptian Cultural Bureau at London for funding and supporting me during this course work through Newton-Mosharafa PhD programme scholarships.

I am deeply indebted to my parents who dedicated their lives to ensure my success in my academic programme. I am very grateful to them for their moral support and encouragement during my stay abroad. Most special thanks are to my beautiful wife, Anoon and lovely kids; Miso and Dodo for always being there for me. They have given up a lot in order to give me the opportunity to complete this work. They shared the joy and pain with me. I extend my thanks to my brother, my sister and relatives who stood by me.

Finally, I am delighted to acknowledge the support, the encouragement and the pleasant working environment I have received from all my colleagues. In particular, many thanks to my office mates Tata, Tan, Linwei, Lois, Alex, Nadirah, AbdulAziz and Graeme. A warm thanks also to my friend Dr. Umesh Kumar for his guidance and support during his stay in the University of Glasgow.

Table of Contents

List of Tables

List of Figures

Symbols and Abbreviations

Upper case letters

A	Pre-exponential factor, (units vary)
C	Concentration (mol/m^3)
D	Diameter (m)
$D_{i,m}$	Mass diffusion coefficient for species *i* in the mixture
$D_{T,i}$	Thermal diffusion coefficient for species *i*
D_t	Turbulent diffusivity
E	Energy, (kJ/mol)
GH	Hearth Load, (Nm^3/ (h.m^2))
G_b	Turbulence kinetic energy due to buoyancy
G_k	Turbulence kinetic energy due to the mean velocity gradients
H	Enthalpy, (kJ/mol)
H_{reac}	Heat released by the surface reaction
I	Unit tensor
J_i	Diffusion flux of species i
K	Kinetic constant, (s^{-1})
M	Molecular mass, (kg/mol)
P	Pressure, (Pa)
R	Net rate of formation, (mol m^{-3}s^{-1})
Re	Reynolds number
R_i	Net rate of production of species *i* by chemical reaction
S_i	Mass added to the continuous phase from the dispersed phase
S_k	Source terms for the kinetic energy
S_ϵ	Source terms for rate of dissipation
Sc_t	Schmidt number for turbulent flow
T	Temperature, (K)
T_R	Temperature of radiation (K)
V	Volume (m^3)
Y_i	Mass fraction of species *i*
Y_M	Contribution of the fluctuating dilatation in compressible turbulence to the overall dissipation rate

Lower case letters

$\frac{dm_p}{dt}$	Rate of evaporation (kg/s)
f_h	Particle absorbs fraction of heat
g_i	Gravitational body forces
h	Convective heat transfer coefficient (W/m^2.K)
h_{fg}	Latent heat (J/kg)
m_a	Mass of ash particle (kg)
$m_{p,0}$	Initial particle mass at injection
m_p	Mass of the particle (kg)
$m_v(t)$	Volatile yield up to time t
u	Fluid velocity (m/s)
$\overrightarrow{u_p}$	Particle velocity (m/s)
x_i	Number of mole species

Subscripts

a	Atmospheric
d	Drying
f	Fuel
g	Gases
i	Species
l	Liquid
p	Particle
th	Thermal

Greek letters

ρ	Density
$\sum$	Summation
Δ	Change in state
$\tau_{i,j}$	Stress tensor
μ	Molecular viscosity
σ_k	Turbulent Prandtl numbers for *k*
σ_ε	Turbulent Prandtl numbers for ϵ
μ_t	Turbulent viscosity

ρ_p	Density of the particle
ϵ_p	Particle emissivity
σ	Stefan Boltzmann constant, (5.67×10^{-8} $\frac{kg}{s^{-3}K^{-4}}$)
α_1, α_2	Yield factors

List of Acronyms

MC	Moisture content, (%)
A/F	Air to fuel ratio
ER	Equivalence ratio
CRF	Char reactivity factor
HR	Heating rate, (K s^{-1})
HHV	Higher heating value (kJ/kg)
G	Gases
Nm^3	Normal cubic meter
Py	Pyrolysis
CFD	Computational Fluid Dynamics
DPM	Discrete phase model
PRESTO	PREssure Staggering Option
RANS	Reynolds Averaged Navier-Stokes
VOF	Volume of Fluid

List of Publications

Journals

1. **Ahmed M. Salem**, IlmanNuranZaini, Manosh C. Paul, and WeihongYang, "The Evolution and Formation of Tar Species in a Downdraft Gasifier: Numerical Modelling and Experimental Validation", BIOMASS AND BIOENERGY, Vol 130, November 2019, 105377.
2. **Ahmed M. Salem**, and Manosh C. Paul, "An integrated kinetic model for downdraft gasifier based on a novel approach that optimises the reduction zone of gasifier", BIOMASS AND BIOENERGY, 2018, 109, pp 172-181.
3. N. Bianco, Manosh C. Paul, George P. E. Brownbridge, Daniel Nurkowski, **Ahmed M. Salem**, Umesh Kumar, Amit N. Bhave, Markus Kraf. ‘’Automated Advanced Calibration and Optimisation of Thermochemical Models Applied to Biomass Gasification and Pyrolysis’’. Energy & Fuels, 2018, 32, 10, pp10144-10153.
4. **Ahmed M. Salem**, and Manosh C. Paul, "Advanced Kinetic Modelling of Biomass Gasification Based On Optimum Height Of The Reduction Zone", International Journal of Advances in Science Engineering and Technology, 2321-9009, 4(2), 2016.

Book Chapter

1. **Salem AM**, Kumar U, Izaharuddin AN, Dhami H, Sutardi T and Paul MC. Advanced Numerical Methods for the Assessment of Integrated Gasification and CHP Generation Technologies. Springer, ISBN: 978-981-10-7334-2, Page No.-307-330.

Conferences

1. **A. M. Salem**, and M. C. Paul, “Detailed Kinetic Modelling for Tar Species Evolution in a Downdraft Gasifier", ‘’EHST_107‘’ in EHST'19 - 3rd International Conference of Energy Harvesting, Storage, and Transfer, Ottawa, Canada, June 18-19, 2019. Accepted for publication.
2. **A. M. Salem**, U. Kumar, and M. C. Paul, "Kinetic Modelling for Tar Evolution and Formation in a Downdraft Gasifier," ‘’ICME_69‘’ in World Congress on Engineering, 800-804, London, U.K., 4-6 July 2018.
3. Umesh Kumar, **A. M. Salem** and M. C. Paul. (2017) Advanced biomass gasification technology, All Energy Conference Glasgow, UK.
4. Umesh Kumar, **A. M. Salem** and M. C. Paul (2017) Investigating the Thermochemical Conversion of Biomass in a Downdraft Gasifier with a Volatile Break-Up Approach. In: 9th International Conference on Applied Energy (ICAE2017), Cardiff, UK, 21-24 Aug 2017.

Poster Presentations

1. Umesh Kumar, **Ahmed M. Salem**, Jamie Bell and Manosh C. Paul*, ‘’ Advanced Biomass Gasification Technology’’, Poster Presentation at All Energy Conference and Exhibition, Glasgow, 10-11 May 2017 and also in Innovation in Gasification and CHP Technology (IGATE), Glasgow, 23 May 2017)
2. **Ahmed M. Salem** and Manosh C. Paul, ‘’ A Novel Four-zone Kinetic Modelling Approach for Biomass Gasification’’, Poster presentation at IBioIC’s 2nd Annual Conference: 28- 29 January 2016, Technology and Innovation Centre (TIC), The University of Strathclyde, Glasgow.

Chapter 1 Introduction

1.1 Overview

Most of the coal-fired power stations are struggling with the pollution issues and the strict regulations to control them. According to the report published by Guardians [1], coal power plants have to be shut down by 2030, or they have to tackle the climate change challenges, which would potentially lead a financial loss of around €22 Bn. On the other hand, renewable energy costs are falling rapidly which encourages to build more power plants based on renewables or a mixtures of coal-renewables power stations. Coal is in a "death spiral", as seven nations including the UK already announced to end the use of coal power plants by 2030 [1]. Moreover, clean energy sources are required to potentially solve the issues of the global energy crisis and environmental pollution caused by the heavy use of fossil fuels.

All the previous factors are leading the world to look for new alternatives which are clean and renewable. Biomass is considered to be a clean and environmentally friendly renewable source of energy and could be a good alternative to fossil fuels. Biomass with a suitable choice of processes can be converted into solid, liquid and gaseous fuels that could be used for energy production. Therefore, researches have been working on the various techniques for the enhancement of energy production using biomass [2]. With regard to the production process, biomass gasification is one of the most promising techniques used to convert solid fuels into useful gaseous fuels which can be broadly used in many domestic as well as industrial applications like electric generation and internal combustion engines. The most common use of biomass for energy is direct combustion, followed by gasification, carbonisation, and pyrolysis [3]. Biomass gasification is significantly increasing in terms of industrial and market applications because of the several reasons [4];

- It is a renewable energy source.
- Can be used as good alternative for electricity production, or for reducing electric consumptions during peak times.
- A good waste disposal system.
- Can be used in CHP applications.

Furthermore, gasification also has some advantages over the other techniques e.g. pyrolysis and combustion as follows;

- The direct usage of products in internal combustion engines and gas turbines makes gasification of a great importance compared to other technologies.
- Negligible emissions compared to direct combustion.

- Wide variety of applications like heat, electricity and steam production, and chemicals.
- The gaseous products produced are of a high value in terms of syngas composition.

Gasification is a thermochemical process that converts a solid fuel into a gaseous fuel at temperatures between (700- 900) ^{0}C [3]. It produces carbon monoxide, hydrogen and small amounts of methane as desired products with other undesired gases like nitrogen, carbon dioxide, and other hydrocarbons. In gasification, organic volatiles are not quickly condensed so these are typically carried with the gas products, forming a viscous substance called tar. Both tar and char are undesirable for any downstream applications, e.g. when using producer gases in internal combustion engines and gas turbines [5]. Separation of tar is a major challenge for using the syngas produced because it will condense and cause blockage at engines and valves. Biomass gasification occurs through four main steps, as shown in Figure 1.1, which are

- **Drying** – by which moisture content in biomass is reduced,
- **Pyrolysis** – in which biomass is separated into volatiles and char,
- **Combustion** – by which heat required for the whole process through oxidation of the gasifying medium is provided, and
- **Reduction/Gasification** – which occurs when the amount of supplied air is less than the theoretical (stoichiometric) value to produce syngas through a series of chemical reactions to be illustrated in the following sections.

Moreover, during gasification of biomass, the material is heated to a high temperature up to 1500 K, which causes a series of physical and chemical changes that result in the evolution of volatile products and carbonaceous solid residues. The amount of volatiles produced and their compositions depend on the reactor temperature, type, and characteristics of fuel material. There are several types of biomass gasifiers, each comes with its own specific advantages and disadvantages. However, selection of an appropriate gasifier is usually based on biomass type, its moisture content, gasifying agent used, output power required and economical consideration for each type. Gasifiers can be classified generally as fixed bed, fluidized bed and entrained flow gasifiers [6].

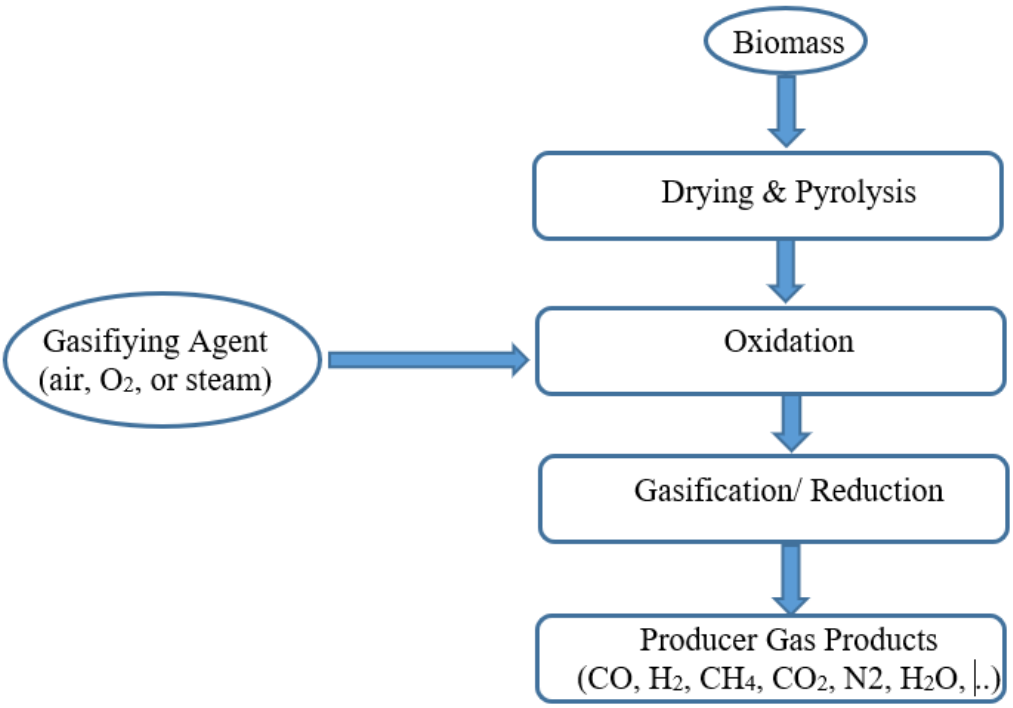

Figure 1.1: Gasification steps for syngas production.

- **Fixed bed gasifiers**

Fixed-bed gasifiers are economical and have a simple design, which is one of their major attractions. On the other hand, their range of applicability is from 10 kW to 1000 kW. For this reason, a large number of small-scale fixed-bed biomass gasifiers are in use around the world [5]. They can be classified into updraft and downdraft fixed-bed gasifiers based on the direction of biomass feed and syngas produced.

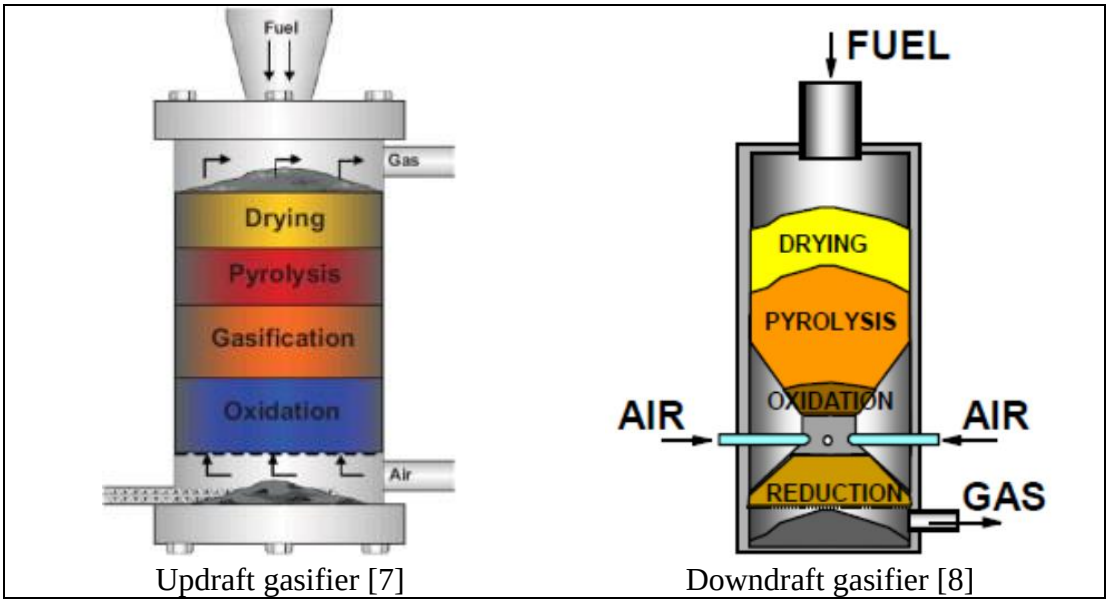

Updraft gasifier [7] Downdraft gasifier [8]

Figure 1.2: Schematic of updraft and downdraft gasifiers.

Both gasifiers, Figure 1.2 includes the four main zones of gasification; drying, pyrolysis, combustion, and reduction. However, the flow of syngas production is different. In the updraft gasifiers, the air/gasifying medium and fuel are at opposite direction, and usually syngas is produced from the gasifier top. On the other hand, in downdraft gasifiers both flows are in same direction, and syngas is discharged from bottom of the gasifier. Although updraft gasifiers can accommodate high moisture levels and ash content, they tend to produce too high tar content (30-150 g/Nm^3) [5]. As a result, gas produced from them can only be used in simple application like direct firing where gas does not need any cleaning. Downdraft gasifiers on the other hand produces small tar amounts (up to 6 g/Nm^3) and can start up quickly (30 min). The gas produced from downdraft gasifier can be used in internal combustion engines and some other applications [5]. Despite the small amounts of tar produced from downdraft gasifiers, the gas produced still needs further cleaning to be used in some practical applications e.g. gas turbine engines, and hence the modelling process of tar formation along downdraft gasifiers could help in getting more understanding of the whole process, and leading to further tar reduction.

- **Fluidized bed gasifiers**

Fluidized-bed gasifiers generate better mixing and uniform temperature distribution than fixed bed gasifiers, because of their design compared to other gasifiers design. The fluidized bed is made of granular solids called bed materials, kept in a semi-suspended condition by the velocity of gasifying medium through them, Figure 1.3. They have a wide range of applications depending on the design and size of gasifier but generally at a large scale, 1-100 MW [5]. While their tar production is between updraft and downdraft gasifiers (~ 10 g/Nm^3).

- **Entrained Flow Gasifiers**

Entrained flow gasifiers (Figure 1.3), are successful and widely used for large applications of gasification. However, they are classified as the most expensive because of their design and working conditions (grinded particles, and gasifying medium). On the other hand, they have the highest power production (up to 1000 MWth) depending on required capacity [5].

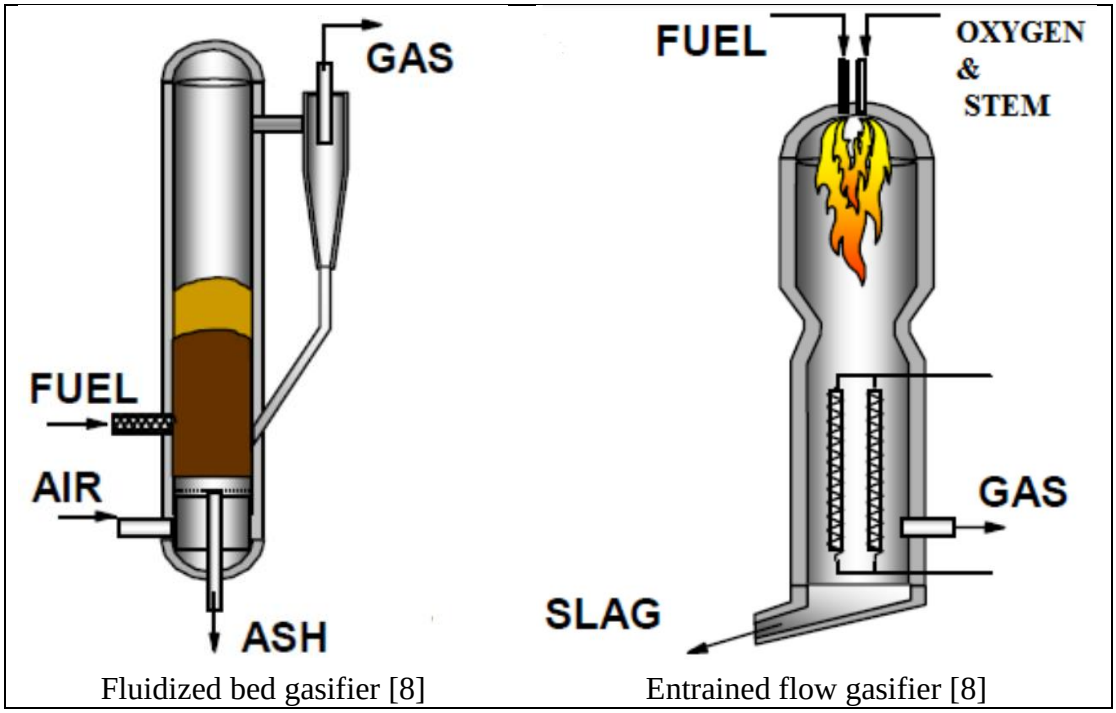

Fluidized bed gasifier [8] Entrained flow gasifier [8]

Figure 1.3: Schematic of Fluidized bed and entrained flow gasifiers.

Due to the previous comparisons and illustrations for different gasifiers types, the downdraft biomass gasifiers have great advantages. The main advantages can be concluded in small tar production rate, quick start-up, easy maintenance and operation, lower running costs, and the ability of using producer gas directly [5]. Downdraft gasifiers also can be easily used in farms, houses, remote areas and some industrial applications like power generation, internal combustion engines, and gas turbine engines. As a result, the focus on this study will be on downdraft biomass gasifiers; with an aim to improve their design and optimisation process, and to make them applicable for more market applications.

1.2 Feedstocks used in the gasification process

A wide range of materials can be gasified to produce valuable producer gas. Coal and biomass are used widely in the process of gasification and combustion. In the current study, different materials will be used for the process of downdraft gasification, focusing on agricultural, and forestry residues. The main focus on the study is to develop modelling processes that can simulate the gasification process of downdraft air-blown gasifiers using biomass and agricultural residues. As a result, an attempt to build up an integrated initial model to simulate the gasification of biomass, will be followed by the model development to accommodate the gasification of biomass and agricultural feedstocks.

The global population is estimated to rise from approximately 6.5 billion to 10 billion by 2050 [9]. Over the next 30 years, global energy demand is expected to increase by 56% [10]. It is expected that global consumption of fossil fuels will increase from 390-60 EJ, (a 57%

increase), which will result in an increase in emissions by 58% from 2005-2030 [4]. Challenging times lie ahead for the next generation to reduce our dependency on fossil fuels and utilise our waste. More recently, the use of agricultural and forest residues for energy production has gained wide attention due to its availability, diversity, and how it helps to reduce greenhouse gases emissions [11]. So, the use of agriculture and forest residues in generating clean energy is one of the main aims of current research.

The process of modelling and design of a downdraft gasifier that can handle biomass and agricultural residues is a promising way to reduce waste and generate energy. The process is gaining high importance in the market of bioenergy. The model aims to produce and develop gasifiers that could be applicable for industrial applications; e.g. to generate heat or other energy applications. On the other hand, syngas produced can be directly fed into a generator to produce electricity. At the same time, heat generated from the gasifier can be used through a recovery process to produce steam or hot water for other purposes. It can also be used for combustion-based CHP systems that are flexible and operate on a variety of fuels such as oil, natural gas or biogas. Since CHP is generated locally, the technology is not susceptible to losses from distribution, and therefore proves advantageous over conventional power generation and distribution. Distribution of electricity and heat locally proves more efficient and advantageous over conventional power generation and distribution. As a result, CHP plants can achieve higher overall efficiency in comparison to its counterparts.

1.3 Modelling and simulation of downdraft biomass gasifiers

Downdraft gasifiers are varying from small to industrial scale for power production as discussed earlier. The gasifier should be designed based on experimental or numerical data. Experiments are more reliable and accurate; however, it is not always available with changing fuel, dimensions, and other working conditions/parameters. Modelling of gasification process and gasifiers design can be helpful for prediction of operating conditions, syngas production, emissions, and to study the variations and effect of changing of fuel, loading, and working parameters. It is also a cost-effective tool that can be used without depending on experimental methods that can be expensive and more time consuming. Researchers have been developing various modelling techniques to optimise and predict the behaviour of biomass gasifiers such as

- **Thermodynamic equilibrium models**

This modelling depends on chemical balance, which is based on combining the equilibrium constants with the minimisation of Gibbs free energy through one global or multiple

reactions e.g. ([12], [13], [14], [15]). Although it gives reasonable prediction of syngas production and maximum temperature, it usually over predict some species (e.g. CO, and CH_4). It also cannot predict or consider other parameters like gasifier design, velocity, and temperature distributions.

- **Kinetic modelling**

Kinetic models are widely used and can cover a wide range of parameters that cannot be studied by equilibrium models. It takes into account detailed chemical reactions taking place inside the gasifier. It can also predict gasifier design, fuel feeding rate, residence time, and reactor hydrodynamics e.g. ([16] - [17]). While promising, kinetic model has some limitations in gasification process. The interactions between solid and gas phase reactions during gasification process needs clear understanding and cannot be covered during kinetic modelling.

- **Computational Fluid Dynamics (CFD)**

CFD models can study the effect of changing gasifier design on syngas composition and quality because kinetic models does not depend on reactor geometry. A CFD model involves a combined solution of mass, momentum, energy, turbulence and hydrodynamics of the flow. It can give a clear understanding of interactions between different phases and reactions inside the gasifier ([18], [19] and [20]).

1.4 Research challenges

As mentioned, downdraft gasifiers usually produce lower tar amounts than updraft and fluidized bed gasifiers. However, the producer gas coming out with these small tar amounts cannot be used directly in internal combustion engines and gas turbine engines without further cleaning. Hence, one of the main aims of this work, is to predict tar formation along downdraft gasifiers with aims to reduce its amount. Additionally, the wide variety of materials that can be used in gasification process (e.g. biomass, waste, and agricultural residues) makes the design process very complicated. The building up of a single gasifier, that is able to handle all these materials and able to operate under different working conditions, is a big challenge.

The way to study all this starts from modelling which to the best of our knowledge, few works considers the detailed formation of tars in downdraft gasifiers. Also, tar formation and destruction were rarely mentioned in CFD modelling of downdraft gasifiers. As far as this

can be researched, building up a kinetic code that is able to simulate the full work and design of a downdraft gasifier including detailed tar species has never been discussed.

As a result, the key challenges in the current research work is to optimise the gasification process based on a single gasifier design that is able to handle a wide range of materials with high efficiency and applicable for a wide range of industrial and domestic applications.

1.5 Research objectives

The research aims to develop robust thermochemical kinetic as well as computational fluid dynamics (CFD) models of biomass gasification which will be applied to investigate the syngas and detailed tar species production. Optimising the various processes in gasification would lead to the production of high-quality syngas with low tar content but with higher heating value. Modelling predictions will be assessed with experimental testing data available in the literature and also using a gasifier in the university labs plus experiments carried out by the author at KTH institute, Stockholm, Sweden.

The modelling process will include the design of a downdraft gasifier that is able to handle a wide range of materials under different working conditions with an optimum gasification efficiency leading to the production of higher quality syngas.

Furthermore, the model will study the formation and destruction of four main tar species (benzene, naphthalene, toluene, and phenol) using detailed kinetic reactions. The yield of tar species will be discussed for different zones of a gasifier based on temperature of each zone. Mass and energy balance will be calculated. The aim of studying all these parameters is to help in understanding the nature of tar species formation, leading to the reduction of its amount inside the gasifier as well as within the syngas production.

A CFD model will also be built to predict the gasifier performance. The CFD model is applicable for different biomass materials with a wide variety of working parameters and design conditions. The main goal of this research work is to optimise the work of downdraft biomass gasifiers for the maximum power production with lower particulates.

1.6 Novelty and key findings

The research work aims to find the optimum working conditions that lead to the production of higher quality syngas, thus making the product gas efficient for direct use in several applications without any gas cleaning process (e.g. gas turbine engines, and internal combustion engines).

A detailed and novel kinetic model is successfully built to simulate and predict the downdraft gasifiers' performance. The model is composed of different sections considering, gasifier design, syngas composition, detailed tar species formation, and temperature variations across the gasifier. The model is able to handle a wide range of feedstocks under different working conditions.

On the other hand, a CFD model is built to simulate the work of downdraft gasifiers considering different tar species formation which has been rarely discussed in previous works. Both the kinetic and CFD models are verified against well-known experimental data and further been used to optimise the gasification process.

As far as this can be researched, the data simulated by the current model (e.g. gasifier design dimensions, producer gas composition and yield, detailed tar species formation, and temperature distribution along gasifier height) have never been mentioned nor introduced in a single kinetic model. The model is also built by the author using Matlab coding without relying on any external sources (e.g. Aspen). The kinetic model can be used as a guide for the optimisation process of designing downdraft gasifiers. The results and findings of the model are leading to higher production of syngas with lower tar amounts.

The models designed can be directly used in the bioenergy industry as a guidance for downdraft gasifiers design and optimisation. The applicability and wide variety of materials the models can handle makes it a unique addition to the bioenergy sector. On the other hand, the new feedstocks tested by the models proved its capability to be gasified, thus giving a promising and wide attention to make use of agricultural and farm residues in the gasification and encourage governments to make a beneficial use of these feedstocks. Additionally, the model is encouraging for the waste management and reduction strategy, showing the opportunity of utilising different waste materials in gasification process.

1.7 Thesis structure

The thesis is outlined as follows;

In **Chapter 1**, introduction of the thesis is provided. The introduction section discusses the use of biomass and world's need to find new sources of clean energy production. The gasification process has been described widely in downdraft gasifiers showing also the different types of gasifiers and the difference between them in syngas production, temperature levels, and applications. The gaps between the current and previous works are discussed with the aim to fill these gaps, thus showing the novelty and key findings of the current research.

While in **Chapter 2**, literature review showed the previous modelling and simulation of downdraft gasifiers including equilibrium, kinetic and CFD models. The modelling of tar inside different gasifiers is further emphasised. The gaps and shortage in the previous works regarding modelling are highlighted and linked to the current work aims.

Chapter 3 discusses the build-up of thermochemical kinetic modelling code that is able to simulate downdraft gasifiers. The model will be validated for different types of feedstocks. Model novelty will be clarified and further, a sensitivity analysis will be carried out to study its effect on syngas production. Gasifier design will be addressed in this chapter and different species distribution along gasifier height will be studied.

In **Chapter 4**, some limitations of the kinetic code are pointed out and the ways to solve them and make the code applicable for a wide range of biomass materials has been discussed and verified against experimental data. The model is further used to optimise the working conditions of a downdraft gasifier through sensitivity analysis.

In **Chapter 5**, tar species formation has been discussed. The different kinetic rate reactions and empirical relations/equations of tar formation have been shown. The build-up of a combined code that is able to simulate the design/work of downdraft gasifiers including tar formation has been discussed widely in this chapter followed by optimisation process. To validate the modelling results, experimental work has been carried out where the different instruments and set-up used are discussed in details.

In **Chapter 6**, the build-up of a 2D CFD model of a downdraft gasifier has been discussed. The model is validated and further used to study detailed tar species formation and different gas species in both steady and transient states.

Lastly, **Chapter 7** concludes the current research further highlighting the novelty and key findings. Also, recommendations for future works are mentioned.

Chapter 2 Literature Review

2.1 Introduction

A gasifier design is a complex process requiring detailed information including its dimensions, nozzles set-up, gas cleaning and feeding systems for the economic and optimum production of producer gas. Modelling of biomass gasification is one of the most favourable techniques, which allows simulating the gasifier design, output parameters, temperature variations, velocity, and pressure variations along the various zones/processes of a gasifier. Modelling techniques can be developed based on the processes involved and considered to be less expensive and less time consuming compared to experiments. Usually, a gasification model can be classified as equilibrium, kinetic, or CFD based model.

The key focus of this research work is on the process optimisation of gasification in an air-blown downdraft gasifier. And, this will be addressed through building up an advanced kinetic code in which gasification processes to be simulated with the identification of design conditions of downdraft gasifiers. The code will examine a wide range of materials including the effects of tar species formation and evolution. A CFD model of downdraft gasifier will be built to further investigate the processes occurring inside the reactor domain.

2.2 Equilibrium models

Thermodynamic equilibrium models are based on the principles of chemical and thermodynamic equilibrium, which are calculated by combining the equilibrium constants and minimisation of the Gibbs free energy through global reactions based on biomass type. Chemical equilibrium models provide a reasonable prediction for the final composition and monitor the maximum temperature in the gasifier for each zone [14]. Thermodynamic modelling, however, uses some assumptions, which are;

- uniform temperature distribution,
- gasifier is considered as zero dimensional,
- fast reaction rates, and
- the residence time is long enough to reach the equilibrium state [5], [14], and [21].

It is a modelling tool used to predict the maximum yield of producer gas based on specific working conditions. The calculation process is independent of gasifier design. However, it gives a reasonable prediction of syngas composition, and maximum gasification temperature. From the name (equilibrium), it is a balance equation that can be either one global reaction (eqn. 2.1) for the whole gasification process or a balance reaction for every process in the gasifier.

$$Dry\ Biomass\ (CHON) + w\ H_2O_{liq} + z(O_2 + 3.76N_2) \rightarrow x_1\ C + x_2\ CO + x_3\ CO_2 + x_4\ CH_4 + x_5\ N_2 + x_6\ H_2 + x_7\ H_2O + tar \quad (2.1)$$

The prediction process depends on the mass balancing in both sides with the elemental composition of biomass (CHON), and also uses additional equations depending on the number of unknowns. The additional equations could be found by using the chemical equilibrium constants which can be calculated from correlations depending on temperature [22] or could be derived from tables [23] or by minimization of the Gibbs free energy.

Dutta et al. [24] built a stoichiometric model for a downdraft gasifier based on equilibrium constants. The results obtained from their equilibrium modelling study were fairly in good agreement with experimental results for five different feedstocks. Ejirefe and Paul [25] introduced a pure thermodynamic equilibrium model for biomass gasification in a downdraft gasifier. This model was built on the basis of one global reaction step for biomass gasification, and the study focused on the effect of moisture content on the product gas composition. They compared their results with numerical model which showed a fairly good agreement. Carvalho et al. [26] showed a new method by modifying / correcting equilibrium constants. They first developed an equilibrium model called M1 and tested against experimental data. After which, they modified this model to M2, which is a quasi-equilibrium model and showed better accuracy. Perez et al. [14] discussed a mathematical model for biomass gasification in a downdraft biomass gasifier. The model was relatively easy to implement and predicted with accuracy the influence of air/fuel ratio and moisture content on producer gas composition.

Nevertheless, a pure thermodynamic model cannot predict accurately the gas composition of a gasifier because it gives an over prediction for higher heating value of CH_4, and H_2 outputs, and also lower amount of CO, Grace et al [27]. Further, Altafini et al. [28] presented a kinetic modelling scheme and reported that the reduction reactions are generally slower than the oxidation reactions by several orders of magnitude. The way to assess these effects was driven through the reaction rates which are the key for identifying the reaction formation and speed. Using high temperatures in reduction (more than 800 °C) which is preferred for higher syngas production because of higher reaction rates and more destruction of tars, the equilibrium model products of gas composition and temperature may deviate from reality. Thus, kinetic models are more suitable and accurate to predict gas composition.

2.3 Kinetic models

A model built through detailed kinetic mechanisms can predict the design of a gasifier which usually depends on the kinetic rate reactions taking place in the gasifier. Kinetic

models involve many parameters that cannot be covered by equilibrium models such as; fuel feeding rate, particle size, superficial velocity, residence time, gasifier length and design, reaction rates and hydrodynamics of reactor [29]. Kinetic models are built up by integrating each zone (step by step) of a gasifier through detailed reactions that can easily predict many factors of gasifier design/output. A kinetic model is a one-dimensional steady state model that is time consuming but gives accurate results [30].

Researchers usually developed one-step model for a specific zone e.g. reduction or pyrolysis, as it is complicated to include reactions of all zones in one model. Dividing gasifier model into sub-models gives more accuracy for the model than the prediction relying on a single zone.

Tinaut et al. [31] introduced one dimensional steady-state model for downdraft biomass gasifiers. The model takes into account the mass and energy balance and exergy exchange between solid and gaseous phases and heat transfer by radiation. They included all the gasification sub-processes (e.g. drying, pyrolysis, combustion, reduction by char and hydrocarbons reforming). Particle size effect and biomass feeding rate were also studied experimentally. A good agreement was found between the modelling and experimental data and they concluded that smaller particle size and lower equivalence ratio (ER) result with higher efficiency.

Budhathoki [8] introduced a model by combining the kinetic approach for the reduction zone and the thermodynamic equilibrium for the other zones. This model was compared with other experimental works for wood biomass and was found to be in a good agreement for the gas composition except for methane in which it gave higher prediction rates. The model introduced a sensitivity analysis to study the effect of changing ER and moisture content (MC) on the producer gas composition. While Ratnadhariya and Channiwala [15] proposed a new model for modelling biomass gasification. It is composed of three different zones, in which drying and pyrolysis are the first zone followed by combustion zone and reduction zone. The model is a combined system of stoichiometric model and assumptions for pyrolysis and oxidation zones for predicting the output gas. This model also provided a good agreement for woody biomass materials with varying working parameters. Dejtrakulwong et al. [32] built a four-zone kinetic model showing the effect of MC and ER on the temperature and height of each zone, which is useful in the gasifier design evaluation. The model incorporates empirical and equilibrium relations for drying, pyrolysis, and combustion zone, while reduction zone was based on detailed kinetic rate reactions.

Di Blasi [33] introduced a one-dimensional unsteady model for downdraft (stratified) biomass gasifiers. The model incorporates heat and mass transfer coupled with biomass

drying, pyrolysis, char combustion, gasification, and thermal cracking of tars. Di- Blasi considered moisture evaporation as a diffusion-limited process and represent it by an empirical expression while pyrolysis was represented as a one-step global reaction. Tar secondary cracking reactions have been estimated based on literature [34]. Again, reduction zone was based on detailed kinetic reactions. The results allowed to study the effect of working parameters on the gas quality and process dynamics. The model also was able to predict axial temperature profile as well as gas composition. Giltrap et al. [22] built a steady-state model based on kinetic rate reactions in reduction zone. It was able to predict temperature and gas composition though it found over prediction for methane. The model did not include pyrolysis and tar reactions. All reactions were based on Arrhenius-type temperature dependent rates which were taken from Ref. [35]. The model incorporates all of mass and energy balance as well as pressure and velocity variations. The results were verified against experimental data of [36] and [37], and found a good agreement for syngas components with higher values for CH_4.

In the model of Jayah et al. [38], they presented a model composed of two sub-models for pyrolysis and reduction zones. Pyrolysis model is an equilibrium model with mass and energy balance to estimate maximum temperature and gas composition leaving pyrolysis. The products of pyrolysis were used as feeding to reduction zone. They [38] also carried out experiments to validate results coming out of the model. The model was validated, and the results of gas composition and temperature of gasification and pyrolysis were found to be in good agreement with the variations of ± 5.8%. They recommended using reduction zone length more than 33cm to achieve an acceptable conversion efficiency.

Koufopanos et al. [39] introduced a simple kinetic model for biomass pyrolysis in details where they stated that the rate of pyrolysis is the sum of corresponding rates of biomass components. Each of these components was described by kinetic model. Their work was built as shown in Figure 2.1 which shows the reactions in pyrolysis of biomass. The model shows that biomass first decomposes into volatiles and gases, then these components further react with each other to form the final gases, volatiles and char from pyrolysis. Then Babu and Chaurasia [40] used the model of [39], solved the pyrolysis equations derived from their work at different working conditions and specified the optimum parameters of pyrolysis zone e.g. temperature, heating rate and time of pyrolysis. They also reported the concentration of char and other volatiles of pyrolysis products.

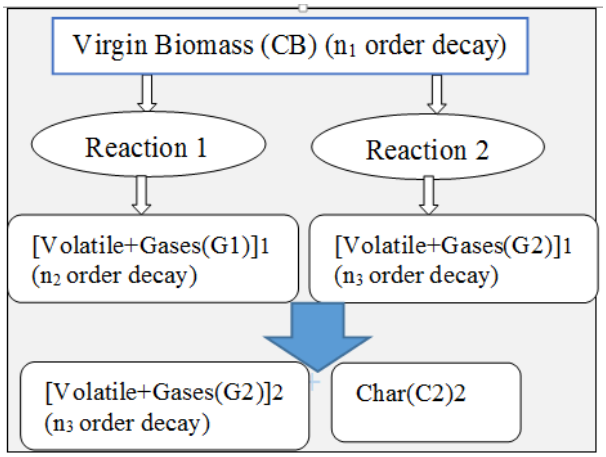

Figure 2.1: Biomass devolatization [39].

Babu and Chaurasia [40] solved the ordinary differential equations (ODE) of [39] numerically using the fourth order Runge–Kutta method for a wide range of temperatures (773-1773K) and heating rates (25–360 K/s). They used two different orders of reactions and found optimum values (for thermal degradation) for non-isothermal pyrolysis. At the pyrolysis times 9.53 and 2.636 s, the optimum values of the heating rates were found to be 51 and 184.38 K/s, respectively, considering the same temperature (1259.03 K) for both the orders of reactions.

Gordillo and Belghit [41] developed a numerical model for solar downdraft gasifier fed by char biomass with steam as gasifying medium. The model ignored pyrolysis and cracking reactions and only considered gasification reactions from Ref. [35]. The results were validated against experimental data and found in a good agreement for temperature and gas composition. The highest yield was found for hydrogen followed by carbon monoxide with lower amounts of carbon dioxide and negligible amounts of methane.

Di Blasi and Branca [42] proposed a detailed mathematical kinetic model for downdraft gasification of wood pellets. The model assumes two air jets; primary from top and secondary at certain height from bed. The air amount variations between primary and secondary air was studied on the effect of wood degradation, temperature, tar and char conversions. The results showed a good agreement with pilot scale gasifier ([43], and [44]) with reduction of tar amount and higher conversion of char.

In the model of Sharma [17], a one-dimensional kinetic model was built to predict the downdraft biomass gasifier performance. Chemical equilibrium is used for combustion process while empirical correlations were used for pyrolysis and kinetic rate reactions for reduction zone. They used mass and momentum conservations with heat transfer analysis, which were solved in integral form combining pressure, temperature and product gas composition. The experimental set-up built by Sharma [30] for a 20 kW downdraft gasifier

was used for model validation in the present work, and the model found good agreement for heating value, gas composition, and flow rate, temperature and efficiency.

While Simone et al. [45] presented a one-dimensional mathematical model to validate their experiment on a throated biomass gasifier running on wood residues. The model incorporates mass and heat transfers as well as kinetic reactions of char combustion/gasification and tar cracking. The detailed kinetic reactions were for reduction zone while one global reaction was used for devolatilization process [33]. Simulations and experiments were carried out at different loading rate of biomass to study its effect on gasification performance.

Budhathoki [8] reported that his model is only valid for wood biomass material, and it does not take into account any tar formation and higher hydrocarbons. Several other researchers (e.g. see [13], [46]and [47]) only discussed the effect of changing biomass moisture content on producer gas heating value and showed that higher moisture content reduces the heating value. But they did not show any possible effect of those on residuals and tar content. Further, they did not discuss the effect of other working parameters like equivalence ratio.

Although kinetic models are a powerful tool in designing a gasifier, they still have some limitations. To the best of the author's knowledge, there is no previous kinetic model that is capable of including the design of a downdraft gasifier and tar formation along with the prediction of producer gas production in a single kinetic model. Also, previous models did not consider the detailed species formation and distribution along gasifier height/length. So, the current research work proposes to develop a novel integrated kinetic model that will overcome the limitations highlighted above.

2.4 Tar formation and modelling

Tar was defined in various ways as per the previously published works. For example, Ref [48] reported it as an organic compound produced during thermochemical reactions including oxidation and gasification of any organic material. Tar is also assumed to be largely an aromatic compound and has a wide range of boiling points consisting of one- to five-ring aromatic hydrocarbons as reported by [49]. Generally, tar can be defined as a hydrocarbon that has a molecular weight higher than benzene C_6H_6 [50]. Further, tars could be formed in hundreds of different chemical compounds, but in most cases, about 20 species are present in significant amounts [35] (Figure 2.2). Finally, tar is a totally undesirable product from biomass gasification, as it can create many problems like condensation and subsequent plugging of downstream equipment [5].

An effective tool to use syngas directly as a fuel, is to limit the formation of tar, or reduce it to a specific limit. As a result, studies are carried out to investigate the nature of formation and destruction of tar compounds. Experimental works regarding tar formation and destruction is a cost and time-consuming tool. On the other hand, tar is a complex compound, and because of this, many researchers only consider it as a one compound like benzene [16], while others mainly take into account the formation of poly Aromatic Hydrocarbons (PAH) [51]. Another effective tool to study tar compounds formation in gasification processes is the modelling either by kinetic codes e.g. [51] and [52], or by CFD modelling e.g. [53].

Tar is produced primarily from pyrolysis through depolymerisation process at temperature 200-500 °C. Biomass components such as cellulose, hemicellulose, and lignin in this temperature range starts to break down the process to lead primary tar (wood oil, or wood syrup) [48]. At above 500°C, primary tars tend to form smaller, lighter non-condensable gases and a series of heavier molecules called secondary tars. At the temperature above that range, primary tars are destroyed and as a result, tertiary tars are formed.

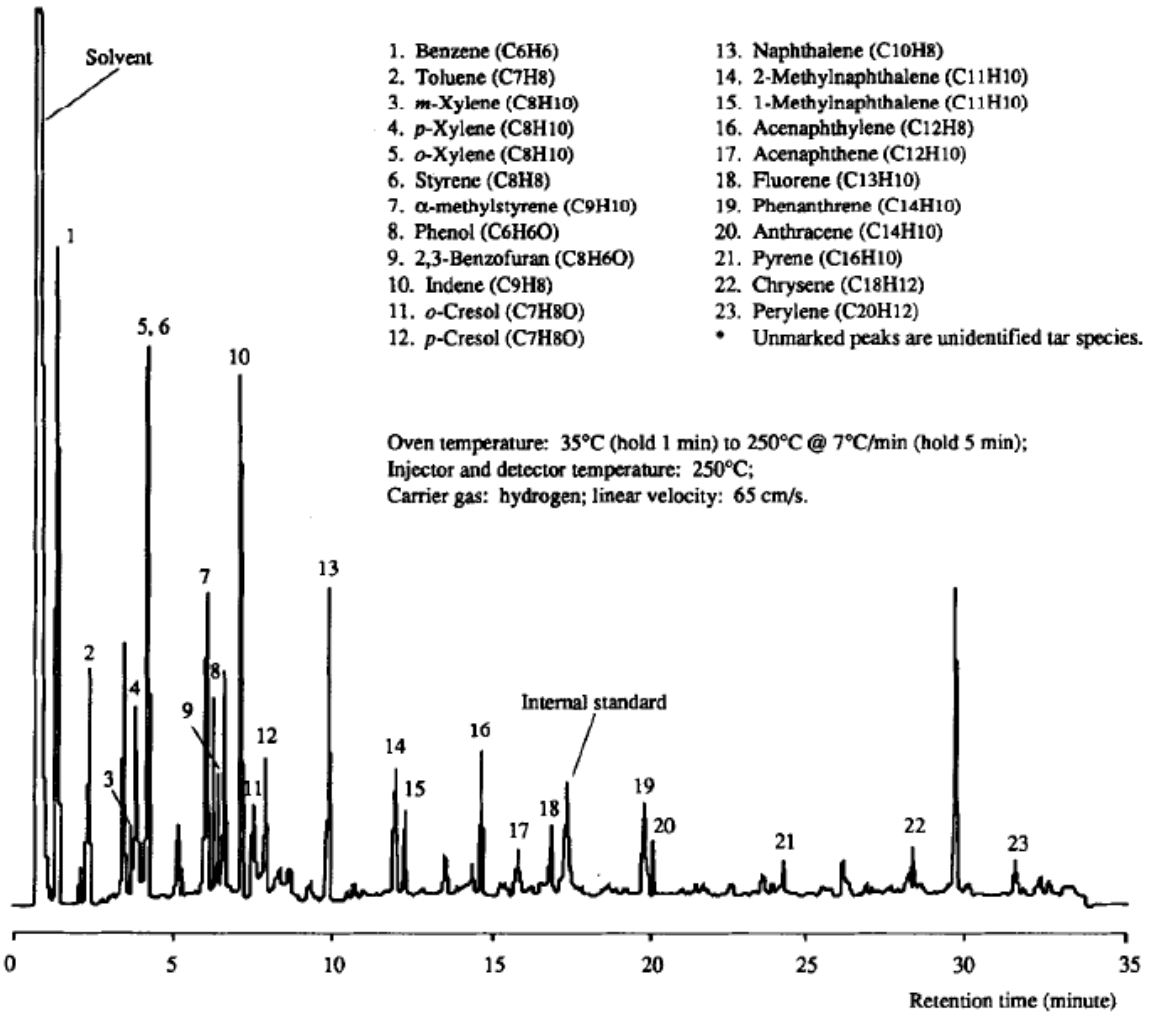

Figure 2.2: Chromatogram of tar species [35].

In more depth, tars can be classified as described below;

- Primary tars: Oxygenated, primary organic and condensable molecules. They come mostly from the breakdown of cellulose, hemicellulose, and lignin under 500 °C, like phenol, acetol (biggest portion [54]), acetic acid, Guaiacol, and Furfural.
- Secondary tars: As the temperatures rise above 500 °C, primary tars rearrange to form gases and secondary tars (phenol, cresol, indene, and olefins).
- Tertiary tars: Aromatics, toluene and indene which are formed at higher temperatures. Condensed tertiary tars make up the PAHs (Benzene, naphthalene (most important [54]), acenaphthylene and pyrene). All primary tars are converted to secondary and tertiary tars as the temperature of gasifiers increases further.

Tar formation and cracking in downdraft gasifiers have been simulated using kinetic models previously e.g. see [55], and [56]). Kinetic tar models could be built by using a one single compound representing all tar species such as $C_6H_{6.62}O_{0.2}$ as a tar representative compound and it assumed to give tar amount as a percent of total gas production [16]. Other models chose a heavy aromatic compounds as tar representative. For example, Liu et al. [57] used toluene as a tar compound to study the tar destruction process using gliding arc technology. Also, Zhao et al. [58] used toluene in tar steam reforming modelling during pyrolysis of biomass. Toluene was chosen for its stability as a good representative of tar produced during pyrolysis. Other compound like phenol was also used as a tar representative as described by [59].

2.4.1 Single compound tar models

The use of Naphthalene as a single compound for tar representation was illustrated in the model of Jess [60]. The model studied pyrolysis conditions for tar in hydrogen and steam environment. The main products of tar cracking were methane, benzene, and C_2 hydrocarbons with minor amounts of toluene and indene. Soot was also formed and further converted by cracking with other hydrocarbons to CO, and CO_2 at temperatures above 1473K. The model was verified by an experimental work built by Jess and found good agreement. It also found that benzene is the main component during tar conversion and cracking.

Ji et al. [61] used phenol as tar compound for air-blown fluidized bed biomass gasifiers. They found that phenol as a primary tar further decomposes during cracking reactions to naphthalene, benzene, soot, steam and non-condensable gases. The results were compared with experimental data ([62], and [63]) and found a good agreement. They also discussed the effect of ER and temperature on hydrogen production considering overall thermodynamic efficiency of fluidized bed gasifiers.

While Zhao et al. [58] used steam reforming of toluene as a tar representative during biomass pyrolysis with catalysts in downdraft gasifiers. They used temperatures within the range of 1023-1173 K as it is an optimum range for ultimate hydrogen production. Thermodynamic equilibrium model was built, and experiments were carried out at same working conditions to validate the model results. The main products of toluene reforming were benzene and naphthalene with small amounts of phenol and styrene. However, naphthalene was found to decrease with temperature while benzene was increasing.

2.4.2 Detailed kinetic models

Detailed kinetic models discuss tar formation along different zones of gasifier. Unlike a single compound model that uses one compound representing tar, a detailed kinetic model selects different tar compounds which are generated during the process of gasification.

Norinaga et al. [64] introduced a detailed chemical model to predict pyrolysis and combustion of hydrocarbons (benzene, naphthalene, or toluene). The model is used to predict and evaluate the steam reforming of aromatic hydrocarbons in presence of hydrogen and steam. The modelling results were initially verified with [60], at temperatures 1073-1673K, and found the major products to be CO, CO_2, and CH_4 in addition to some trends of aromatic hydrocarbons. The results showed good comparison and validation except for soot and C_2 hydrocarbons. For naphthalene conversion, they further studied the effect of hydrogen partial pressure on products composition.

Corella et al. [65], on the other hand, built a lumped model considering six tar groups. The groups were benzene, one-ring compounds, naphthalene, two ring compounds, three to four-ring compounds, and phenolic compounds. They used a set of 6 different kinetic equations with 11 kinetic constants to model the tar formation and cracking in a fluidized bed biomass gasifier. They reported that phenolics were most likely to be formed while naphthalene was hard to be cracked. While Fuentes et al. [66] built a model to predict the yield of benzene, toluene, and naphthalene, plus phenol and pyrene under pyrolysis conditions of wood biomass materials in temperature range of 973-1373K. The model was divided into two sub-models; devolatilization, and further volatiles and tars are converted by

secondary reactions. They reported that toluene is the best representative for secondary tars while naphthalene as a PAH represents tertiary class tars. [52] Also stated that the four compounds, (benzene, naphthalene, toluene, and phenol) were used for their model who simplified 10 tar species to those four lumped tar species. They also reported that toluene conversion is affected by hydrogen presence, and lighter compounds are formed with benzene as the main conversion product. Benzene yield was well predicted with a maximum yield around at 1073-1273K.

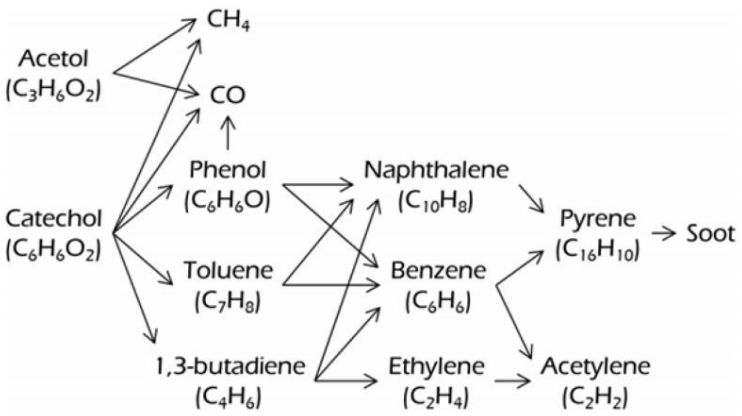

Figure 2.3: Scheme of reactions proposed by [66].

Abdelouahed et al. [52] introduced their model to simulate a steam blown fluidized bed gasifier. Their model consists of three sub models; devolatilization, secondary reactions of steam gasification, and char oxidation model. Pyrolysis model was based on an empirical correlation for the devolatilization of wood biomass to different gas species and four tar compounds. The correlations were derived from the experimental data of [67] depended on the reactor temperature. Secondary reactions and char oxidation were based on detailed kinetic rate reactions. The results of gas composition, tars, heating value and flow rate were compared with the corresponding data from two gasifiers and found good agreement.

Fourcault et al. [68] modeled thermal decomposition of tars coming of a gasifier at 800°C. They used naphthalene and toluene as model compounds. The model used to study working parameters on degradation efficiency. However, they did not validate their findings against any experimental data. Nevertheless, the results were validated with an equilibrium model and showed good agreement. Their model used a set of 15 different kinetic rate reactions to study the products of cracking and concentration of tar species.

A recent study by Veksha et al. [69] illustrated the modelling and experimental investigation for tar produced during gasification of municipal solid waste (MSW) in a downdraft gasifier. They studied the effect of changing working parameters on tar produced

using air gasification. The formation and evolution of styrene was modeled as it showed the biggest portion i.e. 13–29% wt. of tar species released during gasification of MSW. As a result, the variations of styrene during experiments and modelling were studied at different working conditions to optimise the process of gasification. The effect of varying temperatures such as 800, 850 and 900 °C in combination of ER of 0.2, 0.3 and 0.4 and moisture content of 10, 25 and 40% was studied. The results concluded that styrene amounts can be minimised in the range of 900-950 °C at higher ER of 0.3-0.35, and moisture content >20%.

Ledesma et al. [70] built a lumped model for biomass tar cracking using 4-propylguaiacol as a model compound that represents the primary tars formed during pyrolysis between 300°C and 900°C. The products showed three major classes; oxygen-containing compounds, single- and multi-ring aromatic hydrocarbons, and permanent gases. Results revealed the great effect of temperature on gases and tar products. The model was validated against experimental data and further expanded to lumped kinetic model with 8 first-order irreversible reactions. The results were validated and showed that the model is capable of describing the behaviour of secondary vapour-phase cracking of biomass tar.

Li et al. [71] studied the elimination of heavy tar compounds by modelling and experiments. The modelling process was carried out based on a kinetic model ([72], and [64]) using CHEMKIN code. Temperature and residence time increase showed an increase of heavy tar decomposition. They showed that temperatures above 1573 K will crack heavy tars to lighter compounds/gases and soot. The results proved that steam reforming is an effective tool to reduce heavy tar. Their results provided with the useful information for 3D simulations, design and operation of tar cracker.

2.4.3 Experimental studies on tar formation

A detailed experimental study was conducted by Dufor et al. [73]. They experimentally studied pyrolysis of wood chips increasing temperature from 700°C to 1000 °C, at a varying heating rate of 20–40 °C/s and reported the mass balance for CHO. Permanent gases, char, water, and 10 aromatic tar compounds were considered in the balance calculations. They mentioned that higher gas yield and higher heating rates are achieved by using fine particles <1 mm. They, however, found a large difference in the gas yield and composition when changing the temperature, heat transfer rate and residence time. Benzene was the most stable tar compound, representing more than 80% mol. of tars at 900-1000 °C, and it is a key compound of aromatic tars conversion which has good agreement with [74]. The char yield

was found to decrease with the increase of temperature. It can be clearly shown in Figure 2.4, that benzene concentration is increasing with temperature, while the other compounds are decreasing. On the other hand, the total tar produced is increasing until 800 °C, then tends to decrease again.

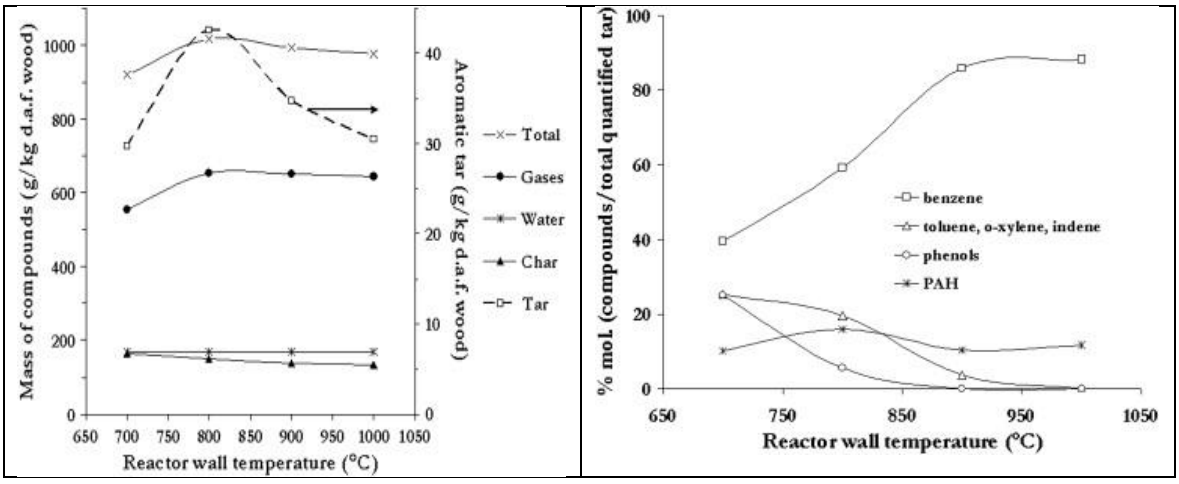

Figure 2.4: Products from wood pyrolysis (left), and tar species evolution (right) [73].

The same results trend was showed by Phuphuakrat et al. [74] who studied experimentally the tar yields in the syngas produced in a downdraft gasifier from sewage sludge. The results showed that benzene is always the highest portion of tar produced, Figure 2.5. The study also discussed the effect of air supply (ER) on the reduction of tar amount.

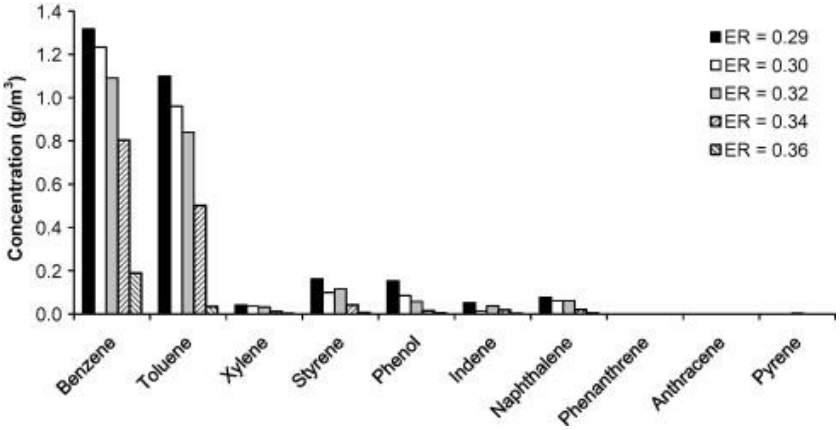

Figure 2.5: Averaged concentration of each tar component [74].

Based on the review of tar modelling, it can be clearly concluded that tar formation in downdraft gasifiers has not been widely expanded when considering the aspects of detailed formation of tar species, cracking and distribution along gasifier height. Some models were built to represent only one compound (usually considering a general formula of tar, or selecting one species as a tar representative [51]), while other models focused on tar but formed in specific zones (e.g. pyrolysis [58]). To the best of the author's knowledge, there has been no model that takes into account the modelling of tar species along gasifier height or at the different zones of a downdraft gasifier. So, one of the current research goals is to

build up a tar formation model with detailed species and chemical kinetics along gasifier height and investigate the evolution of tar at both steady and transient state conditions. The model will also address the optimum conditions that would potentially help to reduce the tar amount.

2.5 CFD models

Computational fluid dynamics (CFD) modelling codes are facing some challenges in the area of biomass gasification/combustion, because of the biomass variety and also the lack of understanding of tar modelling [75]. On the other hand, it is a very advanced numerical modelling technique that allows studying all the relevant processes within a gasifier. It also provides better understanding of the interactions between the solid and gas phase reactions during gasification process ([18], and [19]). A CFD model involves a combined solution of the transports of mass, momentum and energy, along with turbulence and hydrodynamics of flow field [29]. Several commercially available CFD software could be used in the modelling of gasification such as ANSYS FLUENT, Star CCM, and Phoenics. However, CFD modelling of biomass gasification needs more clear understanding of the process gasification. Also, different chemical kinetics were used for same reactions, which makes uncertainty and variations in results [76]. On the other hand, the process of tar formation along gasifier has not been covered widely using CFD modelling and thus needs more investigation and research. In CFD models, variation of operating and design parameters could be implemented and impacts on the syngas quality could be further investigated [18]. However, based on the literature review on the CFD modelling of biomass gasification in downdraft gasifiers, the selection of chemical kinetics significantly influence on the models stability ([76], [77], and [74]).

A CFD based model was built by Fletcher et al. [78] based on CFX4 package, for biomass gasification in an entrained flow gasifier. They used Lagrangian approach to model biomass particles entering gasifier, which then release volatiles and goes under gasification. Transport equations and heterogeneous reactions are solved to get the concentration of different gas species. The model succeeded to present temperature and syngas composition under different working conditions.

A 2D CFD model was also built recently by Kumar and Paul [18], for a downdraft biomass gasifier. The model used ANSYS Fluent software to simulate a 20-kW downdraft gasifier work. Eulerian-Lagrangian model was used in the modelling procedure including gasification's 4 main zones; drying, pyrolysis, combustion and reduction. They used different set of chemical reaction data to validate the model against experimental and kinetic

results from literature. After the model validation, they studied the effect of ER on the producer gas composition and the variations of using different feedstocks from Sottish agricultural residues. Detailed results of gas species formation along gasifier and temperature profile were presented at different ER >0.35, as the models were unstable for lower ER. Under this condition, the model provided a good stability in predicting the various from the gasifier and thus has potential in designing and simulation downdraft biomass gasifiers.

L. Yu et al. [79] presented numerical simulation model for a bubbling fluidized bed (BFB) coal gasifier using the kinetic theory of granular flow (KTGF). They combined the kinetic theory of granular flow (KTGF) and Arrhenius rate reactions for coal gasification to simulate BFB. The results were verified against experimental data for gas composition at exit and found good agreement. The model was further used to study the relation between gasifier height and gas composition, temperature, and velocity along gasifier bed.

Janajreh, Al Shrah [20] build up an axi-symmetrical CFD numerical model for a small-scale downdraft biomass wood chips gasifier. The CFD model used a high-resolution mesh for accounting the solids and gases interaction, and the k–ε turbulence model combined with reaction kinetic models containing water evaporation, devolatilization, gas phase and particle surface reactions as discrete phase. The modelling results were compared with experimental data as well as equilibrium model and found good agreement.

Rogel and Aguillón [80] used PHOENICS, with an IPSA algorithm to build a 2D CFD model for thermal and flow fields inside a stratified downdraft biomass gasifier for pine wood. The model used Eulerian conservation equations consisting transports of mass, momentum, and energy, chemical kinetics, and turbulence. The Eulerian approach was used to solve for the velocity, specific enthalpy, particles and gas phase reactions by taking into account of usual gasification steps including drying, pyrolysis, homogenous and heterogeneous phase reactions in combustion/reduction. They used the standard κ-ε and RNG κ-ε models to simulate turbulent flow inside the gasifier. The model was able to predict gas composition, temperature profile, heating value and reactor performance for different working conditions. The model showed an acceptable value of gas composition when compared with the experimental results.

Wu et al. [81] developed a 2D CFD model for simulating gasification in a downdraft biomass gasifier with highly preheated air and steam considering all thermochemical processes in the gasifier; drying, pyrolysis, combustion and reduction. The Euler-Euler approach was used to solve gas-solid phase interactions considering mass, momentum, and energy balances using the standard κ-ε model in the gas phase. The results were validated

and found good agreement with their experimental small-scale downdraft biomass gasifier for the temperature and gas species concentration. They also studied the effect of increasing preheated temperature and steam to air ratio and found that they increase the syngas production rate while decrease tar amount.

Murugan and Sekhar [82] built a 2D numerical simulation of imbert biomass gasifiers to study and select the biomass availability at remote areas. They used species transport with the κ-ε RNG to model the main four zones of a downdraft gasifier. They also studied the effect of changing different feedstocks (e.g. coconut shell, cow dung, rice husk, rubber seed kernel shell, and rubber wood). They showed the effect of changing ER on the product gas quality, composition and heating value. The model was validated against their experimental results as well as with other data from literature and found good agreement for temperature and gas composition. Their results further demonstrated that ER within the rage of 0.24- 0.26 gave the best performance of a gasifier, and the use of rubber seed kernel shell was the most suitable feedstock to be used in Nagercoil, Tamilnadu, India for producing higher heating value syngas.

Gupta at al. [83] presented a 2D CFD model to study the performance analysis of a 10-kW downdraft biomass gasifier using ANSYS software. The modelling was carried out through species transport theory with volumetric and particle surface reactions to study temperature and different gas species along gasifier. The model used some assumptions including spherical particle shapes with 25 mm diameter and used O_2 as an oxidizer (zero N_2) under steady state condition. Turbulence was simulated again using the standard and realizable κ-ε RNG model with the usual governing equations of mass, momentum, and energy. P1 simple radiation model was used for simulations. Results of gas species mass fractions and temperature along gasifier were validated with the experimental gasifier and found good agreement with a reasonable error of 4-6 %. They further presented pressure, temperature, char consumption in reduction zone, and contours of different gas mass fractions along gasifier height.

Unlike the kinetic models, CFD modelling can handle a wide range of parameters and working conditions (e.g. gasifier design effect). Kinetic models depend on chemical reactions that are not affected by gasifier geometry. As a result, gasifier design's effect on the syngas production and quality cannot be widely studied through the kinetic models. Species formation and distribution along gasifier at transient state also can be studied through a CFD model. Based on the review carried out, previous CFD models did not present any detailed tar species and also, a very few previous published works studied the effect of changing feedstocks on their gasifier design. Hence, the main focus on this research work is

to address these challenges through a detailed CFD model developed using ANSYS software. The model will be able to simulate the working conditions of a downdraft gasifier when operating with a wide range of materials (such as biomass and agricultural residues). The model will also study the different gas species and detailed tar species formation along the gasifier domain. Further, one of the main aspects and novelty in the current research work of the CFD modelling is implementation and modelling of the detailed tar species formation along the gasifier under both steady and unsteady state conditions.

Chapter 3 Integrated Novel Kinetic Model for Biomass Downdraft Gasifiers

3.1 Introduction

A novel kinetic model was built to estimate the optimum working parameters of a downdraft gasifier, in which a set of chemical kinetics at each zone of the gasifier was described. The model deals with a wide range of biomass types with the elemental composition ranges of (38≤C≤52) %, (5.5≤H≤7) %, and (36≤O≤45) %. This model is able to predict the gas composition, tar content, temperature and height of each zone, as well as temperature, velocity and pressure distributions at the reduction zone with the heating value of product gas. The model also gives the full design dimensions of a downdraft gasifier to be further discussed. The final results, which proved to be in good agreement with the experimental works under different working conditions of biomass type, moisture content, and air to fuel ratio, were based on a new approach that includes the calculation of the optimum height of the reduction zone.

All the previously published articles discussed the gasification kinetic model with a constant height of reduction (e.g. see [15] , [32], [17], and [22]). Based on the review, this is the first time the model presented in this work incorporates the effect of optimum height of the reduction zone on the concentration of different species of product gas as predicted. Taking into account a wide range of biomass materials covered by the model, the study will also focus on the prediction of tar content and find the optimum working conditions leading to the production of high quality syngas as well as biomass materials that give a high yield of syngas with a low tar content. The model will also provide useful information for the full design of a downdraft gasifier based on a desired thermal power. Further to be noted that, to the best of the author's knowledge, there appears to be no previous model that includes the product gas composition, tar content and a full design of gasifier in one kinetic model. The model will address the gasifier design based on the key parameters like throat diameter and fuel feeding rate and its effect on other working parameters.

3.2 Kinetic modelling

The proposed model is built through a set of chemical kinetic schemes to predict the full design principles for a downdraft gasifier which depends on a series of reactions taking place in the gasifier. Biomass gasification is done through four main steps: drying, pyrolysis, oxidation and gasification / reduction as shown in Figure 3.1. Kinetic modelling involves initial steps including the calculation of main parameters used in the whole process e.g.

air/fuel ratio, biomass chemical formula, heat of formation for biomass, and temperature calculations.

3.2.1 Air to fuel ratio

The theoretical (stoichiometric) amount of air to fuel (AF) ratio was calculated from [5]

$$0.1153\ C + 0.3434\ (H - \frac{O}{8}) \quad \text{(kg air/kg biomass)} \tag{3.1}$$

where H, O and C indicate respectively the mass fraction (%) of hydrogen, oxygen, and carbon content in biomass from its ultimate analysis, and the actual amount based on the equivalence ratio (Φ) is calculated from

$$(AF)_{actual} = \Phi\ (AF)_{theoretical} \quad (kg\ air/kg\ biomass) \tag{3.2}$$

$$m = \ (AF)_{actual_{moles}} = \frac{M_{biomass}}{M_{air}} (AF)_{actual} \tag{3.3}$$

where M is the molecular weight of dry biomass.

3.2.2 Chemical formula of biomass

The chemical formula of biomass ($C_a\ H_b\ O_d$) was calculated based on its elemental composition from its ultimate analysis as follows

$$a = 1\ ,\ b = \frac{H*M_C}{C*M_H}\ ,\quad \text{and}\ \ d = \frac{O*M_C}{C*M_O} \tag{3.4}$$

where Mc, M_H and M_O are their molecular weight.

3.2.3 Water molar fraction

The water molar fraction in biomass is calculated as

$$w = \frac{h*M_{biomass}}{M_{H2O}\ (1-h)} \tag{3.5}$$

where h is the moisture content of biomass.

3.2.4 Heat of formation of biomass

Biomass heat of formation (h_f) is used in calculating temperature distribution. It is derived from its heating value as the Hess's law states that the difference of enthalpy (ΔH) for a reaction can be found indirectly by summing the ΔH values for any set of reactions which then sums to the desired reaction [84]. The enthalpy of formation of biomass is assumed to be equal to the biomass higher heating value which is calculated from [15].

$$HHV\ (MJ/kg) = \quad 0.519 * C + 1.625 * H + 0.001 *\ O^2\ - 18.87 \tag{3.6}$$

$$HHV\ (kJ/mol)\ =\ HHV\ (MJ/kg)\ *\ M_{\ biomass} \quad (3.7)$$

3.2.5 Temperature variation across the gasifier

Heat balance between the input and exit of each stage is made to predict the temperature of pyrolysis, combustion and gasification processes. It is done through the energy balance for the reactants and products of pyrolysis zone as follows;

$$\left(h_f\right)_{biomass} + w.\left(h_f + C_p.\Delta T\right)_{H_2O_{liq}} = \sum X_i\,.\left(h_f + C_p.\Delta T\right)_{pyrolysis\ products} \quad (3.8)$$

where X_i is the concentration of products in mole, ΔT is the temperature difference between air supplied and pyrolysis products in K, C_p is the specific heat at constant pressure (J kg^{-1} K^{-1}), and h_f is the heat of formation of different species (kJ/mol) from [23]. Same energy balance is carried out for the different zones to get temperature.

3.3 Kinetic model formation

A schematic drawing of a downdraft gasifier is shown in Figure 3.1, in which biomass is fed from the top of the gasifier into the drying zone, while air is fed into the oxidation zone for combustion process. The product gas is driven from the down of the gasifier. Tar is collected in the bottom of the gasifier. Modelling involves an integration of the four zones and the thermochemical kinetic processes associated with the main zone are elaborately explained in the following sections. The output of each zone such as the gas composition and temperature is considered as an input for the next one based on the process illustrated in Figure 3.1. Modelling of each zone is described in the following sections whereby all the zone models are combined together in one code (i.e. an integrated model).

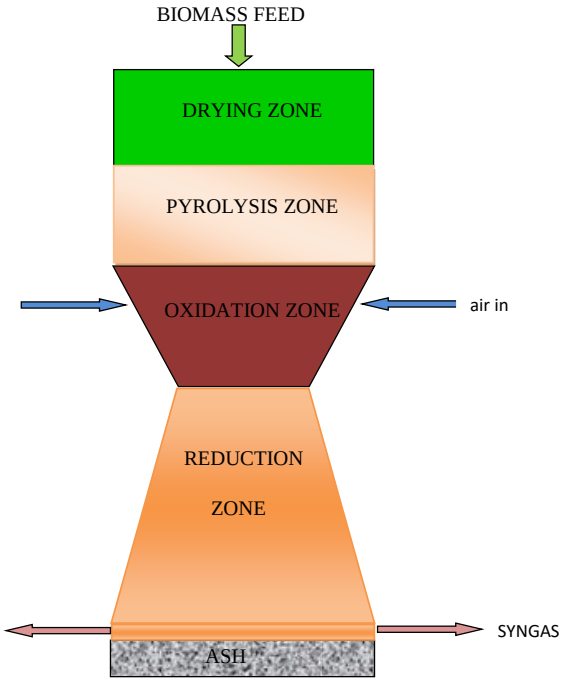

Figure 3.1: Schematic view of a downdraft gasifier.

3.3.1 Drying model

The drying zone receives heat from oxidation which leads to an increase of temperature. The initial temperature is supposed to be 298 K, however when the temperature reaches 373 K, the vaporization of moisture content starts until it reaches 473 K as mentioned by [32]. At this temperature, the pyrolysis begins automatically, thus the devolatization of biomass occurs [32]. The rate at which the drying reaction taking place is determined based on the modelling proposed by ([32] and [85]). Constant drying temperature is used in calculations as 400K to ensure that the drying process is complete.

$$r_d = K_d . C_{H_2O,l} \quad (3.9)$$

$$K_d = A_d exp\left(\frac{-E_d}{R\,T_d}\right) \quad (3.10)$$

where, constants used in the drying model are summarised in Table 3.1, where r_d is the drying rate, K_d is the drying equilibrium constant, and C_{H2O} is the moisture concentration in biomass. A_d is the pre-exponential factor, s^{-1}, E_d is the activation energy of drying reaction, kJ/mol, R is the universal gas constant, and T_d is the drying temperature used, K.

Table 3.1: Data for drying model [32]

A_d, (s^{-1})	K_d, (s^{-1})	E_d, (kJ/mol)	T_d, (K)
5.13×10^6	0.1652	88	400

3.3.2 Pyrolysis model

Biomass after drying first decomposes into volatiles and char, then these components further react with each other to form char and volatiles again as shown in Figure 2.1 of Chapter 2. The kinetic equations below are taken from [25]

$$\frac{dC_B}{dt} = -K_1 C_B^{n1} - K_2 C_B^{n1} \quad (3.11)$$

$$\frac{dC_{G1}}{dt} = K_1 C_B^{n1} - K_3 C_{G1}^{n2} C_{C1}^{n3} \quad (3.12)$$

$$\frac{dC_{C1}}{dt} = K_2 C_B^{n1} - K_3 C_{G1}^{n2} C_{C1}^{n3} \quad (3.13)$$

$$\frac{dC_{G2}}{dt} = K_3 C_{G1}^{n2} C_{C1}^{n3} = \frac{dC_{C2}}{dt} \quad (3.14)$$

Where,

$$K_1 = A_1\, exp[\,(D_1/T) + (L_1/T^2)] \quad (3.15)$$

$$K_2 = A_2\, exp[\,(D_2/T) + (L_2/T^2)] \quad (3.16)$$

$$K_3 = A_3\, exp[\,(-E/RT)] \quad (3.17)$$

The model shows that biomass (with an initial concentration C_B) first decomposes into volatiles and char (*G1*, and *C1*), then these components further react with each other to form the final gases, volatiles and char (*G2*, and *C2*) from pyrolysis. The values of *A*, *D*, and *L* for equations (3.15), (3.16), and (3.17) are illustrated in Table 3.2. The following initial conditions are used for solving the coupled ordinary differential equations (3.11)-(3.17), e.g. at t= 0, C_B = 1 and $C_{G1} = C_{C1} = C_{G2} = C_{C2}$ =0.

Table 3.2: Parameters of the pyrolysis model [39] and [40].

R	*A*, (s^{-1})	*D*, (K)	*L*, (K^2)	*E*, (kJ/mol)
1	9.973×10^{-5}	17254.4	-9061227	
2	1.068×10^{-3}	10224.4	-6123081	81
3	5.7×10^{5}			

Equations (3.11-(3.14) are solved until the conversion of biomass reaches 0.03 from its initial concentration (100%), because beyond this point the pyrolysis is very slow and there is little experimental and practical importance [40]. Matlab code ODE45 was used to solve these sets of equations to get the products. The products of this model were plotted against time, as shown in Figure 3.2.

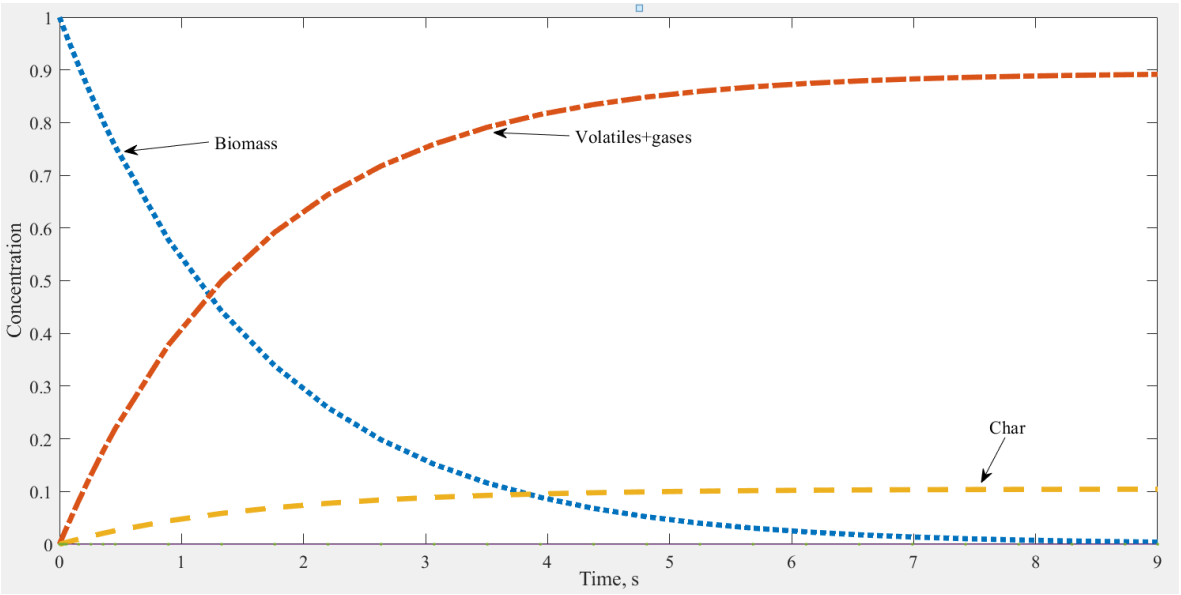

Figure 3.2: Products concentration of biomass devolatization.

The results illustrated in Figure 3.2 shows the biomass devolatilization with time and its corresponding products. While the temperature increases inside the gasifier and pyrolysis zone, biomass starts to decompose into volatiles, gases and char as clearly shown in the figure. The highest portion is for volatiles followed by char.

Babu et al. [40] determined the optimum parameters for pyrolysis through a wide range of heating values (25–360 K/s) and temperatures (773-1773K) during the isothermal and non-isothermal processes and found that the optimum conditions for the non-isothermal process are as stated in Table 3.3. Optimum parameters ensure that all the biomass successfully converted into volatiles and char, and the final concentration of virgin biomass left is less than 0.03. While they showed that the optimum temperature for pyrolysis is 1259 K, the temperature is still very high to handle before oxidation and this will require higher temperature in the oxidation zone plus the specific design materials for gasifier. As a consequence, we choose a temperature of 873 K to start with as the pyrolysis process below 773K is very slow, as reported by [32]. The volatiles are assumed to be CO, CO_2, CH_4, H_2, H_2O, and tar. The importance of this part is that it gives the final concentration of char and volatiles; after which the concentration of char is known at the end of devolatization and is used for the next step in which the volatiles concentration is predicted.

Table 3.3: Optimum values of non-isothermal pyrolysis [40].

T, (K)	*HR*, (K/s)	Time, (sec)	n_1	n_2=n_3
1259	51	9.53	1	1.5

Sharma [17] introduced a new model to predict the percentage composition of volatiles and he considered one-step model for the biomass pyrolysis as follows

$$C_a H_b O_d \rightarrow x_1 C + x_2 CO + x_3 CO_2 + x_4 CH_4 + x_5 H_2 + x_6 H_2 O + x_7 C_6 H_{6.2} O_{0.2} \quad (3.18)$$

Where $C_a H_b O_d$ represents biomass, *x* is the concentration of different species of pyrolysis products in mol, $C_6H_{6.2}O_{0.2}$ is the tar chemical formula as considered by many researchers e.g. [17]. The mass fraction (*Y/Y*) empirical relations used are

$$\frac{Yco}{Y_{CO_2}} = \exp\left(-1.845 + \frac{7730.3}{T} - \frac{5019898}{T^2}\right) \quad (3.19)$$

$$\frac{Y_{H_2O}}{Y_{CO_2}} = 1 \quad (3.20)$$

$$\frac{Y_{CH_4}}{Y_{CO_2}} = 5 \times 10^{-16} \times T^{5.06} \quad (3.21)$$

The char concentration was derived initially from solving equations (3.11(3.17), then a mass balance calculation for CHO is carried out using equation (3.18), and the other equations of mass fraction correlations are used to complete the solving procedure and predict the pyrolysis products.

3.3.3 Oxidation model

The oxidation zone supplies the required heat for drying and pyrolysis. Oxidation requires air to complete. If the air is less than the stoichiometric amount required, the gasification (reduction) process will take place to produce syngas. The oxidation process taking place through a set of thermochemical reactions and their reaction rates are illustrated in Table 3.4 and Table 3.5. Pyrolysis products are oxidized in an order that depends on the reaction rate [17] as follows;

- Oxidation of all the hydrogen completes first (R1).
- Oxidation of CO then takes place (R2).
- If oxygen still remains, it will oxidize methane from pyrolysis (R3).
- If more oxygen is available, it will oxidize tar and char according to their reaction rates (R4 and R5).

An energy balance is made for the combustion stage to determine the oxidation temperature based on equation (3.22)

$$\sum X_i \,.\, \left(h_f + \, C_p.\Delta T\right)_{pyr.\ prod} = \sum X_i \,.\, \left(h_f + \, C_p.\Delta T\right)_{comb.\ prod} + Q_{loss} \qquad (3.22)$$

The heat loss Q_{loss} is mentioned in the oxidation zone only, as it is higher in temperature than the other zones, and the overall heat loss is assumed to be 10% of the product of the equivalence ratio and HHV [86] . The same energy balance principle is made for the pyrolysis and reduction zones. Based on the energy balance, assumptions only were made for the inlet temperature (298K), then the overall temperature profile along the gasifier was calculated.

Table 3.4: Oxidation reactions ([30] and [31]).

R	Reaction	A_j	E_j/R
1	$H_2 + 0.5\ O_2 \ \leftrightarrow H_2O$	1.6×10^9	3420
2	$CO + 0.5\ O_2 \ \leftrightarrow CO_2$	1.3×10^8	15106
3	$CH_4 + 1.5\ O_2 \ \leftrightarrow CO + 2H_2O$	1.585×10^9	24157
4	$C_6H_{6.62}O_{0.2} + 4.45\ O_2 \ \leftrightarrow 6CO + 3.1H_2O$	2.07×10^4	41646
5	$C + 0.5\ O_2 \ \leftrightarrow CO$	0.554	10824

Table 3.5: Rate expressions for the oxidation reactions ([30] and [31]).

R	Reaction rate, (mol m^{-3} s^{-1})
1	$r_{H_2} = A_1 T^{1.5}\, exp\left(-\frac{E}{RT}\right).[C_{co_2}][C_{H_2}]^{1.5}$
2	$r_{co} = A_2\, exp\left(-\frac{E}{RT}\right).[C_{co}][C_{o_2}]^{0.25}[C_{H_2O}]^{0.5}$
3	$r_{CH_4} = A_3\, exp\left(-\frac{E}{RT}\right).[C_{o_2}]^{0.8}[C_{CH_4}]^{0.7}$
4	$r_{tar} = A_4\, T.P_A^{0.3}.exp\left(-\frac{E}{RT}\right).[C_{o_2}][C_{tar}]^{0.5}$
5	$r_C = A_5\, exp\left(-\frac{E}{RT}\right).[C_{o_2}]$

3.3.4 Reduction model

The concentration of different gas species and temperature at the end of oxidation zone are used as a feed for the reduction zone to calculate the reduction zone outputs. Initially, the reduction zone length is calculated using equation (3.23), then the rates of formation of different gas species are calculated following Table 3.6 Table 3.7). Afterwards, the

concentration of different gas species of the producer gas is estimated and temperature is then calculated using the energy balance. The change in the mole fractions of any gas species at the reduction zone along the distance *z* (reduction height/length) is determined as [32] ;

$$\frac{dn_x}{dz} = \frac{1}{v}\left(R_x - n_x \frac{dv}{dz}\right) \tag{3.23}$$

Where n_x is the concentration of specific species (x), and R_x is the net rate of formation, and v is the velocity at the end of combustion zone. The reactions considered for the reduction zone are illustrated in Table 3.6, and the corresponding reaction rates r_i are given in Table 3.7. The velocity, temperature, and pressure variations along the reduction zone are obtained through the solutions of the following differential equations [17],

$$\frac{dv}{dz} = \frac{1}{\sum_i n_i C_{pi}}\left[\frac{\sum_i n_i C_{pi} \sum_i R_i}{n} - \frac{\sum_i r_i \Delta H_i}{T} - \frac{dP}{dz}\left(\frac{v}{T} + \frac{v \sum_i n_i C_{pi}}{P}\right) - \sum_i R_i' C_{pi}\right] \tag{3.24}$$

$$\frac{dT}{dz} = \frac{1}{v \sum_i n_i C_{pi}}\left[\sum_i r_i \Delta H_i - v\frac{dP}{dz} - p\frac{dv}{dz} - \sum_i R_i' C_{pi} T\right] \tag{3.25}$$

$$\frac{dP}{dz} = 1183\left(\frac{\rho_{gas}}{\rho_{air}} v^2\right) + 388.19\, v - 79.896 \tag{3.26}$$

Where $\frac{dv}{dz}$, $\frac{dT}{dz}$, and $\frac{dP}{dz}$ are the change of velocity, temperature and pressure, respectively, over the height of the reduction zone (z). n_i is the concentration of specific species (i), and R_i is the net rate of formation, while r_i is the reaction rate.

And to get the heating value and cold gas efficiency, the following equations are used [5]

$$HHV_{product\ gas}\ (MJ/Nm^3) = y_{H_2}.HHV_{H_2} + y_{CO}.HHV_{CO} + y_{CH_4}.HHV_{CH_4} \tag{3.27}$$

$$\eta_{cold\ gas} = \frac{HHV_{product\ gas} * \sum n_i * 22.4}{HHV_{biomass}\ (MJ/kg)} \tag{3.28}$$

where *HHV* is the higher heating value, y is the mol% of different gas species, and $\sum n_i$ (kg / kmol) is the amount of product gas per kg of fuel (biomass) and estimated by,

$$\sum n_i = \frac{N_2(wt\%\ in\ air) * (A/F)}{N_2(wt\%\ in\ product\ gas) * M_{N_2}} \tag{3.29}$$

In the numerical solution procedure, the set of governing equations stated above is first discretized by dividing the reduction zone into equal small zones and solved simultaneously. The initial conditions or the inlet conditions of the reduction zone are taken from the outputs of the combustion zone. The initial pressure is considered to be 1.005 atm and the initial temperature from the oxidation temperature is around 1300 K ([87], and [22]). The equations were solved with a Matlab code *ode45* which is based on an explicit Runge-Kutta 4th order accurate scheme giving the residual tolerances in the order of 10^{-6}. The volume percentage of the product gases, velocity, temperature, and pressure distribution in the reduction zone are obtained and discussed in the result sections.

Table 3.6: Reduction reactions [17] and [35].

R	Reactions		*A*, (1/s)	*E*, (kJ/mol)
1	Boudouard	$C + CO_2 \leftrightarrow 2\,CO$	36.16	77.39
2	Water-gas	$C + H_2O \leftrightarrow CO + H_2$	1.517×10^{4}	121.62
3	Methane formation	$C + 2H_2 \leftrightarrow CH_4$	4.189×10^{-3}	19.21
4	Steam Reforming	$CH_4 + H_2O \leftrightarrow CO + 3H_2$	7.301×10^{-2}	36.15

Table 3.7: Rate expressions for the reduction reactions [17] and [35].

R	Reaction rates, (mol m^{-3} s^{-1})
1	$r_1 = A_1\, exp\left(-\frac{E_1}{RT}\right).\left(y_{CO_2} - \frac{y^2{}_{CO}}{K_{eq,1}}\right)$
2	$r_2 = A_2\, exp\left(-\frac{E_2}{RT}\right).\left(y_{H_2O} - \frac{y_{CO}\,.y_{H_2}}{K_{eq,2}}.\right)$
3	$r_3 = A_3\, exp\left(-\frac{E_3}{RT}\right).\left(y^2{}_{H_2} - \frac{y_{CH_4}}{K_{eq,3}}\right)$
4	$r_4 = A_4\, exp\left(-\frac{E_4}{RT}\right).\left(y_{CH_4}y_{H_2O} - \frac{y_{CO}.y^3{}_{H_2}}{K_{eq,4}}\right)$

3.3.5 Optimum height of the reduction zone

Optimum height of the reduction is the height at which char in this stage is completely consumed as reported by [32]. While, in gasification experiment, this is perhaps unlikely to happen, the current modelling set up will be based on the optimum consumption of char. The assumption will be further tested and validated through a wide collection of experimental data. We shall then use equation (3.23) with the initial concentration of char as

received from the oxidation zone. The final concentration is considered to be zero (i.e. an ideal case). Then we have the rate of destruction of different species, velocity distribution, and velocity at the beginning of the reduction zone. The only unknown in the equation is (z), which will be the optimum height for the reduction zone. Calculations for the different species concentrations will then be built upon this optimum height.

3.3.6 Gasifier design principles

The velocity of pyrolysis gas flow (v_g) through the gasifier is calculated from the following equations [32];

$$v_g = \frac{2RT_p}{P}\sum_{i}^{n} N_{g,i} \tag{3.30}$$

$$N_{gi} = \frac{4\, x_{gi}\, m_b}{\pi\, D^2} \tag{3.31}$$

Where T_p is the pyrolysis temperature K, P is the pressure in Pa, x_{gi} is the concentration of different gas species at the pyrolysis zone, m_b is the biomass mass, and D is the pyrolysis diameter. The biomass feeding rate m_f, is calculated from Rathore [88] based on the capacity/power (W_{th}) of a gasifier

$$m_f = \frac{W_{Th}}{HHV_f} \tag{3.32}$$

Equation (3.33) describes how the throat diameter at the end of combustion zone is calculated.

$$GH = \frac{2.5\, m_f}{A_{th}} \tag{3.33}$$

Where A_{th} is the throat area and D_{th} is the throat diameter. The hearth load (GH) is defined as the amount of produced gas at normal conditions per unit area of throat [88]. The recommended value of GH is within the range of 0.1-1 [89] and [88]. A value of 0.35 is used in our calculations based on what suggested in [89] and [90]. In addition, Ref [91] reported that the throat angle of around 45° gives a higher conversion efficiency. After calculating the throat diameter, the "fire box" (pyrolysis and drying) zone diameter is estimated using [88],

$$D_{pyrolysis} = 3.5\, D_{th} \tag{3.34}$$

The height of drying and pyrolysis is finally calculated from the ratio of the volume of biomass consumed V_{py} to the cross-sectional area of pyrolysis A_{py} as follows

$$H_{pyrolysis} = \frac{V_{py}}{A_{py}} = \frac{m_b}{\rho_{bm} A_{py}} \quad (3.35)$$

Where A_{py} is the pyrolysis area. The air nozzle area is given as a ratio of 0.05-0.09 from the throat area and it is recommended that the air nozzles will be located around the oxidation zone with a number of 4-6 nozzles in a position to prevent any dark zones in combustion [88]. The diameter at which the air injection starts is in the position where the diameter of the oxidation zone is 2-2.5 of the throat diameters [91]. Air injection at this diameter will keep away any dark zones at the oxidation area. Reduction zone diameter is assumed to be the same as the diameter of pyrolysis.

3.4 Results and discussions

A full Matlab Program was built to solve the set of equations stated earlier in which the elemental composition, *ER*, moisture content of biomass, and required thermal power are the input data. Different feedstocks from literature (Table 3.8) are used in the model validation and further sensitivity analysis. The elemental composition of all the feedstocks used in the comparison based on the ultimate analysis is shown in details in Table 3.8.

Table 3.8: Ultimate analysis for different feedstocks

	Feedstock	C %	H %	O %	Exp. results from
1	Rubber wood	50.6	6.5	42	[25]
2	Wood Pellets	50.7	6.9	42.4	[43]
3	Gulmohar	44.43	6.16	41.9	[24]
4	Bamboo	48.39	5.86	39.21	[24]
5	Neem	45.1	6	41.5	[24]
6	Dimaru	44.85	5.98	41.84	[24]
7	Sisham	45.85	5.8	40.25	[24]
8	Saw Dust	52	6.07	41.55	[28]
9	Wood	50	6	44	[13]
10	Olive wood	46.43	5.63	44.91	[92]
11	Rice husk	38.5	5.5	36.6	[93]

3.4.1 Producer gas composition

A wide range of biomass materials (38≤C%≤52, 5.5≤H%≤7, and 36≤O%≤45) as shown in Table 3.8, are tested with the various working conditions to validate the model as presented in Figure 3.3.

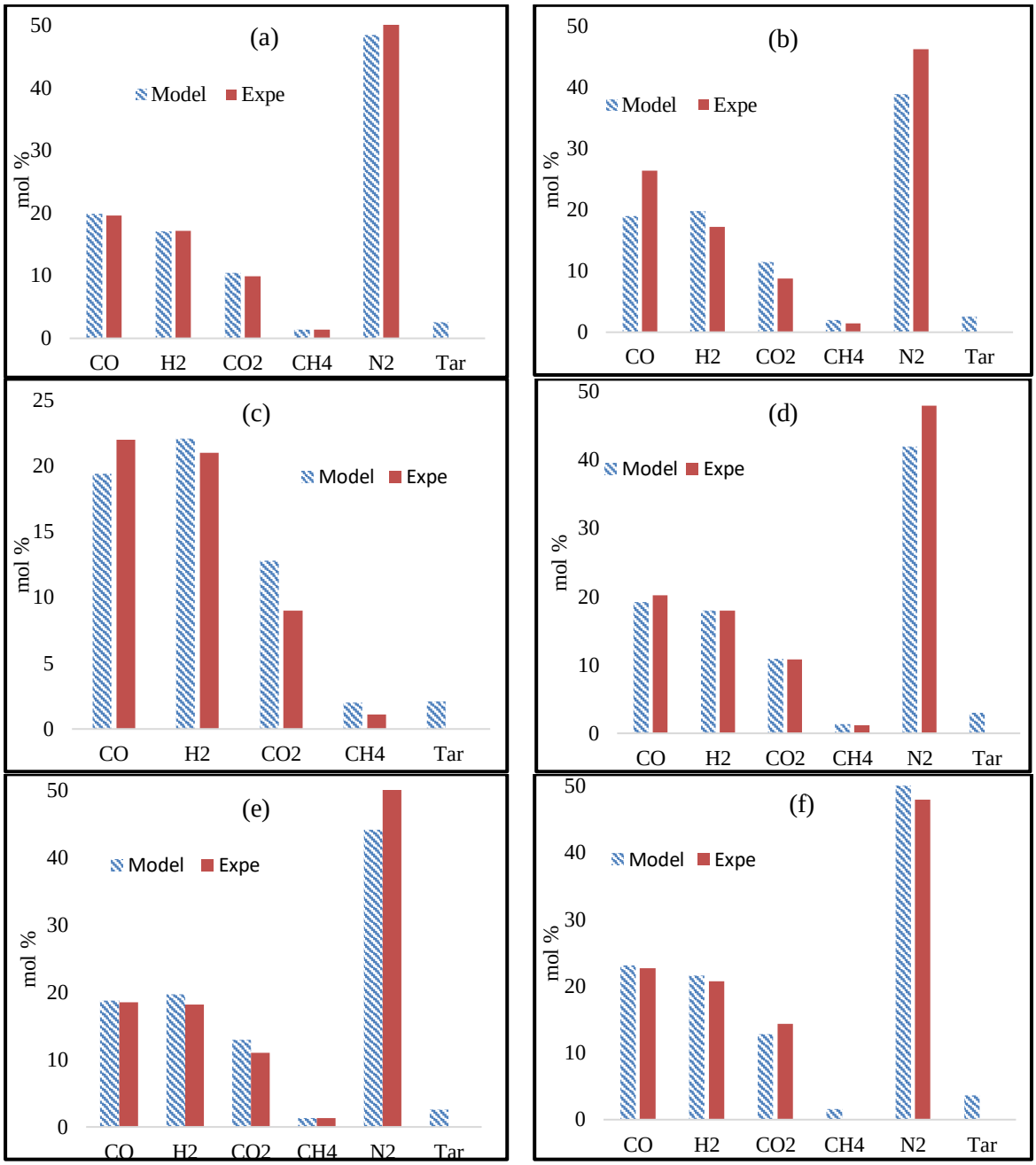

Figure 3.3: Comparison for gas vol.% between the present work and the other experimental work for same (feedstock, Φ, and MC), (a) Rubber wood, (b) Wood pellets, (c) rice husk, (d) Bamboo, (e) Neem, and (f) saw dust.

Table 3.9: Working conditions used in comparison

	Feedstock	MC%	Φ
1	Rubber wood	18.5	0.326
2	Wood Pellets	8	0.259
3	Bamboo	10	0.3

4	Neem	20	0.3
5	Saw Dust	20	0.2796
6	Rice husk	10	0.3

Different boundary conditions of moisture content (MC), and air/fuel ratio used (Φ) in the comparison and validation process are shown in Table 3.9.

The results of the producer gas show a fairly good agreement with the other experimental results, which proves the ability of the kinetic model to operate under different working conditions for a wide range of biomass composition tested, Figure 3.3. The results mainly focused on the wood biomass materials which have widely been used including some other materials with a lower CHO content like rice husk, to further study the model stability over the range of these ultimate analysis data. The results showed a good versatile and model validation over the feedstocks and working range selected. Sensitivity analysis will be carried out to study and optimise the downdraft gasifiers.

Tar formation is also taken into account which was not discussed clearly by previous numerical models. While previous experimental models on downdraft gasifiers rarely mention the tar formation, other experimental data [94] was used to validate the results of the current model. Figure 3.4 shows a comparison between the experimental results [94] and current model for the tar yield in producer gas. The results again show good agreement which also demonstrate the ability of the present model to simulate the tar content in the producer gas.

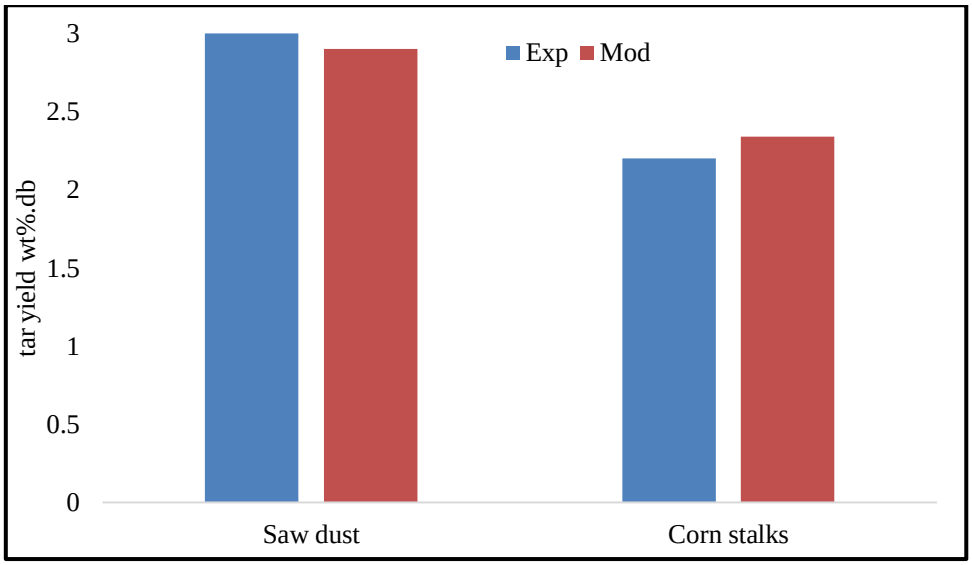

Figure 3.4: Comparisons between the experimental [94] and present work for the tar concentration in producer gas.

3.4.2 Gasifier design principles

Table 3.10 shows a comparison between the results of gasifier dimensions from the present model and theoretical design model of [95]. The results show a fairly good agreement for all the dimensions except for the reduction zone length. However, it was stated in [95] that the reduction length was not based on any known calculations but was based on assumptions. While ref. [32] shows that the reduction zone length varies from 20-50 cm which is in good agreement with the results derived from the present model.

Table 3.10: Comparison between the present work and experimental work for gasifier dimensions

Working parameters	20 kW power, Palm shell, MC 14%, Φ = 0.3	
	Model	Exp. [95]
Fuel feed (kg/hr)	4.0	4.32
H_{pyr} *(cm)*	48.9	40
H_{oxd} *(cm)*	11	--
H_{red} *(cm)*	30.9	15
D_{py} *(cm)*	22.4	23.8
D_{th} *(cm)*	6.4	6.8
$D_{air\ injection}$ *(cm)*	17.9	20

3.4.3 Optimum height of reduction zone

Optimum height of reduction is the height at which char in this stage is completely consumed [32]. Equation (3.23) is solved to get the optimum height for the reduction zone and calculations of the different species concentrations are done and compared based upon this optimum height.

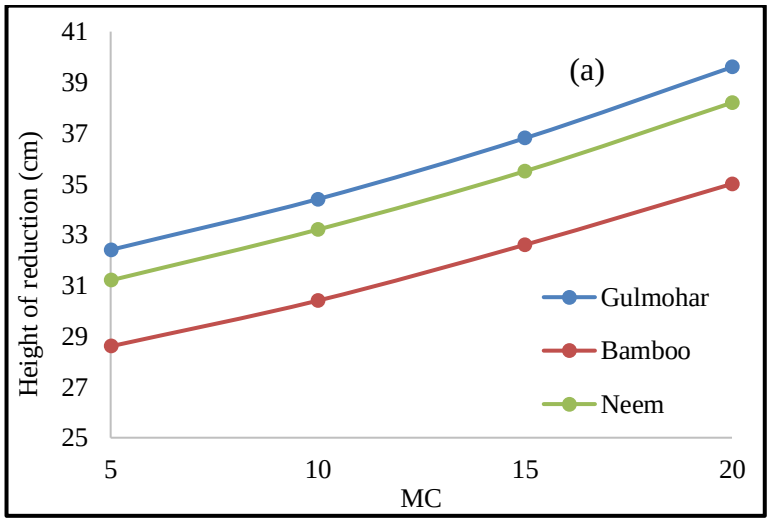

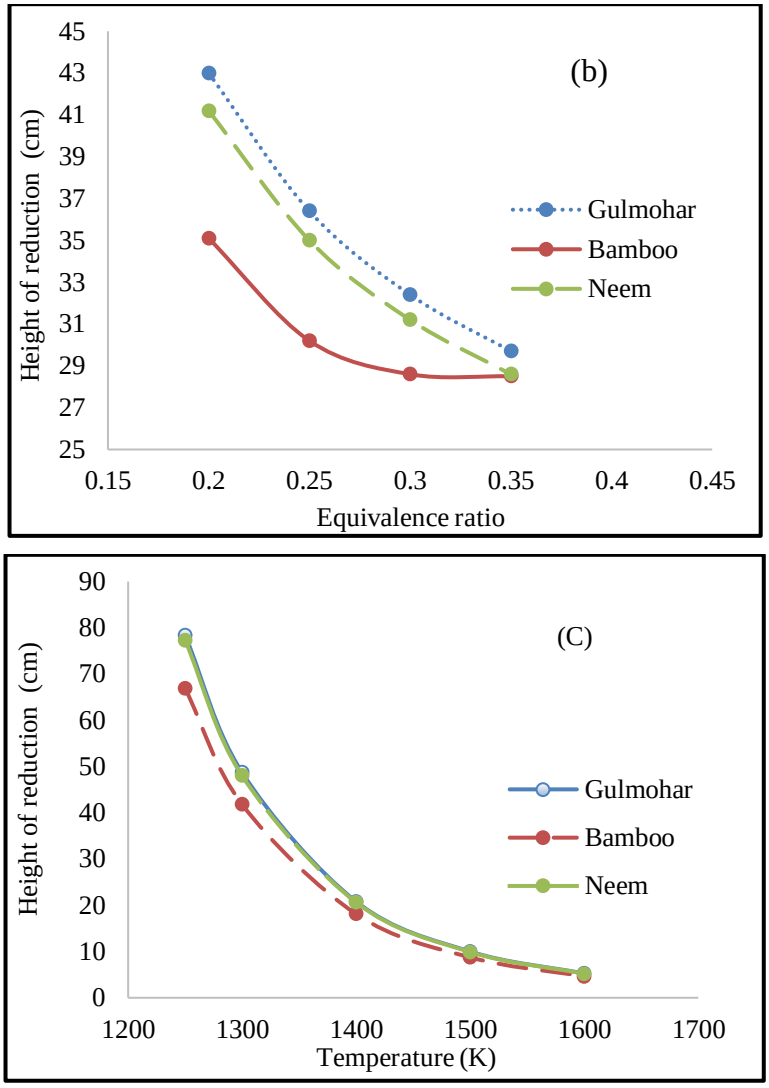

Figure 3.5: Effect of varying moisture content (a), equivalence ratio (b) and temperature (c) on the height of reduction zone.

Several factors such as biomass moisture content, air to fuel (AF) ratio, and temperature at the beginning of reduction affect the height of reduction zone. Figure 3.5(a) shows the relation between the moisture content and reduction zone height for Gulmohar, Bamboo, and Neem [24]. It is clearly seen that as the moisture content increases, the height of the reduction zone increases. This is because higher water content in biomass requires more heat for evaporation and hence decreasing the temperature at the oxidation and reduction zones. The temperature decrease leads to a decrease in the reaction rates and hence decreases the height of reduction zone.

Figure 3.5(b) illustrates the effect of a varying equivalence ratio on the height of reduction zone. It also shows that as the equivalence ratio increases, the height decreases. This is because increasing the equivalence ratio increases the amount of air added and this in turn increases the oxidation temperature and hence the reduction temperature.

The effect of varying the inlet temperature of reduction on the height of reduction zone is presented in Figure 3.5(c). As the temperature increases, the height decreases because higher temperatures give higher reaction rates and formation of the different gas species. This subsequently affects the destruction of carbon in the reduction zone and hence a decrease in the height as shown. The figure presents the temperature at the end of the oxidation/beginning of the reduction zone. Although 1600K is used in the model testing, it is considered to be too high and unlikely to happen at the end of the oxidation zone in a gasifier. However, it was used just as an indication to illustrate that the increasing temperature decreases the length of the reduction zone.

3.4.4 Sensitivity analysis

After validating the current model, it was used to address the optimum working conditions for a gasifier to get higher quality syngas. The term higher quality in the current study will focus on the increasing product gas heating value, yield and lower tar content without discussing any other impurities in syngas. Figure 3.6 presents the results of the effect of changing the moisture content on the output product gas in terms of the higher heating value (HHV) for different feedstocks at a fixed working condition of power (20 kW) and air to fuel ratio (0.35).

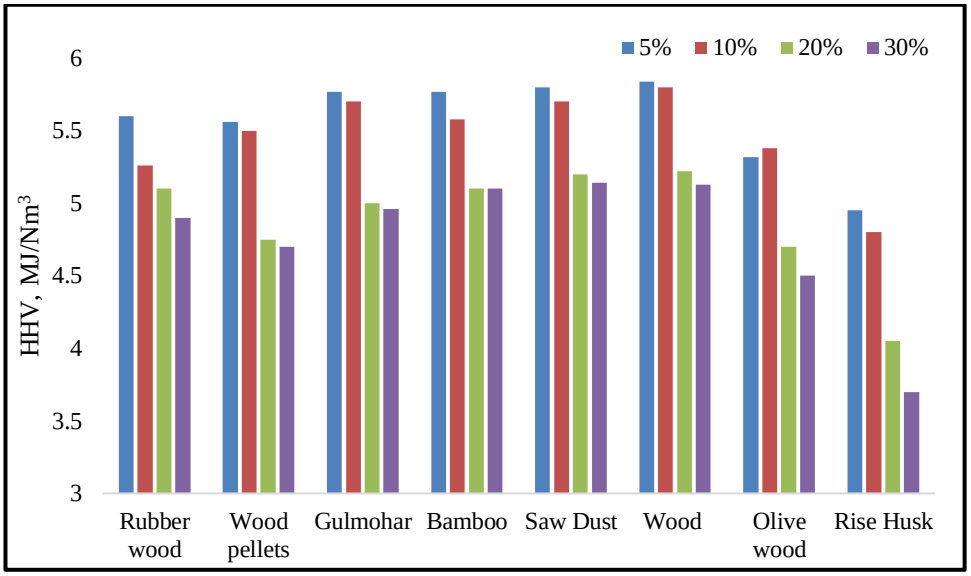

Figure 3.6: Effect of changing moisture content on producer gas heating value.

The results clearly show that a lower amount of water content in biomass leads to a significant increase in the heating value which has a good agreement with [84], [8] and [46] where they showed that the heating value of producer gas decreases with the increase of moisture content. Moreover, lower moisture content leads to a significant increase of CO

and H_2 which then leads to an increase of the heating value. In contrast, higher levels of moisture content require more energy for removal, which is never recovered again. This energy loss affects the produced gas and reduces its heating value. The results also show that a decrease of biomass moisture content from 20% to 5% leads to an increase of the produced gas heating value by 10-22%. Rice husk shows lower values of heating value, while wood is showing higher values. This is because the CHO values of rice husk are low compared to the other materials used in the comparisons, while wood shows higher amounts which leads to higher volatiles and syngas production based on the equilibrium equations used in pyrolysis and hence the other syngas products tends to increase the higher heating values.

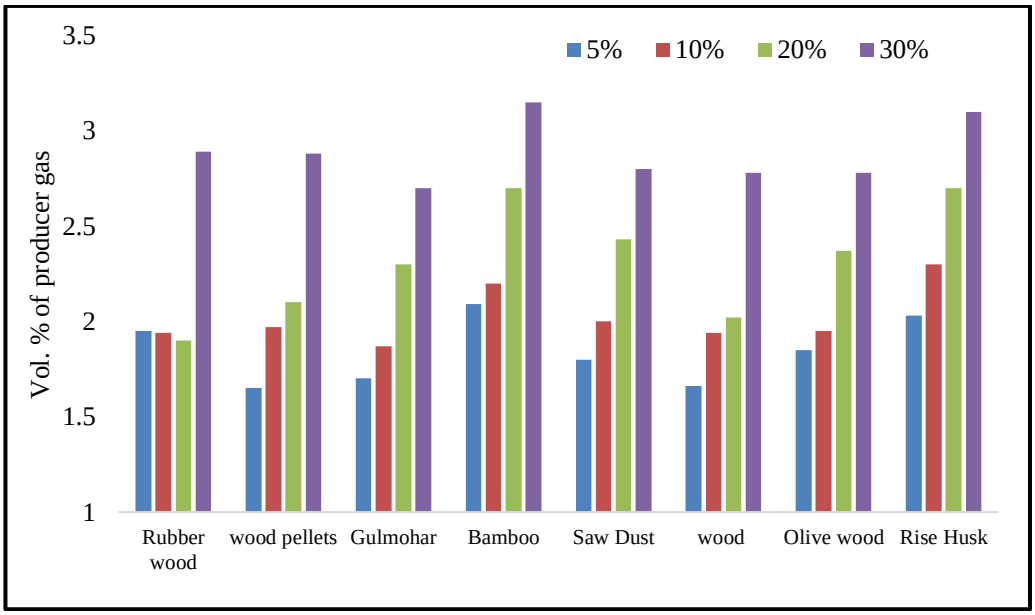

Figure 3.7: Effect of changing moisture content on producer gas tar content.

On the other hand, Figure 3.7 discusses the effect of moisture content on the produced gas quality. The results show that higher moisture content levels lead to an obvious increase of tar content. Tar formation starts from the pyrolysis zone and during combustion, more water vapour tends to reduce the tar cracking reactions, because of lower temperature, and also lower reaction rate compared to the CO and H_2 oxidation based on reactions stated in Table 3.4. Additionally, steam reforming reaction has very low reaction rate and unlikely to affect the process because of the lower values of CH_4 in the reduction zone. Moreover, higher moisture content levels in biomass tend to decrease other volatiles and combustible gases which affect and decrease the oxidation exothermic reactions (R1, R2, and R3 in Table 3.4). The exothermic reactions tend to increase the temperature and hence more tar cracking. Furthermore, higher moisture content levels require more energy for removal and hence decrease the oxidation temperature which obviously decrease the tar cracking reactions leading to higher tar formation levels.

The results also show that a decrease of biomass moisture content from 20% to 5% leads to decrease of tar content of about 18-26%. Based on the current study about the effect of moisture content on the produced gas, lower amounts of moisture lead to higher value gases with a lower amount of tar. Recommended values of moisture content that give a higher yield and quality of syngas should be no more than 10%. Again, rice husk shows the higher tar production rate, because of its low volatiles and CHO content that decrease the combustion reactions and temperature inside the gasifier, thus leading to lower tar cracking. While wood biomass materials with higher CHO and volatile content are leading to increase the temperature inside the gasifier, and hence, lower tar formation.

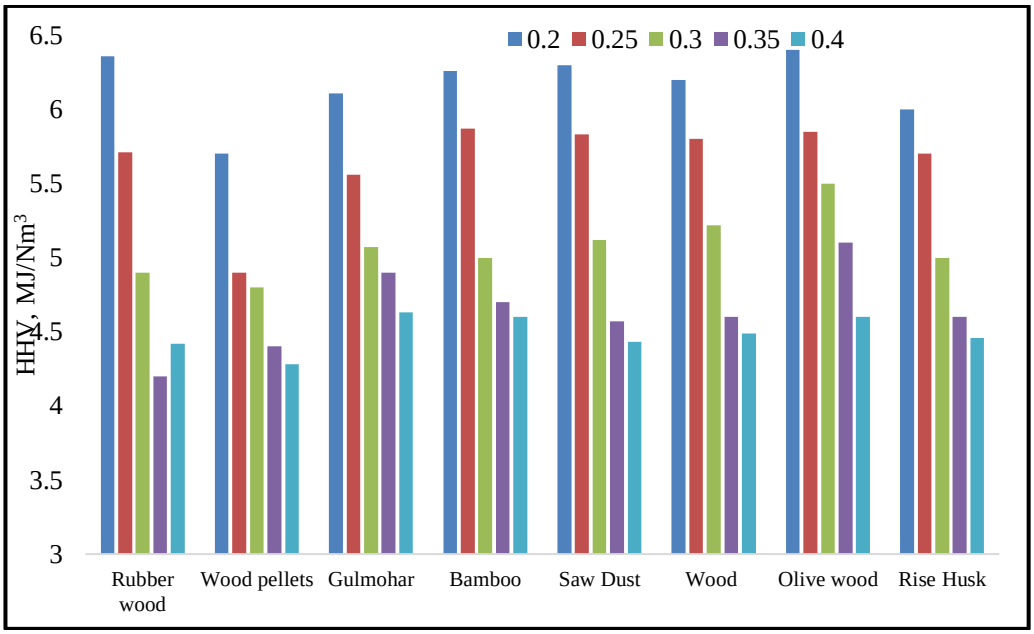

Figure 3.8: Effect of changing equivalence ratio on producer gas heating value.

Figure 3.8 illustrates the effect of changing equivalence ratio on the producer gas heating value for different feedstocks at the fixed working conditions of power (20 kW), and moisture content (10%). The results show a gradual increase of the heating value with a decreasing equivalence ratio. Referring to the oxidation reactions and their equivalent rate, more air supply in the combustion zone encourages the oxidation reactions to occur with more CO_2 and H_2O. This also leads to a decrease in tar content due to the tar cracking reaction that takes place with more oxygen supply in the oxidation zone, as clearly seen in Figure 3.9. Moreover, the results show an increase in the producer gas heating value of 25-30% while decreasing Φ from 0.4 to 0.2. Tar yield also increases from 16% to 50% with the same level of magnitude drop in Φ. Most feedstocks are showing similar values for heating value, however, rise husk is showing the lowest values, while wood materials are presenting higher heating values under different ERs. For the same reasons mentioned earlier regarding CHO lower contents for rise husk and higher values of CHO content in wood materials that

tends to produce more volatiles and syngas content, and hence, higher heating values. Higher volatiles tend to increase the reactions in oxidation zone which leads to higher temperature and more tar cracking leading to reduce the amount of tar produced.

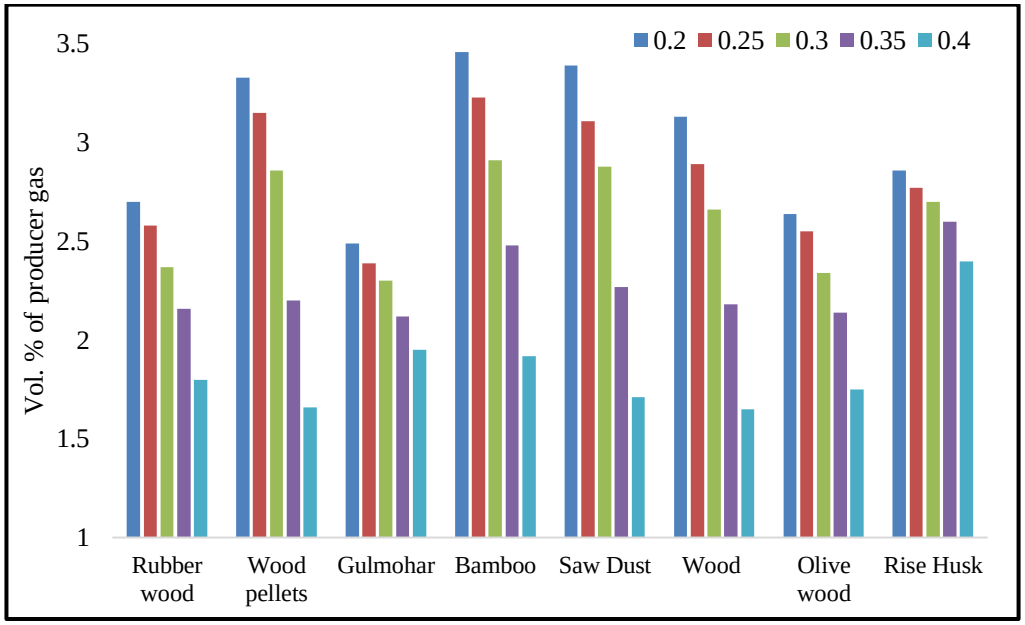

Figure 3.9: Effect of changing equivalence ratio on producer gas tar content.

In conclusion, an equivalence ratio of 0.3-0.35 with lower amounts of moisture content less than 10%, gives a higher yield of syngas composition with reasonable amounts of tar content (~ 2 vol. % of producer gas). In particular, woody biomass materials give a higher yield of syngas with lower tar amounts compared to other feedstocks. Olive wood has the heating value up to 6.4 MJ/Nm^3 at Φ=0.2 and MC of 10%, and tar content was the lowest for wood (1.65%) at Φ=0.4. Higher values of Φ reduces the heating value accordingly.

3.4.5 Distribution of different gas species along the reduction zone

Gas concentrations and variations along the reduction zone are calculated based on equation (3.23). Figure 3.10 shows a linear distribution for all the different gas species in the reduction zone. Rubber wood with MC 20% and Φ 0.32 is used in this case.

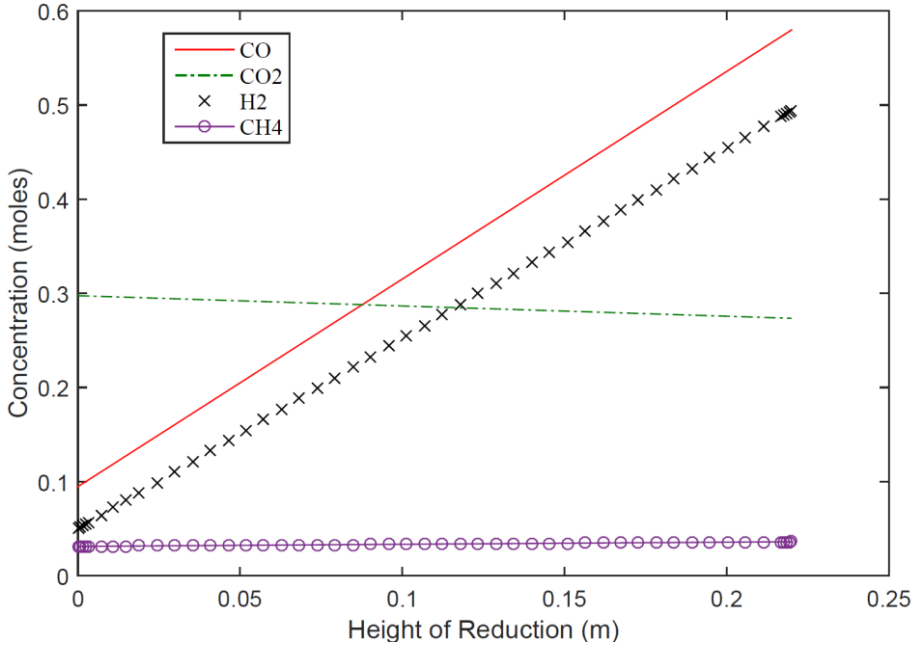

Figure 3.10: Variation of different gas species concentrations for rubber wood along the reduction zone

The reactions in reduction are very fast due to the high temperature in the reduction zone (around 1000K), Figure 3.14. The formation of different gas species depends on the velocity, temperature, and concentration of gas species at the end of combustion zone. Referring to equation (3.23) which describes the formation of gas species along the reduction zone height, and also Table 3.6 and Table 3.7 which describes the reduction reactions and their equivalent rate of formation, higher rates of formation for CO and H_2 are expected. However, variation of CH_4 is very small as its concentration is very small at the beginning of reduction and its formation rate is also small due to lower reaction rates. Formation of CO_2 is expected to decrease along the reduction zone as it is converted into CO based on the reduction reactions. The results also show a good agreement with those reported in [87]. The results showed a linear formation/destruction along the height of reduction zone. However, the way to judge this case cannot be experimentally studied and the way to access this is expected to be through the CFD modelling part. On the other hand, the initial and final concentrations of the zone are in good agreement with previous experimental data as illustrated earlier in the validation part.

3.4.6 Gasifier design and operating conditions

Table 3.11 illustrates the effect of changing the biomass type on the gasifier design. The results show a variation in the fuel feeding rate dependant on the biomass composition from carbon, hydrogen and oxygen.

Table 3.11: Effect of changing biomass on the gasifier design.

Biomass	Rubber wood	Wood Pellets	Gulmohar	Wood	Saw Dust	Rice husk
Fuel feed (kg/hr)	3.65	3.52	4.51	3.8	3.65	6.3
H_{pyr} (cm)	48.8	48.9	49.1	48.7	48.9	48.9
H_{oxd} (cm)	10.9	10.7	12.1	11.2	10.9	14.4
H_{red} (cm)	33.02	29.9	31.3	31.2	29.1	30.2
D_{pyr} (cm)	21.8	21.4	24.2	22.34	21.8	28.7
D_{throat} (cm)	6.23	6.11	6.9	6.4	6.23	8.1
$D_{air\ injection}$ (cm)	17.4	17.1	19.4	17.8	17.4	22.9
Total air area (cm^2)	2.13	2.1	2.6	2.24	2.13	3.6

There are also small variations predicted in the oxidation and reduction height, pyrolysis and throat diameter, and air injection area. The gasifier dimensions are quite similar for most of the biomass tested except for the rice husk. Rice husk has very low carbon and hydrogen contents which affect the heating value of biomass. The decrease in heating value leads to an increase in the throat diameter and hence, increase in the pyrolysis diameter and oxidation height. This is because biomass heating value decrease will require more feeding rate of biomass to achieve the required capacity of a gasifier, equation (3.32), and hence bigger gasifier dimensions.

Varying the thermal power is also found to affect the gasifier dimensions, but it has no effect on the gas composition. The effect of changing thermal power is related to the fuel feeding rate which is again related to the volume occupied by biomass inside the gasifier and thus, it changes the gasifier design. While changing both of the moisture content and equivalence ratio (Φ) analysed in the previous sections have a great effect on the gas composition and its heating value, it is found to have no effect on the gasifier design.

3.4.7 Key design parameters and its effect on the working conditions

Throat diameter and fuel feeding rate are the key parameters in designing a gasifier. All the other dimensions can be generated using these two parameters. Based on the gasifier design, equations (3.30(3.35), the feeding rate is affecting height of pyrolysis, while throat diameter is affecting pyrolysis and reduction diameters, and oxidation zone height. As a result, studying the effect of varying thermal power from 1kW to 1MW for different biomass types is investigated as shown in Figure 3.11 and Figure 3.12.

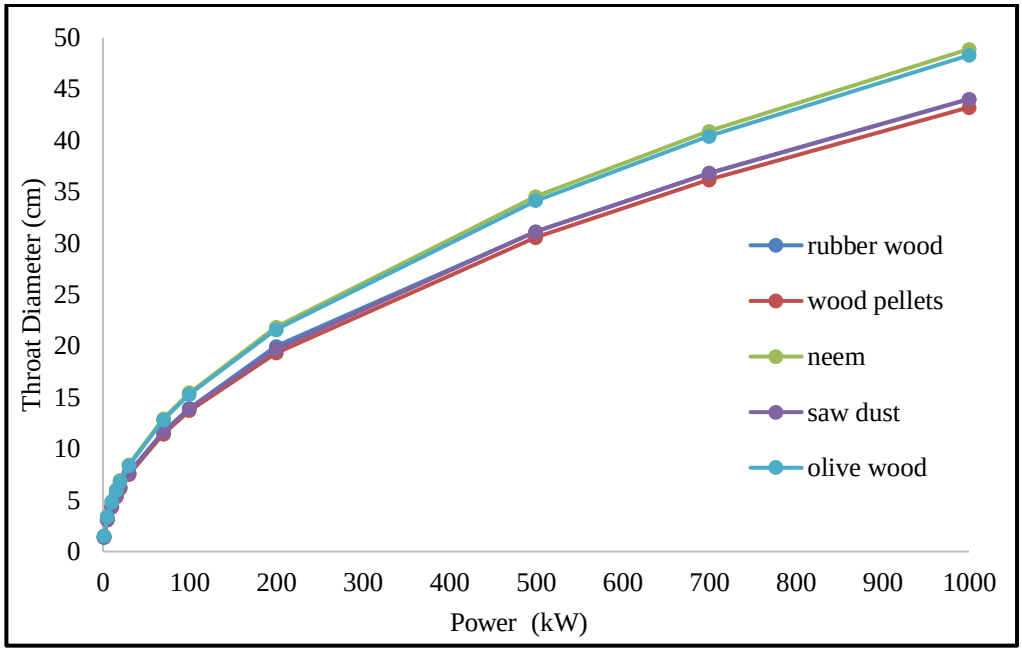

Figure 3.11: Effect of changing power on gasifier throat diameter.

Figure 3.11 shows the effect of changing the required thermal power on the throat diameter design. The results show higher throat area for higher power. This is because higher power requires more biomass feeding and hence, bigger volume for the pyrolysis and combustion zones.

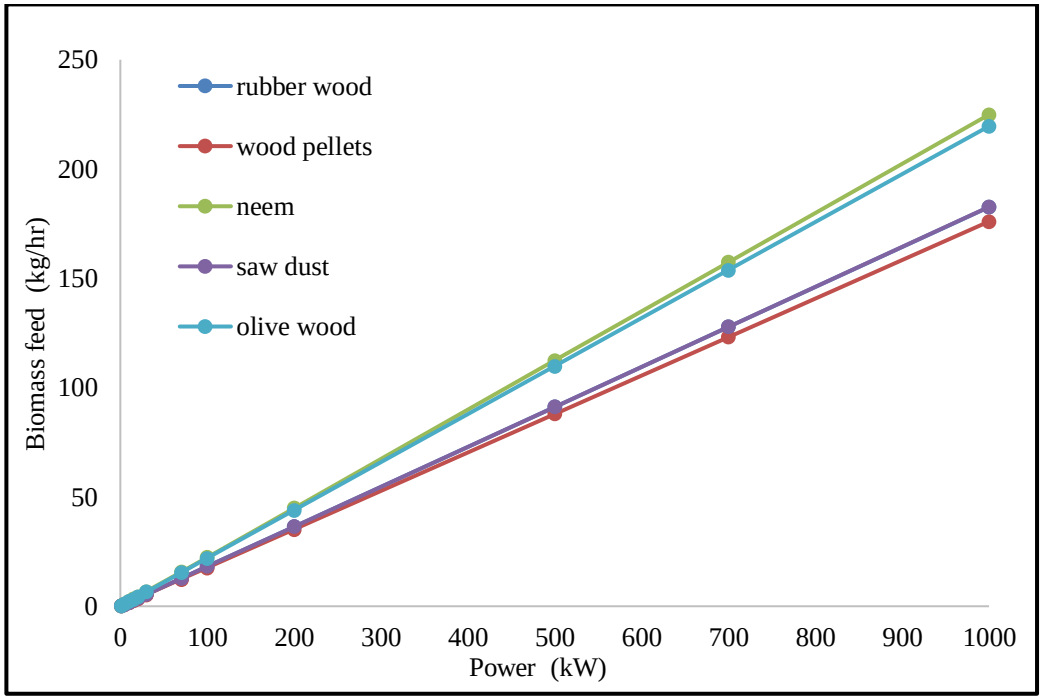

Figure 3.12: Effect of changing power on biomass feeding rate.

Figure 3.12 shows the effect of changing the required thermal power on the biomass feeding rate. The results show a linear variation for the feeding rate as it is calculated from

equation (3.32) which has a linear relation among the thermal power, feeding rate, and biomass heating value.

3.4.8 Different gas species distribution along gasifier

Gas species distribution along the gasifier height is of great importance to understand the gasification process within downdraft gasifier. The gases formation and destruction will help to optimise the whole process leading to the production of higher quality syngas with high heating values and lower tar amount. In the following sections, the effect of moisture content and equivalence ratio on the gas species distribution will be discussed in details.

3.4.8.1 Moisture content effect on different gas species

The effect of changing moisture content on different gas species along the gasifier is addressed in this section. Results are derived from the kinetic model where the output from each zone is feeding to the next one. At every zone, temperature is estimated first based on the gas production of every zone using energy balance, then a recalculation is carried out again to estimate the exact gas composition.

The results of gas, char and temperature distribution along the gasifier height is widely illustrated in Figure 3.13Figure 3.15), and Figure 5.12-Figure 5.18). The calculation process is based on the ultimate gas production and the maximum temperature at every zone. Starting from the room temperature (398 K) and the initial concentration of different gas species (zero), the gas concentrations at the middle of every zone are estimated and plotted as a point. The intervals between every point is too complex to be experimentally measured. However, for the model simplicity, a curve fitting is used for the main four points in the current work for better shaping the gases and temperature distributions along the gasifier height. The output gas concentration of the gasifier has been widely validated (Figure 3.3), and hence, it is more likely to give accurate predictions at different points along the gasifier height. Because the model is integrated, each point depends on the previous point calculations stating from pyrolysis to oxidation and reduction. The same strategy for the similar plots will be implemented throughout the whole thesis.

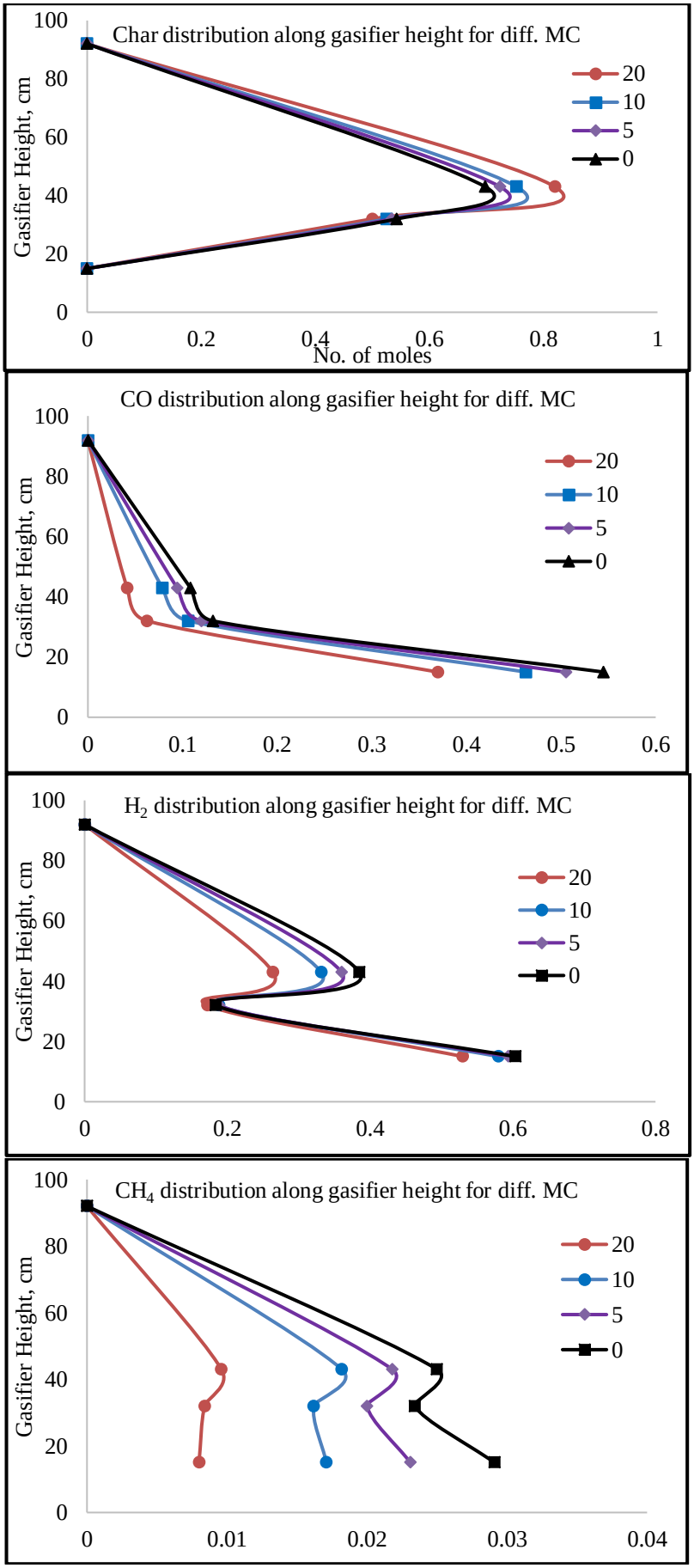

Figure 3.13: Different gas species variation along gasifier height with moisture content for wood pellets.

The results of different gas species and tar compounds were tested for different moisture content levels. The equivalence ratio has a negligible effect on the pyrolysis temperature as the main factor at pyrolysis is the moisture content for specific feedstock and, therefore, the results of different gas species are the same as long as the temperature is constant. The results are discussed based on one mole of biomass gasified.

$$dry\ biomass(C\ H_a\ O_b)\ + w\ H_2O_{liq}\ \rightarrow\ x_1\ C\ +\ x_2\ CO\ +\ x_3\ CO_2\ +\ x_4\ CH_4\ + x_5\ H_2\ +\ x_6\ H_2O\ +\ x_7\ tar \quad (3.36)$$

Figure 3.13 shows different gas species distribution along the gasifier height with different MC levels, for wood pellets at a fixed ER of 0.27. Lower moisture content levels are favourable for the production of useful gas species (CO, H_2, and CH_4) and that is because higher moisture content levels tend to decrease other products. The biomass, after the drying process, decomposes into volatiles, tar, and char. Furthermore, based on the global reaction of pyrolysis (equation (3.36)), increasing moisture content tends to increase vapour in volatiles which affects other gases and consequently lowers them as shown in Figure 3.13. On the other hand, char was found to increase with moisture content, whereas the hydrogen and oxygen in biomass tend to be converted to volatiles including water vapour. The char included in biomass is converted to CO, CO_2, and a very small amount of tar. As long as the volatiles decrease, then obviously, char amount will increase.

Increasing moisture content tends to increase water vapour in volatiles which affect and decrease other gases and consequently reduces them as shown in Figure 3.13. Combustion reactions (Table 3.4) show higher rates for reactions 1, 2, and 3. Those reactions tend to rapidly increase all the H_2O and CO_2 levels during oxidation and this has a great effect on reducing H_2, and CH_4 levels. On the other hand, char is consumed in combustion forming CO, and CO_2 which lead to a reduction in char amount in the combustion zone. As shown in Figure 3.14, combustion temperature decreases with moisture content because higher moisture content levels affect gasifier temperature and tend to reduce it. Nitrogen concentration remains the same because the ER is constant, and the model does not consider any NO_x formation or nitrogen reactions and conversion to other compounds.

The results also show a gradual increase for all the gas products coming out of the reduction zone. Based on the reduction reactions, a higher reaction rate is found for reactions 1 and 2. Higher moisture content tends to increase CO, and H_2 based on water gas reaction. However, the total amount of vapour is increasing and, therefore, reduces the final concentration of those gases. CH_4 was found to increase slightly, depending on the char and

vapour concentration. Because the heating value depends on the amount of CO, H_2, and CH_4, it, therefore, reduces with the moisture content increase. Moisture content levels are preferred to be low in order to achieve a higher heating value.

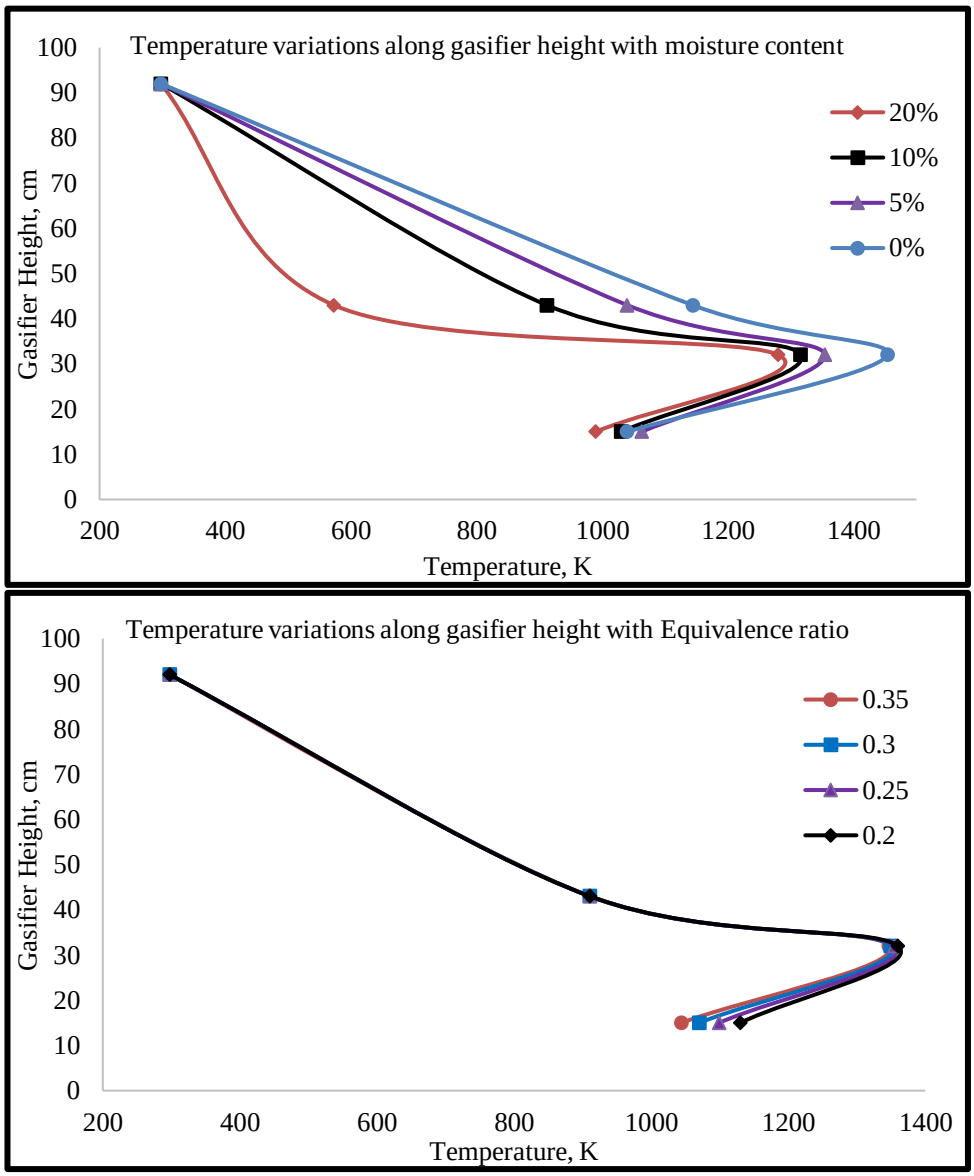

Figure 3.14: Temperature variation along gasifier height levels for wood pellets.

Temperature along the gasifier is calculated by the energy balance at the end of every zone. It is found that the temperature drops along the gasifier as the moisture content levels in biomass increase (Figure 3.14). This is because higher water content in the feedstock requires more energy to remove and convert it to vapour and, therefore, the temperature decreases. The highest temperature is found to be 1410K, at MC=0% for wood pellets in the combustion zone, at ER of 0.27, while the lower temperature is at the pyrolysis zone, 732K, at 20% MC for the same feedstock and ER. Temperature variations along the gasifier height with varying ER are also studied for wood pellets at fixed MC=10%. Higher ER means more

air addition, which increases the oxidation reactions (exothermic), thus resulting in more heat release and subsequently increasing the temperature inside the gasifier.

3.4.8.2 Equivalence ratio effect on different gas species

Figure 3.15 illustrates the variation in different gas species along the gasifier height with varying equivalence ratio. The calculations are carried out at a fixed MC of 10% for wood pellets gasification.

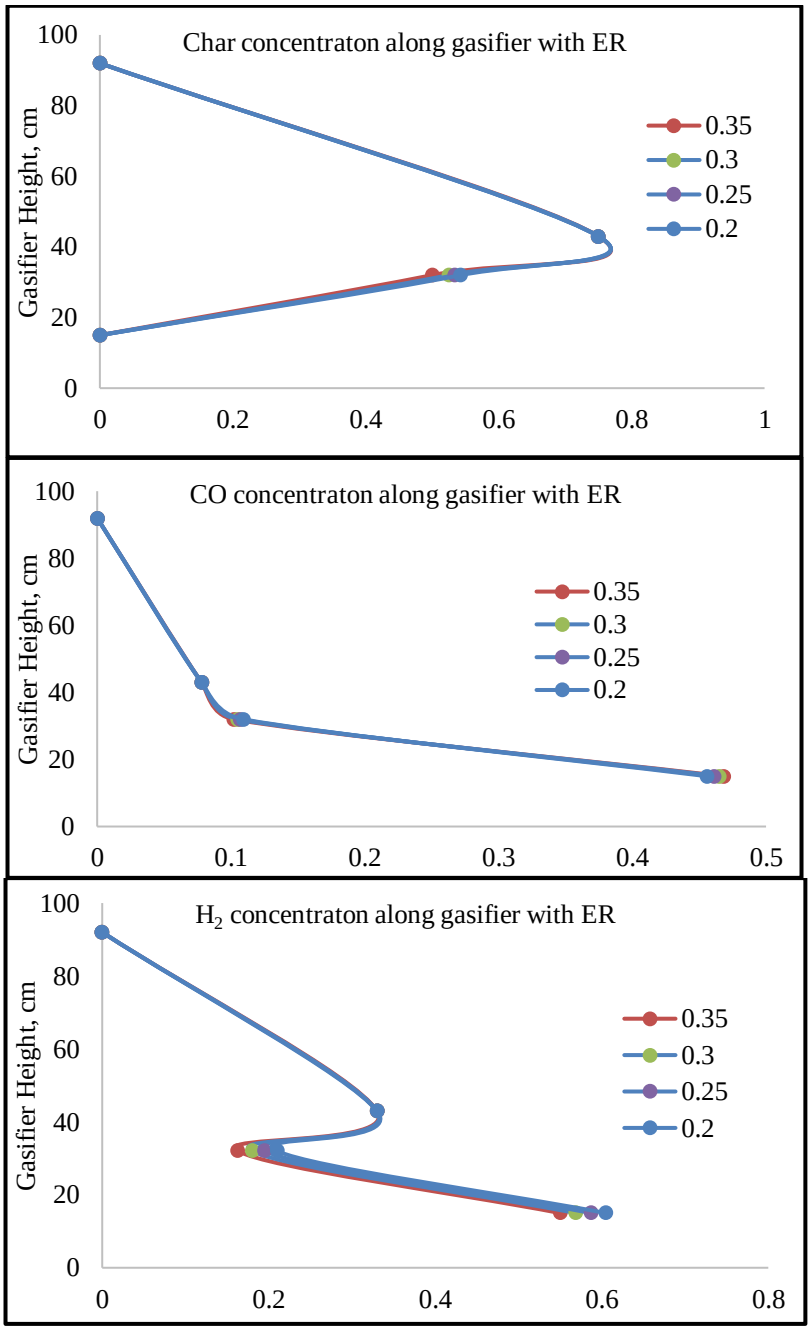

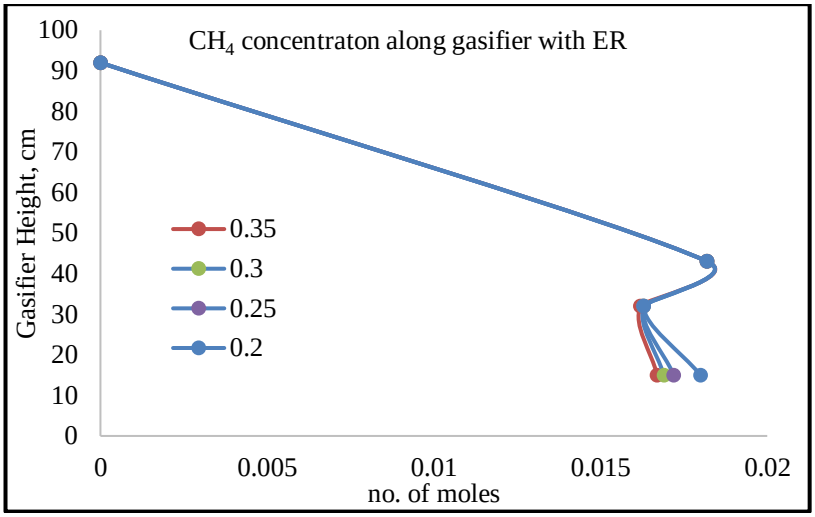

Figure 3.15: Equivalence ratio effect on different gas species along gasifier height for wood pellets at MC=10%.

There is no variation in the pyrolysis zone as the MC is fixed and, therefore, pyrolysis temperature is constant as discussed earlier. That is because, as MC is fixed, then pyrolysis temperature will be constant which means the same gas production from pyrolysis as the main factor affecting the pyrolysis volatiles is temperature.

Char concentrations starts to increase then tends to be constant in the pyrolysis zone, then decrease at combustion with the oxidation of char and convert to CO, and CO_2. At reduction zone, char is further consumed, and based on the model assumptions, char is fully consumed at reduction zone.

While CO, H_2, and CH_4 concentrations follow the same trend in pyrolysis as char (fixed amount), they in most cases tend to be fully oxidised and converted to CO_2, and H_2O depending on the equivalence ratio. Higher equivalence ratios tend to consume all H_2, and CH_4 in the oxidation zone. Based on the reduction reactions, the concentration of CO, H_2, and CH_4 tends to increase again at the reduction zone. Lower equivalence ratios produce more CO, H_2, and CH_4 concentrations in producer gas. This is because lower oxidation reactions, and hence lower consumption of CO, H_2, and CH_4 in combustion, which increase their concentrations during reduction zone.

Lower equivalence ratio tends to increase the rate of gasification reactions and reduces the rate of combustion reactions. Combustion reactions depend on the amount of air supplied which increases the formation of CO_2, and H_2O (Table 3.4, and Table 3.5). As seen from the combustion reactions in (Table 3.4, and Table 3.5) higher reaction rates are found in R1, R2, and R3, ([30] and [31]), which tends to produce more CO_2, and H_2O, depending on O_2 amount in the oxidation zone. This also means lower combustible gases like CO, H_2, and CH_4. The amount of oxygen is mainly identified by the equivalence ratio, which means lower

Φ is favourable for the production of lower amounts of CO_2, and H_2O, which increase syngas production through more CO, H_2, and CH_4. On the other hand, more air supply reduces the useful gases (CO, H_2, and CH_4) as a result of their oxidation and conversion to steam and CO_2, while lower equivalence ratios tend to reduce the oxidation reaction rates. That might be a reason for increasing CO, H_2, and CH_4 with a reduction in CO_2 amounts. Lower equivalence ratios are favourable for the production of higher value producer gas. Higher values of char and syngas are found at lower ERs and the corresponding heating value is higher as well (Figure 3.8). Higher ER tends to increase the oxidation temperatures and oxidation reactions that consume char and lead to the destruction of useful gases and increase water vapour and CO_2.

3.5 Conclusions

The current work presents a unique four-zone kinetic model for a downdraft gasifier in which the gasification products are determined using a novel approach that includes an optimum length of the reduction zone. According to model validation, it gives accurate results for the producer gas composition, tar content, and gives also the predictions for dimensions of a downdraft gasifier. Previous models never combined altogether in one work. The design theory in this model was built based on the optimum height of reduction zone, which was never discussed before in any published data. Finally, the results from this model was used to test a wide range of biomass materials to conclude the optimum working conditions and best feedstocks that give higher yields of syngas with a lower tar content. Key design parameters for a downdraft gasifier are mentioned and the effects on working conditions are discussed using the current model.

Additionally, sensitivity analysis was carried out through studying the effect of varying moisture content and air equivalence ratio on producer gas composition, tar content, and higher heating value. Furthermore, different gas species distribution along gasifier was discussed with the effect of changing working parameters.

The results show that a decrease of biomass moisture content from 20% to 5% leads to an increase of the produced gas heating value of 10-22%, and a decrease of tar content of about 18-26%. Moreover, the results show an increase in producer gas heating value of 25-30% while decreasing Φ from 0.4 to 0.2. Tar yield also increases from 16% to 50% with the same level of magnitude drop in Φ.

In conclusion, an equivalence ratio of 0.3-0.35 with lower amounts of moisture content less than 10%, gives a higher yield of syngas composition with reasonable amounts of tar content. In particular, woody biomass materials give a higher yield of syngas while olive

wood has a heating value up to 6.4 MJ/Nm^3 at Φ=0.2 and MC of 10%. Higher values of Φ gives a lower heating value for wood pellets and saw dust. The tar content was also lower for wood (1.65%) at Φ=0.4.

It is also found that the throat diameter and fuel feeding rate are the key parameters in designing a gasifier. All the other dimensions can be generated using these two parameters.

Chapter 4: Kinetic Model's Limitations, Improvement, and Gasifier design optimisation based on Scottish Agricultural Waste

4.1 Introduction

The kinetic model presented in the previous chapter has been verified and tested over a wide range of biomass materials and found to be in good agreement with the various experimental data. Furthermore, it has been used to optimise the gasification process through a detailed sensitivity analysis. However, this kinetic model becomes very sensitive to the unconventional feedstocks (outside the range specified in Chapter 3), sourced from Scottish Farms, and in some cases, it fails to simulate the gasification processes, primarily due to the variation in the chemical contents of these feedstocks. Thus, the focus of the work in this chapter is to improve the kinetic model, with an aim to investigate the gasification potential of Scottish agricultural waste. For that, the kinetic model is used an improved set of boundary conditions with an adaptation of the temperature variations inside the gasifier, to make the model applicable for a wide range of materials including biomass, waste, and agricultural residues.

Based on the literature review, there is no previous model presented the gasification of agricultural feedstocks in downdraft gasifiers. The model will further be used to make a sensitivity analysis for agricultural feedstocks addressing the optimum working conditions that lead to higher syngas production with better quality and lower amounts of tar. Furthermore, the model will be used to address the design limitations and challenges of using multiple feedstocks and attempt to produce the optimum design that suits the wide range of materials and working conditions.

4.2 Limitations of the previous kinetic model

The model was used initially to attempt to test some of the agricultural feedstocks with their ultimate analysis data, as shown in Table 4.1. Most of these feedstocks are out of the working range of this model based on the materials tested for the kinetic model in Chapter 3. The model is an integrated model, where each zone of gasifier (drying, pyrolysis, oxidation, and reduction) is integrated, and the result of each zone is used as an input for the next zone. A failure in any zone calculations will result in a failure in the syngas prediction and other model results.

Table 4.1: Ultimate analysis of agricultural feedstocks.

Biomass type	C%	H%	O%	MC%

1	Wood chips	49.7	6	43.6	11.9
2	Wood Pellets	52	6.9	41	18.4
3	Wheat straw	48.1	5.8	42.6	10
4	Barley screenings	45	6.2	44.8	11
5	Spent barley	49.8	6.4	35.6	30
6	Barley dust	46.1	5.7	40.6	11.3
7	Spent hops	50.6	6	30.3	67.4
8	Livestock bedding	44.3	5.2	37.4	10.5

Eight different feedstocks have been collected from several Scottish agricultural farms, as seen in Figure 4.1. Agricultural feedstocks used in the model and their corresponding ultimate and proximate analysis are shown in Figure 4.2. Feedstocks analyses were carried out at SGS United Kingdom Limited [96]. As noted from the analysis data, the values of C, H and O are mostly lower than those of typical biomass and wood materials, which might cause instability of the model, because all the model calculations are based on the ultimate analysis data.

Samples have been collected from Cragnathrow, Kinkell, and Foulis farms in Scotland, based on a project led by the University of Glasgow to utilise and generate energy from farm waste.

Figure 4.1: Different feedstocks used in the current study.

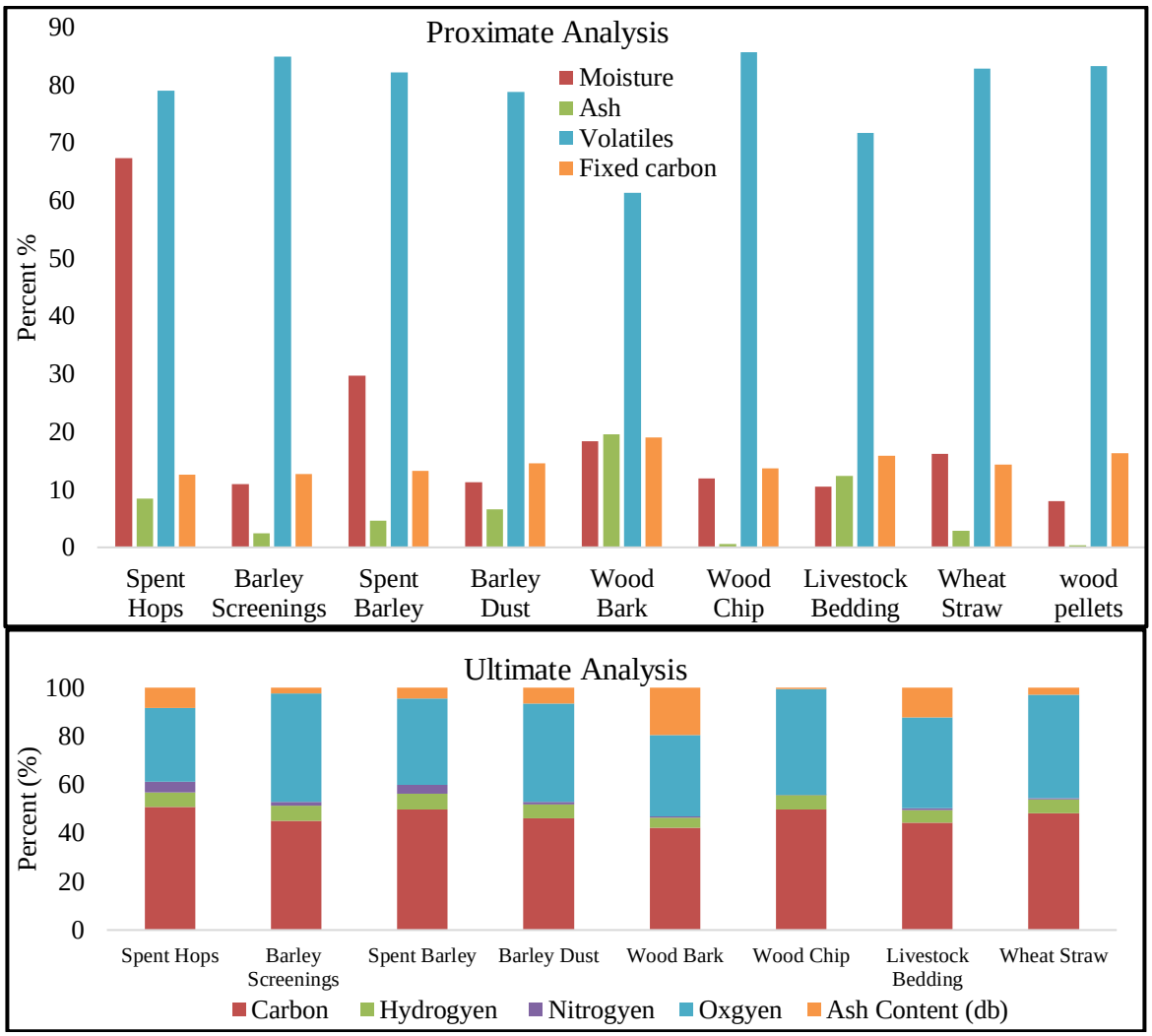

Figure 4.2: Proximate and ultimate analysis for feedstocks used in current study.

All the feedstocks appear to possess the normal values of C, H, O content and moisture content levels suitable for gasification process. Spent hops and spent barley have higher moisture content levels and need first to be dried to less than 20% moisture content to make the gasification process economically viable.

Most of the feedstocks have high volatile content, which make it suitable for gasification because it will release more volatiles and hence more syngas production. However, ash content is high in some feedstocks (livestock beddings, spent hops, and barley dust) which might affect the gasification process because of lower volatiles and, consequently, decrease the syngas production as it is mainly the inorganic content of any biomass [5]. Furthermore, it needs a greater amount of cleaning after every experiment. Heating value of all the feedstocks seems normal compared to that of the woody biomass materials. The ultimate analysis data (C, H, and O) appear to be in the normal range to be considered in the kinetic model; however, the oxygen values are all outside of the working range, and the hydrogen

values are low compared to the wood materials. Based on this, the model first needs to be tested over the selected materials to study its stability.

4.2.1 Modifications on the kinetic model

As discussed in the previous section, the temperature of pyrolysis has the greatest impact first on the pyrolysis products and subsequently on all of the other zones' calculations. The temperature was found to exceed the normal values of pyrolysis temperature in some cases of varying MC and ER. Hence, a further modification was made for a temperature limitation to overcome this critical problem. The equations including temperature calculations and corresponding equations (3.19(3.21) were revised and modified. The calculations are converted to be all based on equilibrium modelling for the pyrolysis zone by combining equations (3.18(3.21), and further energy balance to get pyrolysis temperature is carried out. Some limitations and control equations are added to control the temperature variations along the gasifier. Maximum pyrolysis temperature is limited to 1000K, based on [40], where it was stated that optimum pyrolysis temperature is around 1066K. Also [3] stated that for slow pyrolysis, moderate temperature is about 873K, while maximum temperature is around 1073K. In the possibility that the temperature calculation exceeds this range, the program was iterated to recalculate the gas composition using the modified temperature in the normal pyrolysis temperature range. After modifying the energy equations and the mass fraction empirical correlations, the model is verified against experimental data and found a good agreement. The new advanced model was tested and compared with the experimental and other results to validate its prediction accuracy.

4.3 Results and discussions

The kinetic model as described earlier in Chapter 3 has limitations related to the feedstocks used. While the received agricultural feedstocks are all out of the working range of the kinetic model described in Chapter 3, an initial attempt to run the code with these feedstocks proved the model failure to study the gasification process using these feedstocks. This is because of the lower oxygen and hydrogen content of the selected feedstocks, which lead to failure in calculating the pyrolysis temperature, and hence followed by an incorrect estimate for all the consequential calculations. This might be because of the lower heating values compared to typical biomass materials and hence, overprediction of temperature based on energy balance (equation (3.22).

4.3.1 Model validation

The model is first validated with the well-known experimental data [38] and [24]. The comparison was made at the same working conditions such as moisture content (18.5%) and equivalence ratio of (0.326) for (a), rubber wood; and for (b), moisture content (20%) and equivalence ratio of (0.3) as shown in Figure 4.3 (a, and b).

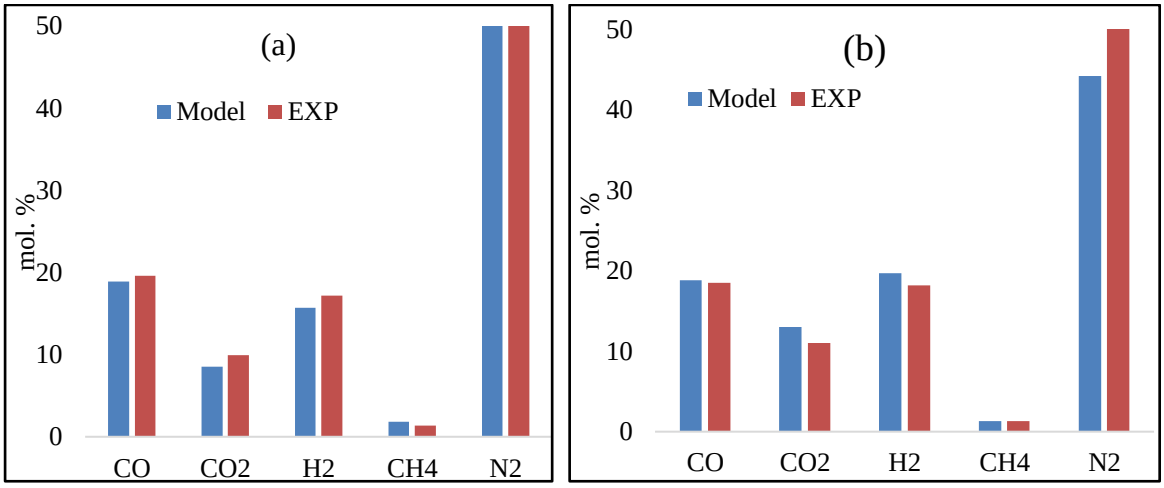

Figure 4.3. Gas volumetric composition comparison for new advanced model, and experimental results for a: rubber wood [38] and b: Neem [24].

The results display a good agreement for both the feedstocks. Small variations are noticed as the kinetic model predicts tar formation, which was not mentioned in the experimental works used for the comparison; however, the tar formation predictions were validated in [16]. The validation was done using the biomass materials from the previous experimental results, as there was no previous data to use for agricultural feedstocks. However, in the previous validation for the initial model, some agricultural feedstocks were also used e.g. rice husk in Figure 3.3. On the other hand, based on the ultimate and proximate analysis data presented in Figure 4.2, the CHO composition of agricultural feedstocks is quite similar to biomass materials. As a result, similar trend of syngas production and temperature variations are expected to take place by gasifying agricultural residues as it will be illustrated in the coming sections.

4.3.2 Results variations and optimum working conditions

After validating the new model, a wide range of materials were tested under different working conditions in order to test the ability of kinetic model to predict gasifier work.

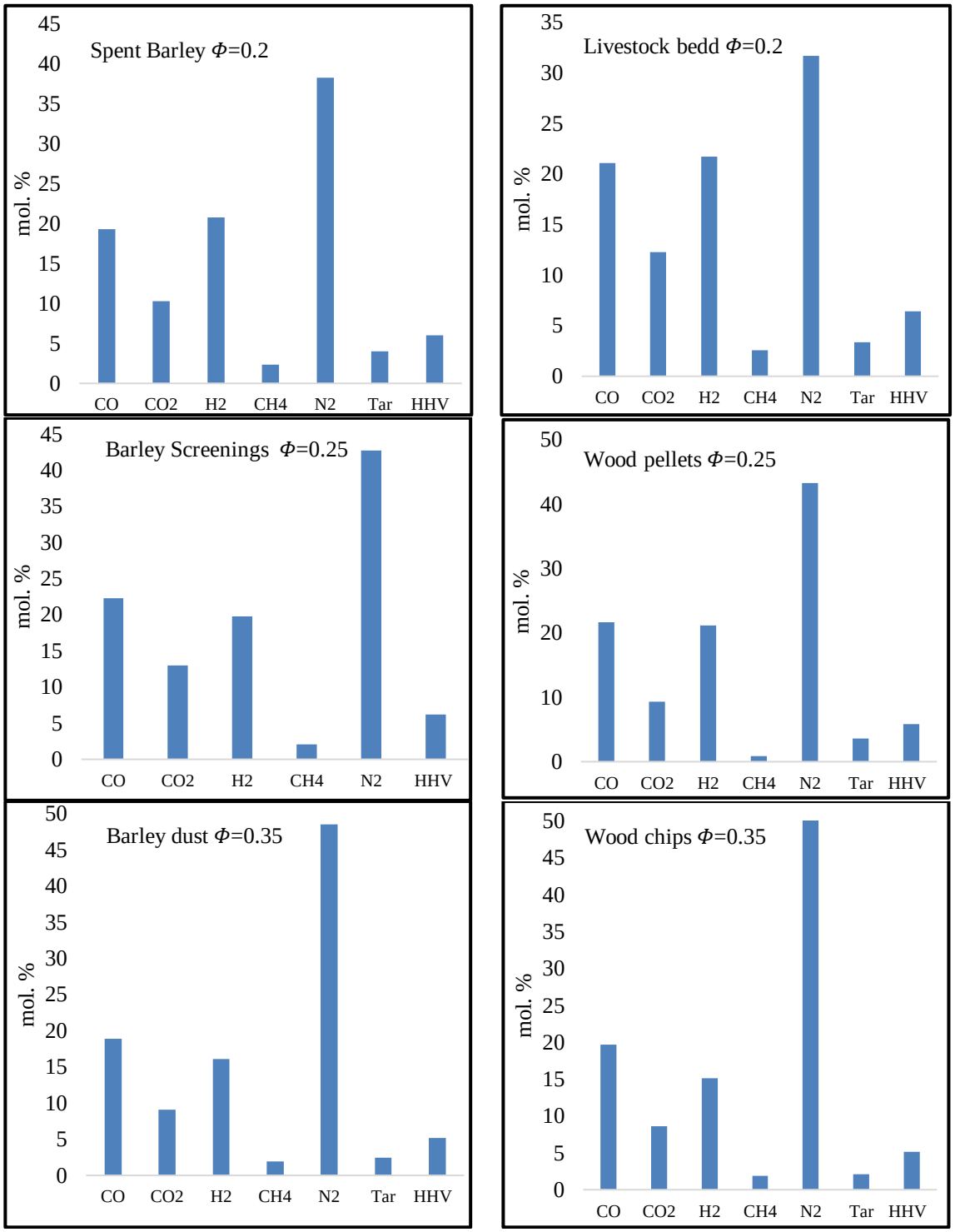

Figure 4.4. Results for volumetric gas composition for different feedstocks at different working conditions of moisture and equivalence ratio.

The set of results shown in Figure 4.4 proved the stability of the advanced kinetic model to simulate gasifier work for a wide range of biomass and waste materials at different working conditions. The model shows the stable results while varying the moisture content, equivalence ratio, or the ultimate analysis of different feedstocks. Moisture content was chosen as received for every feedstock (Table 4.1), while the equivalence ratio varied from (0.2-0.35) to cover a wide range of air/fuel ratios. The working conditions were also varied

to study the model stability and syngas production rate. However, further comparisons will be made through the sensitivity analysis to report the most suitable feedstock for gasification, as well as the optimum working parameters leading to the production of higher quality syngas. In the results, livestock beddings are found to have the highest syngas yield and highest heating value, because of its low moisture content level (as received), and the lower equivalence ratio used. On the other hand, wood chips are found to have the lowest heating value, due to the use of a higher equivalence ratio, however, it will be further studied through sensitivity analysis at same working conditions for better comparison. As discussed, the results in this section show the model stability, which will be further expanded to optimise the gasification process through studying the effect of varying the working conditions on the quality of the whole gasification process.

4.3.3 Feedstocks' validity for gasification

The model is further used to test all of the feedstocks and judge its ability to produce acceptable quality of syngas with reasonable tar amounts (< 2% of producer gas vol.). Equivalence ratio and moisture content will be fixed and syngas production, heating value and tar amount will be tracked for every feedstock. The same boundary conditions are used to compare between the different feedstocks' outputs.

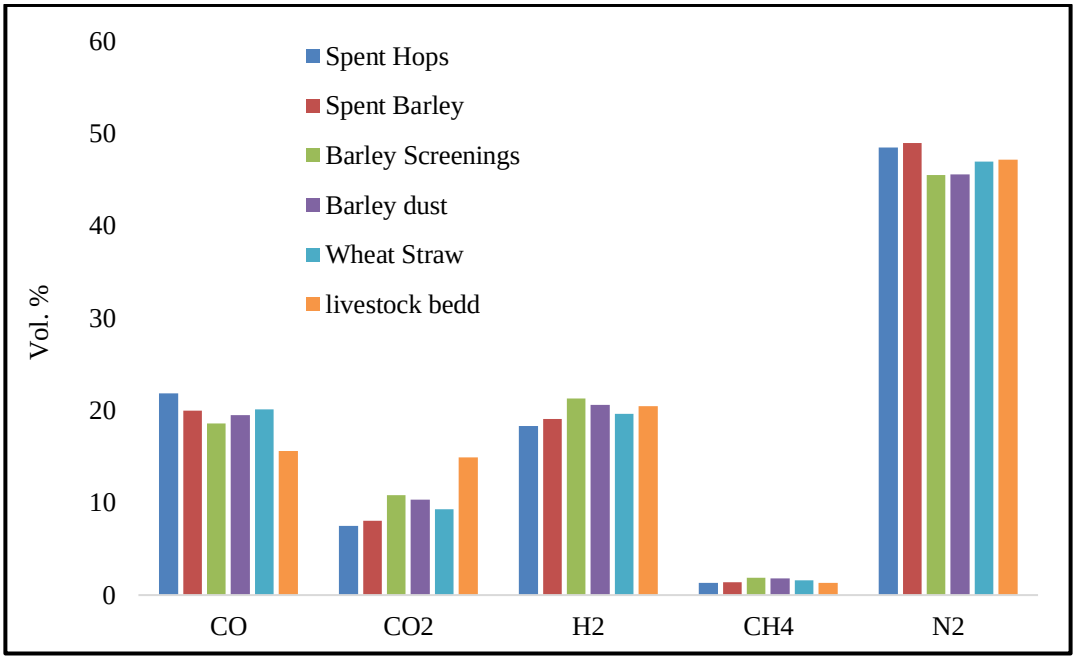

Figure 4.5. Results for volumetric gas composition (vertically), for different feedstocks at MC 10% and ER=0.35.

Figure 4.5 illustrates the producer gas production for all of the feedstocks when gasified at moisture content 10%, and equivalence ratio 0.35. Boundary conditions are selected based on the recommendations of previous works ([16], [51], and [68]), for higher syngas production rate (ER 0.3-0.35, and MC <10 %). Wood biomass materials are not included in this part as the focus is on the agricultural feedstocks and a comparison between their gasification outputs, including the model's stability against the different materials with sensitivity analysis. All feedstocks give reasonable results for the syngas production, which therefore proves that they can be used for gasification and produce syngas with reasonable rates.

For the same working conditions (i.e. 10 % MC, and 0.35 ER), CO shows higher values for spent hops and spent barley. This is because of their higher carbon content when compared to the other feedstocks. On the other hand, H_2 shows higher values for barley screenings and barley dust; however, all the values of hydrogen appear to be similar, varying between (15.3-16.1) %. Hydrogen values are the smallest in the ultimate analysis data when compared to C, and O. CH_4 values also show very small amounts, varying between (1.3-2) %. Syngas production, tar and heating value are all very important when considering the whole gasification process. The results of gasification are further discussed by studying the heating value and tar content in the producer gas, as illustrated in Figure 4.6.

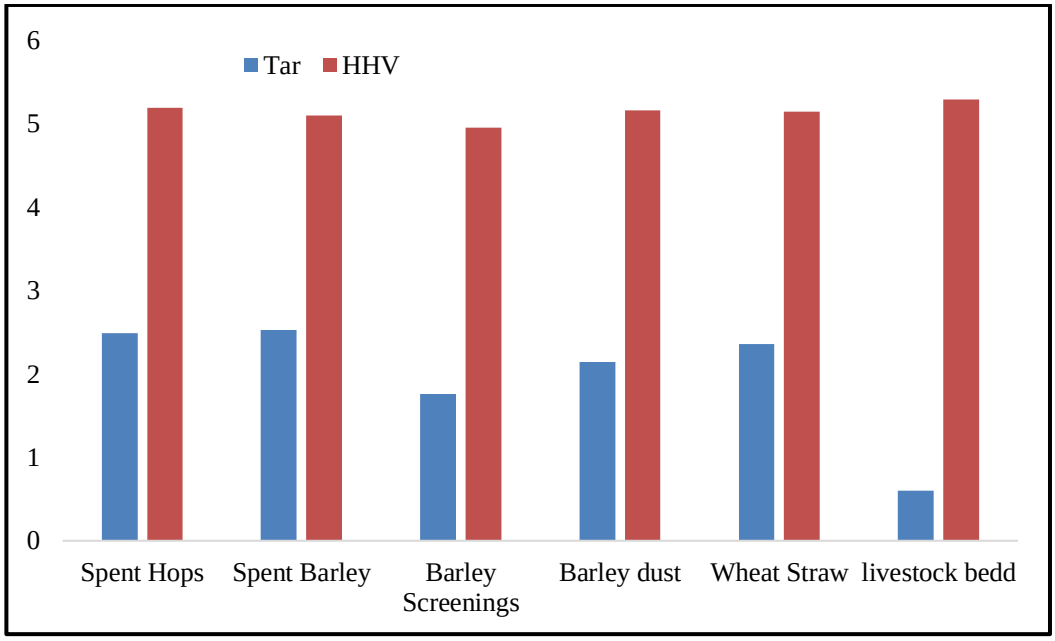

Figure 4.6: HHV (MJ/Nm^3) and tar (mol % of producer gas) content at 10% MC and Φ =0.35.

As shown in Figure 4.6, the highest heating value is found for spent hops and livestock beddings (~5.2 MJ/Nm^3) with a moderate tar content level less than ~2.5% from the producer

gas mole content. All of the feedstocks have a relatively similar heating value with a slight variation in the tar production rate. This is because of the similar C and H contents in most feedstocks that tend to produce the higher syngas composition, and also more burning of tar, converting it into useful compounds and hence a reduction in the levels of tar. On the other hand, the lowest heating value is found for barley screenings (4.95 MJ/Nm^3) which has the lowest carbon content. Lower carbon in feedstock tends to decrease the char oxidation reactions, which decrease the amount of syngas produced and hence, lower heating values. Spent hops was found to have the highest tar content (2.88 %). This is due to lower oxygen content, which tends to decease the oxidation reactions, in turn leading to lower the temperature in combustion, and hence lower burning and cracking rates for tar and higher levels of tar.

The results of agricultural feedstocks gasification are very close to wood biomass materials, as most of the feedstocks are similar in their ultimate data to biomass materials. The use of agricultural feedstocks will greatly impact economically and reduce waste too.

4.3.4 Sensitivity analysis

The effect of working parameters (equivalence ratio Φ, and moisture content MC) will be addressed in this section in order to study their influences on the quality of producer gas yield. This will be represented by studying their effect on the gas heating value and tar content. This will further give a clear indication for the optimum working conditions of the gasification of agricultural feedstocks.

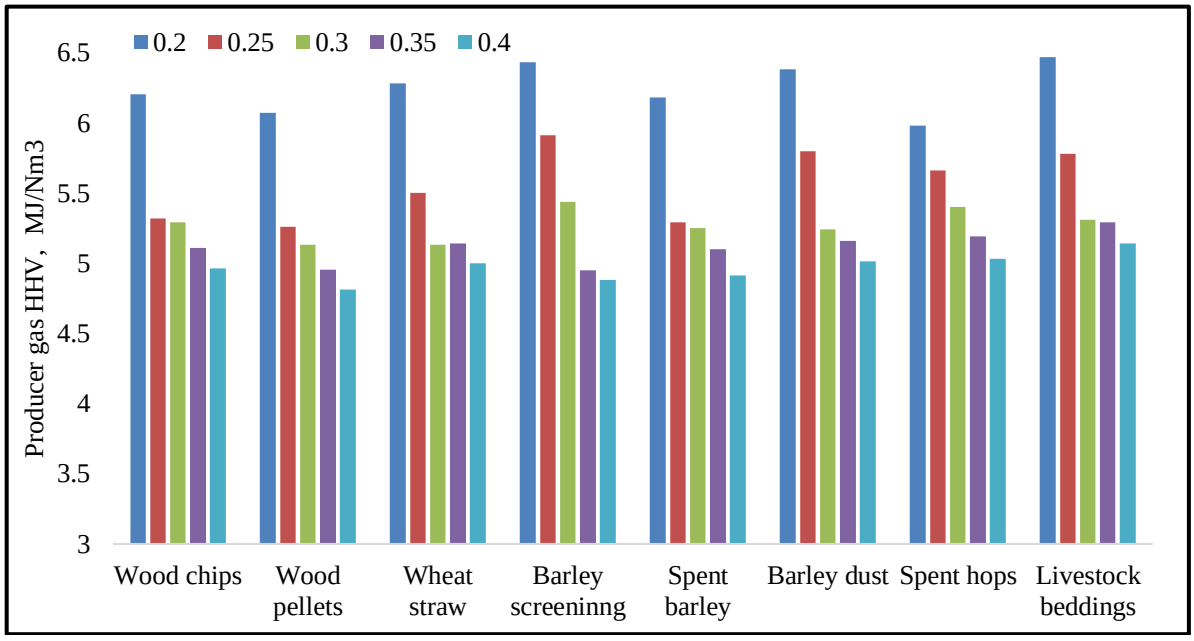

Figure 4.7: Effect of equivalence ratio on the producer gas heating value.

The results in Figure 4.7 show the effect of a changing equivalence ratio on the producer gas heating value. Fixed MC value was used as 10 %, and the equivalence ratio varies between (0.2-0.4). The results reveal that lower equivalence ratios are favourable for producing higher value syngas. This is mainly because lower air amounts (i.e. with low Φ) reduce the oxidation reactions ([16], [17] & [31]) and subsequently tend to reduce the amounts of CO_2 and H_2O. On the other hand, this also leads to an increase in the useful gases such as CO, CH_4 and H_2. Higher air amounts in the oxidation zone tend to further increase the oxidation of CO, char, CH_4, and H_2, which convert them to steam and CO_2, reducing the syngas products based on the combustion reactions ([16], [17] and [31]). Furthermore, increasing air amount tends to increase air dilution for syngas produced by adding more N_2 to the producer gas.

Maximum heating value varies between 6-6.4 MJ/Nm^3 at a lower equivalence ratio of 0.2, while the lowest values are between 4.8-5.14 MJ/Nm^3 for a higher equivalence ratio of 0.4. Most feedstocks show close values for HHV. However, livestock beddings, barley screenings and barley dust show higher rates of heating values ~ 6.4 MJ/Nm^3. The ultimate analysis data shows that those feedstocks require the lowest values of air for the same ER, when compared to the other feedstocks; this means lower air amounts when compared to the other materials. This further leads to lower combustion reaction rates and lower consumption for CO, CH_4, and H_2 in the oxidation zone, and hence, increases their values in syngas production, consequently giving a higher heating value. However, as noted, all of the materials show the same trend, and the value of heating value is similar to that of woody biomass materials. The results, therefore, further prove that using agricultural waste materials will provide the potential results.

Furthermore, the results generally show an increase in the producer gas heating value of 25–30% while decreasing Φ from 0.4 to 0.2. These results also show a strong agreement with previous work on the topic, such as ([17], [51], and [68]).

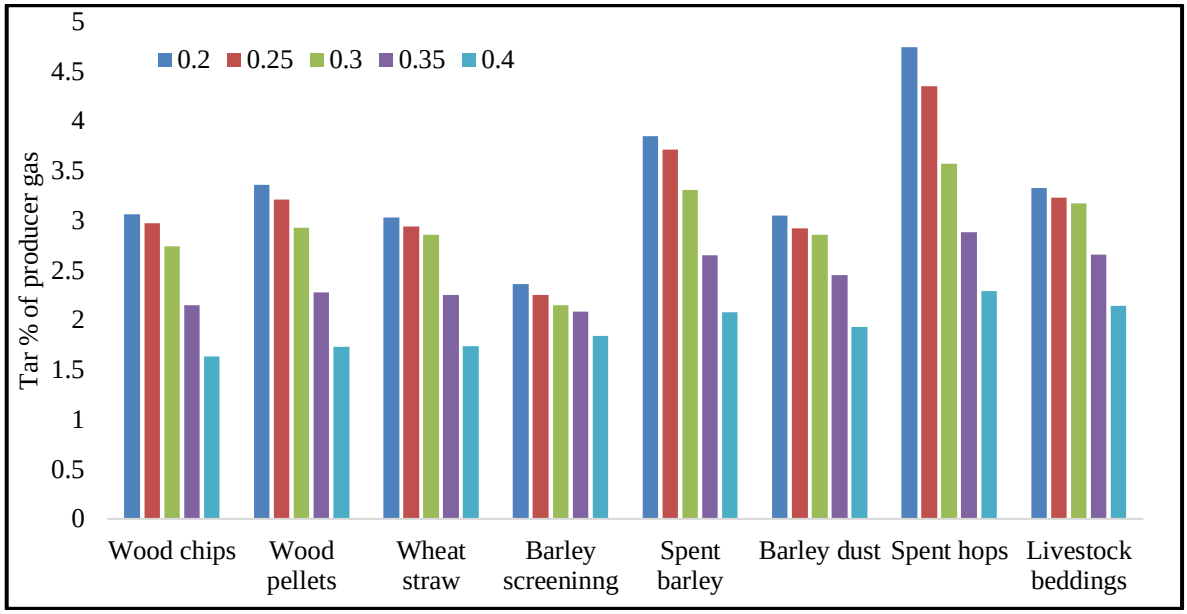

Figure 4.8: The effect of equivalence ratio on tar content

The model is used to study the effect of equivalence ratio on the gas quality (tar content), as shown in Figure 4.8. Other impurities and ash content are not included in the model for model simplicity, and the massive hazards caused by tar species in syngas. As a result, the main focus is on tar formation modelling. Comparisons are made at the fixed moisture content of 10% with varying ER (0.2-0.4) to see its effect on the gas quality. The results show that higher equivalence ratios are preferred for producing lower tar amounts. Referring to the oxidation zone reactions ([31], [16], and [17]) that depend on the amount of air supplied, a larger air supply (i.e. high Φ) will increase reaction rates. Increasing the rate of the combustion reactions leads to an increase in the combustion temperature, as most of these reactions are exothermic and hence, the temperature inside the gasifier will rise up. As a result, higher Φ tends to encourage the oxidation and tar cracking reactions to take place. Increasing the temperature inside the gasifier is favourable for cracking any heavy tars to convert them into lighter compounds. The results show with decreasing Φ from 0.4 to 0.2 tar yield increases from 16% to 50% [16].

Spent hops show the highest tar yield (4.74 mol% of syngas) at an equivalence ratio of 0.2. This is due primarily to the lower air amounts, including the lower oxygen content in this feedstock, which affected the oxidation temperature and led to lower cracking reactions. Wood biomass materials show lower tar production rate (1.6-1.7 mol% of syngas). These results also show good agreement with the previous works [16]; this is due to higher volatiles and lower ash content in wood materials. More volatiles tend to increase the syngas production rate and hence lower tar amounts, because it increases the temperature inside the gasifier due to higher rate of the oxidation reactions (which depend on the concentration of

CO, H_2, CH_4, and O_2). On the other hand, it also tends to encourage the oxidation reactions and cracking of tar molecules, converting them into lighter compounds.

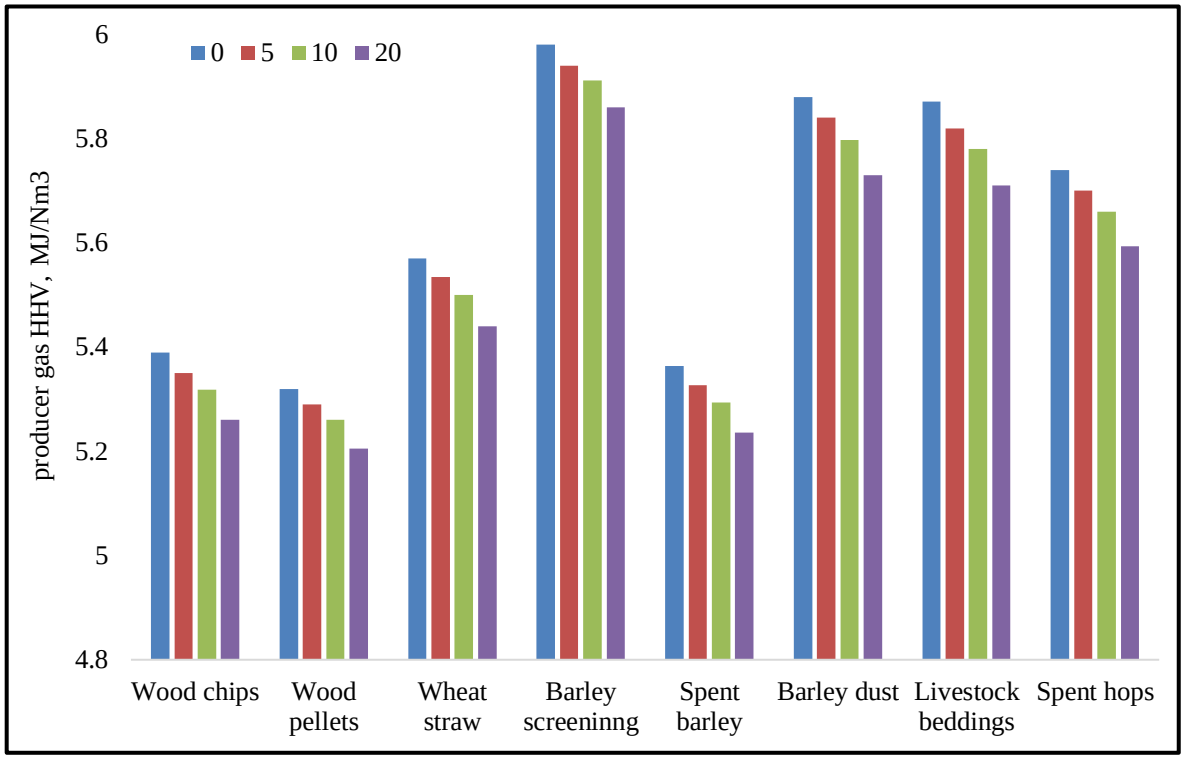

Figure 4.9: The effect of moisture content on producer gas heating value

Moisture content has a great effect on the quantity and quality of the gasification products. The results are carried out at fixed equivalence ratio of 0.25, while varying moisture content in the range of (0-20%). Higher moisture content levels tend to decrease gas heating value, as shown Figure 4.9. As MC increases, more energy will be required to remove it from biomass. This energy is not recovered again and reduces the gasification efficiency and also affects oxidation and gasification reactions, because of reducing the temperature inside the gasifier. The fact that it will decrease the amount of syngas produced with the producer gas, which decreases the heating value. It also results in increasing moisture levels inside the gasifier and as a result, a decrease in syngas yield through dilution with moisture. Higher MC tends to decrease the temperature inside of the gasifier, reducing gasification reaction rates and hence lower amounts of syngas produced. The results further show that a decrease in biomass moisture content from 20% to 5% leads to an increase in the produced gas heating value of 10–22%. Barley screenings, barley dust and livestock beddings show a higher production of syngas, and hence higher heating values for the same reasons discussed earlier.

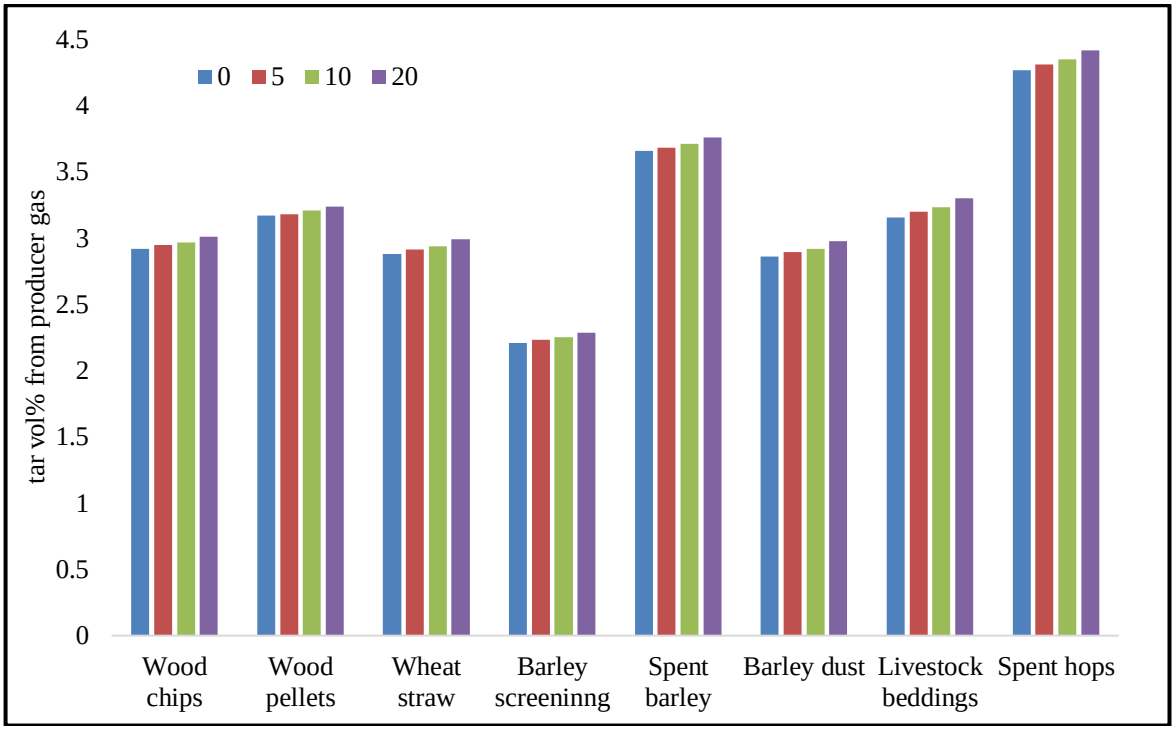

Figure 4.10: The effect of moisture on tar content

Figure 4.10 shows the effect of moisture content on tar produced. As mentioned, higher MC tends to decrease the temperature inside of the gasifier, which in turn leads to a decrease in cracking reactions and higher tar content levels. The results also show that a decrease of biomass moisture content from 20% to 5% leads to decrease in tar content of about 18–26%. Spent hops consistently show higher values of tar content; as mentioned earlier, this is because their lowest oxygen content based on the ultimate analysis data. The moisture content levels in the same material (~67%) mean that the gasification process is impossible unless drying for the recommended values (<10%) takes place before gasification. Other values of tar content show close values to wood materials, proving that the selected agricultural feedstocks can be utilised for gasification and syngas production in an economic and environmentally friendly way.

4.3.5 Gasification efficiency

Gasifier efficiency is calculated using the following relation [97];

$$\eta_{th} = \frac{G_p\, Q_g}{Q_b}, \tag{4.1}$$

$$Q_b = 0.339\, C + 1.029\, H + 0.109\, S - 0.112\, O - 0.025\, MC \;\; MJ/kg \tag{4.2}$$

Where, Q_g is the LHV of syngas in MJ/Nm^3; G_p is the gas yield in Nm^3/kg; and Q_b is the LHV of fuel/biomass in MJ/kg. The capacity of the gasifier is derived from the fuel feeding rate, along with the heating value of biomass used. A comparison is made between the

current modelling results for the gasifier efficiency and other experimental results [97] for the same biomass (Table 4.2).

Table 4.2: Ultimate analysis of corn straw.

Proximate (% wt. db)		Ultimate analysis	
Fixed carbon	13.75	C	43.83
Volatile matter	75.95	H	5.95
MC% (as received)	6.17	O	45.01
Ash	5.93	N	0.97
LHV(MJ/kg), daf	17.75	S	0.13

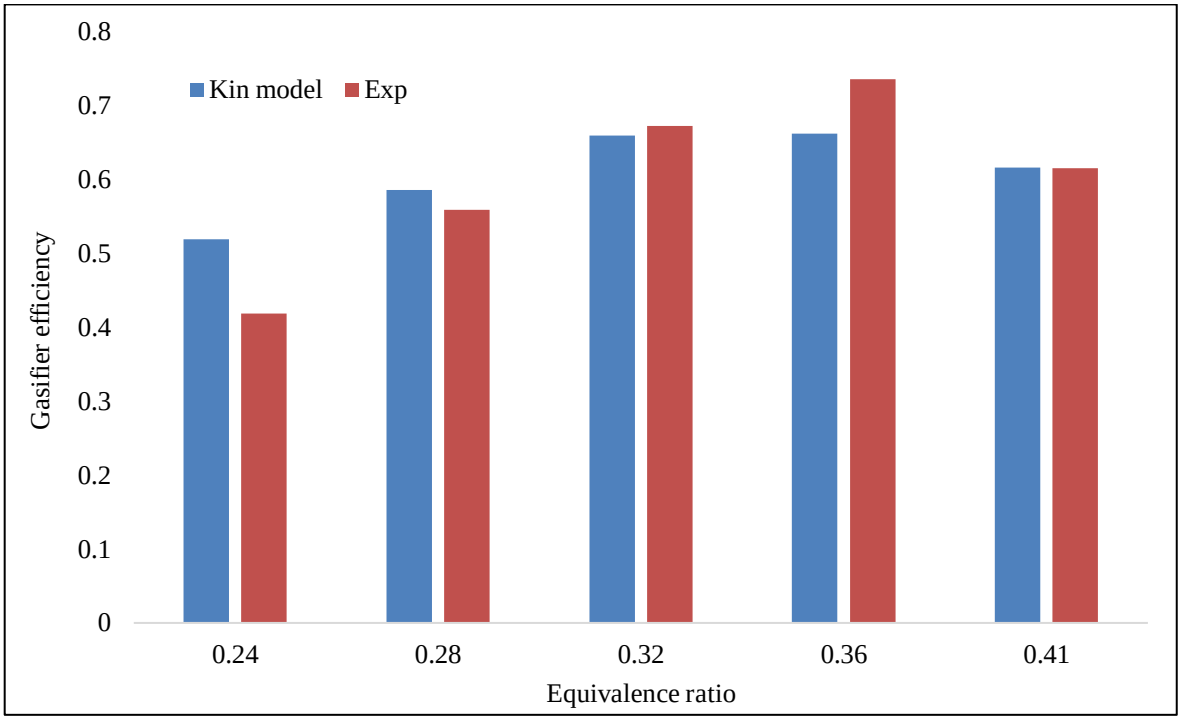

Figure 4.11: Comparison between gasification efficiency for the current model and experimental [97] work for the same working parameters.

The experimental results from [97], (Figure 4.11) are used for validating the current model results for gasification efficiency. They used different equivalence ratios and kept moisture content as received. For comparison, the same working conditions are used and found good agreement with the experimental results [97]. Gasification efficiency at different ERs shows good agreement (0- 9%), while at lower ER (0.24), it was found that the gasification efficiency is lower than the expected value by 19%. This might be because the lower air amounts calculated in the model compared to the experiments leading to lower gas yield and hence, lower gasification efficiency. However, all the other results look stable and within the acceptable range of the gasification efficiency. After validating the results from

the current kinetic model, the model was used to compare the gasification efficiency of different feedstocks (Figure 4.12).

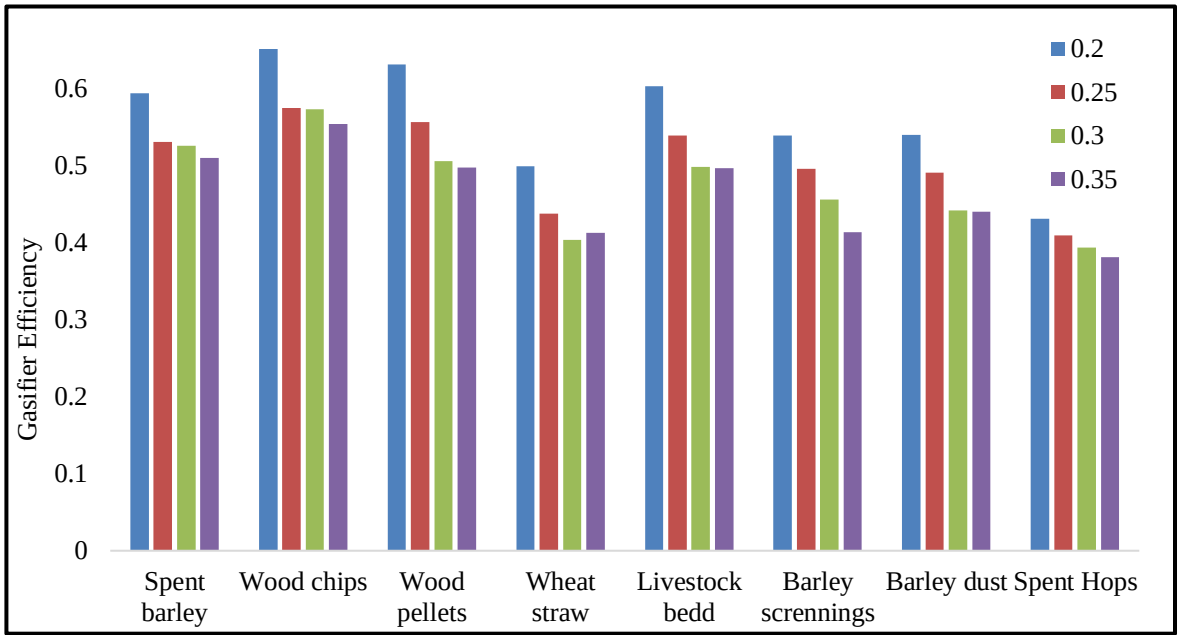

Figure 4.12: Gasifier efficiency for different feedstocks at different equivalence ratios.

Figure 4.12 illustrates the variations of gasification efficiency for a downdraft gasifier for different feedstocks. Moisture content kept fixed at 10% with varying ER, for easier comparisons between different feedstocks. Gasification of wood chips show as having a higher efficiency of approximately 66%, particularly for lower values of equivalence ratio (Φ 0.2). This is because a lower equivalence ratio tends to decrease the amount of air used in the gasification, and at same time leads to higher yield of producer gas, higher heating value of syngas, and hence increases gasification efficiency.

On the other hand, a higher equivalence ratio with high moisture content levels tends to decrease the amount of producer gas for the same reasons illustrated earlier.

Woody biomass materials show higher gasification efficiency (~65%), due to a higher yield of syngas. This is due to higher C, H, and O levels based on the ultimate analysis and reasonable values of moisture content. Again, livestock beddings, spent barley and barley screenings show high gasification efficiency and have very close values to the wood biomass materials. On the other hand, spent hops show the lowest gasification efficiency (~38 %), and as discussed earlier, also show higher values of tar content, making the feedstock unusual for gasification unless drying is considered.

4.3.6 Producer gas yield

Lower equivalence ratios tend to produce higher value syngas (higher heating values). On the other hand, it tends to produce higher tar amounts. Furthermore, the syngas yield produced has a high importance in the gasification process.

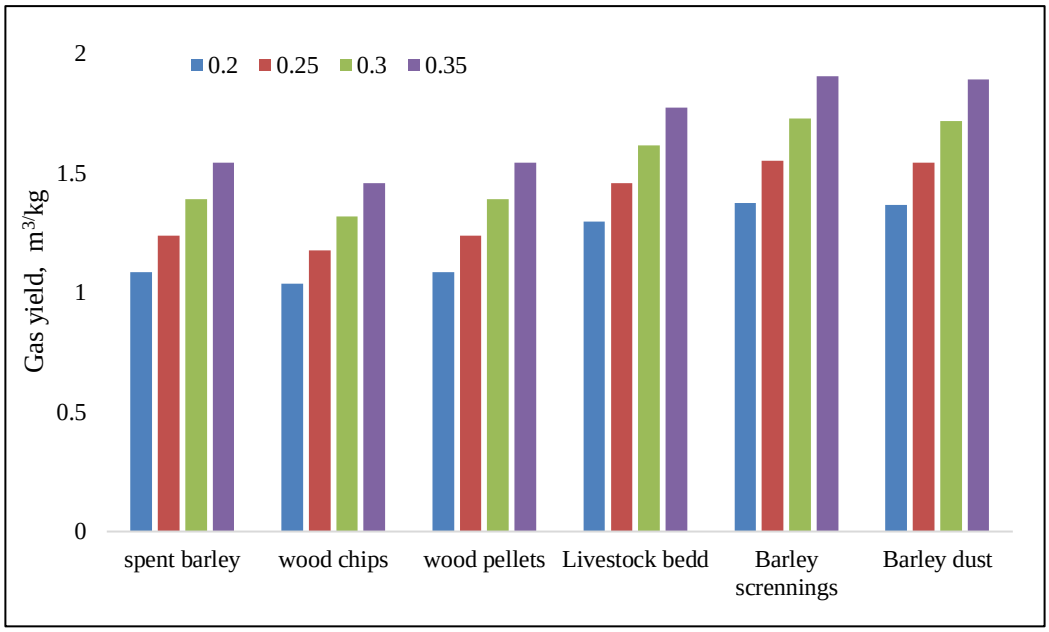

Figure 4.13: Producer gas yield production with different equivalence ratios.

The rate of syngas production (m^3 of producer gas/ kg of biomass) during the gasification of different feedstocks with varying ER is illustrated in Figure 4.13. As discussed earlier, lower ER tends to produce higher value syngas (higher syngas concentrations). However, it was found that the producer gas yield drops with ER. This is because lower ER tends to inject lower air amounts for combustion, and hence lower production rate of gas. On the other hand, lower air amounts decrease the combustion reactions inside the gasifier, and subsequently decrease the temperature as illustrated earlier, which in turn decrease the yield of syngas produced. Wood biomass materials tend to produce moderate value of syngas production rate, while barley screenings produces the highest production rate (1.9 m^3/kg) at higher ER of 0.35. This is because barley screenings has higher H, and O concentrations from its ultimate composition data, which requires higher feeding rate based on a constant power requirement of a gasifier. The higher fuel feeding rate in turn will require higher air amounts than other feedstocks for the same ER, and hence the higher production rate of producer gas. A moderate value of ER ~0.3 tends to produce higher value syngas (higher heating values with higher production rate) with lower tars.

4.3.7 Temperature variations across the gasifier

After validating the new modified model and testing it over a wide range of biomass materials, the model was used to study temperature variations along gasifier height.

Temperature variations across gasifier height are shown in Figure 4.14 and Figure 4.15. The results show variations in temperature while varying equivalence ratio. Moisture content is chosen to be constant as received in the feedstock, and for comparison and validation of the current model.

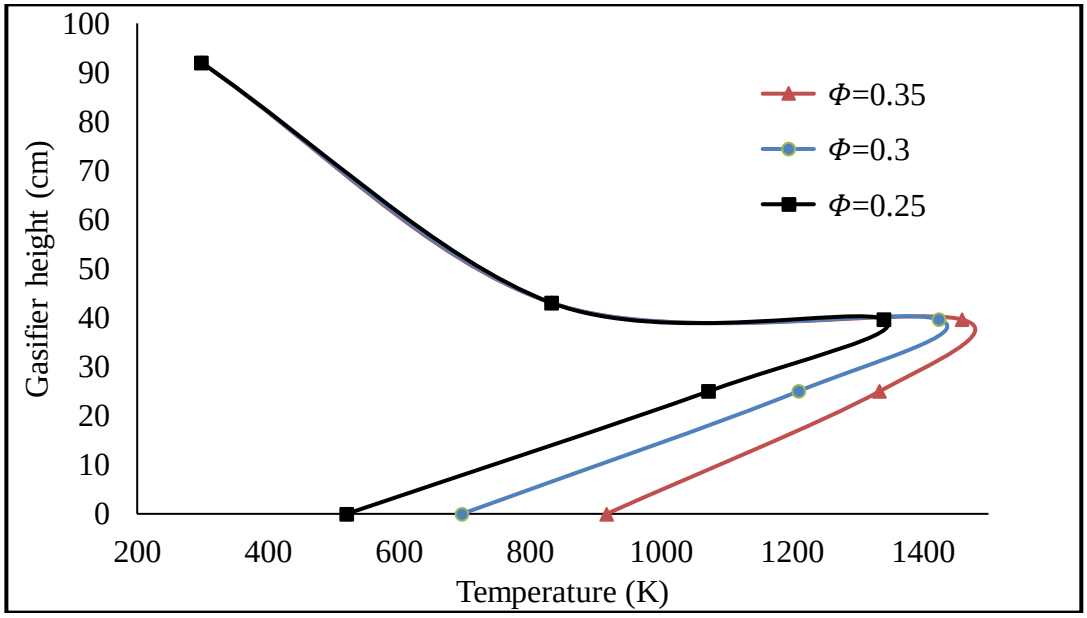

Figure 4.14: Temperature variations across gasifier height for rubber wood at MC=18.5%.

The results in Figure 4.14 shows good agreement with the data presented by Jayah et al. [38] where they showed that the maximum temperature in the reduction zone for rubber wood (ER of 0.35) was around 1400 K, while the exit temperature was 900K. For the same feedstock and working conditions, Ref [8] showed in their experimental data that the oxidation and pyrolysis temperatures are 1400 and 810 K respectively. In the present work, the oxidation and reduction temperatures are found to be 1460, and 917 K respectively. Also, Ref [8] showed the fixed pyrolysis temperature while varying the equivalence ratio. But the equivalence ratio has a negligible effect on the pyrolysis temperature, while the moisture content plays the dominant role affecting the pyrolysis process and its parameters. A biomass type with specific amount of moisture content will require a constant amount of heat for removal of moisture and start of devolatilization process. As long the biomass with fixed amount of mass, moisture and specific heat, then its pyrolysis temperature will remain constant. The results also show increase in temperature along gasifier height while equivalence ratio is increased. Increasing equivalence ratio tends to increase the amount of air inside the gasifier and hence encourages the oxidation (exothermic) reaction to take place;

the fact that increase oxidation temperature and corresponding temperatures along gasifier height. The same results are shown for another feedstock Figure 4.15.

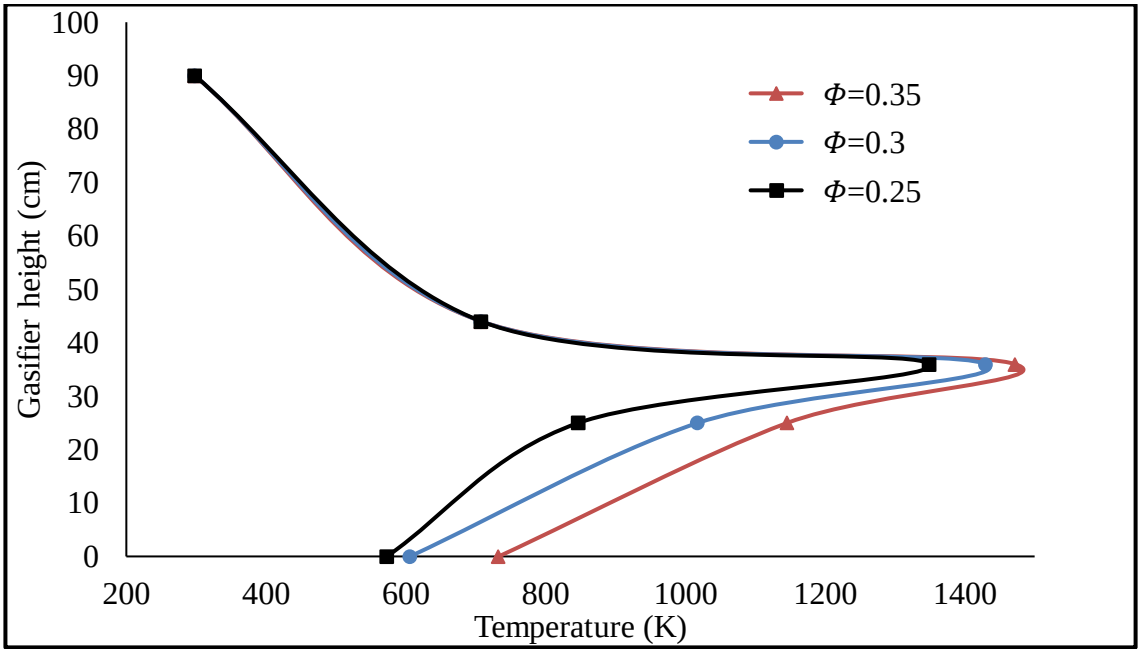

Figure 4.15: Temperature variations across gasifier height for wood pellets at MC=7.58%.

The results shown in Figure 4.15 illustrate a fairly strong agreement with Barrio et al. [43]. They showed the oxidation and reduction temperatures of 1373K, and1023K, respectively. Fixed pyrolysis temperature was also found, as the moisture content kept at a constant of 7.58%, and ER of 0.25. The results show that while increasing the equivalence ratio, the temperature also increases along the gasifier.

4.3.8 Gasifier design limitations and challenges

Designing a gasifier depends on many variables: feedstock, working conditions, and required thermal power. A gasifier design dimension is discussed in detail in chapter 3, [16].

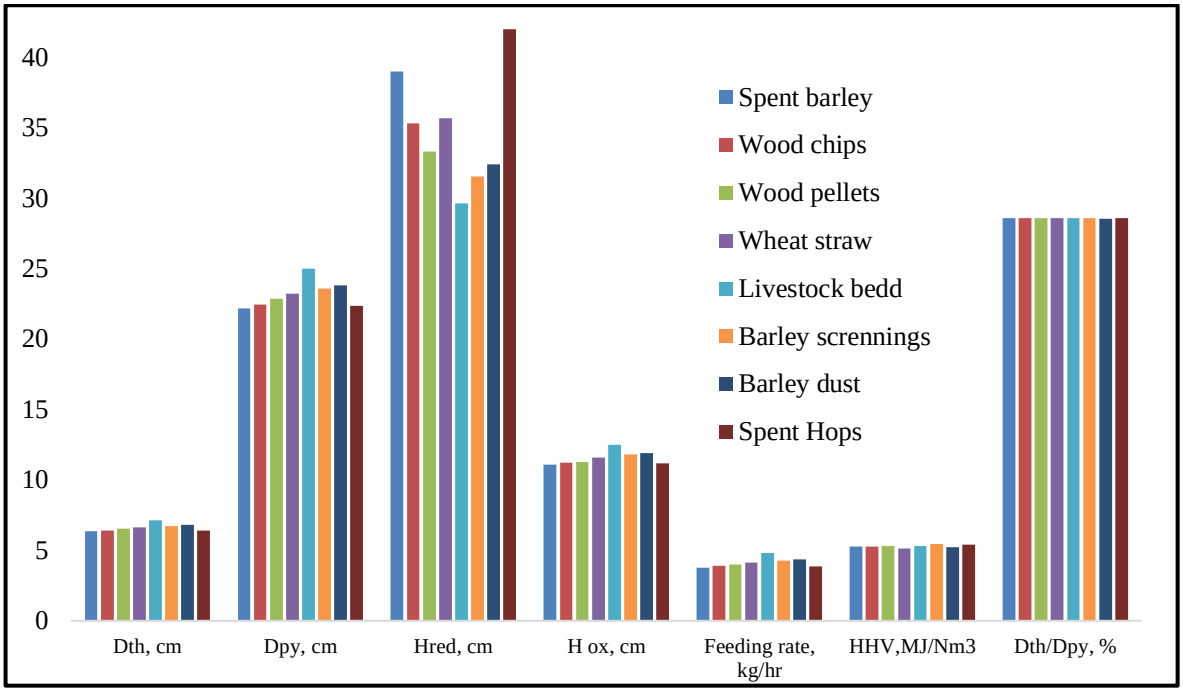

Figure 4.16: Gasifier design for different feedstocks.

The ultimate analysis and chemical composition variations of agricultural feedstocks might affect the gasifier design to obtain a specific power and syngas production rate. The set of results discussed in Figure 4.16 shows the main gasifier dimensions obtained from the kinetic code, for equivalence ratio of 0.3 and moisture content of 10%. However, it was found that different working parameters have no effect on gasifier design based on a specific capacity, because fixed capacity will mean fixed feeding rate, and hence fixed dimensions. The results show similarity in all the dimensions apart from the reduction zone length, which varies between (29-42) cm. This is because the kinetic code was designed based on the optimum height for the reduction zone. The theory behind this is based on full consumption of char at reduction zone. As a result, the higher reduction zone length will not affect the syngas production or power of a gasifier. Slight variations are also found in the throat (6.4-7.15) cm, pyrolysis diameter (22.2-25) cm, and oxidation zone lengths (11.1-12.5) cm.

On the other hand, a key design parameter – the ratio of throat to gasifier diameter (D_{th}/D_{py}) – is affecting the syngas produced and power required [98]. The results show an optimum value for all the feedstocks of around 29%, while it was in the range of 40% as discussed by [98]. In their research they performed CFD modelling and compared between different ratios to achieve the optimum ratio. While in the current research work, the design is taken and validated from previous experimental data ([24] and [25]).

Based on this discussion, a gasifier design based on spent hops and spent barley will suit most of the agricultural materials been discussed. Higher (C and H) content in those

materials gives higher char in the combustion and reduction zone, which affects the reduction reactions, thus requiring a higher length of reduction zone to be fully consumed. Also, H_2 higher levels increase the reduction reactions that again depend on the amount of H_2, further affecting the reduction zone length. On the other hand, they have a moderate value for the other design dimensions of gasifier based on the fixed power rate. To prove this point further, a reverse calculation is performed to assess the effect of using the fixed gasifier on the change of syngas production and heating value of producer gas.

4.3.9 Gasifier design optimization

All biomass, waste and agricultural materials possess different ultimate and proximate analysis data. These data affect gasifier design for a required power and syngas output. As a result, the design of a gasifier that is able to handle different feedstocks with different working parameters and ultimate data is a big challenge. A backward calculation takes place using the kinetic code to observe the effect of using a fixed design of a gasifier on the producer gas rate and its quality (Figure 4.17).

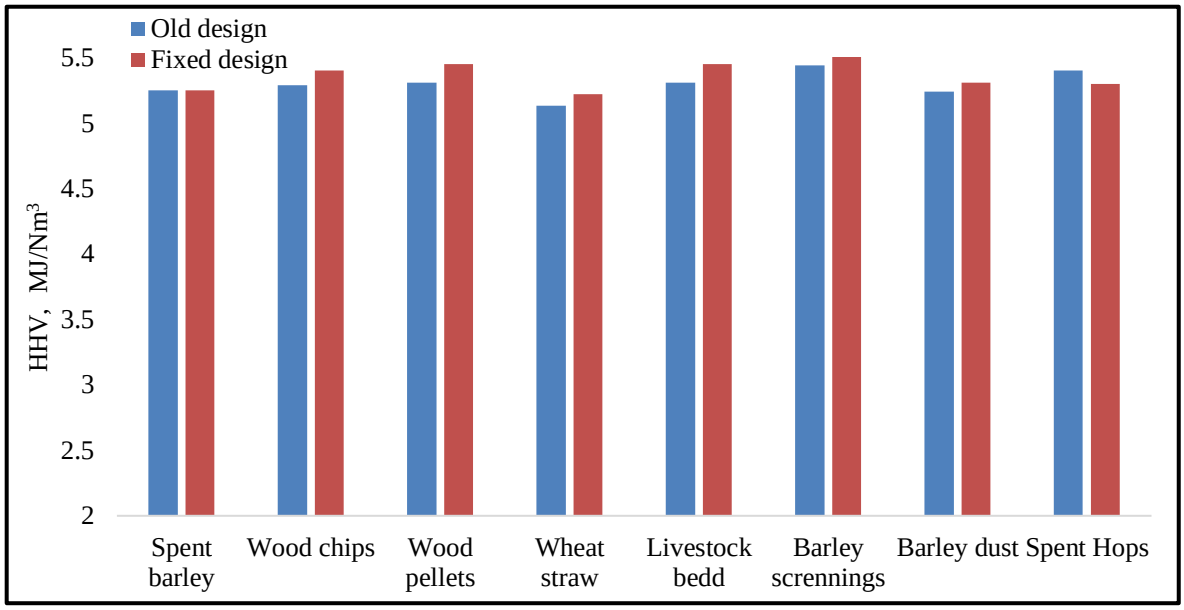

Figure 4.17. The effect of a fixed gasifier design for different feedstocks.

A single design is used by fixing the thermal power (20 kW) and gasifier dimensions for the spent barley feedstock and applied this design for all the other feedstocks. As a result, a fixed gasifier is used for all the feedstocks at the same working conditions of ER=0.3, and MC of 10 %. The effect of this on the syngas quality will be discussed and compared that with the separate designs for every feedstock.

As seen from Figure 4.17, the results of the heating value show a negligible difference when using one gasifier design. Based on the discussion, designing a gasifier based on the highest (C and H) content of a specific feedstock will work properly with other feedstocks and give the expected syngas production. This is because these feedstocks require the specific dimensions (bigger reduction zone length), which ensure all the char consumption inside the reduction zone, thus providing the ultimate production of syngas with the highest heating value.

4.3.10 Optimum working parameters

The model is used to address the working parameters that lead to a higher production of syngas with lower amounts of tar when considering gasification efficiency. These factors will optimise the gasification process.

Based on the results obtained by the model thus far, lower equivalence ratios are seen to lead to an increase in syngas composition and hence, a higher heating value. On the other hand, it was found that this can also lead to an increase in the produced amount of tar, and lower syngas yield, which is not economic for the gasification process. As a result, using moderate values of the equivalence ratio will be of great impact for producing higher syngas (i.e. higher heating values), with lower levels of tar.

Moisture content in biomass is shown to have a significant impact on both tar and heating value. It was found that higher levels of moisture content are unacceptable and lead to a decrease in syngas production and also an increase in tar yield. Lower or no moisture content makes gasification of a great potential and gives the highest yield of syngas and lowers the amount of tar. However, drying biomass before gasification to zero would require more energy for removal, and this would make the process economically inefficient, as well as decreasing the whole efficiency of the process. As a result, using lower moisture content levels is recommended.

Gasification efficiency is a key parameter that should be considered for higher syngas production and the whole optimisation process. A lower equivalence ratio and moisture content are both favourable for higher gasification efficiency.

The results generally show an increase in the producer gas heating value of 25–30%, and tar yield increases from 16% to 50% while decreasing Φ from 0.4 to 0.2. The results further show that a decrease of biomass moisture content from 20% to 5% leads to an increase of the produced gas heating value of 10–22%, and a decrease of tar content of approximately 18–26%. Wood biomass materials show a lower tar production rate (1.6-1.7 mol% of syngas), finding a good agreement with previous work. Other values of tar content show

close data and similarity to wood materials, which proves that the selected agricultural feedstocks can be utilised for gasification and syngas production in an economically efficient and environmentally friendly way.

Woody biomass materials show a higher gasification efficiency (~65%) (Figure 4.12), due to a higher yield of syngas and higher C, H, and O levels, based on ultimate analysis and reasonable values of moisture content, as seen in Table 4.1. Agricultural feedstocks such as livestock beddings, spent barley and barley screenings, show high gasification efficiency and very close values to wood biomass materials. On the other hand, spent hops show the lowest gasification efficiency (~38 %), and as discussed earlier, also show higher values of tar content, which makes the feedstock unusual for gasification unless drying is considered. The moisture content level in the same material (~67%) means that the gasification process is impossible unless drying for the recommended values takes place before gasification.

The robustness of the model has been examined and the results show that the equivalence ratio (Φ) at 0.3-0.35, and with a moisture content less than 10%, gives a higher yield of syngas with a higher gasification efficiency and lower tar content.

Based on the discussion, designing a gasifier based on the highest (C and H) content of a specific feedstock will work properly with other feedstocks and give expected syngas production. This is because these feedstocks require specific dimensions (such as bigger reduction zone length), which ensure all char consumption inside the reduction zone and gives ultimate production of syngas and hence, the highest heating value.

4.4 Conclusion

The previous kinetic model (Chapter 3) limitations has been discussed and further improvement is carried out on the model to make it applicable for different materials including biomass and agricultural residues. The model is further used carry out sensitivity analysis through studying the effects of air equivalence ratio and moisture content levels on produced gas quality. Furthermore, gasification efficiency is studied, and the model was used to address design limitations and challenges regarding the use of different feedstocks.

All feedstocks (biomass, waste and agricultural) possess different ultimate and proximate analysis data. These data affect gasifier design for a required power and syngas output. As a result, the design of a gasifier that is able to handle different feedstocks with different working parameters and ultimate data is a huge challenge. The final results discuss the optimisation process of a gasifier design that can handle and operate under different working conditions for various feedstocks and still able to produce higher quality syngas. Based on the discussion, designing a gasifier based on the highest (C and H) content of a specific

feedstock will work properly with other feedstocks and give expected syngas production. This is because these feedstocks require specific dimensions (such as bigger reduction zone length), which ensure all char consumption inside the reduction zone, which in turn provides ultimate production of syngas and hence, the highest heating value.

Agricultural feedstocks, livestock beddings, spent barley and barley screenings show high gasification efficiency and very close values to wood biomass materials. On the other hand, spent hops show the lowest gasification efficiency (~38 %), and also, as discussed earlier, also show higher values of tar content, which makes the feedstock unusual for gasification unless drying is considered. The moisture content levels in the same material (~67%) make the gasification process impossible, unless drying for the recommended values takes place before gasification.

The robustness of the model has been examined and the results show that the equivalence ratio (Φ) at 0.3-0.35, and with a moisture content less than 10%, gives a higher yield of syngas with a higher gasification efficiency and lower tar content. Temperature variation across the gasifier was also studied and the gasification temperature was found to increase, with an increase of Φ. The results are close to wood biomass materials, as most of the feedstocks are similar in their ultimate data to biomass materials. The use of agricultural feedstocks will be of a great impact economically and in reducing waste too.

The model designed could be directly used in the bioenergy industry as a guidance for the design of downdraft gasifiers and optimisation. The applicability and wide variety of materials the models can handle makes it a unique toolkit that could add a significant value to the bioenergy/industry sectors. On the other hand, the new feedstocks tested by the models proved its capability to be gasified, thus gives a promising and wide attention to make use of the agricultural and farm residues in the gasification and also would encourage the governments to make a beneficial use of these feedstocks. Additionally, the model is encouraging the waste management and reduction by showing and highlighting the different waste materials outputs using the process gasification.

Chapter 5 Tar Species Evolution and Formation: Experimental Investigation and Numerical Modelling

5.1 Introduction

During the gasification process, organic volatiles formed are condensed slowly, so these are typically carried with the gas products, forming a viscous substance called tar. Tar is undesirable for any downstream applications e.g. when using producer gases in internal combustion engines and gas turbines. Separation of tar is a major challenge for using the syngas produced because it will condense and potentially cause blockage at engines and valves. Furthermore, tar content in syngas limits its direct use and thus requires additional removal techniques. An effective way to use syngas directly as a fuel is to limit the formation of tar or reduce it to a specific level. Therefore, studies have been particularly focused on investigating the nature of the formation and destruction of tar compounds. However, experimental studies regarding tar formation and destruction are a cost and time-consuming process. The modelling of tar formation, conversion and destruction along a gasifier could give a wider understanding of the process and help in the tar elimination and reduction. Furthermore, tar is a complex mixture of hydrocarbons containing hundreds of species [35] and that makes the modelling process hard and computationally intensive, because the chemistry of the formation and the combustion of many species has not yet been fully studied.

A novel and unique kinetic code was built to simulate downdraft gasifiers including selected tar species and gas species formation along the gasifier height, and gasifier design. As far as can be researched, the data simulated by the current model have never been mentioned nor introduced by any single kinetic model.

Few studies about the detailed tar modelling in downdraft gasifiers have been done recently and most studies have mainly focused on syngas production, because tars are difficult to analyse, and sample compared to other gases. As a result, a novel aspect of this work is that it shows a detailed kinetic code for modelling tar and gas species formation along downdraft gasifiers in one code.

The current work is a combination of modelling and experimental investigation for tar species evolution in air-blown downdraft gasifiers. A tar evolution model is built and combined with an existing model developed recently by the author and presented in the previous chapters – a four-zone integrated kinetic model allowing prediction of the optimum working parameters of a downdraft gasifier [16]. The model was tested and verified over a

wide range of biomass materials. The model has been used currently to optimise and design gasification and pyrolysis of biomass [99].

The detailed kinetic model for the evolution and formation of tar from downdraft gasifiers incorporates four main tar species (benzene, naphthalene, toluene, and phenol) with a total of eighteen different kinetic rate reactions implemented in the code for every zone. Tar species evolution will be tracked along the gasifier height from the pyrolysis to the oxidation and reduction zones. A good understanding of the evolution of different gas species and tar, and their relationship to the temperature at each zone and other working parameters, will be of great importance when designing a gasifier and also in reducing the tar content in producer gas. The results can be used to optimise the work of downdraft gasifiers that lead to the production of higher value syngas. Experimental work was carried out to investigate the tar species contents along with a validation of the results of the kinetic code where a good agreement is found. Sensitivity analysis was also carried out by the kinetic code to optimise the working parameters of a downdraft gasifier that led to a higher calorific value of syngas with lower tar content.

Based on the review made, the novelty in current research work is addressed through building up the proposed kinetic code for simulating downdraft air-blown gasifiers. The code is developed using Matlab and does not depend on any external modelling codes (e.g. Aspen). Additionally, most of the earlier published works only takes into account tar formation as a total amount or selected species [100], but the current model predicts the formation of the four main tar species based on their kinetic rate reactions along the gasifier height.

5.2 Experimental setup

The experiments were carried up at the KTH institute, Stockholm, Sweden on a small-scale gasification unit. Wood sample was used as feedstock. Gas species, total tar, and detailed tar species were analysed. The experiments were carried out at three different equivalence ratios (ER) at three different temperatures (800, 900, and 1100 °C).

5.2.1 Gasification unit

A pilot-scale gasification unit designed for gasification, combustion and pyrolysis of different feedstocks using air and/or steam mixtures was used. A schematic view of the test rig is shown in Figure 5.1. The combustor is an axial cylinder surrounded by a heater connected to a control panel which can heat up to 1150 °C. The system is connected to a water/isopropanol path to collect tar generated (Figure 5.2a) followed by a filter for tar and

particulates removal, then gas flows to a micro GC system to analyse the syngas. The sample boat/holder is 10 cm length, while the internal combustor diameter is 24 cm, surrounded by a heater of 1.5 mm thickness. The axial combustor length is 50 cm, while the total length of the test rig is 100 cm.

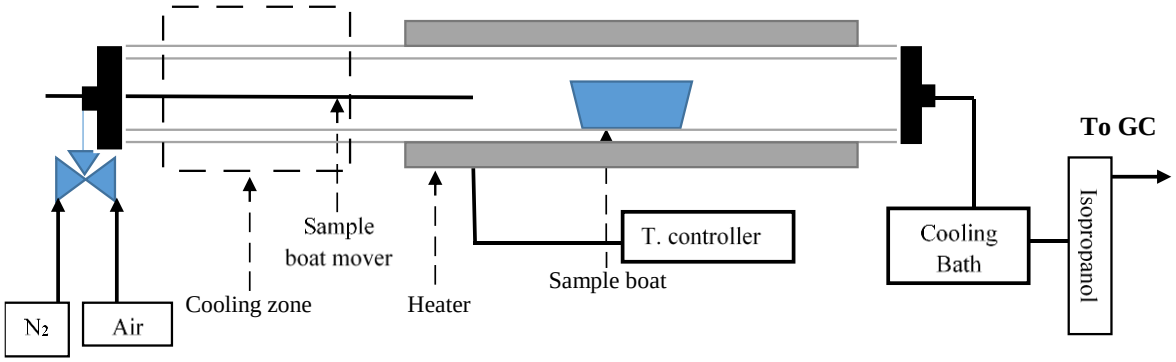

Figure 5.1. Schematic diagram of gasification test rig used in experiments.

Two thermocouples were connected to the system. The first was connected to the heater that was controlled by the control panel, while the second thermocouple was connected to the sample holder to measure the temperature of gasification during the experiment.

5.2.2 Materials and feedstock' preparation

Wood was used as a feedstock with the ultimate analysis shown in Table 5.1. Wood samples are formed from fine particles and been used directly in the experiments after drying. The analysis was carried out by BELAB AB, Sweden [101]. Samples were first dried in an oven for twenty-four hours at 100℃ to reduce the amount of water content, since dry samples have the advantage of easier tar sampling and analysis. Three different equivalence ratios (ER) were used (0.25, 0.3, and 0.35) at three different temperatures (800, 900, and 1100℃).

Table 5.1: Biomass analysis of feedstocks used [101].

Ultimate Analysis, db	
C	49.1
H	6.1
O	43.8
N	0.12
S	0.026
Ash	0.8
Moisture%	14.1
Vol. %, db	84.2

5.2.3 Experimental procedure

After drying samples in the oven, a sample holder was filled with a sufficient amount of wood (4.7g). The sample holder was weighed before and after the sampling to measure the accurate amount of sample. A specific scale was used for weighing the samples and bottles with an accuracy of 0.001 g. Glass bottles for tar collection were washed and dried and their weight was measured individually. The inner tube of the reactor was cleaned by methanol to ensure that there was no tar or ash left inside. The temperature of the experiment was then set by the control panel which heats up the system at a rate of 35 degrees/min. Nitrogen was also used for a leakage test to ensure there was no gas leakage from the system. The sample was then placed at the start of the reactor tube (at around 150℃). The amount of air based on the required ER was calculated and nitrogen was fed first to ensure that no air remained in the reactor. Air amount for every run was calculated based on the ER wanted, and for 40 min experiment time it was supplied through three-way valve and been adjusted using air flow meter.

The tar collection bottles were immersed inside the bath of the cooler at a temperature of -20℃. This temperature is below the condensation temperature of all the well-known tar species. The air flowrate was adjusted by a flowmeter based on a specific residence time of the experiment to ensure a sufficient amount of gasification medium based on the calculations of ER. When the temperature inside the tube reached the required experiment temperature, the sample holder was pushed to the middle of the reaction tube and air replaced nitrogen. The temperature and time were recorded for every run.

(a) (b)

Figure 5.2. (a) Cooler bath used to condense tar, and (b) glass bottles used to collect tar samples

Once the sample was placed in the middle of the reactor and air flows, tar started to form and was collected in the bottles and syngas continued to flow to be analysed in the micro-GC system. Heavier tar molecules were collected in the first bottle followed by lighter molecules in the following bottles. Before gas analysing through the GC, gas cleaning take place through different filters and collecting liquids. The gas coming out of the reactor is coming through tar collecting system, then passing through a specific filter fitted at last bottle, followed by isopropanol collecting system, then finally passing through another filter to ensure that gas is cleaned from all tar and other impurities before going to the gas chromatograph.

5.2.4 Tar sampling and Solid Phase Adsorption (SPA) method for tar analysis

In Figure 5.3 (a), condensed tar species in the bottles is shown for wood fibre gasification at 900℃, for an ER of 0.3. After collecting tar, it is further diluted using Dichloromethane (DCM) in order to be analysed and to give a tar species concentration. Figure 5.3 (a) shows heavier tar compounds (darker colours) collected in the first bottle, followed by lighter compounds in the following bottles. Condensation takes place as a result of lower bath temperature (-20 ℃). Bottles are then weighed after each run to measure the total amount of tar produced.

Tar collection as shown in Figure 5.3 (b) in order to identify detailed tar species in the tar produced from the gasification of biomass. The tar collected in 100 ml of syngas was sent to be further analysed using the SPA method. A specific syringe with 100 ml internal volume is used for collecting tar inside this volume where the gas coming out of the system is subjected to the syringe until it is totally filled.

(a) (b) (c)

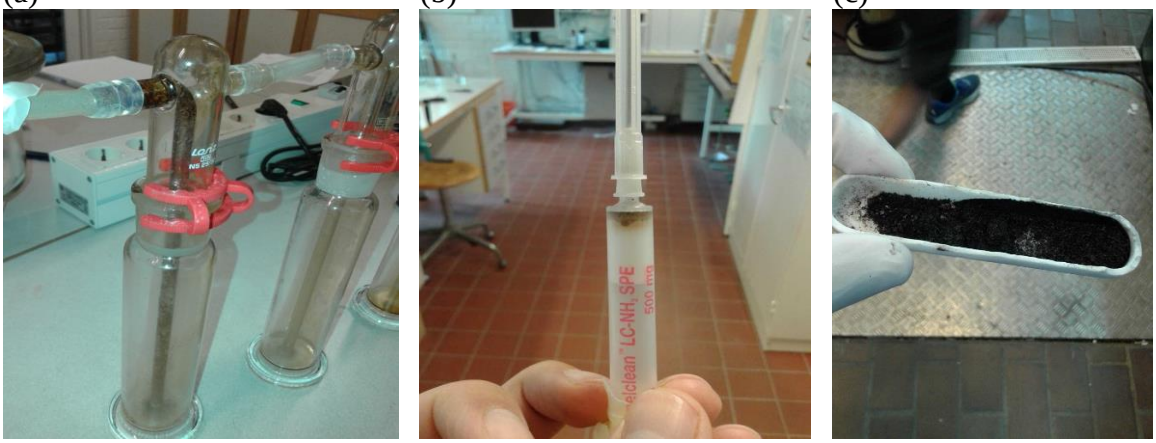

Figure 5.3. (a) Tar collected in bottles, (b) tar collection by SPA method syringe, (c) ash collected after the experiment.

The detailed SPA (Solid Phase Adsorption) method is an offline collection method used to analyse tar compounds. It is used to detect and analyse tar compounds that have a boiling point up to 400 °C which is sufficient for most gasification applications as the gasifier temperature is obviously higher than that [102]. With a rapid sampling time (around 1 minute), a wide range of aromatic and phenolic compounds can be detected in μg for every 100 ml of gas.

Tar is collected in the gas phase (250-300 °C) by being trapped in a small disposable polypropylene column in a small syringe with the help of a 100 ml syringe (Figure 5.3(b)) Tar is later analysed by a gas chromatograph (Varian CP-3800) with a flame ionization detector (FID). The main compounds detected by this method are shown in Table 5.2.

Table 5.2: Detectable compounds of SPA tar collection method

Aromatics	**Phenolics**
Benzene	Phenol
Toluene	o-Cresol
m/p-Xylene	m-Cresol
o-Xylene	p-Cresol
Indan	2,4-Xylenol
Indene	2,5/3,5-Xylenol
Naphthalene	2,6-Xylenol
2-Methylnaphthalene	2,3-Xylenol
1-Methylnaphthalene	3,4-Xylenol
Biphenyl	
Acenaphthylene	
Acenaphthene	
Fluorene	
Phenanthrene	
Anthracene	
Fluorantene	
Pyrene	

Ash content after the experiment is shown in Figure 5.3 (c) which ensures that the sample amount is gasified.

5.3 Numerical model

A detailed kinetic code for tar evolution and destruction is built and combined with the kinetic code previously developed by the author (Chapter 3) [16]. The model uses a set of kinetic rate reactions and balance equations for the different zones of a downdraft gasifier. The kinetic code was able to predict the downdraft gasifier performance through a wide range of output variables and control parameters. The model was also able to predict the producer gas composition, temperature variations along the gasifier height, velocity and pressure variations, gasifier design and tar formation as a one general compound. The model was tested and verified over a wide range of materials and working parameters against the well-known experimental data and further used to optimise the downdraft gasifier work based on the sensitivity analysis [16]. As illustrated, the main kinetic code was an integrated model considering gas species formation zone by zone, where the input of every zone is the feeding to next zone. The model was based on a 20-kW downdraft gasifier where all the design parameters were described in details (Chapter 3).

In this Chapter, four main tar species were added to the model to represent the tar formation using detailed kinetic reactions. The yield of tar species at different zones of a gasifier is discussed based on the temperature of each zone. Mass and energy balances are calculated. Eighteen different kinetic reactions are implemented in the kinetic code to predict the optimum working conditions that lead to the production of a higher value producer gas.

5.3.1 Pyrolysis sub-model

Tar decomposition based on the pyrolysis temperature is addressed and discussed in the present work. Ref. [52] reported parameters for the empirical correlations of pyrolysis products, as shown in Table 5.3, based on the experimental data taken from [67] which gives the mass yield of tar evolution during the pyrolysis process in g tar/ kg biomass.

Table 5.3: Correlations for pyrolysis products [52]

	a	*b*	*c*
C_7H_8	-6E-5	0.10701	-48
$C_{10}H_8$	-0.0001	0.218	-115.32
C_6H_6	-0.0003	0.7017	-387.6
C_6H_6O	2E-5	-0.068	46.42

The mass yield of different tar species *Y*, in g/kg biomass, can be derived by using the following equation:

$$Y = aT^2 + b\,T + c \qquad (5.1)$$

After calculating the mass yield of the four main tar species at the pyrolysis zone, they are added to the pyrolysis products and an energy balance is carried out in order to calculate the pyrolysis temperature through equation (5.2).

$$\sum X_i \,.\, \left(h_f + \, C_p.\Delta T\right)_{pyrolysis} = \sum X_i \,.\, \left(h_f + \, C_p.\Delta T\right)_{comb} + Q_{loss} \tag{5.2}$$

5.3.2 Tar species in combustion and reduction zones

The products of pyrolysis are used as a feed to the oxidation zone. The reactions stated in Table 5.4 are implemented in the kinetic model for both the combustion and reduction zones. These reactions are taken from the references mentioned in the Table. Other reactions for the gasification and combustion were already discussed in Chapter 3 and will not be repeated here. The same way of calculating gas species is followed to calculate different tar species.

Table 5.4: Reactions of tar species implemented in the model.

	Reactions and rate expression	A (s^{-1})	E (kJ/mol)	Ref
1	$C_7H_8 \rightarrow 0.17C_{10}H_8 + 0.89C_6H_6 + 0.67H_2$ $r_1 = k_1\,[C_7H_8]$	2.23E13	315	[66]
2	$C_{10}H_8 \rightarrow 10\,C + 4H_2$ $r_2 = k_2\,[C_{10}H_8]^2\,[H_2]^{-0.7}$	5.56E15	360	[103]
3	$C_{10}H_8 + 4H_2O \rightarrow C_6H_6 + 4CO + 5H_2$ $r_3 = k_3\,[C_{10}H_8]\,[H_2]^{0.4}$	1.58E12	324	[103]
4	$C_7H_8 + H_2 \rightarrow C_6H_6 + CH_4$ $r_4 = k_4\,[C_7H_8]\,[H_2]^{0.5}$	1.04E12	247	[103]
5	$C_6H_6 + 5H_2O \rightarrow 5CO + CH_4 + 6H_2$ $r_5 = k_5\,[C_6H_6]$	4.4E8	220	[103]
6	$C_6H_6 + 7.5\,O_2 \rightarrow 6CO_2 + 4H_2O$ $r_6 = k_6\,[C_6H_6]^{-0.1}\,[O_2]^{1.25}$	17.83	125.5	[103]
7	$C_6H_6 + 3O_2 \rightarrow 6CO + 3H_2$ $r_7 = k_7\,[C_6H_6]\,[O_2]$	1.58E15	202.6	[103]
8	$C_7H_8 + 9\,O_2 \rightarrow 7CO_2 + 4H_2O$ $r_8 = k_8\,[C_7H_8]^{-0.1}\,[O_2]^{1.25}$	14.26	125.5	[103]
9	$C_6H_6O \rightarrow CO + 0.4C_{10}H_8 + 0.15\,C_6H_6 + 0.1CH_4 + 0.75H_2$ $r_9 = k_9\,[C_6H_6O]$	1.0E7	100	[52], [54]

5.3.3 Different gas species in combustion and reduction zones

Gas species formation in the reduction zone follow the same kinetic modelling illustrated in Chapter 3 with the same kinetics reactions. But the equilibrium approach that was implemented in combustion cannot be applicable after using the kinetic rate reaction for tar species. As a result, a detailed kinetic rate reaction for different gas species formation and destruction at the oxidation zone is employed considering the pyrolysis products as feed.

5.4 Results and Discussion

Since the initial model has been modified, the validation of the new model to simulate downdraft gasification needs to be re-considered. Syngas production will be validated first, followed by the tar species validation as total amount and detailed species. Furthermore, a sensitivity analysis will be carried out to optimise the process of gasification.

5.4.1 Producer gas species validation

The set of materials used in comparison and validation are illustrated in Table 5.5.

Table 5.5: Working conditions used in comparison

	Feedstock	MC%	Φ	Ref.
a	Rubber wood	18.5	0.326	[38]
b	Wood Pellets	8	0.259	[44]
c	Bamboo	10	0.3	[24]
d	Neem	10	0.3	[24]
e	Rice husk	10	0.3	[93]
f	Saw Dust	20	0.2796	[28]

Different materials are used for validation, with different working conditions of moisture content and air equivalence ratio to study the model stability and robustness as shown in Table 5.5.

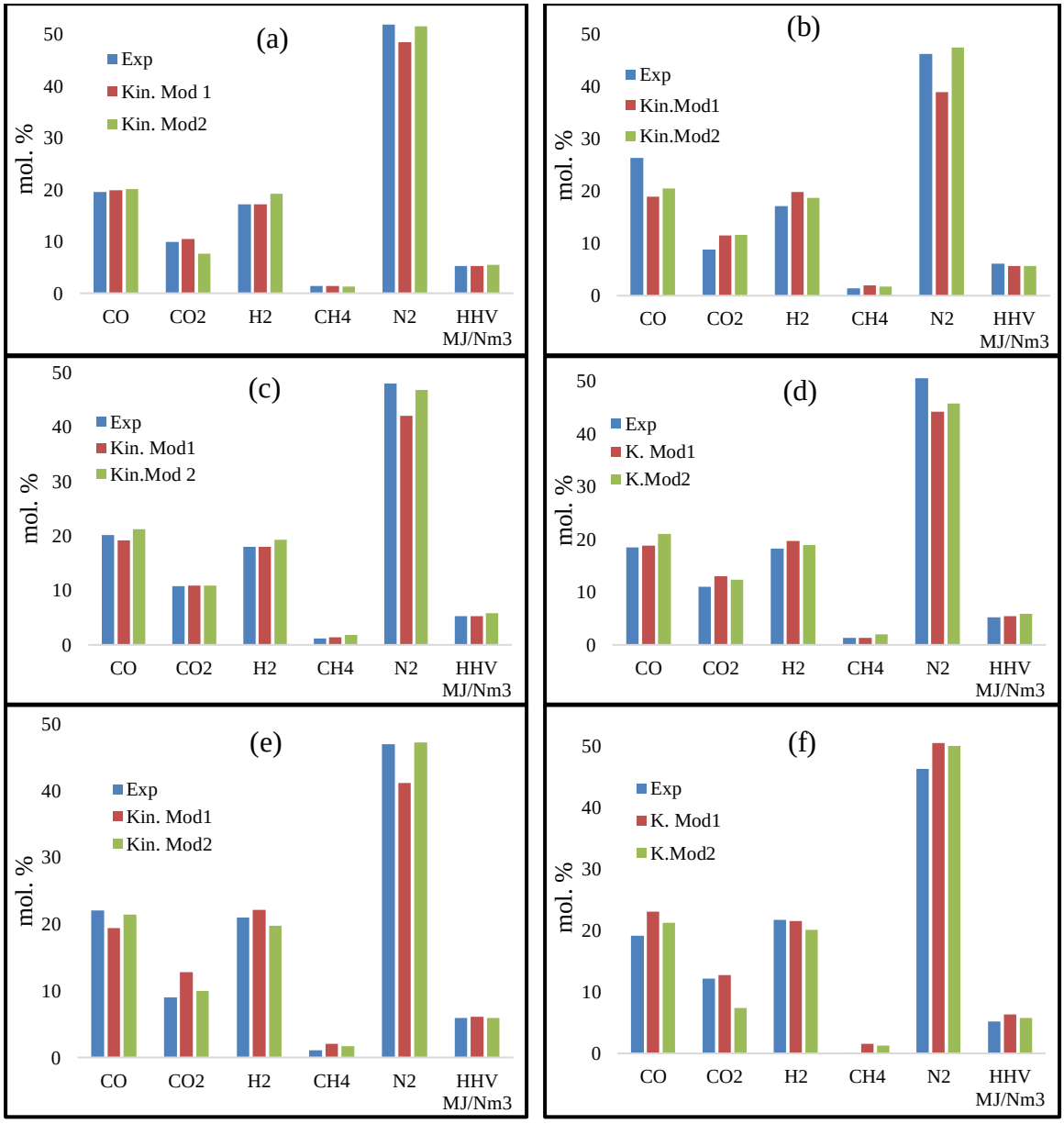

Figure 5.4: Comparison between the producer gas compositions for the current model (Kin. Mod2), the previous model (Kin. Mod1), and the experimental data.

The set of results shown in Figure 5.4 illustrates the volumetric gas composition derived from the current model (Kin. Mod2) for different feedstocks. The results are compared with the previous model (Kin. Mod1) developed and also with the experimental data from literature to study the model stability and ability to work under wide variations of working conditions and feedstock changes. The results of the current model show more accurate and stable results for some species (N_2), which was slightly underestimated in the previous model. All the results are derived at a fixed required thermal power of 20 MW_{th}, although it was found that changing thermal power has no effect on the gas composition, and heating value for producer gas, as already illustrated previously in Chapter 3.

After model has been validated, tar formation will be discussed and validated separately as it is the main focus of this chapter, and further will be followed by sensitivity analysis to show optimum working conditions for downdraft gasifiers.

5.4.2 SPA tar results

Tar samples were collected and further analysed in order to obtain detailed tar species as presented in Figure 5.5. The results illustrate the area covered by the different aromatic and phenolic species for wood sample gasification.

The experiment was carried out at an ER of 0.35 and temperature of 1100 °C and the results are further converted to amount (μg) per 100 ml of syngas based on the area covered by every single species as shown in Table 5.6 .Further, GC analysis was performed to confirm the retention time for tar species. Based on the literature [35], hundreds of tar species can be detected. However, in the present work, only twenty-six species were found in significant amounts (Table 5.6), varying between aromatics (such as benzene, naphthalene and xylene) and phenolics (such as phenol and cresol). Under all the working conditions and changing parameters (e.g. MC, and ER), it was seen that the tar species selected for modelling (benzene, toluene, naphthalene, and phenol), are always in large amounts of approximately 70-95%. The concentration of remaining tar species (such as xylene, indene, pyrene, cresol and xylenol) can be ignored because of their small amount or a lack of chemical data and kinetic rate reactions that can help in building a stable kinetic code.

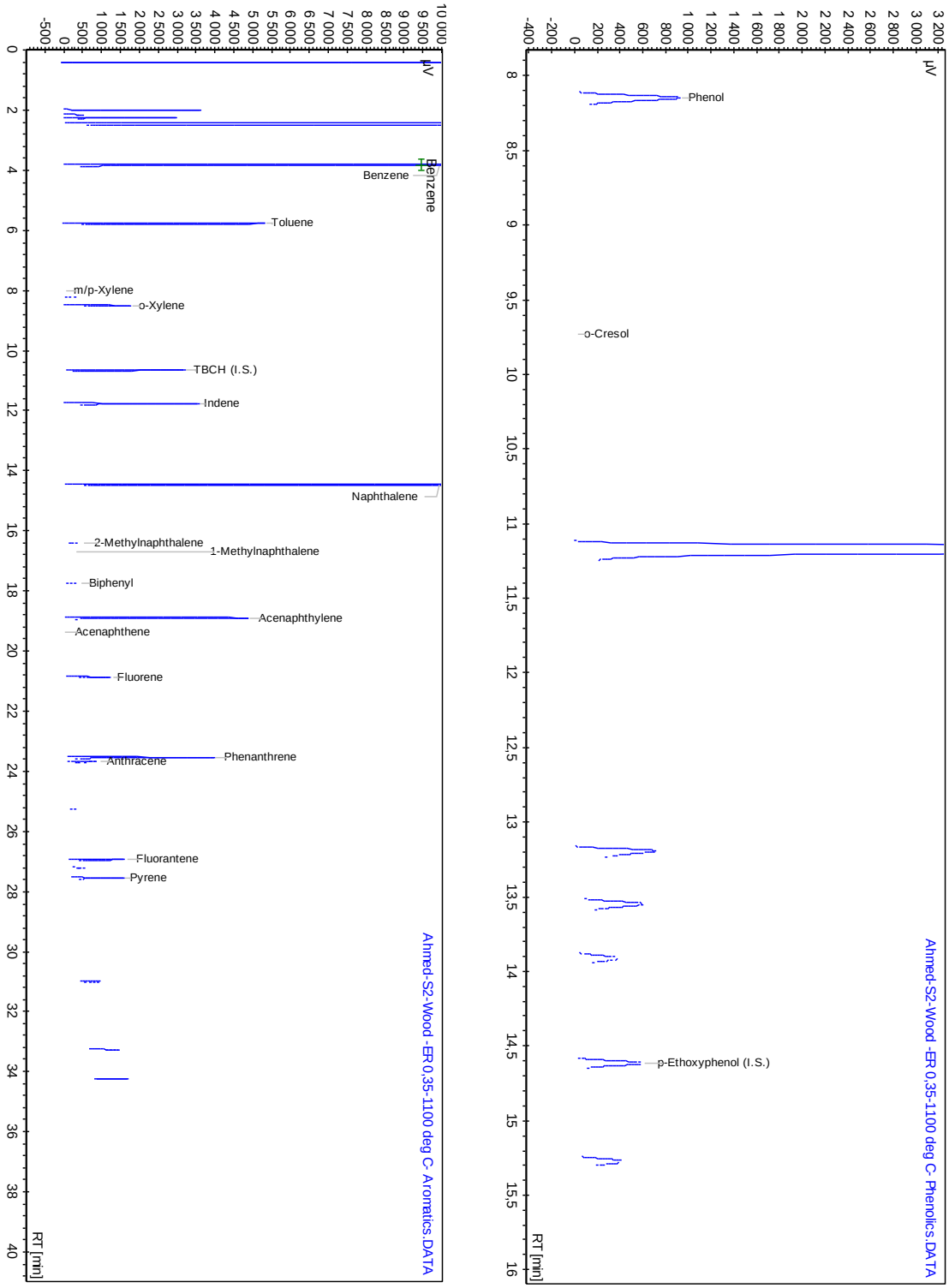

Figure 5.5. Tar species released during GC analysis of wood sample.

The results also show that benzene and naphthalene are the highest amounts of tar formed. That is because their nature as tertiary tars and all the primary and secondary tars are further converted to tertiary tars due to higher temperatures inside the gasifier. On the other hand, both compounds are not easy to be cracked under lower temperatures as will be illustrated further in the coming sections.

Table 5.6: Sample results from SPA tar analysis method, per 100 mL

S2-wood-ER 0.35-1100 deg.C -Aromatics						
	Name	Time [Min]	Quantity [µg]	Area [µV.Sec]	Area [µV.Min]	Area % [%]
1	Benzene	3.83	767.17	29169.7	486.2	18.504
2	Toluene	5.78	266.84	10288.5	171.5	6.527
4	m/p-Xylene	8.02	2.07	84.6	1.4	0.054
6	o-Xylene	8.5	108.04	4438.8	74	2.816
7	TBCH (I.S.)	10.66	0	6018	100.3	3.818
0	Indan	11.59	N.D.	N.D.	N.D.	N.D.
10	Indene	11.77	176.97	7468.5	124.5	4.738
16	Naphthalene	14.46	793.38	35477.5	591.3	22.506
18	2-Methylnaphthalene	16.41	33.48	1412.5	23.5	0.896
19	1-Methylnaphthalene	16.69	18.44	862.3	14.4	0.547
21	Biphenyl	17.76	30	1353.7	22.6	0.859
26	Acenaphthylene	18.9	294.74	9831.9	163.9	6.237
27	Acenaphthene	19.38	1.15	50.1	0.8	0.032
33	Fluorene	20.87	68.8	3016.8	50.3	1.914
42	Phenanthrene	23.54	183.34	7993	133.2	5.071
43	Anthracene	23.68	51.22	2257.7	37.6	1.432
51	Fluorantene	26.94	80.6	3466.9	57.8	2.199
54	Pyrene	27.55	75.31	3184	53.1	2.02
Total			2951.57			
S2-wood-ER 0.35-1100 deg.C - Phenolic						
#	Name	Time [Min]	Quantity [µg]	Height [µV]	Area [µV.Min]	Area % [%]
1	Phenol	8.15	53.01	951.1	46.9	3.154
2	o-Cresol	9.73	2.28	37.7	1.8	0.119
0	m-Cresol	9.98	N.D.	N.D.	N.D.	N.D.
0	p-Cresol	10.2	N.D.	N.D.	N.D.	N.D.
0	2,4-Xylenol	11.78	N.D.	N.D.	N.D.	N.D.
0	2,5/3,5-Xylenol	11.86	N.D.	N.D.	N.D.	N.D.
0	2,6-Xylenol	12.24	N.D.	N.D.	N.D.	N.D.
0	2,3-Xylenol	12.44	N.D.	N.D.	N.D.	N.D.
0	3,4-Xylenol	12.58	N.D.	N.D.	N.D.	N.D.
7	p-Ethoxyphenol (I.S.)	14.61	0	612.8	26.9	1.811
Total			55.29			

Phenol shows very small amounts compared to the other species and can be negligible, while toluene is found in considerable amounts. The results also show that the four main tar species selected for modelling are forming more than 60% of the total tar formed during gasification process which founds a good agreement with the previous works (e.g. [67], [60], and [51]) , and this will be further illustrated in the coming sections.

5.4.3 Tar model validation

The model validation will be carried out through different ways. Mass balance is calculated for the input and output species. In addition, the total amount of tar estimated by the model will be compared with the experimental data. Furthermore, every detailed species amount will be compared with the results derived from the experiments.

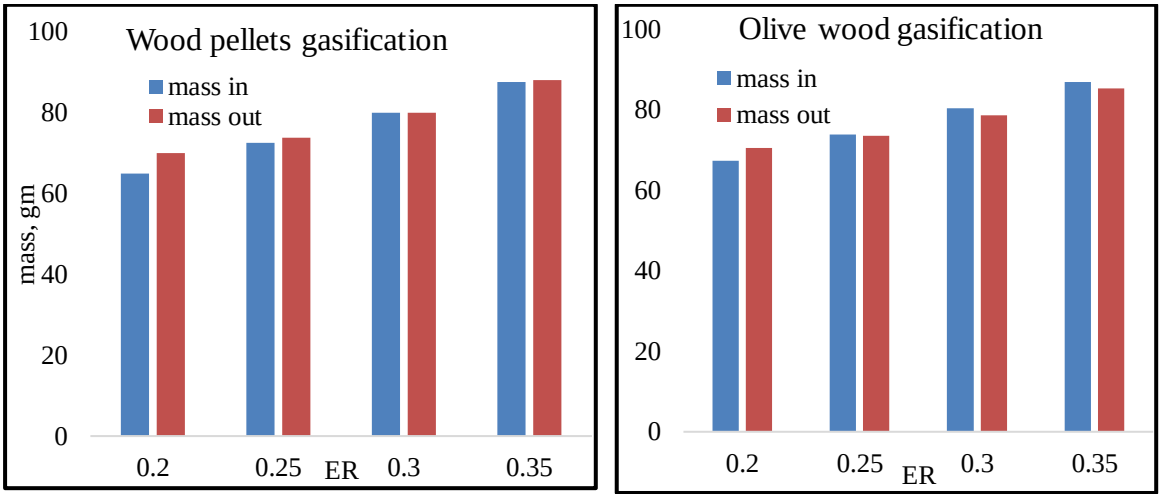

Figure 5.6. Mass balance calculations for different feedstocks.

Figure 5.6 shows the mass balance calculations for wood pellets and olive wood [92] at different equivalence ratios with a constant moisture content of 10% for the results derived from the kinetic code. These calculations are based on the numerical results driven from the kinetic code. Total mass input, including biomass and air, is calculated and mass output includes the producer gas and tar species. All the results are based on one mol of biomass decomposition. Unlike equilibrium models that should give the exact results for the mass balance, the kinetic code which depends on many variables (e.g. zones temperature, gas species concentration and gas velocity) is expected to have slight variations between the mass input and output. However, this discrepancy has to be within a specific limit. The results presented tend to be fair although a slight variation is found at a lower equivalence ratio for wood pellets which might be because of the lower air content that leads to a mass decrease compared to that of the higher ERs. However, the results look stable (with only 1-8 % variations), and show the model's stability at different working conditions such as the equivalence ratio. Earlier experimental results reported by [104] showed there is a slight mass balance variation during their experiments under different conditions up to 10%, which again provides the good agreement with the current work.

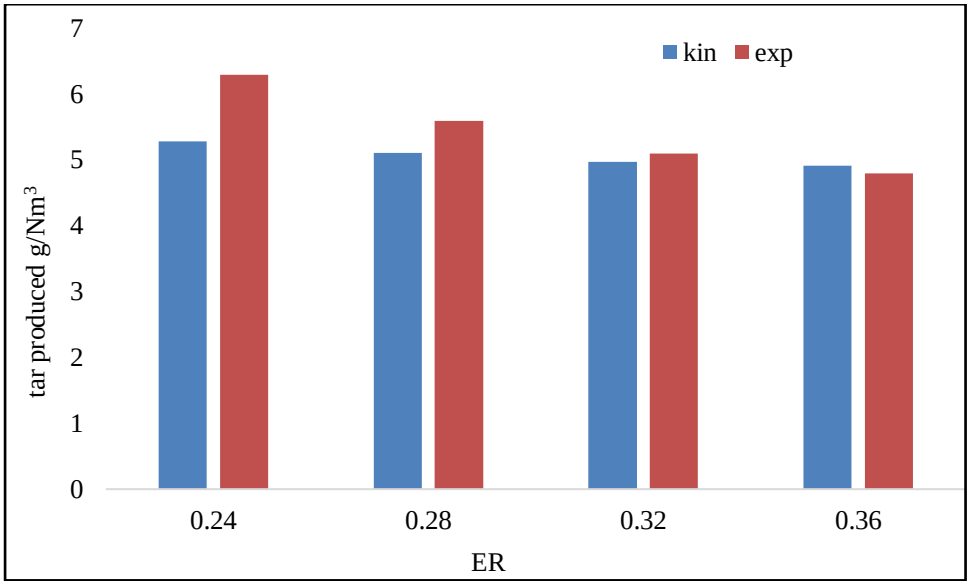

Figure 5.7. Total tar formation comparison between the present model and experimental results [97].

The comparison shown in Figure 5.7 between the results obtained by the present model and the other experimental data [97], demonstrates having a good agreement for the total tar amount. The model is following the same boundary conditions used in the experiments for correct validation, where MC is fixed at 6.17% and ER is varied from 0.24-0.36. Maximum tar produced by the model shows values approximately 5 g/Nm^{3}and it is also in agreement with [105], where they stated that tar produced in downdraft gasifiers is in the range of 0.01-6 g/Nm^3. In the experimental work of [97], they used corn stalks with a moisture content level of 6.17%, and the comparison is made for the different values of the air equivalence ratio to measure the stability of current model for a normal range of working conditions.

The experiment is carried out at an axial combustor while the modelling is based on considering a downdraft gasifier. However, the model is relying on the detailed kinetic rate reactions that does not depend on the gasifier geometry, and hence, the results provide strong agreement with experiments.

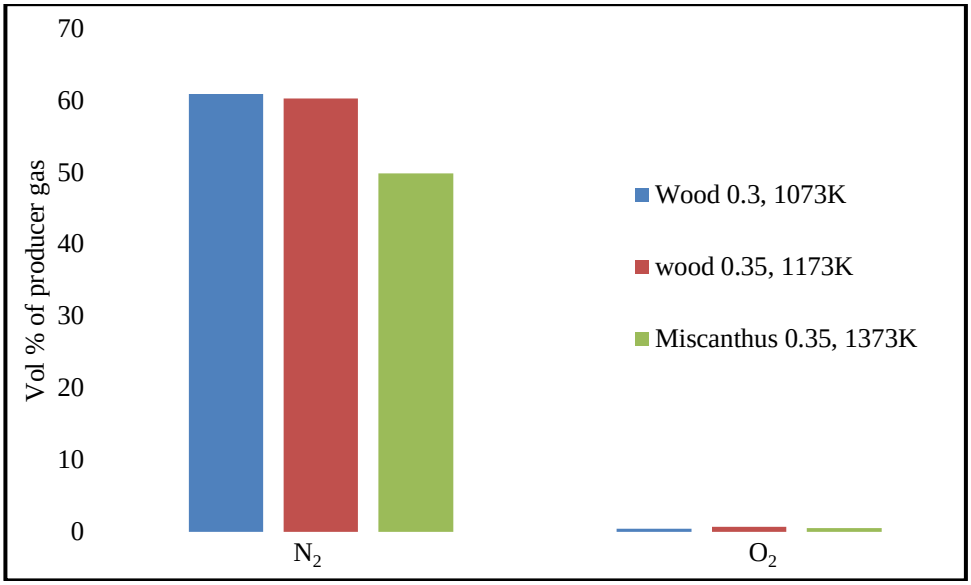

Figure 5.8: Oxygen and nitrogen concentrations with producer gas for different cases.

The set of results shown in Figure 5.8 illustrates the nitrogen and oxygen concentrations (vol%), in the producer gas of different feedstocks .The results are average values recorded during the experiments, and shows that the oxygen is totally consumed or present in negligible amounts, while nitrogen presents in values >50%. The results proves that gasification occured during the experiment.

5.4.4 Total tar produced/100 ml of syngas

Tar produced from the model presents four main tar species, while the data from experiments introduce approximately twenty-six different aromatic and phenolic tar compounds. However, most of these compounds (xylene, indene, pyrene, cresol, xylenol, etc) are negligible, and only a few of them have a considerable amount (Figure 5.5). Further, the basic reasons for choosing four main species in the modelling are that they represent the main tar species (primary, secondary and tertiary) in most cases at 70-95% of the tar produced from downdraft gasifiers. On the other hand, other tar products such as o-Xylene, Methylnaphthalene, and Acenaphthylene have no well-known chemical reaction kinetics although they still have considerable amounts in some cases.

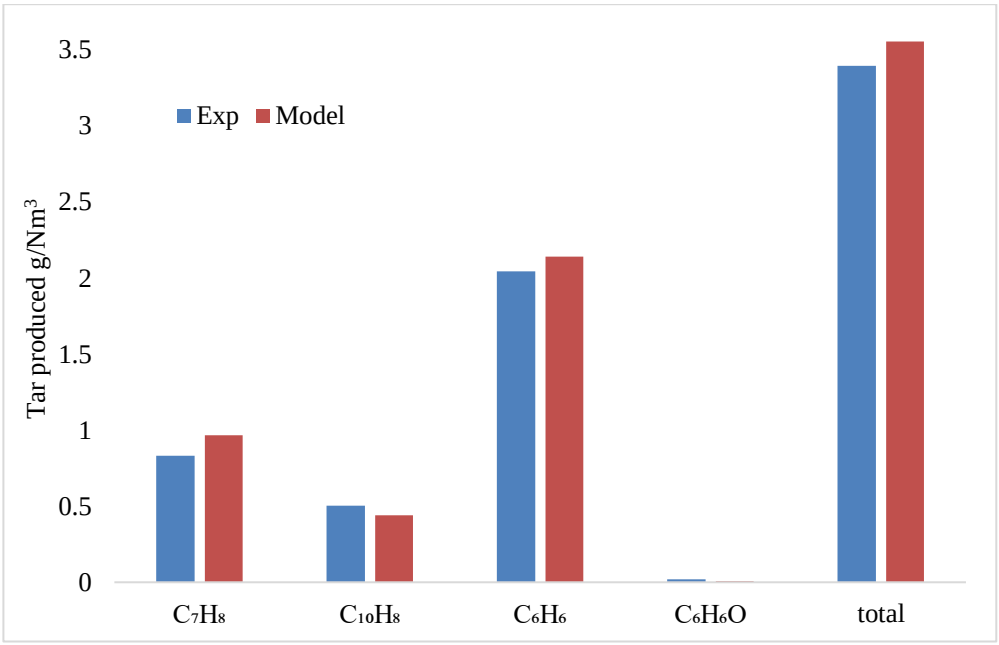

Figure 5.9. Tar species validation for wood gasification ER 0.35.

The set of results presented in Figure 5.9 show the tar species produced during the gasification of wood at an ER of 0.35. Comparisons are made between the results from the numerical model and the corresponding tar collected by the SPA method. Tar amounts are shown in µg/100ml of syngas produced as given in the experimental results and comparison is made at the same gasification temperature of model and experiments (900°C). Experiments were carried out at different gasification temperatures, while the model results showed that wood gasification temperature at ER of 0.35 will be around 1158K = 885°C which can be assumed to be very close to the experimental temperature used in this run ~ (900°C). The results show reasonably good agreement for all the major tar species produced and also for the total tar amount. Phenol concentrations are too small and can be considered as negligible compared to other species because, it is a primary tar compound that tends to be fully cracked and converted to other species at higher temperatures. All tar results have been converted from (µg/100 ml of syngas) to same unit (g/Nm^3), for easy tracking and comparing with other experimental or numerical data as this unit has been used widely in quantifying and estimating tar produced from gasification.

5.4.5 Total tar amount at every run

The experiments were carried out at different temperatures varying between 800 and 1100°C for every feedstock, with three ERs (0.25, 0.3, and 0.35). Tar is collected first in 100 ml of syngas, as already shown in Figure 5.3(b), and every species in the samples is analysed and then the whole amount of tar for every sample is measured and recorded (g_{tar}/feed).

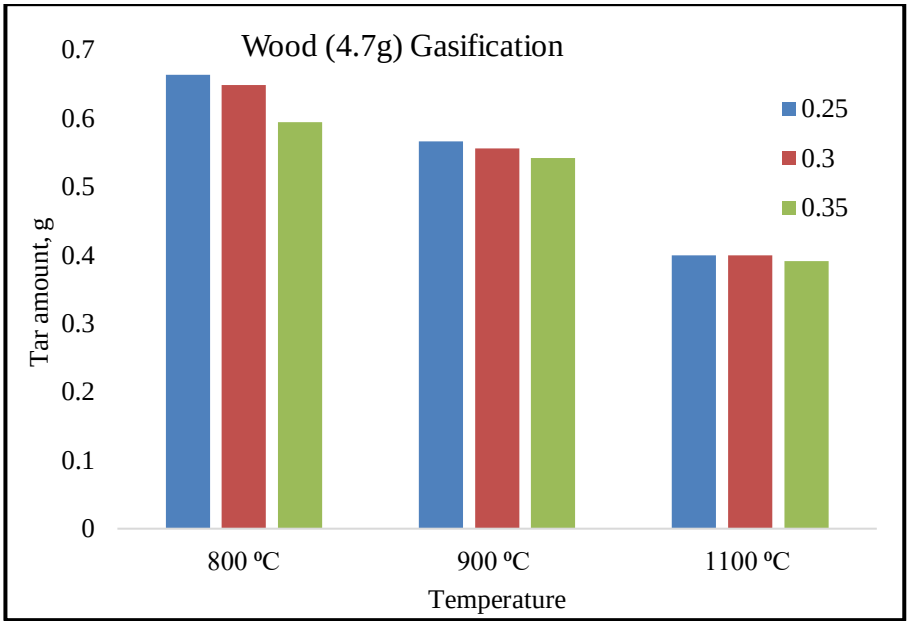

Figure 5.10. Total tar produced per sample with varying ER.

The experimental results in Figure 5.10 reveal a decrease in the tar amount with increasing temperature or ER. Temperature increase encourages cracking reactions and, subsequently, increases their rates which lead to more cracking and a decrease in the tar amount. On the other hand, higher ER leads to an increase in the amount of air (oxidant), which has the same effect of temperature and decreases the amount of tar. This finding also agrees with the previous researches e.g. [73], [14], [54], and [51], who reported a decrease of tar amount with the temperature and/or ER.

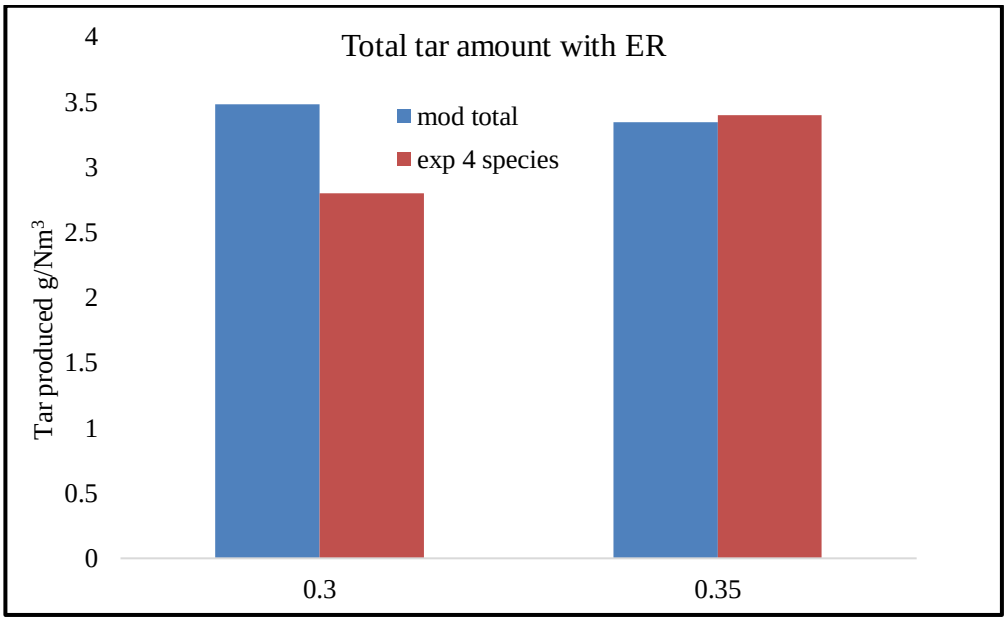

Figure 5.11. Comparison between the model and experiments for the total tar produced.

The results in Figure 5.11 show a comparison between the modelling and experimental data for the total tar produced. The comparison was made for the same ER, with a slight

change in the temperature. For example, at ER 0.3, the model prediction is 842 °C, while the experiment was carried out at 800°C. This might cause slight variations in tar produced as shown in Figure 5.11. However, at ER 0.35, the model and experiment were carried out at a similar temperature as shown in Figure 5.9, and therefore, the results tend to have better agreement. In the experiments, more than twenty different tar species were detected; however, as discussed earlier, only four main tar species were considered.

5.4.6 Sensitivity analysis

After the validation, sensitivity analysis is carried out to study the model ability to work under a wide range of variations and also to optimise the process gasification. The evolution, formation, and destruction of tar species will be tracked along the gasifier height and will be studied with varying moisture content and equivalence ratio.

5.4.6.1 Temperature variations along gasifier with ER/MC

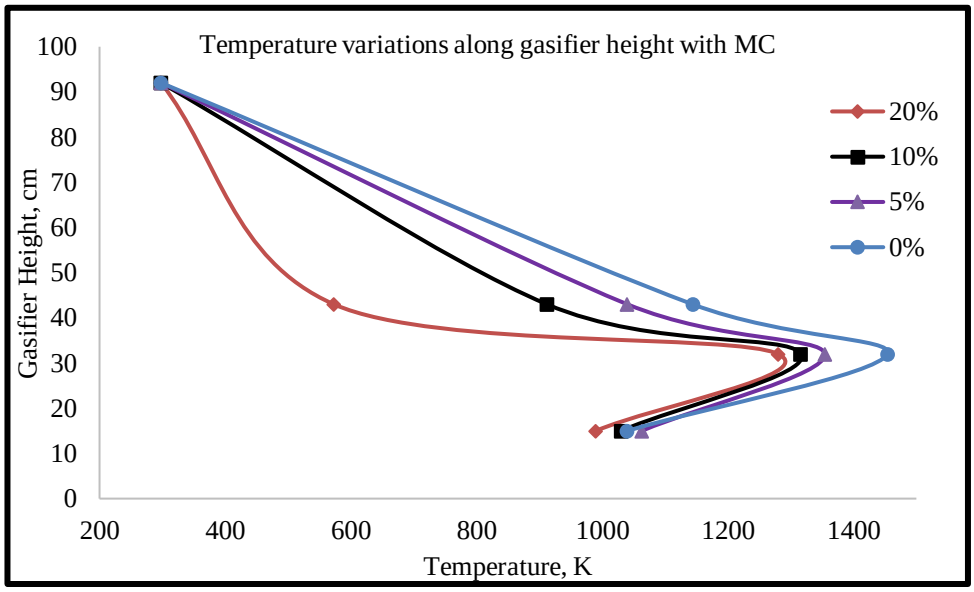

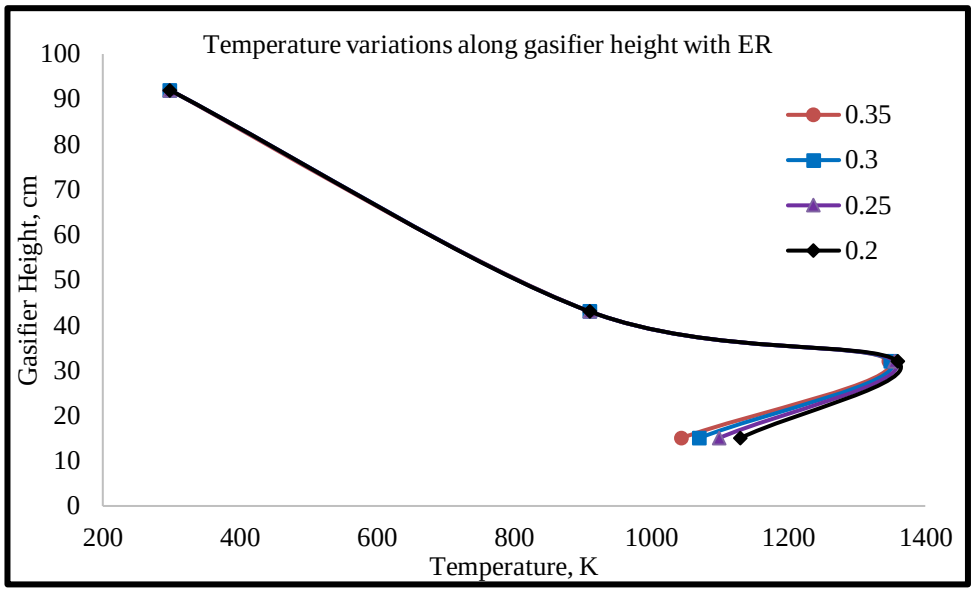

Figure 5.12: Temperature variation along gasifier height levels for wood pellets.

Wood pellets will be used in comparison, with varying all of moisture content and equivalence ratio. The effect of this change on temperature along gasifier is illustrated in Figure 3.14. The results reveal an increase in temperature with ER increase or moisture content decrease. As discussed earlier, the results showed fair agreement with previous works [43].

5.4.6.2 Tar species evolution and formation along gasifier

Tar species tracking from the evolution at the pyrolysis to combustion and reduction zones will be illustrated in the following sections. Tar evolution along the different zones of the downdraft gasifier with a fixed ER will be discussed to study the effect of varying MC on the different tar species formation. On the other hand, the effect of changing ER will also be studied by changing ER with a fixed MC. Different tar species used in the model are traced from their formation in pyrolysis then through the combustion and reduction zones along the gasifier height, depending on the temperature of each zone. The modelling was carried out for rubber wood at a fixed ER of 0.326, and with varying moisture content to study its effect on the tar formation and to obtain the optimum conditions for less tar amount coming with producer gas.

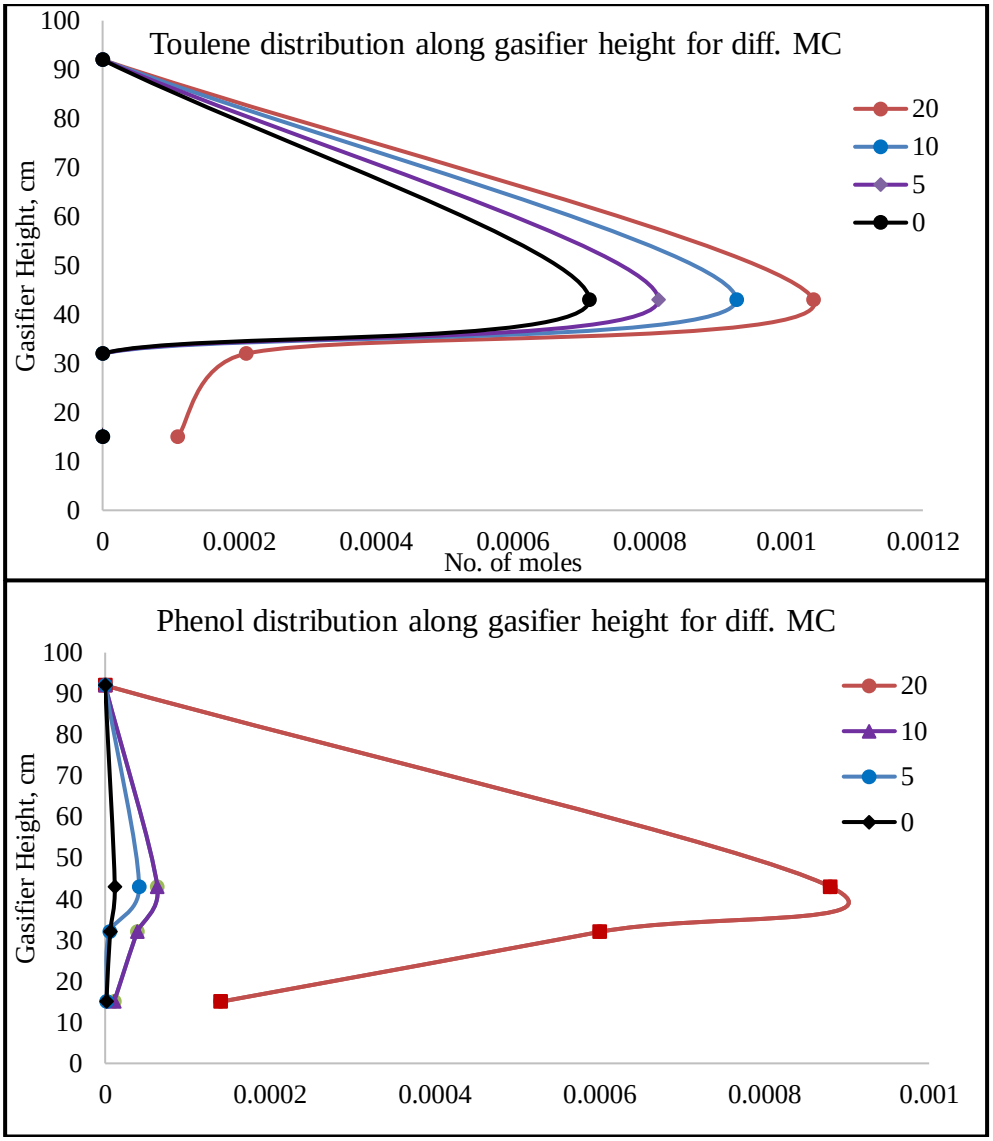

Figure 5.13: Phenol and toluene evolution and formation along gasifier height at different moisture content levels.

Phenol starts forming in pyrolysis and then a reduction in oxidation, then tends to disappear or to exist in very small amounts in producer gas; that is because it is a primary tar compound. Primary tars starts to form at temperatures 673-973 K [51] and, at temperatures above 773 K, primary tars starts re-forming [5], and are converted to secondary then tertiary tars. The temperature profile along the gasifier within different moisture content or equivalence ratio is shown in Figure 3.14. Temperatures of oxidation and reduction zone that are higher than 1173 K are enough to destroy the primary tar species and transform them into other compounds.

Toluene formation along the gasifier has the same trend of phenol, i.e. a higher concentration in the pyrolysis zone, followed by the destruction in the oxidation and reduction zone. Temperatures above 1173 K are enough to crack all the phenol and toluene and convert them into benzene and other lighter species [35], and as a result, toluene concentration at the end of combustion zone is zero, and no toluene formation at the

reduction zone was found. Additionally, the standalone dot at the end of curve is displayed as no toluene formed at this case.

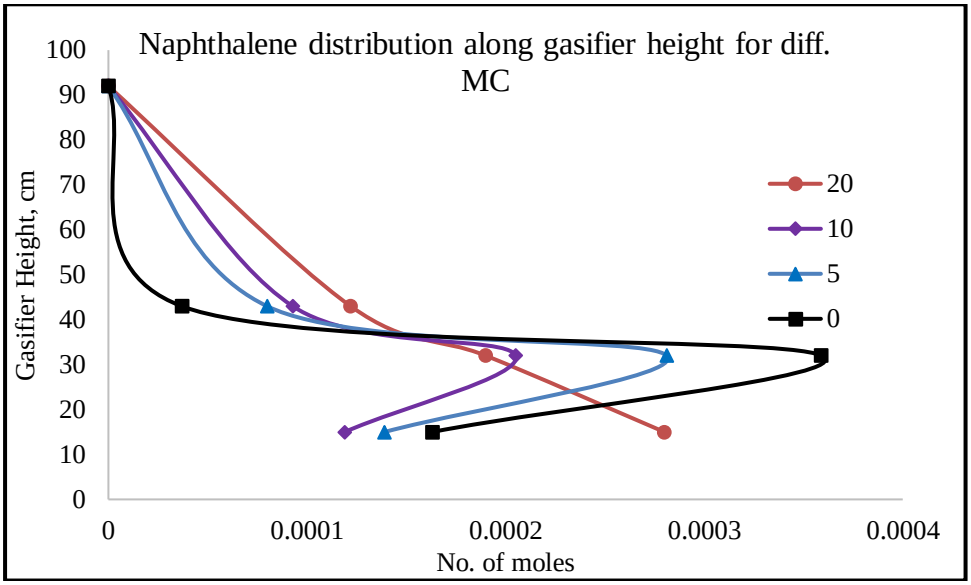

Figure 5.14: Naphthalene evolution and formation along gasifier height at different moisture content levels.

Naphthalene formation follows a different trend from the other species. It is formed and is presented in considerable amounts in producer gas. Small amounts are produced during pyrolysis because it is a tertiary tar which requires higher temperatures to present and form. Higher temperatures in oxidation zone >1300K are favourable for naphthalene formation which starts conversion for temperatures greater than 1300K and achieves total conversion at 1600 K [60]. Based on reactions (2 and 3) in Table 5.4, naphthalene is converted to char, H_2, CO and benzene. Those reactions tend to take place in the combustion and reduction zones; however, it is more likely to happen in the reduction zone because of the presence of water vapour. Higher concentration of naphthalene in the oxidation zone is mainly a result of the conversion of lighter species (phenol and toluene) and also because of oxidation temperature which is in the ideal range of naphthalene formation and it never exceeds the destruction temperatures (>1600 K) [60].

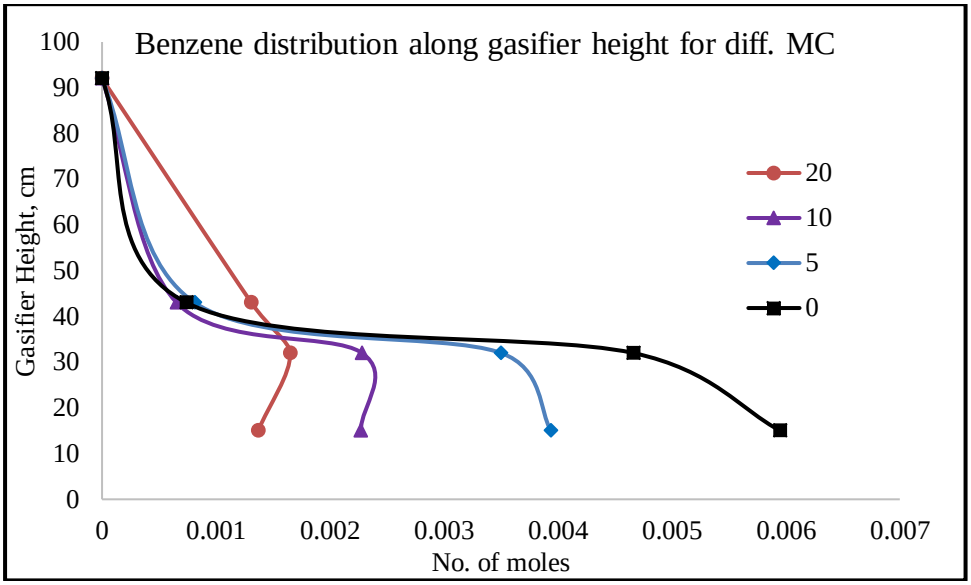

Figure 5.15: Benzene evolution and formation along gasifier height at different moisture content levels.

Benzene has the highest portion of tar species, which is usually greater than 37% from the weight of total tars produced [5]. The results show a different trend of benzene formation and evolution from other species. Small amounts are formed in pyrolysis and then start to increase in the oxidation and reduction zones. Oxidation reactions tend to destroy benzene and convert it to CO, CO_2, CH_4, H_2 and H_2O. On the other hand, these reactions depend on the oxygen amount and have small reaction rates which make it unlikely that it will take place in the oxidation zone, and in fact, will not take place in the reduction zone where no oxygen is present. Other tar species (phenol, naphthalene, and toluene) are converted under this temperature range to benzene and other compounds. In addition, benzene conversion requires very high temperatures to take place, 1400-1700 K [60]. The temperature along the gasifier shows the maximum temperature for the oxidation zone <1500 K, which is not enough to convert all benzene to other species. All the previous factors tend to increase the amount of benzene along the gasifier height with an increase in temperature which agrees with the results of [35].

Higher moisture content levels tend to increase water vapour and hydrogen which further favour the tar formation reactions. Also, higher moisture levels tend to reduce the temperature along the gasifier which has a great effect on tar destruction which is favourable in higher temperatures.

On the other hand, the results shown in Figure 5.16, andFigure 5.17) demonstrate the effect of the equivalence ratio on different tar species evolution along different zones of downdraft gasifier. Rubber wood was used as feedstock with a moisture content of 10%. The same trend shown with varying moisture content also noticed with equivalence ratio. All tar species' evolution starts from pyrolysis.

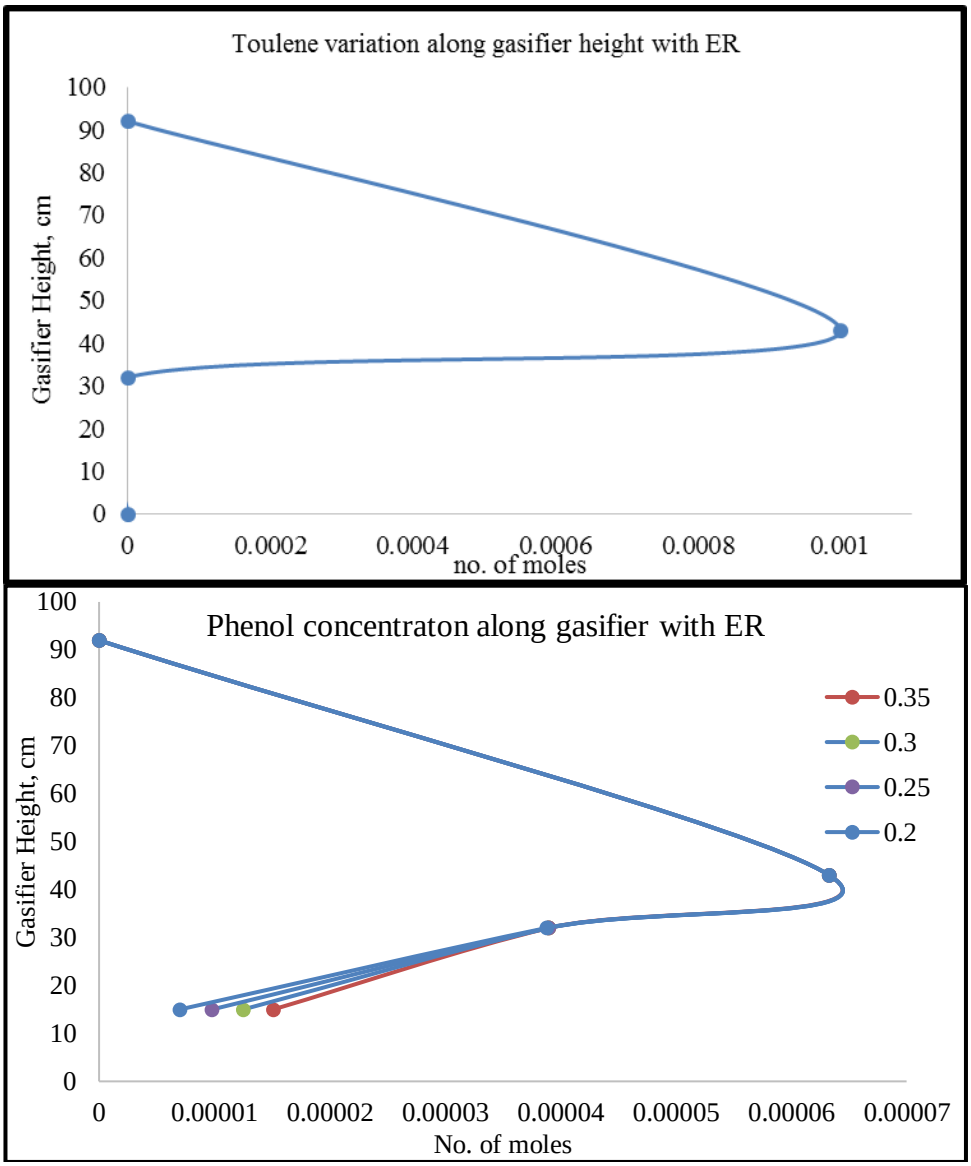

Figure 5.16: Phenol and toluene formation along gasifier height at different ER.

Toluene behaviour is not affected by varying ER. As moisture content is fixed, the highest amount of toluene is formed during pyrolysis and is totally destroyed and converted to other compounds in the oxidation zone. This is because moisture content is the major factor affecting the pyrolysis temperature and whether all tar compounds are derived through these relationships, it depends on temperature (Table 5.3). Therefore, its amount will remain the same in pyrolysis. The amount of all the four tar species used in the model is the same in pyrolysis. Oxidation temperature for different moisture content levels is greater than 1173

K, which is enough to convert all the toluene amounts to other tar species and small amounts of lighter compounds (CO, H_2, and CH_4). Phenol follows the same trend as toluene with small amounts starting to form again in the reduction zone as the temperature drops.

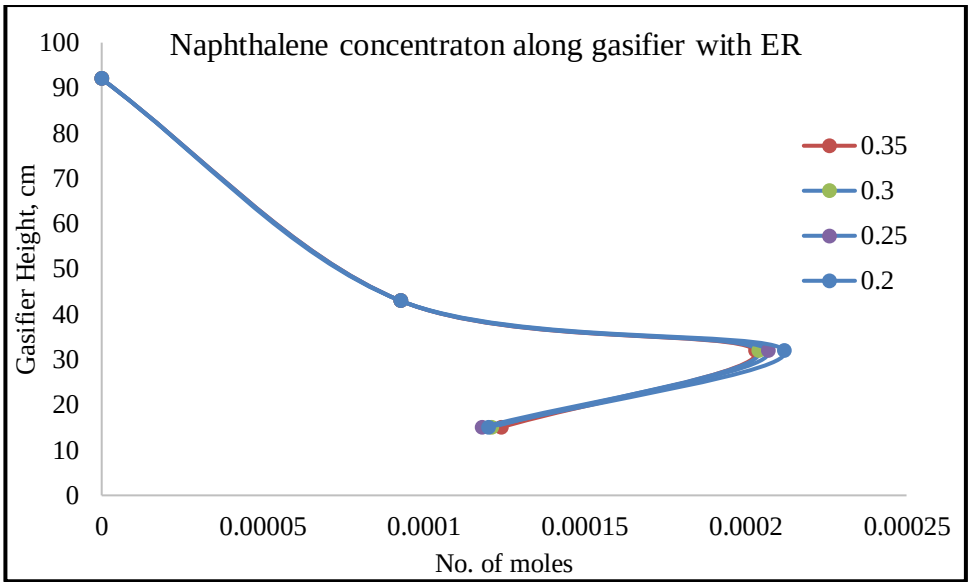

Figure 5.17: Naphthalene evolution and formation along gasifier height at different ER.

Naphthalene formation was found to have relatively high amounts compared to toluene and phenol, following the same trend as changing with the moisture content effect. The temperature of oxidation and reduction has a major effect alongside the amount of water vapour, phenol, and toluene that are converted to naphthalene depending on their amount and reaction rates.

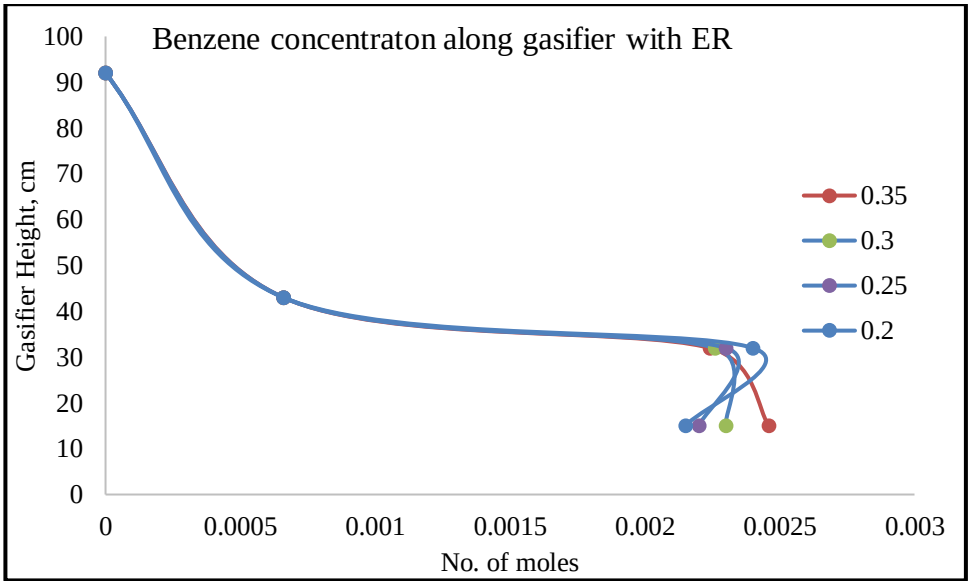

Figure 5.18: Benzene evolution and formation along gasifier height at different ER.

Benzene has the biggest portion of tar produced during biomass gasification. The results of changing moisture content or equivalence ratio show the same trend and find good agreement with other previous works such as [60], [68], [52] and [66] that conclude an increase of benzene with increasing ER or decreasing MC. For benzene, as moisture content decreases, the temperature increases, which is favourable to converting other gas and tar species to benzene. So benzene increases with the temperature which found good agreement with ([60], [73] and [35]). They showed that benzene formation increases with the temperature, and also benzene destruction starts after 1400K, which is almost the highest temperature in the current results at the oxidation zone at 0% MC.

5.5 Conclusion

Tar formed during gasification limits the direct use of syngas and requires additional removal techniques. The modelling of tar formation, conversion and destruction along a gasifier could give a wider understanding of the process and help in tar elimination and reduction. However, tar complexity, which contains usually hundreds of species, makes the modelling process hard and computationally intensive, because the chemistry of the formation and the combustion of many species have not yet been fully studied.

In this work, a detailed kinetic model for the evolution and formation of tar from downdraft gasifiers was built. The model incorporated four main tar species (benzene, naphthalene, toluene, and phenol) with a total of eighteen different kinetic reactions implemented in the code for every zone. Experimental work was carried out to validate the results of the kinetic code and found a good agreement. The experiments were carried out at three different equivalence ratios (ER) and at three different temperatures (800, 900, and 1100 ^{0}C). Sensitivity analysis was carried out by the kinetic code to optimise the working parameters of a downdraft gasifier that led to a higher calorific value of syngas. The results reveal that a tar evolution model is more accurate for wood biomass materials and that using ERs around 0.3, and moisture content levels lower than 10% lead to the production of higher value syngas with lower tar amounts.

The current model is used to address the evolution of different gas species, char and tar species along the gasifier, starting from the devolatilization process to combustion and reduction. Modelling, as well as experiments carried out, shows good agreement and proves model stability and ability in order to predict tar species produced from wood downdraft gasifiers. The four main tar species were found to be a good representative for tar evolution in downdraft wood gasifiers, and in most cases, they form 50-90 % of total tar produced.

Chapter 6 CFD Modelling for Gas and Tar Species in a Downdraft Gasifier

6.1 Introduction

The kinetic modelling of biomass gasification was presented in the previous Chapters (3 and 4). The kinetic model studied a wide range of variables and their effect on the gasification process, syngas composition and tar content. However, the kinetic model has some limitations in regard to the gasification process. The interactions between the solid and gas phases reactions during the gasification process require clear understanding and cannot be covered during the kinetic modelling. Gasifier design also has a strong effect on the syngas composition and quality. Kinetic models depend on a detailed chemical reaction that does not depend on reactor geometry. These limitations in the kinetic models are assessed through a Computational Fluid Dynamics (CFD) model, which involves a combined solution of the transports of mass, momentum, energy, turbulence and hydrodynamics of the flow. It can give a clear understanding of interactions between different phases and reactions inside of the gasifier. As discussed earlier, few works have been used to simulate downdraft biomass gasifiers and possess limitations regarding feedstocks and syngas composition validation([18],and [74]) . CFD modelling techniques face multiple challenges within the area of biomass gasification/combustion [75], like feedstocks' variety, different working parameters change, and tar modelling. On the other hand, it is a powerful tool for studying all parameters included in the process along the gasifier. The limitations of zero- and one-dimensional equilibrium and kinetic models makes CFD models more interesting for the data and results. On the other hand, experimental set-up and time/cost analysis makes CFD models crucial and is able to offer a deeper understanding within the field of research and building fundamental aspects of the gasification processes design.

ANSYS FLUENT software will be used for the current work computational fluid dynamics (CFD) simulation, where a 20 kW, 2D, downdraft biomass gasifier is used in the simulations. The gasifier has been designed and validated based on the kinetic model (Chapter 3) [16]. The model is composed of four main zones: drying, pyrolysis, combustion and gasification. The prediction process is integrated, starting from drying and volatiles break up during temperature rise in pyrolysis zone, followed by combustion and reduction. 20 different kinetic rate reactions are implemented with the ANSYS software to accommodate volatiles break up and other reactions involved in the process. The set of combustion/gasification reactions has been implemented using previous 2D CFD modelling

[18], while the volatile break up and other tar combustion/gasification reactions will be further illustrated in detail employing different references.

The model will be validated using different feedstocks. Furthermore, different biomass and agricultural feedstocks will be used to address optimum working parameters and effect of equivalence ratio on syngas composition. Detailed tar species evolution and formation will be implemented in the code and will be validated.

To the best of the author's knowledge, previous downdraft gasification models have been used to discuss one feedstock, most often focusing on woody materials, and giving full concentration to producer gas composition yield. The current model's novelty is shown by using different biomass, waste, and agricultural materials. Furthermore, the model presents detailed and selected tar species formation along gasifier, which has never been discussed in any published works related to downdraft gasifiers.

6.2 Model description

A schematic diagram of the meshing file is shown in Figure 3.1. The model is developed as 2D, using air as a gasifying agent that is fed through the nozzles attached to the combustion zone. The model design was discussed in detail earlier in Chapter 3. The model is also shown in the meshing file (Figure 6.1), evidencing that the typical mesh distribution has been used inside of the domain of the gasifier geometry.

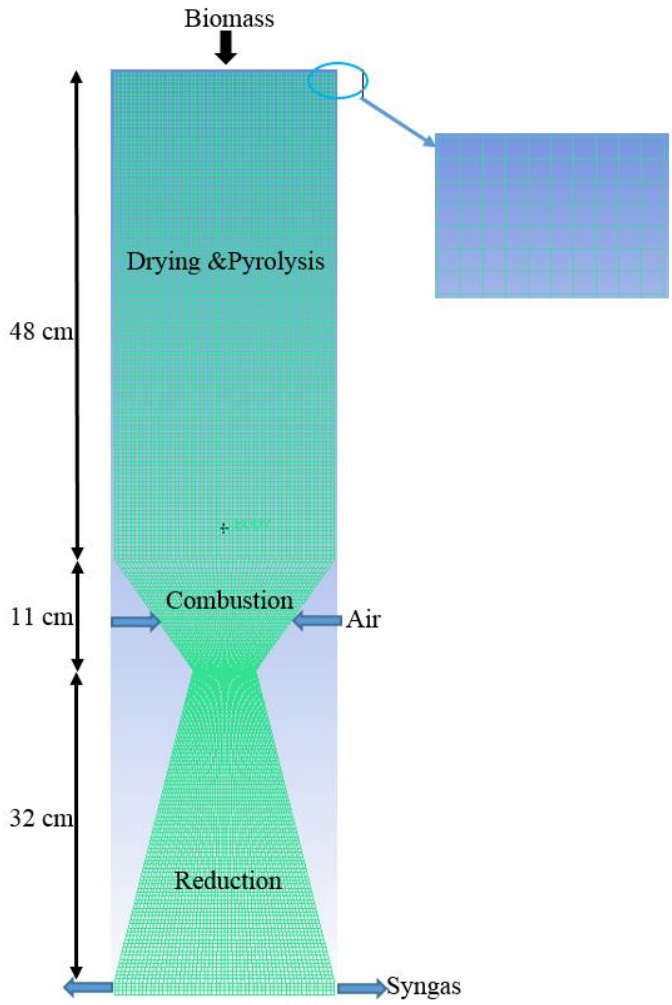

Figure 6.1: Mesh file of the 2D gasifier.

6.2.1 Governing equations

Governing equations include the energy, mass and momentum conservations, and species transport reactions for all species. Viscous and radiation discrete ordinate model are also included and solved with the governing equations. All the equations are solved under steady-state and turbulence conditions depending on a set of reactions in ANSYS fluent [106] and also on the specific rate reaction kinetics which are implemented in the code to match the gasification process.

Mass conservation:

$$\frac{\partial \rho}{\partial t} + \frac{\partial \left(\rho u_i\right)}{\partial x_i} = S_i \tag{6.1}$$

Momentum conservation:

$$\frac{\partial \left(\rho u_i\right)}{\partial t} + \frac{\partial \left(\rho u_i u_j\right)}{\partial x_j} = -\frac{\partial p}{\partial x_i} + \frac{\partial \tau_{ij}}{\partial x_j} + \rho g_i + F_i \tag{6.2}$$

The stress tensor τ_{ij} equation

$$\tau_{ij} = \mu\left[\left(\frac{\partial u_i}{\partial x_j} + \frac{\partial u_j}{\partial x_i}\right) - \frac{2}{3}\nabla.u_{ij}I\right] \quad (6.3)$$

Where S_i the mass added to the continuous phase from the dispersed second phase, ρg is the gravitational body forces, F_i is the external body forces, τ_{ij} is the stress tensor, and I is the unit tensor

The Reynolds Averaged Navier-Stokes (RANS) is derived using time averaging through equations ((6.1)-(6.3) [106]. The Reynolds stresses employed in the equations are modelled through the Boussinesq hypothesis that depends on the turbulence model. Turbulence kinetic energy, k and its dissipation rate ϵ are calculated through the following equations and representing the standard k-ϵ viscosity model.

$$\frac{\partial}{\partial x_i}(\rho k u_i) = \frac{\partial}{\partial x_j}\left[\left(\mu + \frac{\mu_t}{\sigma_k}\right)\frac{\partial k}{\partial x_j}\right] + G_k + G_b - \rho\varepsilon - Y_M + S_k \quad (6.4)$$

$$\frac{\partial}{\partial x_i}(\rho \varepsilon u_i) = \frac{\partial}{\partial x_j}\left[\left(\mu + \frac{\mu_t}{\sigma_\varepsilon}\right)\frac{\partial \varepsilon}{\partial x_j}\right] + C_{1\varepsilon}\frac{\varepsilon}{k}(G_k + C_{3\varepsilon}G_b) - C_{2\varepsilon}\rho\frac{\varepsilon^2}{k} + S_\varepsilon \quad (6.5)$$

Where σ_k and σ_ε are the turbulent Prandtl numbers for k, and ϵ respectively. G_b is the Turbulence kinetic energy due to buoyancy, and G_k is the Turbulence kinetic energy due to mean velocity gradients, Y_M is the Contribution of the fluctuating dilatation in compressible turbulence to the overall dissipation rate, S_k, and S_ε are the Source terms for the kinetic energy, and Source terms for rate of dissipation, The values of constants used are $C_{1\epsilon}$=1.44; $C_{2\epsilon}$=1.92; σ_k=1.0; σ_ϵ=1.3 [22].

The species transport equation is described as

$$\frac{\partial}{\partial t}(\rho Y_i) + \nabla.\left(\rho\vec{u}Y_i\right) = -\nabla.\vec{J}_i + R_i + S_i \quad (6.6)$$

Where Y_i is the mass fraction of species, R_i is the Net rate of production of species i by chemical reaction, and J_i is the Diffusion flux of species i.

While the diffusion flux for turbulent flow is represented by the following form.

$$\vec{J_i} = -\left(\rho D_{i,m} + \frac{\mu_t}{Sc_t}\right)\nabla Y_i - D_{T,i}\frac{\nabla T}{T} \quad (6.7)$$

$$Sc_t = \frac{\mu_t}{\rho D_t} \quad (6.8)$$

Where $D_{i,m}$ is the mass diffusion coefficient for species *i* in the mixture, and $D_{T,i}$ is the thermal diffusion coefficient for species *i* in the mixture, D_t turbulent diffusivity, and Sc_t is the Schmidt number for turbulent flow.

Biomass particles are modelled by discrete phase model; DPM (Lagrangian approach). The model considers particles trajectory by a continuous phase of fluid. The interaction between particles is taken into account considering heat and mass transfer as the main term in the governing equations. Particle trajectory is written and calculated by integrating force balance on a particle where this balance equates particle inertia force with other forces acting on the particle as described in equations (6.9)-(6-11).

Force balance:

$$\frac{\partial \overrightarrow{u_p}}{\partial t} = F_D\left(\vec{u} - \vec{u}_p\right) + \frac{\vec{g}\left(\rho_p - \rho\right)}{\rho_p} \tag{6.9}$$

Where $F_D\left(\vec{u} - \overrightarrow{u_p}\right)$ is the drag force per unit particle mass.

$$F_D = \frac{18\mu C_D \,\mathrm{Re}}{24\rho_p {d_p}^2} \tag{6.10}$$

Where C_D is the drag coefficient, *Re* is Reynolds number, and μ is the viscosity. The temperature of particle T_p, convective heat transfer, and the absorption/emission of radiation of the particle surface are related by the following equation.

$$m_p c_p \frac{dT_p}{dt} = hA_p\left(T - T_p\right) + \varepsilon_p A_p \sigma\left({T_R}^4 - {T_p}^4\right) \tag{6.11}$$

Where *h* is the heat transfer coefficient, A_p is the particle surface area, and T_R is the radiation temperature.

6.2.2 Volatiles break-up approach and biomass decomposition

Due to a temperature rise from the oxidation zone, biomass goes through the drying process first, which allows all of the moisture to vaporise. After drying, the devolatisation of biomass occurs [32] by which it decomposes into volatiles and char. These materials then further react with one another to form char and volatiles again, as was illustrated earlier in Chapter 3 ([39], and [25]). Volatiles break up approach in this work depends on an equilibrium model, as shown in equation (6.13) besides an assumption derived from experimental data, as explained below [73].

$$Biomass \rightarrow Volatiles + moisture + Tar + Char + ASH \tag{6.12}$$

$$Volatiles \rightarrow x_1\,CO + x_2 CO_2 + x_3 CH_4 + x_4 H_2 \quad (6.13)$$

Based on the volatiles ultimate analysis data, calculated from [5] and [106], an elemental mass balance is carried out to calculate the mole fraction of every species. The model proposed by [52], which calculates the mass fraction of every species produced during biomass pyrolysis based on temperature, is also followed in this assumption to calculate CO concentrations. The other gas species are calculated from the mass balance between the volatiles and pyrolysis products. The volatile break up reaction and the stoichiometric coefficients derived from equations (6.12), and (6.13) are added into ANSYS code to start the simulation process.

6.2.3 Gas phase reactions and char surface reactions

The set of reactions used to represent the oxidation and reduction reactions are based on the recommendations provided by [18], where a set of reactions were first used and then built up a modified 2D model based on a series of revised kinetic rate reactions (Table 6.1, and Table 6.2). The current model is further enhanced by implementing the detailed chemical reactions of tar species formation and evolution starting from devolatilization, oxidation and reduction (Table 5.4). The model was further enhanced and showed more stability using 20 different rate reactions for the evolution and formation of different gas species and detailed tar species, as reported in Chapter 5.

Table 6.1: Oxidation zone reactions

	Reactions	*A*	*E* (kJ/mol)	*T*. exponent	Ref.
1	$2C+O_2 \rightarrow 2CO$	147000	112.99	1	[107]
2	$CO+0.5O_2 \rightarrow CO_2$	1.0e+10	126	0	[76]
3	$2H_2+O_2 \rightarrow 2H_2O$	2.2e+09	109	0	[76]
4	$CH_4+2O_2 \rightarrow CO_2+2H_2O$	4.4e+11	126	0	[108]

Table 6.2: Reduction zone reactions

	Reactions	*A*	*E* (kJ/mol)	*T*. exponent	Ref.
5	$C+CO_2 \rightarrow 2CO$	8.268	188.2	1	[107]
6	$C+H_2O \rightarrow CO+H_2$	8.268	188.2	1	[107]
7	$0.5C+H_2 \rightarrow 0.5CH_4$	8.8894e-06	67.16	1	[107]
8	$CH_4+H_2O \rightarrow CO+3H_2$	3e+08	125	0	[76]
9	$CO+H_2O \rightarrow CO_2+H_2$	2.35e+10	288	0	[109]
10	$CO_2+H_2 \rightarrow CO+H_2O$	1.785e+12	326	0	[109]

6.2.4 Boundary conditions

Two feedstocks are initially used for the model validation, followed by the investigation of different feedstocks from biomass to agricultural waste/residues, as stated earlier in Chapters 3 and 4, to study the working conditions and how they affect the producer gas quality. Rubber wood and neem with their ultimate and proximate analysis data are used for validation, as illustrated in Table 6.3. The boundary conditions used in the model are illustrated in detail in Table 6.4.

Table 6.3: Feedstocks data used in validation

		Rubber wood [25]	Neem [24]
Ultimate data %	C	50.6	45.1
	H	6.5	6.0
	O	42	41.5
	N	0.2	1.7
Proximate data %	Volatiles	81.1	81.75
	Fixed Carbon	19.1	12.65
	Ash	0.7	5.6
	Moisture	18.5%	10

Table 6.4: Boundary conditions used in validation.

	Rubber wood	Neem
Equivalence ratio	0.326	0.3
$\dot{m}_{fuel}$, kg/s	0.002027776	0.002498556
$\dot{m}_{air}$, kg/s	0.0011356	0.002053454
Air *T*, K	600	600
Biomass *T*, K	300	300
Gauge *P*, outlet	0	0
Backflow *T*, outlet	1000	1000

The model is a 2D model for a 20-kW downdraft gasifier following the design illustrated in the previous Chapter 3. Two air nozzles are used for the air injection into the combustion zone, so that the amount of air illustrated in Table 6.4 is divided in two at the model for every air inlet.

Biomass is fed from the top of the gasifier as a mass flow rate input boundary condition, while the total number of particles are tracked through a Lagrangian approach (Discrete

phase). The discrete phase model follows the Euler-Lagrange approach, where one phase representing fluid is solved by the Navier-Stokes equations presented above, while the second phase representing dispersed particles is solved by tracking specific number of particles through the flow field. Both phases exchange mass, momentum and energy within one another. The number of particles dispersed due to turbulence is predicted using a stochastic tracking model (Random walk model). The model includes the effect of turbulence on the particles trajectories or tries, which is injected in every cell of mesh [106]. The DPM proved good stability and better prediction for biomass gasification as illustrated in the earlier works, e.g. [110], [111], [20], [98], and [112].

6.2.5 Simulation and convergence

Solution methods and residuals control are all concluded in Table 6.5.

Table 6.5: Solution methods followed in the simulation

Phases	Euler-Lagrangian
Models included	Turbulence k-epsilon 2 equations
	Radiation Discrete ordinates
	Species Transport for Finite rate/Eddy transport kinetic model
Solution methods	Pressure-velocity coupling, Coupled
	Momentum and Energy; 2^{nd} order upwind discretization scheme
	Pressure discretization scheme, PRESTO
Residuals level	10^{-3} for all variables, for Energy and radiation 10^{-6}

The steady state solution of the governing equations of two phases is carried out by an implicit finite volume method. Pressure velocity coupled algorithm is used where it comprises coupled solution for the momentum and pressure-based equations. This solving criterion gives a higher rate of solution convergence [106]. The spatial discretization pressure was solved by the PRESTO (PREssure STaggering Option) method, which is used as a default for multiphase simulations or volume of fluid (VOF) models with mixtures or more than one fluid in the system. The PRESTO system is more applicable for all models and gives more convergence in the solution. Energy, momentum, gas species, and discrete ordinates under spatial discretization uses a second order upwind scheme for a more accurate and stable solution. Convergence criteria for residuals is set as default, where all the relaxation factors are set to 10^{-3}, while the energy and discrete ordinate radiation are set as 10^{-6}, providing stable, accurate solutions. The particles were tracked cell by cell through the

volume where the devolatilization, combustion and gasification takes place with other specified rate reactions.

6.3 Results and discussion

Initially a CFD model is established according to the above simulation setup. A mesh independency test is carried out to study the mesh stability and then to select the most suitable grid in the simulations. Model validation is then carried out using the selected mesh for two different feedstocks in order to study the model compatibility to simulate downdraft air gasifiers. The model is then further used to study the gasification process for different feedstocks, and to get the optimum working parameters to lead to higher production of valuable syngas. Furthermore, four main tar species are implemented within the materials in the code in order to study their evolution, formation and destruction along the gasifier. The results of tar formation will be validated with experimental data and with the results from the kinetic code (presented in Chapter 5). The novelty of the current model is clearly shown by its applicability for using different feedstocks. Previous CFD models used to discuss one feedstock usually focus on wood biomass materials, such as [20], and [80]. The model is able to simulate the gasification of biomass, agricultural waste/residues feedstocks, and their results are compared/validated using the kinetic code. Furthermore, a new aspect of the current model, which has never been discussed in any earlier research, is its integration with the formation of the selected detailed tar species.

6.3.1 Mesh independency test

A mesh independency test is carried out first, considering five different mesh sizes with cells numbers of 22320, 39744, 90770, 203980, and 319780. Producer gas composition, and a higher heating value of rubber wood gasification is shown in Figure 6.2.

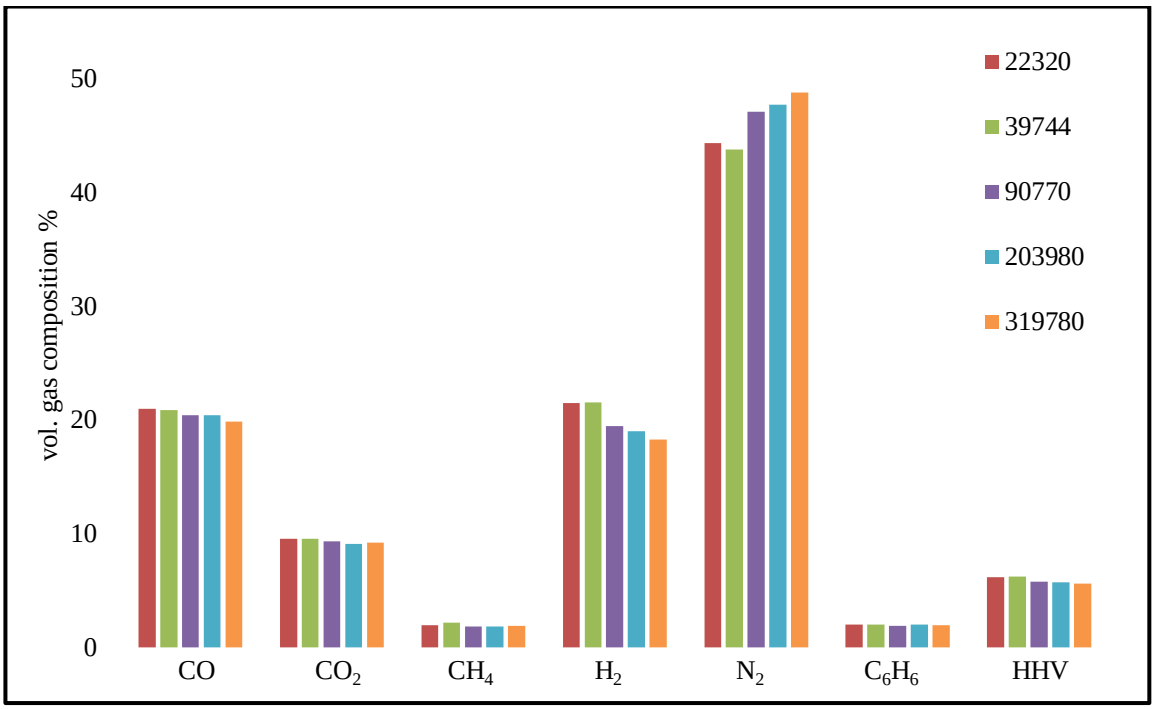

Figure 6.2: Syngas composition at different mesh sizes

The results show slight variations in the gas compositions for all of the grids used. However, starting from 90770 cells, the gas composition does not change much, and the heating value shows almost the same. As a result, the mesh size of 90770 is selected for further simulations presented in the current work, as the higher mesh density is usually time consuming and, as per the test above, would not provide any further benefit. Tar is first represented by a single compound (benzene) and will be further converted to detailed species (benzene, naphthalene, toluene, and phenol).

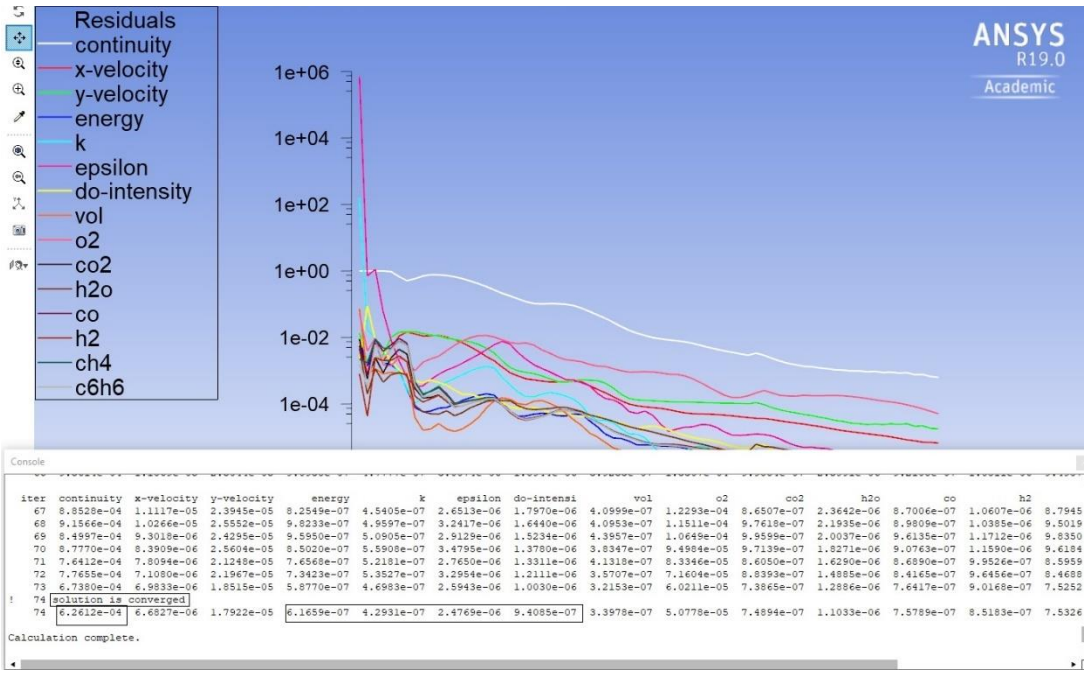

Figure 6.3: Residuals convergence criteria.

The set of data shown in Figure 6.3 illustrates the residuals convergence where the solution finally converges after a small number of iterations smoothly. All of the equations show convergence below 10^{-3}, while the energy and radiation go below 10^{-6}.

6.3.2 Model validation

Two feedstocks are used first to validate the current model: Rubber wood [25], and Neem [24]. Their proximate and ultimate data are shown in Table 6.3.

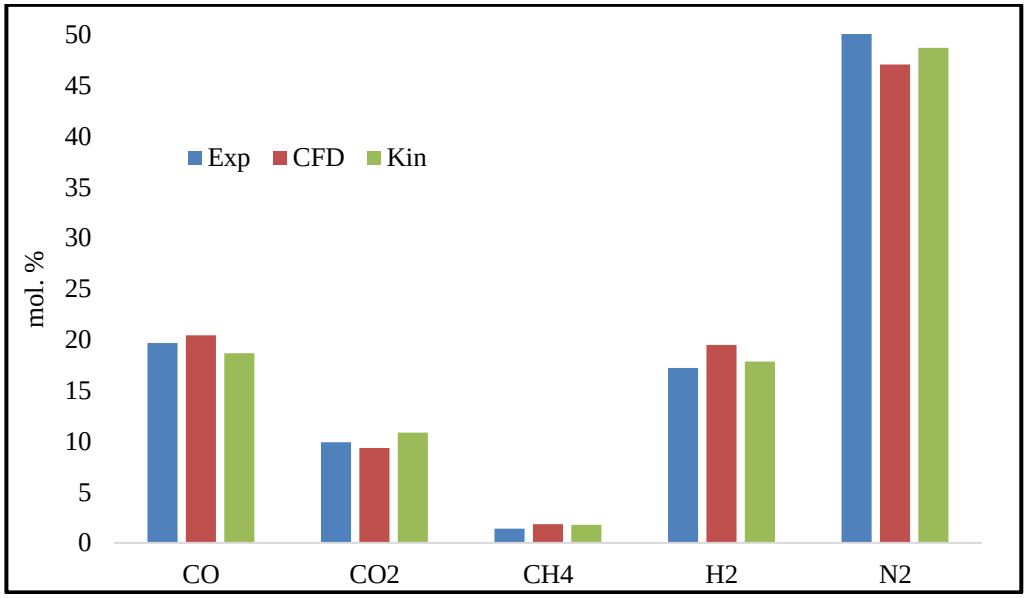

Figure 6.4: Rubber wood comparison.

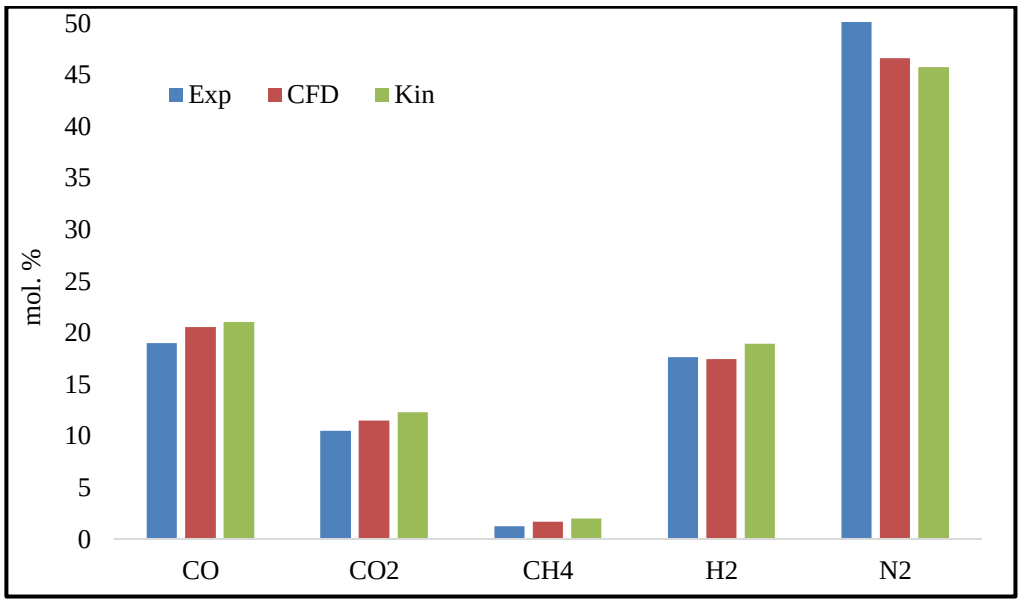

Figure 6.5: Neem comparison.

The results shown in Figure 6.4, and Figure 6.5 demonstrate the model results for the two feedstocks, and its comparison with experimental and kinetic code data. Rubber wood was gasified at ER of 0.326 and MC of 18.5%, while the neem gasification was gasified at ER

of 0.3 with MC of 10%. The results show the dry gas composition at gasifier outlet for the three data. Both feedstocks show fairly good agreement for all of the gas compositions with the kinetic code (Chapter 4) and the experiments ([25] , and [24]). A negligible variation in some gas composition data is found, which proves the current model's stability to simulate the working process of downdraft biomass gasifiers.

6.3.3 Rate of reactions

Different reactions implemented in the code are discussed in this section, starting from the volatiles decomposition and moving onto the other char combustion and gasification reactions.

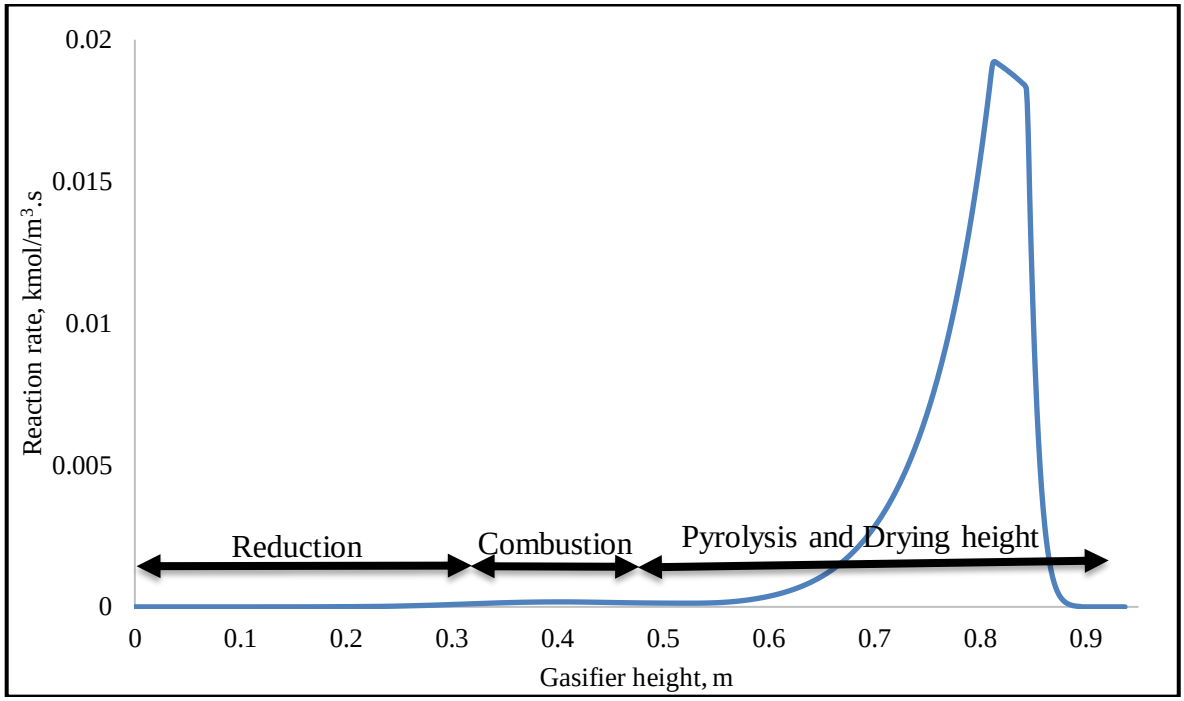

Figure 6.6: Volatiles decomposition reaction rate along centreline of gasifier.

Pyrolysis starts after the drying process, as shown in Figure 6.6. Volatiles decomposition then starts to reach its peak; as biomass is fed towards combustion, the rates of volatiles decomposition decrease until reaching zero, slightly above oxidation zone (~ 55cm from gasifier bottom) where other reactions are taking place. Biomass decomposition into char, tar, and gases takes place in the pyrolysis zone, as shown in Figure 6.6. Most often, all decomposition takes place 40 cm above the combustion zone, which demonstrates that all biomass decomposition takes place in the pyrolysis zone.

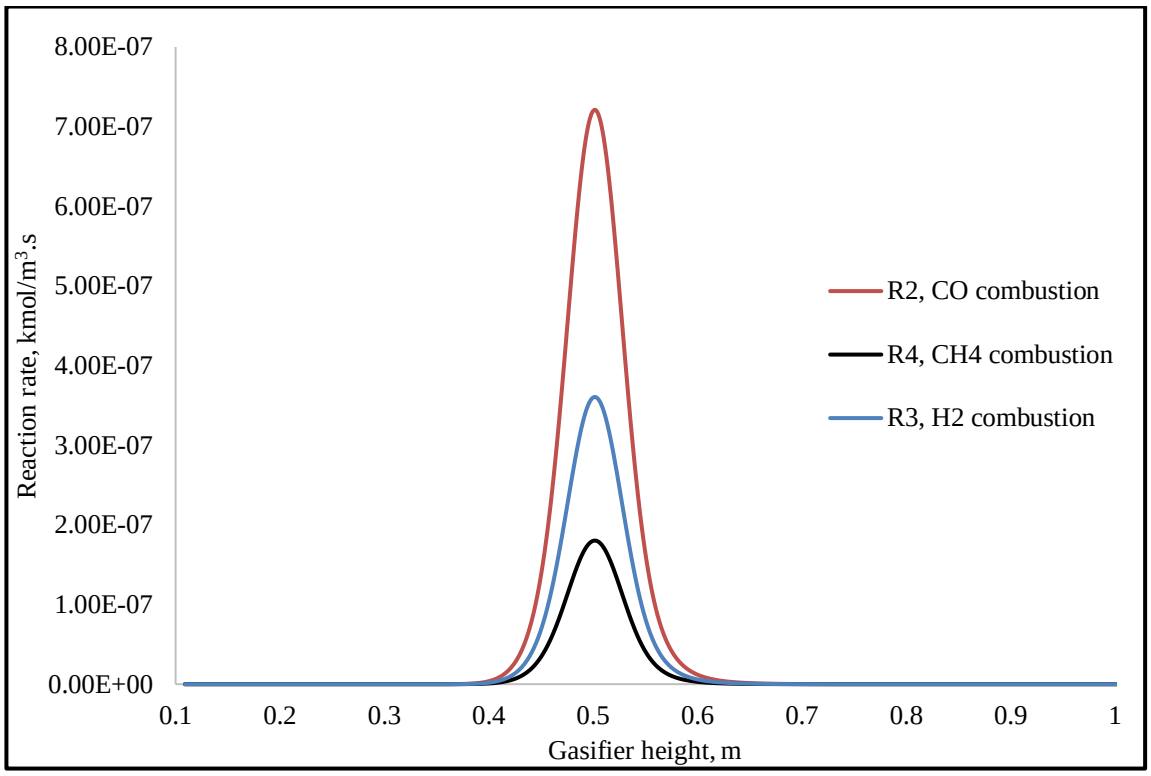

Figure 6.7: Combustion reactions rate along gasifier.

Combustion reactions takes place in the oxidation zone, as illustrated by Figure 6.7. The reaction rates of CO, CH_4, and H_2 combustion is noted for rubber wood gasification at ER 0f 0.326. Oxidation reactions are exothermic, generating heat for the whole process of gasification, leading to biomass decomposition in pyrolysis, and further to reduction reactions in the gasification zone. All combustion reactions as shown take place in the combustion zone, between the heights of 40-60 cm. A higher combustion rate is expected for CO, followed by H_2 and CH_4, as illustrated in Figure 6.7.

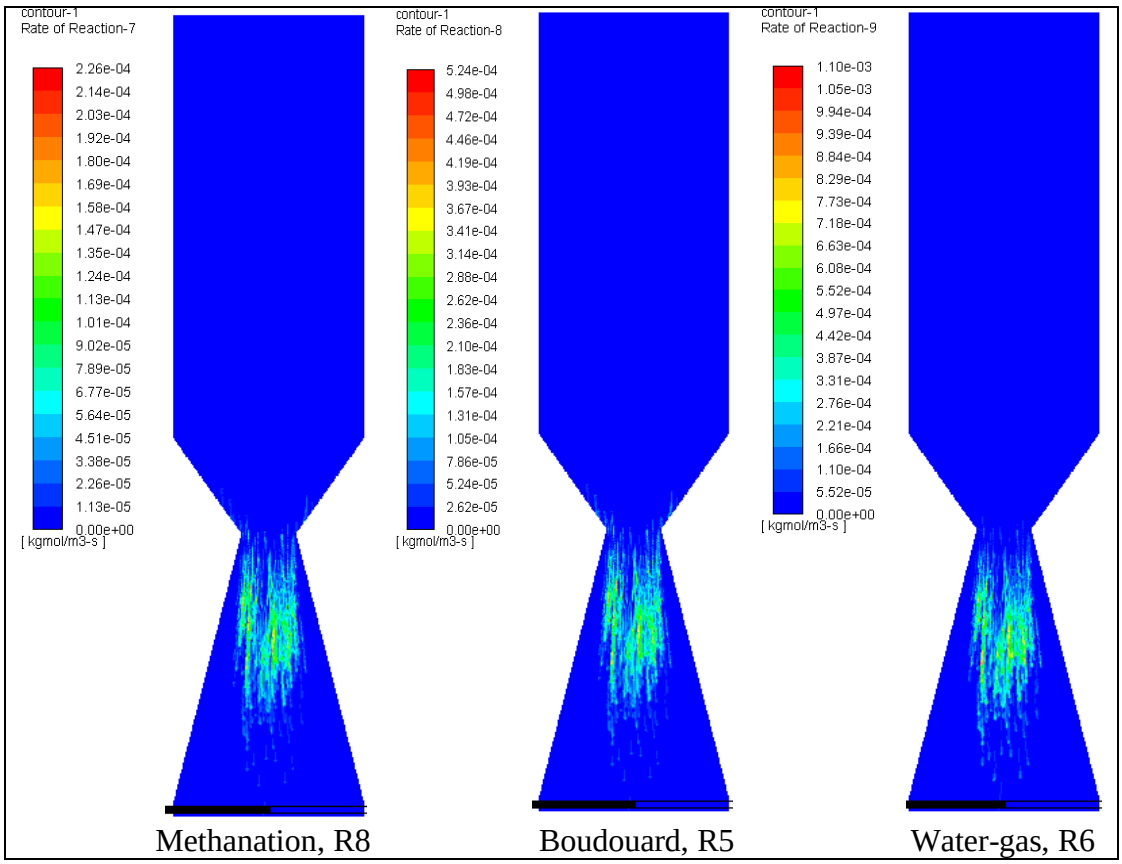

Figure 6.8: Gasification reactions rate along gasifier.

The set of results in Figure 6.8 illustrates the reaction rates taking place in the reduction zone: methanation, boudouard, and water-gas reactions, respectively. Rubber wood is used again, and as seen from the figure; all of the specified reactions take place in the reduction zone. The methanation reaction has the highest reaction rate, followed by the water-gas and the boudouard reaction, which find strong agreement with [18]. All of the reactions start at the end of the combustion zone, with very small rates possibly taking place in the combustion zone; however, usually the gasification reactions take place along the reduction zone length. The boudouard reaction shows the lowest reaction rate due to of the consumption of CO_2, and converting it to CO. This is mainly because CO_2 is a very stable compound and requires heat to be converted to other molecules. Therefore, it finds agreement with previous work, which state that reduction reactions are mostly endothermic and require heat to occur [6].

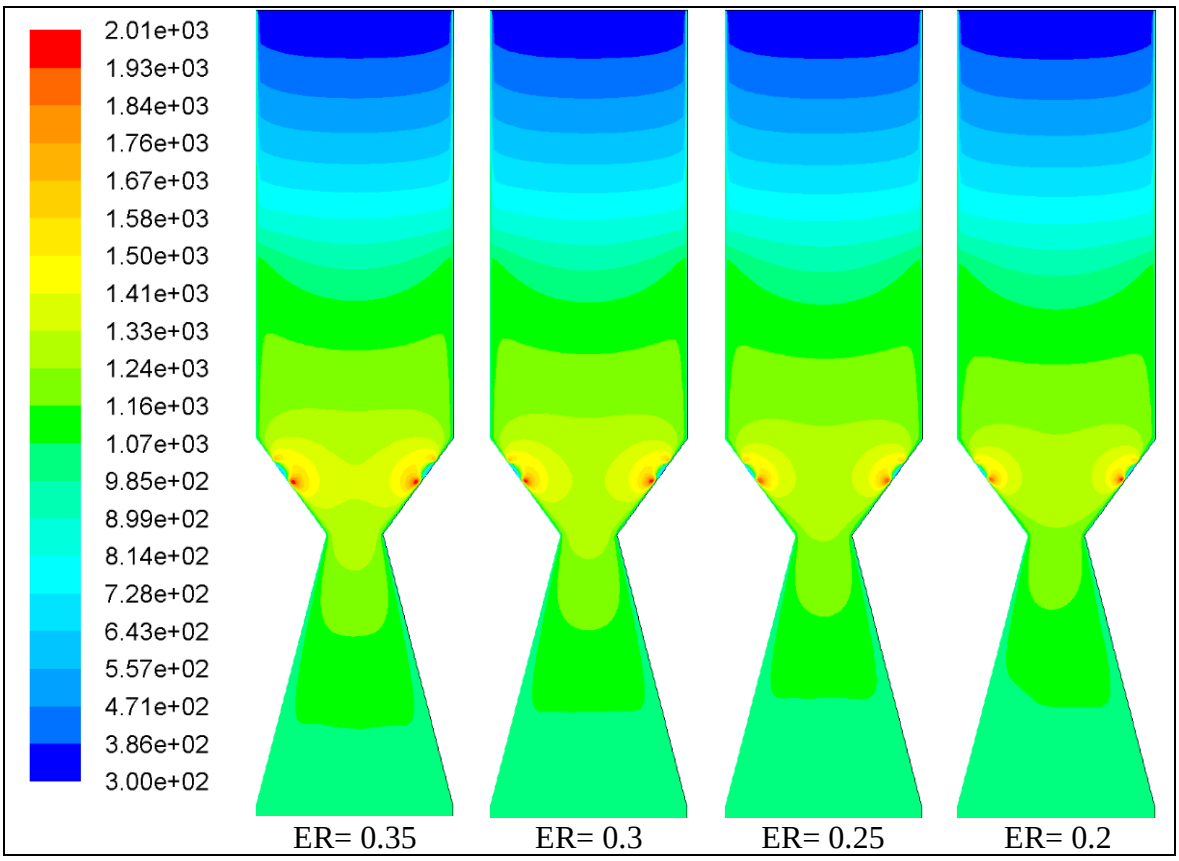

Figure 6.9: Temperature contours along gasifier.

Equivalence ratio and air amount injected inside the gasifier play a critical role in syngas production, chemical reactions taking place, temperature and the whole gasification process. Hence, studying the effects of changing ER on temperature and other parameters, will lead to the understanding of its effect on gasification, in turn leading to higher syngas production and increasing the gasification process efficiency. Figures 6.9 shows the temperature contours inside of the gasifier for rubber wood gasification at different equivalence ratios. The results clearly illustrate the higher temperatures in the oxidation zone ~ 1400K at the centreline of the gasifier, followed by the reduction and pyrolysis zones. The peak temperature, or in other word the ignition temperature, (1900-2015) K shows around the injection points of air; however, it is not the combustion temperature, as the temperature drops again in the middle of the gasifier to its normal levels.

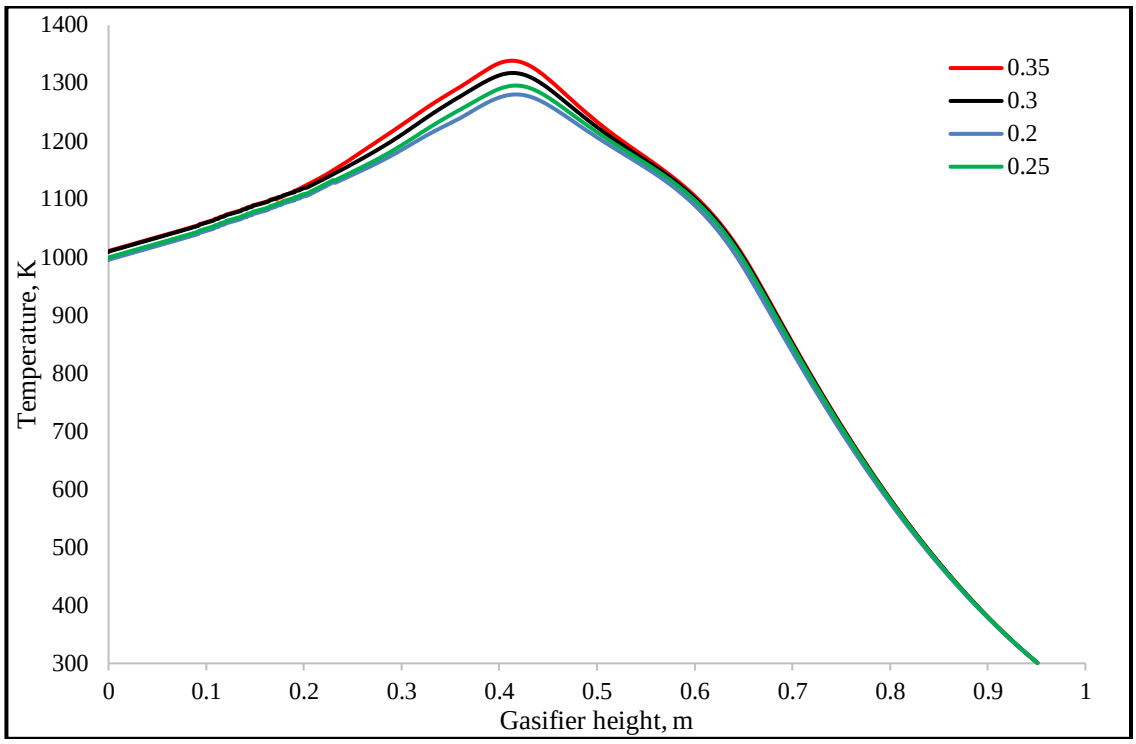

Figure 6.10: Temperature distribution along gasifier centreline.

Further in Figure 6.10, the temperature profile along the gasifier centreline is shown for different ERs. These results are in good agreement with the kinetic code and experimental data. As clearly shown in the figure, more air addition coming from the higher ER tends to increase the temperature inside of the gasifier. Maximum temperature was found for the higher ER of 0.35 and it was around 1340K. When ER decreases, the temperature decreases as well. The temperature rise with ER is also in good agreement with the previous works [38], and [8] as well as with the results derived from the kinetic model (Figure 4.14).

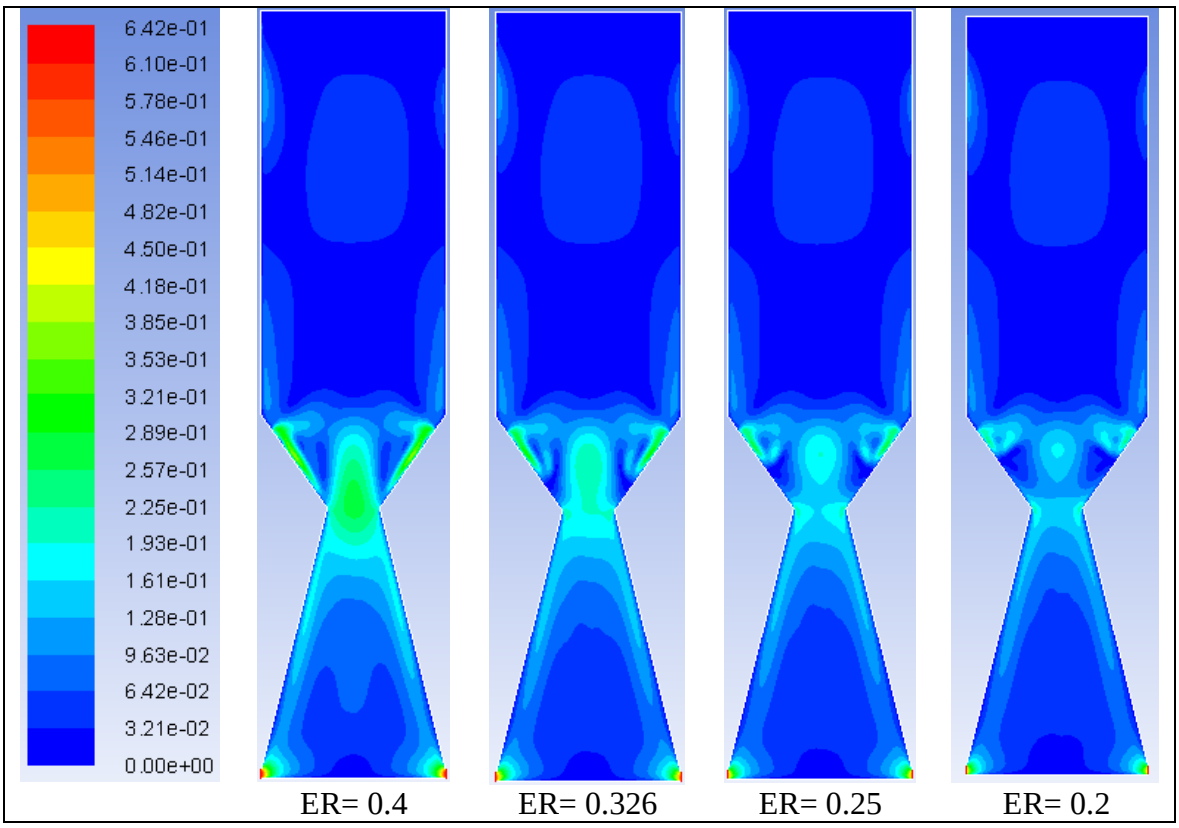

Figure 6.11: Velocity distribution contours along gasifier.

Higher ER tends to increase turbulence and mixing inside of the reactor and higher reaction rates, because of higher velocity at air inlets and around the nozzles, which increase temperatures along the gasifier. As illustrated in Figure 6.11, higher ER tends to increase air amount injection, resulting in higher velocity due to the use of fixed injection air diameter. As a result, higher velocities are produced in the combustion zone, increasing the mixing of gases, and enhancing the combustion process, leading conclusively to higher temperatures.

6.3.4 Species distribution (contours)

All of the species formation, including the volatiles and other gases formation and evolution, will be illustrated in order to have a deeper understanding of their behaviour inside of a gasifier.

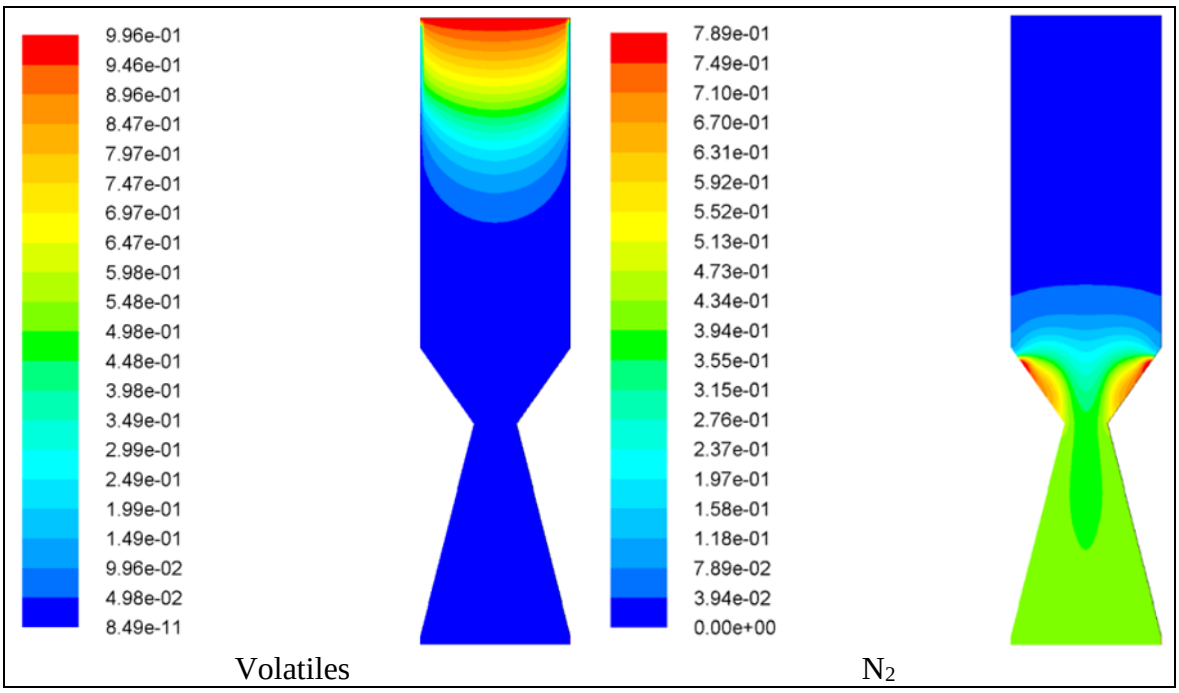

Figure 6.12: Volatiles and nitrogen mole fraction contours along the gasifier.

The results illustrated in Figure 6.12 show the volatiles decomposition, and nitrogen formation contours inside of the gasifier. The highest concentration of volatiles begins from the top of the gasifier; while the temperature increases (Figure 6.9) and the drying process takes place, all of the moisture evaporates and the pyrolysis process starts (Figure 6.6). Volatiles then start to release where it shows its peak in the pyrolysis zone, then decrease, while the other reactions take place during gas phase reactions ((R1-10), as seen in Figure 6.13 and Figure 6.14, as well as the char combustion/gasification reactions (R1, R5, and R6). On the other hand, air gasification produces higher amounts of nitrogen (~ 50%). Nitrogen starts forming from the air injection in the oxidation zone, as illustrated in Figure 6.12. Maximum nitrogen value comes from oxidation, showing higher volume concentrations at air injection, then decreasing while other gases form in the reduction zone until exit points.

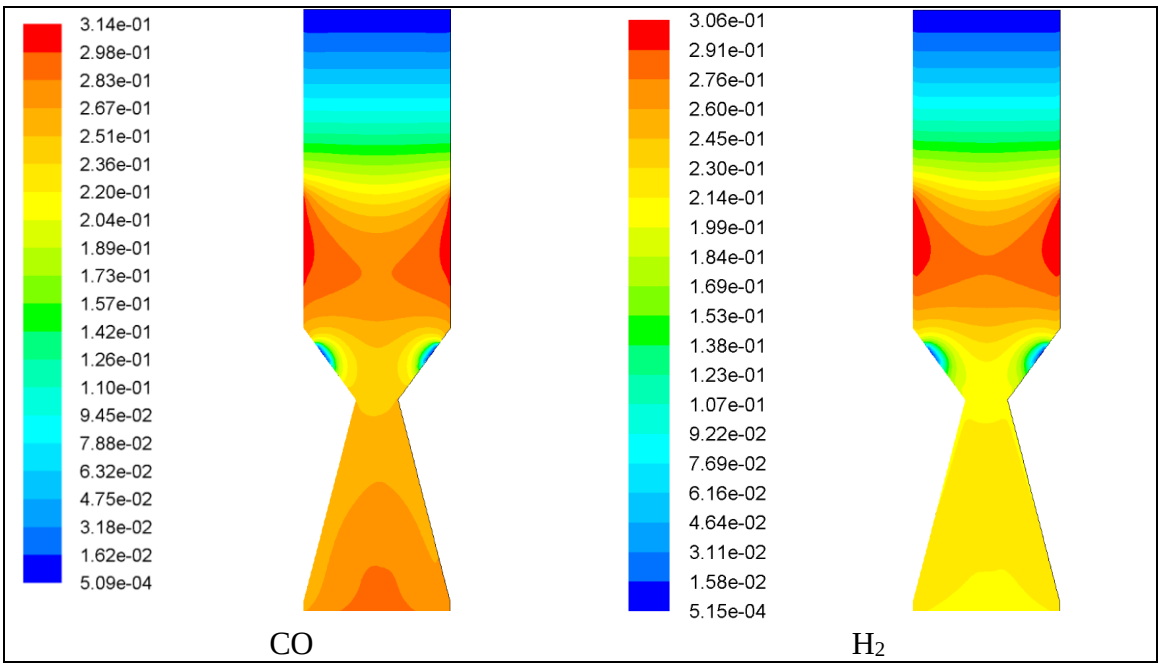

Figure 6.13: CO, and H_2 mole fraction contours along the gasifier.

Both CO and H_2 have the same trend along the gasifier, as shown in Figure 6.13. The results are derived during rubber wood gasification at ER of 0.326. They show a gradual increase after the devolatilization process, and due to gas reactions in pyrolysis they keep increasing slightly above the combustion zone. During combustion, primarily H_2 and Co are consumed based on ER (R2, R3, and R4), and converted to other gases (CO_2, and H_2), as well as tar. After combustion, a slight increase of their value begins formation in the reduction zone; this is due to gasification reactions, particularly the boudouard (R5), and water gas reactions (R6). Both reactions have a very small reaction rate, and hence a lower formation of CO and H_2.

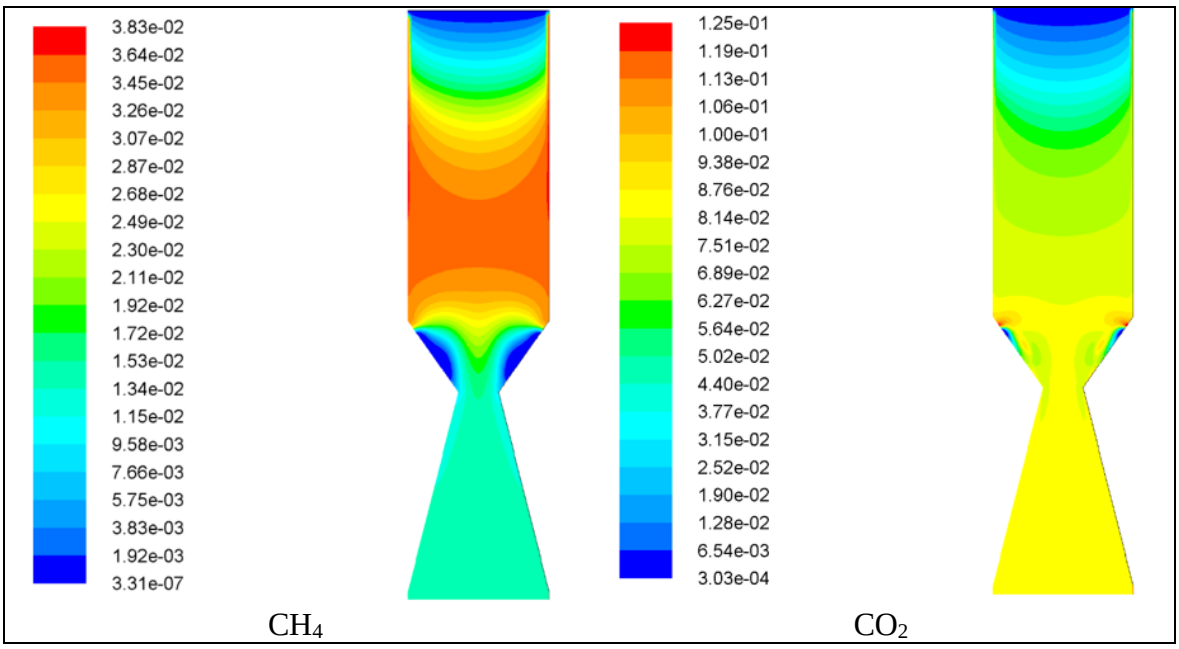

Figure 6.14: CH_4 and CO_2 mole fraction contours along the gasifier.

Methane follows the same trend as CO and H_2, as shown in Figure 6.14. It begins formation in pyrolysis, reaching maximum value at the end of pyrolysis followed by combustion, which leads to a sudden decrease in its amount. During pyrolysis, the amount of methane released is still of a small value; while going through combustion, it tends to decrease due to the methane oxidation reaction (R4). In the reduction zone, it begins formation again due to methanation reactions (R7).

CO_2 follows a different trend to CO, CH_4 and H_2, as shown in Figure 6.14. It starts its release with volatiles in the pyrolysis zone; due to the oxidation reactions, it keeps increasing in the oxidation zone until it reaches its peak value (R1, 2, and 4). During reduction, it decreases slightly again due to gasification (boudouard reaction).

6.3.5 Different feedstocks gasification

The model is further used to simulate the process of the gasification of biomass, waste, and agricultural feedstocks to study model stability. The same feedstocks as used earlier in the kinetic model are used in CFD modelling.

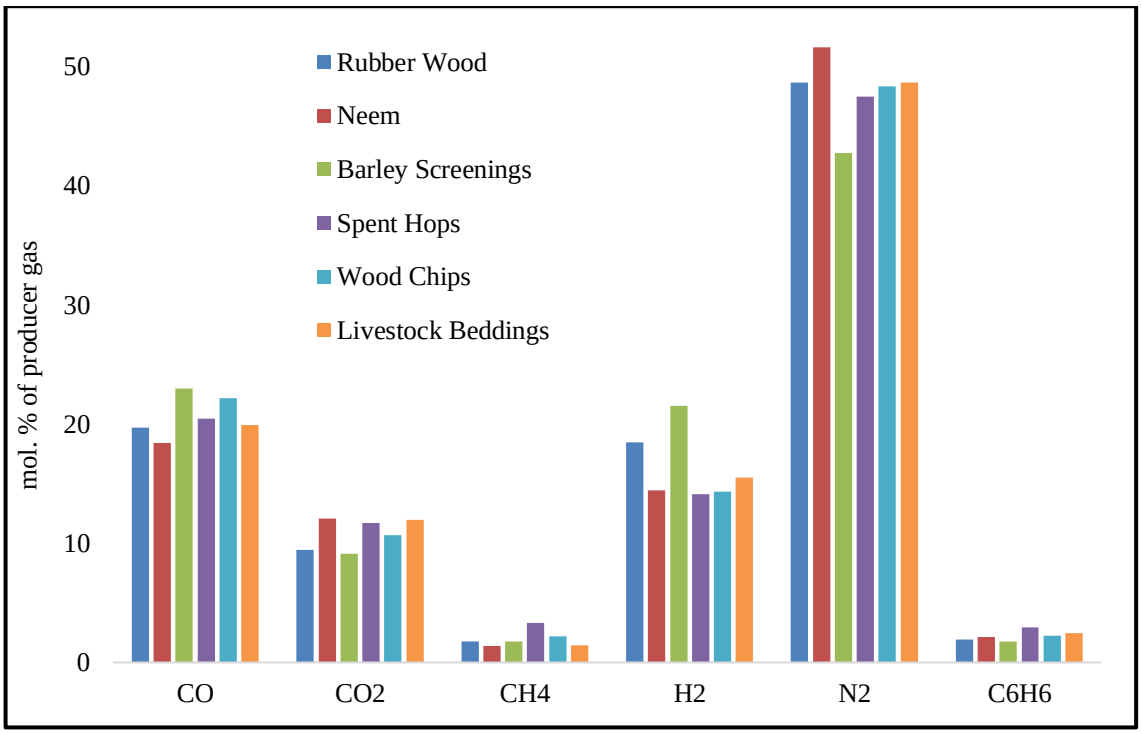

Figure 6.15: Producer gas composition comparison at fixed ER 0.35.

A fixed equivalence ratio (0.35) is used to compare different feedstocks gasification, as illustrated in Figure 6.15. For the same working conditions, barley screenings, and wood chips show higher CO content. This is because of the higher volatiles and fixed carbon

amounts, which lead to the higher CO production rates and formation along the gasification process. It is also noted that both the feedstocks have a higher oxygen content, which favours the CO formation. Higher values of hydrogen are noted for barley screenings and rubber wood, due to the higher volatiles and hydrogen content. On the other hand, the lowest values for CO, and H_2 are noted for neem with a higher CO_2 emission rate. Based on the neem chemical content data, as shown in Table 6.3, neem demonstrates having a lower carbon content, but with higher ash values tends to decrease the useful gas amounts, as shown in the results. Data obtained from the model proves its stability and ability to simulate the process of gasification in downdraft air blown gasifiers for different feedstocks. The results finds agreement with the kinetic code.

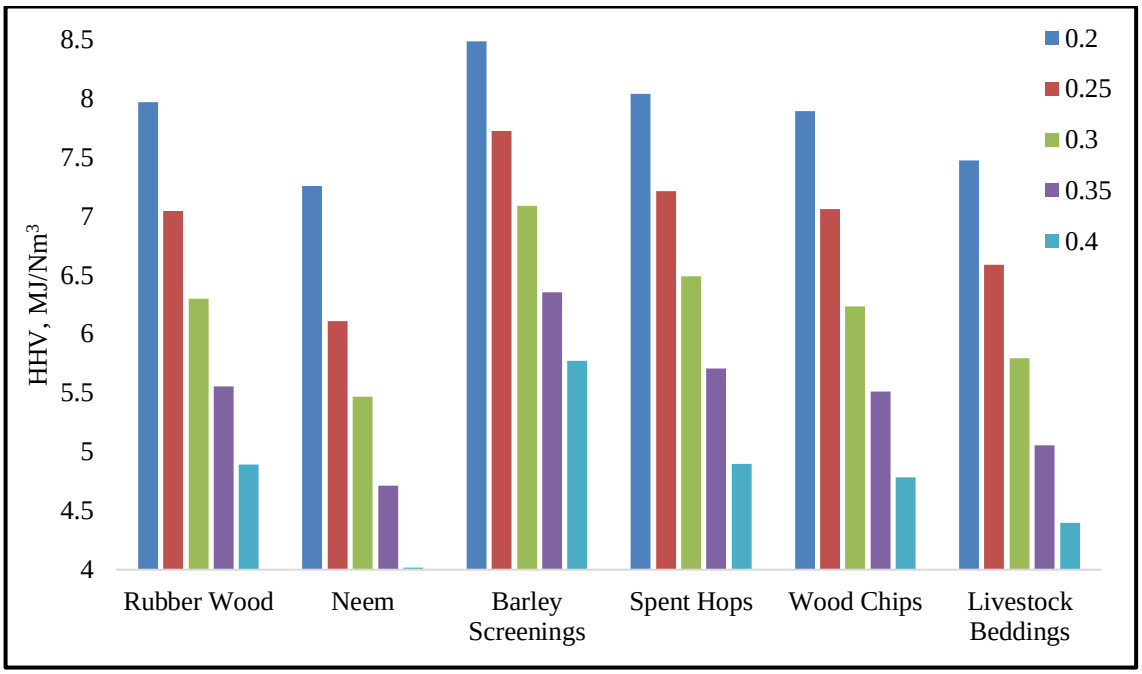

Figure 6.16: HHV of producer gas at different ERs.

Higher heating values derived from syngas composition at different equivalence ratios is shown in Figure 6.16. Lower equivalence ratios tend to produce more CO, H_2, and CH_4, and hence higher values of HHV. This finds a good matching with all previous works on the topic, for reasons stated earlier. On the other hand, higher ER tends to increase non-useful gases, and increase nitrogen dilution in syngas, in turn leading to a decrease in heating values. As shown in the figure, higher values are noted for barley screenings, spent hops, and wood biomass materials, which again show good agreement with the previous work. This is primarily because of the higher volatiles and fixed carbon amounts that lead to increased syngas composition in producer gas. Highest heating value (8.4 MJ/Nm^3) is found for barley screenings at ER 0.2, while the lowest value is found for neem (4.1 MJ/Nm^3) at ER 0.4.

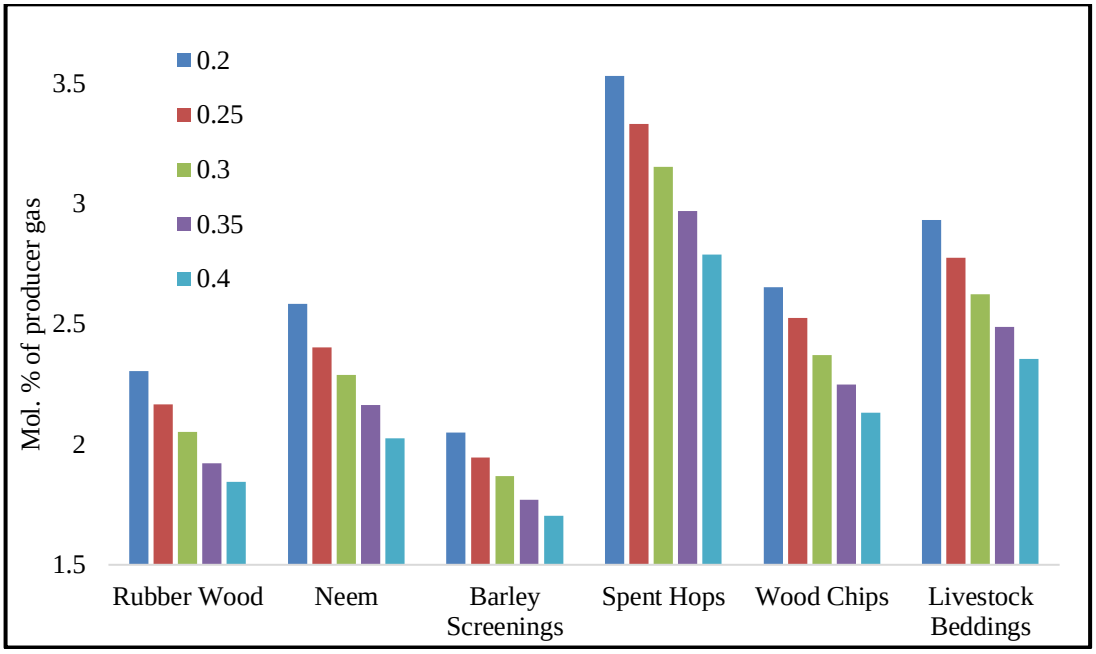

Figure 6.17: Total tar produced with producer gas at different ERs.

Tar produced from the model is also studied at different equivalence ratios, as illustrated in Figure 6.17. Initially, and for easier comparison, the model assumes one compound as tar representative; this compound is benzene (C_6H_6). Based on the review, tar can be identified as all hydrocarbons that have a molecular weight higher than benzene C_6H_6 [50]. As shown in the figure, lower equivalence ratios produce more tar due to lower air amounts, and lower temperature inside of the gasifier which decrease tar cracking reactions. On the other hand, lower tar amounts are found at higher values of equivalence ratios. The results tend to be fair and find agreement with the kinetic code data. The highest value of tar is found for spent hops (3.5 mol %) at ER 0.2, which is similar to same values derived from kinetic model. The lowest value of tar is shown for barley screenings and rubber wood (1.7, and 1.8 mol %), respectively.

6.3.6 Detailed tar species formation

One of the primary goals of the current research study is to build up a tar formation modelling system for downdraft gasifiers. The model was first built by kinetic code and verified against experimental data. In the CFD model, tar was initially assumed as one compound, then later classified into four main species. 9 additional reactions have been added to the CFD code to adapt tar evolution, formation and cracking along the gasifier.

Tar evolution in the pyrolysis zone has been described using the mass yield relations described earlier [73]. In the combustion and gasification zones, tar species formation depends on detailed reaction rate kinetics, [66] and [103].

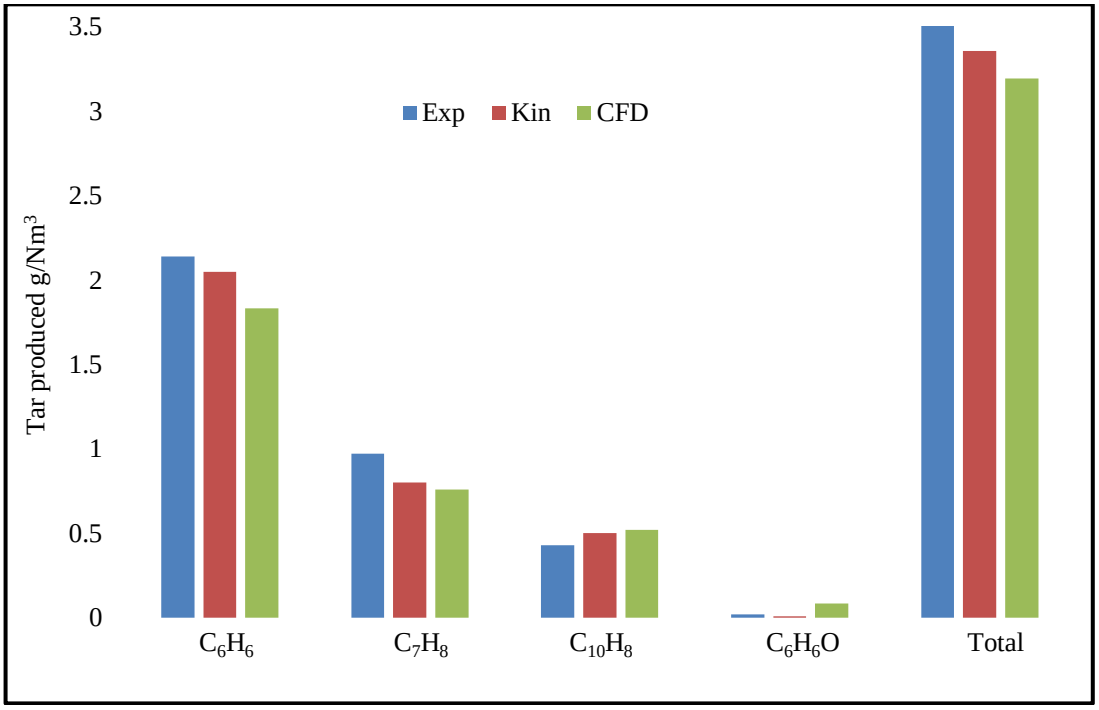

Figure 6.18: Detailed tar species validation.

The model is first validated against experimental data, carried out by the current author, and against kinetic code results, as illustrated in Figure 6.18. The set of results presented show the tar species produced during the gasification of wood at an ER of 0.35. Comparisons are made between the results from CFD, the numerical model and the corresponding tar collected by the SPA method. Tar amounts are shown in µg/100ml of syngas produced, as given in the experimental results and converted to (g/Nm^3). All tar results have been converted from (µg/100 ml of syngas) to the same unit (g/Nm^3), for easy tracking and comparison with other experimental or numerical data, as this unit has been widely used in quantifying and estimating tar produced from gasification. The ultimate and proximate analysis data of material used in validation is previously illustrated in Table 4.1.

The results find reasonably good agreement for all of the major tar species produced, and also for the total tar amount. A negligible decrease in model prediction for the total tar amount is found because of very slight benzene prediction amounts. Phenol concentrations are too small and can be considered as negligible when compared to other species as it is a primary tar compound that tends to be fully cracked and converted to other species at higher temperatures. Based on the kinetic model and CFD model, phenol concentration is zero, while for experiments it is (<0.02 g/Nm^3). Benzene and naphthalene are found to be in fair agreement with both experimental and kinetic code results. Both compounds have the highest portion of tar produced during biomass gasification and represent more than 60% of tar produced in most cases [5]. Toluene concentrations show higher values than the

experiment or kinetic model, of around 50%. This might be due to the toluene reactions, which have small reaction rates, and at same time, the amount of toluene released at pyrolysis based on the model is high. As a result, a considerable amount of toluene cracking does not take place.

6.3.7 Tar species distribution along the gasifier

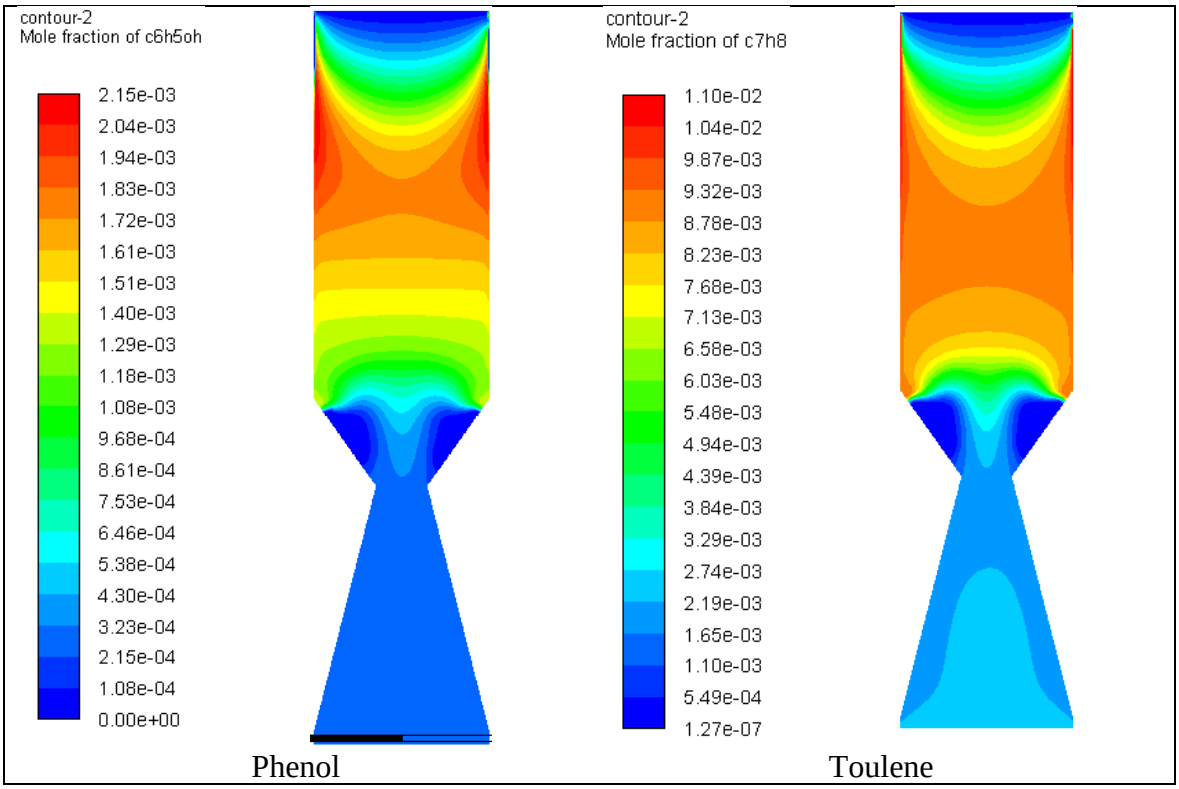

Figure 6.19: Phenol and toluene mole fraction contours along the gasifier.

Phenol concentrations within producer gas are usually close to zero and can be neglected, as evidenced in Figure 6.19. Phenol starts formation in early pyrolysis with large amounts; while the temperature increases, it reacts further with other compounds and converts to other forms. During gasification, it also tends to slightly decrease as the temperature is high enough, and in some cases, it tends to be fully consumed and converted to benzene, naphthalene, and other gas species (CO, H_2, and CH_4).

Toluene formation along the gasifier has the same trend of phenol, a higher concentration in pyrolysis zone, followed by the destruction in oxidation and reduction zone, as evidenced in Figure 6.19. However, in some cases toluene starts reforming again at the reduction zone with small amounts based on reduction reactions and temperature of gasification zone.

At temperatures above 773 K, primary tars starts re-forming ([6], and [35]) and are converted to secondary, then tertiary, tars. Temperatures of oxidation and the reduction zone

that are higher than 1173 K are enough to destroy primary tar species and transform them into other compounds.

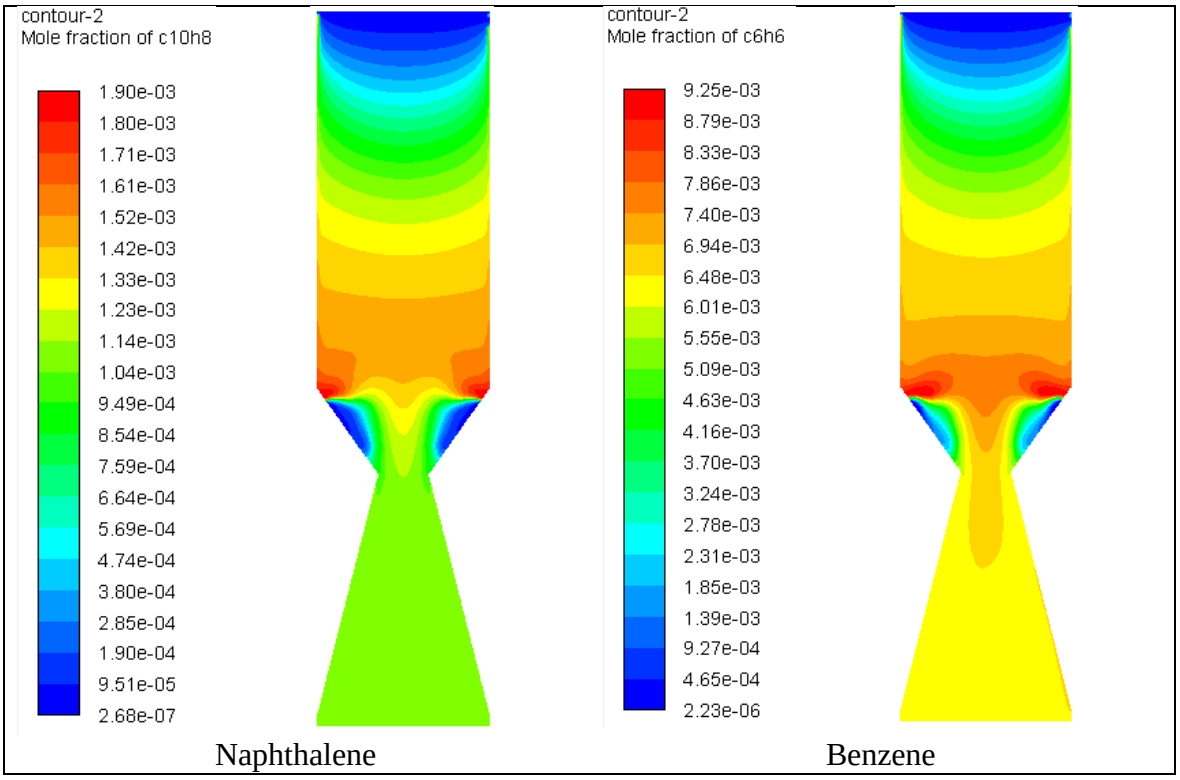

Figure 6.20: Naphthalene and benzene mole fraction contours along the gasifier.

Naphthalene formation follows a different trend from other species. It is formed and presented in considerable amounts in producer gas, as evidenced in Figure 6.20. Small amounts are produced during pyrolysis as it is a tertiary tar, which requires higher temperatures to present and form. Higher temperatures in oxidation zone >1300K are favourable for naphthalene formation, which starts conversion for temperatures greater than 1300K and achieves total conversion at 1600 K [60]. Based on tar kinetic reactions, naphthalene is converted to char, H_2, CO and benzene. These reactions tend to take place in the combustion and reduction zones; however, it is more likely to occur in the reduction zone due to the presence of water vapour.

Benzene has the highest portion of tar species, which is usually greater than 37% from the weight of total tars produced [5]. Benzene starts forming in pyrolysis, followed by a slight decrease in oxidation and increase again in the reduction zone. Oxidation reactions tend to destroy benzene and convert it to CO, CO_2, CH_4, H_2 and H_2O. However, benzene is found in larger amounts, and during oxidation it tends to be slightly cracked. This is due to its higher stability when compared to other tar species, and hence it forms the highest portion of tar compounds during the gasification process [5]. Furthermore, benzene requires very high temperatures to start cracking (1400-1700) K [60]. On the other hand, these reactions

depend on the oxygen amount and have small reaction rates. This makes it unlikely to take place in the oxidation zone and means that it will not take place in the reduction zone where no oxygen is present. Other tar species such as phenol, naphthalene, and toluene are converted under this temperature range to benzene and other compounds. Furthermore, benzene requires very high temperatures to start cracking (1400-1700) K [60]. All of the previous factors tend to increase the amount of benzene along the gasifier height, with an increase in temperature, which agrees with the results of [35].

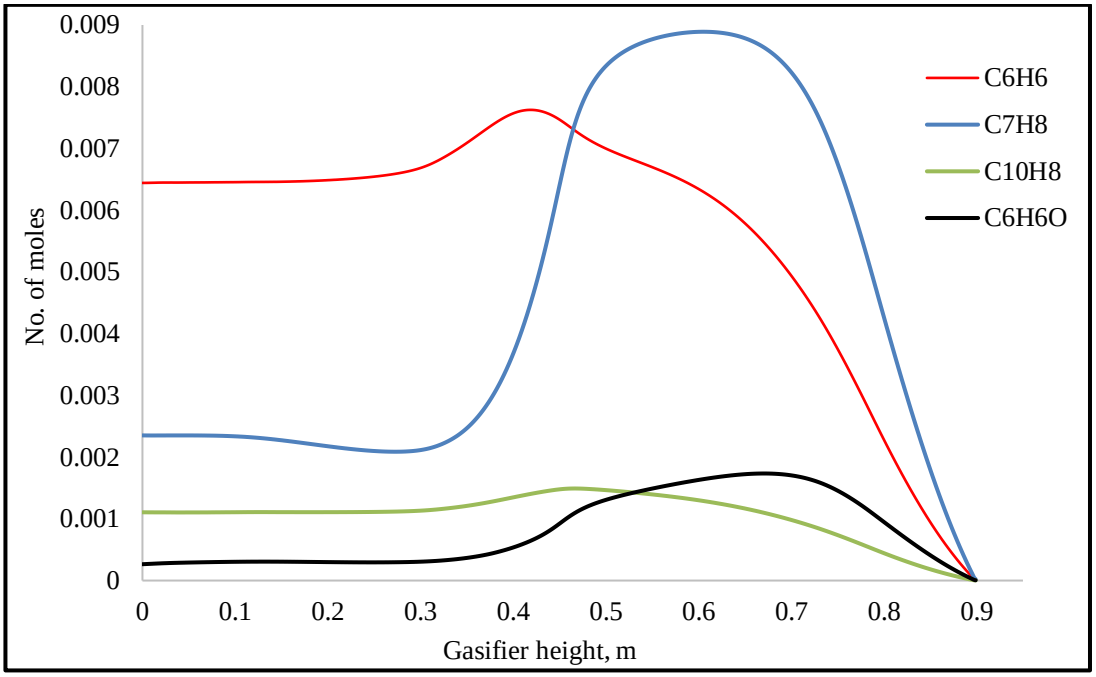

Figure 6.21: Different tar species distribution along the gasifier centreline.

Tar species formation along the centreline is illustrated in Figure 6.21. The results follow the same trend described earlier in Figure 6.19, and Figure 6.20). In the pyrolysis zone, phenol shows higher concentration; this is because it is a primary tar compound, usually formed in higher amounts during the devolatilization process, and has been further formed into secondary and tertiary tars in combustion and gasification. At the gasifier exit, benzene shows the highest portion of tar species followed by phenol and naphthalene, while toluene shows negligible values at the exit of the gasifier, as expected.

6.3.8 Tar species formation with time

Unsteady simulations are also performed to study the formation of different species with time starting from evolution at pyrolysis, followed by combustion and gasification, and also at the syngas exits. A well understanding of tar formation and its nature is the primary requirement that would help to decrease the tar amounts produced with syngas. All the

simulation results of tar species presented below are processed at the mid-location of every zone, while they are face average at the gasifier exit.

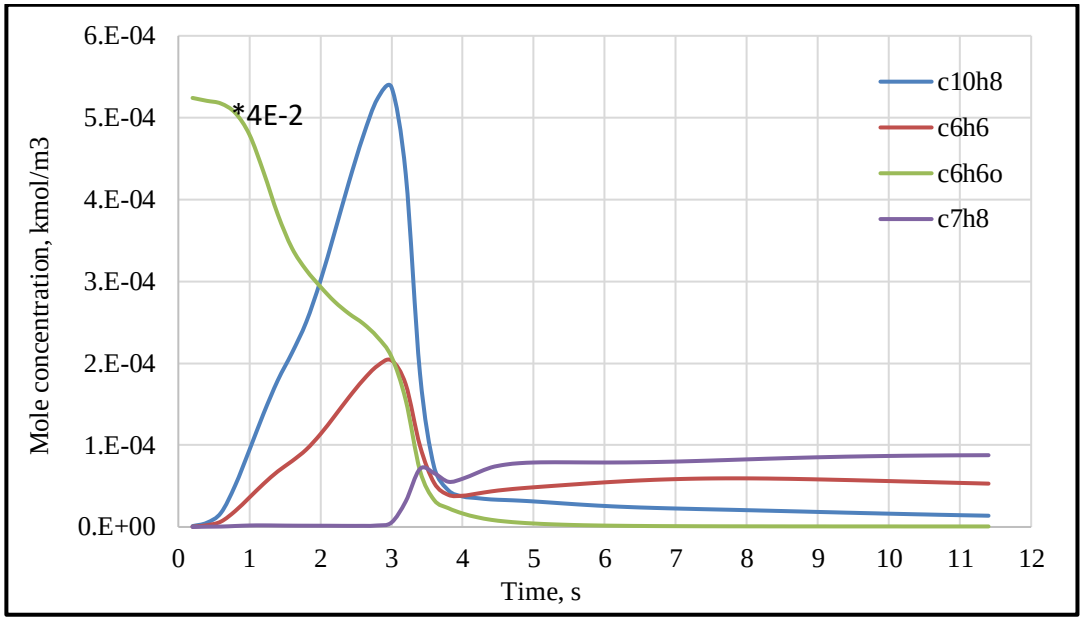

Figure 6.22: Tar species distribution at the pyrolysis zone with time.

The evolution of tar species at the pyrolysis zone with time is shown in Figure 6.22. All the species, apart from phenol, start to increase and reach to their peaks, though at different time, and then decrease and finally stabilise after 5 seconds. Phenol concentrations are found to be very high at the beginning, so the scale of phenol was multiplied by 0.04, for an easy illustration in the chart area. Phenol concentrations are found to be very high because of its nature as a primary tar, which forms at pyrolysis, then by the time and while the temperature increases inside the gasifier, it starts to be cracked and converted to other higher tar compounds and consequently, tends to decrease by the end. On the other hand, toluene was found to have the highest portion of tar species at pyrolysis end, which has a good agreement with the previous and present research findings. Toluene as the most stable primary tar is formed under the usual pyrolysis temperatures and tends to be cracked and converted to benzene and naphthalene at higher temperatures of the oxidation zone. Benzene is found in considerable amounts, while naphthalene is found in lower amounts as a PAH that needs higher temperatures to be formed.

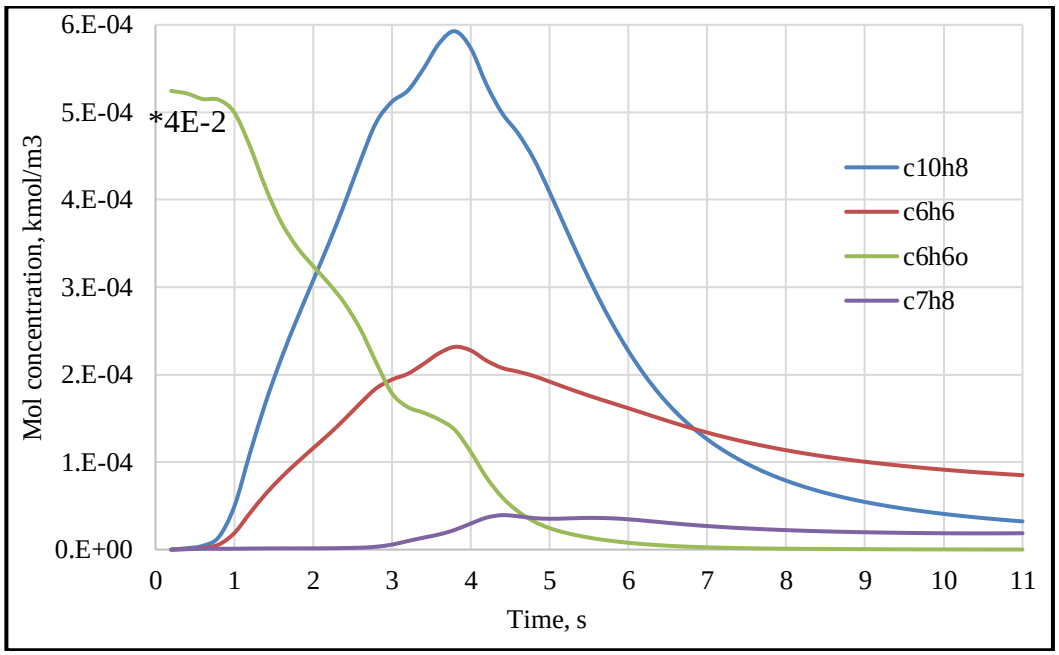

Figure 6.23: Tar species distribution along the combustion zone with time.

The set of results illustrated by Figure 6.23 are showing the distribution and formation of tar species along the combustion centre zone with time. The results start to stabilize after 8 seconds, which should be higher than that was shown in the pyrolysis time (5 seconds). That is because species start formation at pyrolysis then go through the combustion zone which need more time to stabilize. All the species follow the similar trend as found in the pyrolysis zone. However, benzene and naphthalene are forming in higher amounts, because of the higher combustion temperatures (Figure 6.9) that cracks the primary tar molecules and convert them to the secondary and tertiary tars. Toluene is found in small amounts while phenol is fully consumed because of the higher temperature at the oxidation zone. The results are showing a logical trend, where the sum of the tar contents (in kmol/m^3) at the end of pyrolysis (16e-5), and end of combustion (13e-5) decreases. Additionally, the results show that the primary tars are forming the highest portion at pyrolysis (e.g. toluene ~ 8.8 e-5), while at the end of oxidation it shows benzene (tertiary tars) having the highest portion (8.5e-5), followed by naphthalene and toluene, which agree strongly with the previous studies based on the literature data ([67], [48], and [52]).

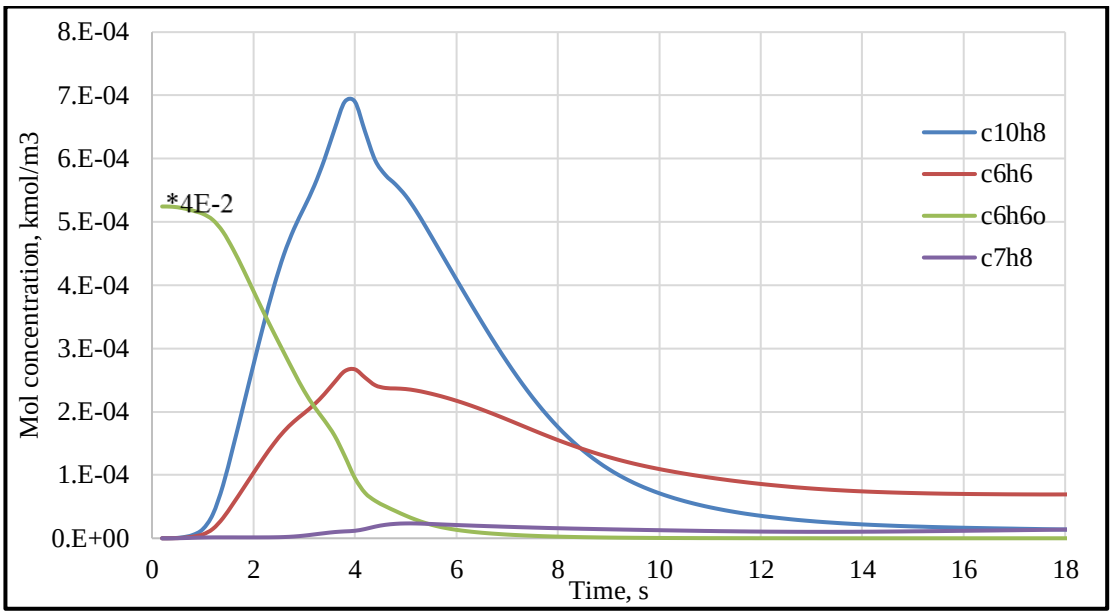

Figure 6.24: Tar species distribution along the reduction zone with time.

Tar species formation at the reduction zone with time is described by Figure 6.24. The results start to stabilize after longer time than combustion and pyrolysis, i.e. around 12 seconds. Tar species formation follows the same trend as in the combustion zone because of again higher temperature.

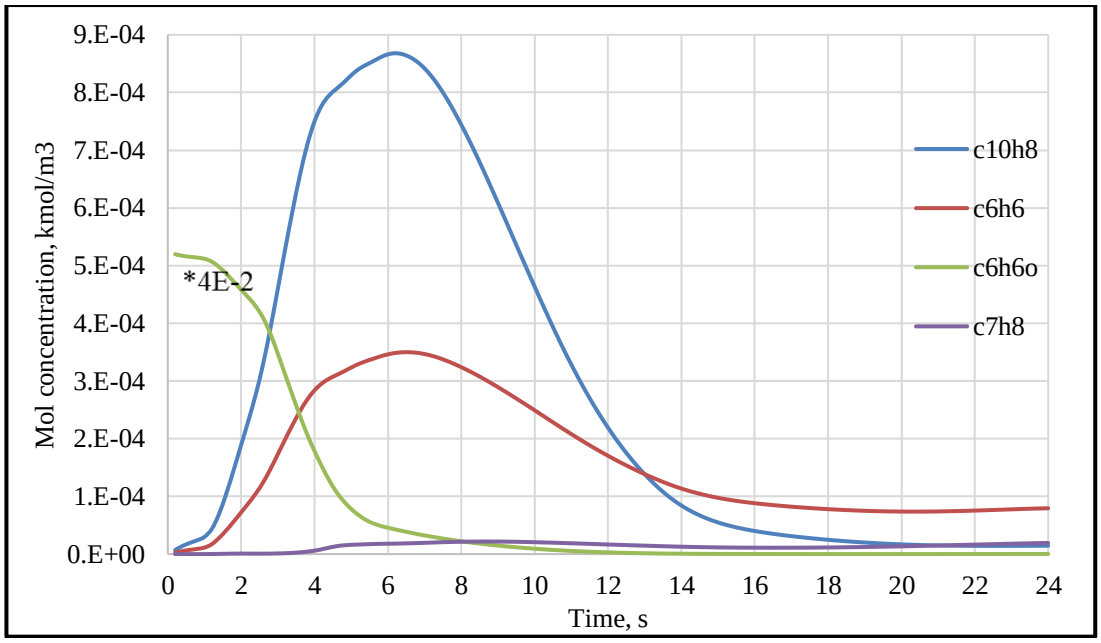

Figure 6.25: Tar species distribution along the gasifier exit with time.

Finally, the average values of tar species evolution at the syngas exits is represented by Figure 6.25. The species formation starts its stabilization at longer times than other zones, around 15 seconds. Initially, phenol is found in large amounts, then it decreases or fully consumed over time and with temperature increase. Benzene and naphthalene are formed in large amounts then by the temperature increase they cracked slightly. While toluene as a

stable compound starts stabilization early and been found in considerable amounts. Eventually, benzene is forming the highest portion of tar species, followed by toluene, naphthalene, and phenol in a very small amount. The results are matching with same findings illustrated earlier by kinetic, CFD, and experiments carried out at the current research, Figure 6.18.

6.4 Conclusions

The 2D CFD model was built using ANSYS software. The model was able to simulate the work of air blown downdraft gasifiers. The gasifier design was based on a 20-kW downdraft gasifier, based on kinetic code predictions. A mesh independency test was carried out for three different grids. The model was initially tested against two different feedstocks and found a good agreement. Additionally, the model was used to study the gasification process using different biomass, waste, and agricultural feedstocks. Furthermore, the model was used to study four main tar species evolution and formation along the gasifier. Benzene, naphthalene, toluene, and phenol were used as tar representatives. They represent primary, secondary, and tertiary tars. On the other hand, they all usually form more than 70-80% of tar formed during the gasification process. The results of the tar species formation were validated against the kinetic code already built, and against experimental data carried out by the current research author at KTH institute in Sweden.

Reaction kinetics were studied, showing rates of reactions for around 20 reactions taking place in the model. Detailed gas and tar species formation along the gasifier and different species concentration along centreline of the gasifier were also studied.

Results showed that the highest heating value (8.4 MJ/Nm^3) is found for barley screenings at ER 0.2, while the lowest value is found for neem (4.1 MJ/Nm^3) at ER 0.4. The highest value of tar is found for spent hops (3.5 mol %) at ER 0.2, which is similar to same values derived from the kinetic model. The lowest value of tar is shown for barley screenings and rubber wood (1.7, and 1.8 mol %), respectively. The model is able to predict different tar species formation accurately, as well as total tar production.

Chapter 7 Conclusions and Future Recommendations

The main focus of this research was towards building up a detailed novel kinetic model that is able to predict downdraft air-blown gasifier's work. The model was successfully built and validated over a wide range of materials including biomass, waste, and Scottish agricultural residues. The model was also able to predict the formation of syngas production from volatiles release in pyrolysis followed by combustion and gasification zones.

The model is integrated four-zone kinetic model in which the outcomes of every zone are the feeding to next one. A novel aspect was used in building up the model depending on the full char consumption at reduction zone. Based on this assumption, the reduction zone length was determined, and all syngas products were calculated. The model also was successfully able to design downdraft gasifiers based on gasifier capacity and feedstock used. Furthermore, the key design parameters such as throat diameter and thermal power required are discussed in details to optimise the design process and produce a gasifier able to accommodate fuel change and other working conditions for higher syngas production.

Additionally, sensitivity analysis was carried out through studying the effect of varying moisture content and air equivalence ratio on producer gas composition, tar content, and higher heating value. Furthermore, different gas species distribution along gasifier was discussed with the effect of changing working parameters.

The results show that a decrease of biomass moisture content from 20% to 5% leads to an increase of the produced gas heating value of 10-22%, and a decrease of tar content of about 18-26%. Moreover, the results show an increase in producer gas heating value of 25-30% while decreasing Φ from 0.4 to 0.2. Tar yield also increased from 16% to 50% with the same level of magnitude drop in Φ.

Robustness of the model was examined, and the results show that the equivalence ratio (Φ) at 0.3-0.35 and with a moisture content less than 10% gives a higher yield of syngas with a higher gasification efficiency and lower tar content. Temperature variation across the gasifier was also studied and the gasification temperature was found to increase with an increase of Φ. In particular, woody biomass materials give a higher yield of syngas while olive wood had a heating value up to 6.4 MJ/Nm^3 at Φ=0.2 and MC of 10%. At Higher values of Φ gives a lower heating value for wood pellets and saw dust. The tar content was also lower for wood (1.65%) at Φ=0.4.

For agricultural feedstocks; livestock beddings, spent barley and barley screenings showed higher gasification efficiency and very close values to wood biomass materials. On the other hand, spent hops showed the lowest gasification efficiency (~38 %), and also as

discussed earlier it also shows higher values of tar content which makes the feedstock unusual for gasification unless draying is considered. The moisture content levels also in same material (~67%) makes the gasification process is impossible unless drying for the recommended values takes place before gasification.

An important step of designing a gasifier and building up the code was tar formation modelling. The model incorporated the formation and destruction of four main tar species (benzene, naphthalene, toluene, and phenol). Kinetic rate reactions were implemented in the main kinetic code to predict tar formation along the gasifier. Experimental work was carried out to validate the results of the kinetic code and found a good agreement. The experiments were carried out at three different equivalence ratios (ER) and at three different temperatures (800, 900, and 1100 °C). Sensitivity analysis was carried out by the kinetic code to optimise the working parameters of a downdraft gasifier that led to a higher calorific value of syngas. The results revealed that a tar evolution model is more accurate for wood biomass materials and that using ERs around 0.3, and moisture content levels lower than 10% lead to the production of higher value syngas with lower tar amounts.

ANSYS was used to build-up a 2D model that was used to simulate downdraft gasification process. The model was first validated against experimental data and found good agreement. Additionally, it was used to test different biomass, waste and agricultural feedstocks stated earlier with the kinetic code. Furthermore, the model used to study and show species formation and other working parameters (T, and V) contours along gasifier. Reaction kinetics were studied showing rates of reactions for around 20 reactions taking place in the model. The model was further used to investigate the evolution, formation and destruction of tar species used in the kinetic model. The final data of both kinetic and CFD modelling are in a good agreement with experimental work carried out by the author in KTH institute, Sweden. Tar species produced by the model were forming up to 90% of total tar produced during biomass gasification process which founds a good agreement with previous experimental works based on the literature data.

Results showed that highest heating value (8.4 MJ/Nm^3) is found for barley screenings at ER 0.2, while lowest value is found for neem (4.1 MJ/Nm^3) at ER 0.4. Highest value of tar is found for spent hops (3.5 mol %) at ER 0.2 which is similar to same values derived from kinetic model. Lowest value of tar is shown for barley screenings and rubber wood (1.7, and 1.8 mol %) respectively. The model is able to predict different tar species formation accurately, and also total tar production.

Both the kinetic and CFD models showed their uniqueness, and novelty can be further concluded in the following points;

- The kinetic code was able to optimise the design process of downdraft gasifiers leading to higher value syngas production with lower tar amounts.
- The code was able to handle and test a wide range of materials over different working parameters change.
- The kinetic code was built on Matlab coding without relying on any external modelling software.
- The model was built on a novel aspect based on the reduction zone optimization for total char consumption which is used for the first time in modelling processes.
- The model was also able to design a gasifier based on the key design parameters leading to a unique design enabling to handle a wide range of materials and with higher gasification efficiency.
- CFD model was used to study the same range of materials discussed earlier by the kinetic code. Also, the model was used to simulate detailed tar species formation in downdraft gasifiers which has never been covered or handled in any previous CFD models.
- Experiments carried out to further validate both the kinetic and CFD models built.
- The applicability and wide variety of materials the models handled makes them an important addition to the bioenergy sector. On the other hand, the new feedstocks tested by the models proved their capability to be gasified, thus gives a promising and wide attention to make use of agricultural, waste and farm residues in the gasification and also encourage governments to make a beneficial use of these feedstocks.
- The prediction of tar species formation along gasifier would help to eliminate and reduce tar amount in gasifiers leading to higher value syngas. This, therefore, would have impact in the industries of bioenergy and waste management globally.

Based on the work carried out, future work should focus more on increasing syngas heating value and developing methods for tar cracking. The key challenges should be towards designing gasification systems that lead to produce lower or even zero tar amounts suitable for direct use. After considering all optimum conditions and working parameters stated in the current research work, it will be valuable to find out more ways to reduce tar amount in producer gas. Further, more attention should be given towards the evolution of tars from pyrolysis zone, and how this will affect the whole gasification process leading to

decrease tar amount, rather than using external or internal tar cracking systems. Another aspect is also converting tar species into light compounds that could add to the heating value of syngas. Additionally, finding out another way to increase the heating value of produced gas is a key challenge in any reassert work related to the gasification. This could be done by increasing hydrogen, carbon monoxide, and methane production. Again, the evolution of different gas species in pyrolysis zone will definitely affect their formation through the whole process. Finally, the gasifier design should be considered with all other previous stated factors to enhance and increase the gasification efficiency.

References

[1] D. Carrington, "The Guardian," 8 Dec 2017. [Online]. Available: https://www.theguardian.com/environment/2017/dec/08/death-spiral-half-of-europes-coal-plants-are-losing-money?utm_content=buffer38db7&utm_medium=social&utm_source=twitter.com&utm_campaign=buffer.

[2] S.V. Vassilev, C.G. Vassileva, and V.S. Vassilev, "Advantages and disadvantages of composition and properties of biomass in comparison with coal: An overview," *Fuel,* vol. 158, p. 330–350, 2015.

[3] Basu P., Biomass Gasification, Pyrolysis, and Torrefaction. Practical Design and Theory. Second Edition, Amsterdam: Academic Press, 2013.

[4] A.V. Bridgwater, A.J. Toft, and J.G. Brammer, "A techno-economic comparison of power production by biomass fast pyrolysis with gasification and combustion," *Renewable and Sustainable Energy Reviews,* vol. 6, pp. 181-248, 2002.

[5] P. Basu, Biomass Gasification, Pyrolysis, and Torrefaction. Practical Design and Theory. Second Edition, Amsterdam : Academic Press, 2013.

[6] P. Basu, Biomass gasification and pyrolysis: practical design and theory, Burlington: Academic press, 2010.

[7] C. Mandl, I. Obernberger, and F. Biedermann, "Modelling of an updraft fixed-bed gasifier operated with softwood pellets," *Fuel,* vol. 89, no. 12, pp. 3795-3806, 2010.

[8] Budhathoki R., Three zone modeling of Downdraft biomass Gasification: Equilibrium and finite Kinetic Approach" MSC Thesis,, University of Jyväskylä, 2003.

[9] J. Gustavsson, C. Cederberg, and U. Sonesson, "Global food Losses and Food Waste," FAO. 2011. Global food losses and food waste – Extent, causes and prevention., Rome, 2011.

[10] M. Masnad, S. John, R. Xiaotao T. BiC, and J. Ellis, "From fossil fuels towards renewables: Inhibitory and catalytic effects on carbon thermochemical conversion during co-gasification of biomass with fossil fuels," *Applied Energy,* vol. 140, pp. 196-209, 2015.

References

[11] S. Razm, S. Nickel, M. Saidi-Mehrabad, and H. Sahebi, "A global bioenergy supply network redesign through integrating transfer pricing under uncertain condition," *Journal of Cleaner Production,* vol. 208, pp. 1081-1095, 2019.

[12] S.M. Chern, W.P. Walawender, and L.T. Fan, "Equilibrium modeling of a downdraft gasifier i – overall gasifier," *Chemical Engineering Communications,* vol. 108, pp. 243-265, 1991.

[13] Z.A. Zainal, R. Ali, C.H. Lean, and K.N. Seetharamu, "Prediction of performance of a downdraft gasifier using equilibrium modeling for different biomass materials," *Energy Conversion and Management,* vol. 42, no. 12, p. 1499–1515, August 2001.

[14] A. Melgar, J. F. Pérez, H. Laget and A. Horillo, "Thermochemical equilibrium modelling of a gasifying process," *Energy Conversion and Management,* vol. 48, pp. 59-67, 2007.

[15] S.A. Channiwal, and J.K. Ratnadhariy, "Three zone equilibrium and kinetic free modeling of biomass gasifier – a novel approach," *Renewable Energy,* vol. 34, no. 4, p. 1050–1058, April 2009.

[16] A.M. Salem, and M.C. Paul, "An integrated kinetic model for downdraft gasifier based on a novel approach that optimises the reduction zone of gasifier," *Biomass and Bioenergy,* vol. 109, pp. 172-181, 2018.

[17] A.K. Sharma., "Modeling and simulation of a downdraft biomass gasifier 1. Model development and validation," *Energy Conversion and Management,* vol. 52, p. 1386–1396, 2011.

[18] U. Kumar, and M.C. Paul, "CFD modelling of biomass gasification with a volatile break-up approach," *Chemical Engineering Science,* vol. 195, pp. 413-422, 2019.

[19] U. Kumar, A. M. Salem, and M. C. Paul, "Investigating the thermochemical conversion of biomass in a downdraft gasifier with a volatile break-up approach," *Energy Procedia,* vol. 142, pp. 822-828, 2017.

[20] I. Janajreh, and M. Al Shrah, "Numerical and experimental investigation of downdraft gasification of wood chips," *Energy Conversion and Management,* vol. 65, pp. 783-792, 2013.

[21] M. J. Prins, K. J. Ptasinski and F. J. G. Janssen, "From coal to biomass gasification: Comparison of thermodynamic efficiency," *Energy,* vol. 32, pp. 1248-1259, 2007.

[22] D.L. Giltrap, R. McKibbin, and G.R.G. Barnes, "A steady state model of gas-char reactions in a downdraft biomass gasifier," *Solar Energy,* vol. 74, p. 85–91, 2003.

References

[23] M. Chase, NIST JANAF thermochemical tables, Am. Chem. Soc, 1998.

[24] P. P. Dutta, V. Pandey, A. R. Das, S. Sen, and D. C. Baruah, "Down Draft Gasification Modelling and Experimentation of Some Indigenous Biomass for Thermal Applications," *Energy Procedia,* vol. 54, pp. 21-34, 2014.

[25] J. Ejirefe, and M.C.Paul, Biomass Gasification: Thermodynamic equilibrium modelling and simulation of gasification process to analyse the effect of moisture content on product gas, Glasgow: MSC Thesis. Glasgow University, 2014.

[26] A.Z. Mendiburu, J.A. Carvalho, and J.R. Coronado, "Thermochemical equilibrium modeling of biomass downdraft Gasifier: Stoichiometric models," *Energy,* vol. 66, pp. 189-201, 2014.

[27] X. T. Li, J. R. Grace, C. J. Lim, A. P.Watkinson, H. P.Chen, and J. R. Kim, "Biomass gasification in a circulating fluidized bed," *Biomass and Bioenergy,* vol. 26, no. 2, p. 171–193, 2004.

[28] C. R. Altafini,P. R. Wander, and R. M. Barreto, "Prediction of the working parameters of a wood waste gasifier through an equilibrium model," *Energy Convers Manage ,44,* p. 2763–77, 2003.

[29] T.K. Patra, and P.N. Sheth, "Biomass gasification models for downdraft gasifier: A state-of-the-art review," *Renewable and Sustainable Energy Reviews,* vol. 50, pp. 583-593, 2015.

[30] A. K. Sharma, "Experimental investigations on a 20 kWe, solid biomass gasification system," *Biomass and Bioenergy,* vol. 35, no. 1, pp. 421-428, 2011.

[31] F.V. Tinaut, A. Melgar, J.F. Pérez, and A. Horrillo., "Effect of biomass particle size and air superficial velocity on the gasification process in a downdraft fixed bed gasifier. An experimental and modelling study," *Fuel Processing Technology,* vol. 89, p. 1076– 1089, 2008.

[32] C. Dejtrakulwong, and S. Patumsawa, "Four Zones Modeling of the Downdraft Biomass Gasification Process: Effects of moisture content and air to fuel ratio," *Energy Procedia,* vol. 52, p. 142 – 149, 2014.

[33] C. Di Blasi, "Dynamic behaviour of stratified downdraft gasifiers," *Chemical Engineering Science,* vol. 55, pp. 2931-2944, 2000.

[34] M. L. Boroson, J. B. Howard, J. P. Longwell, and W. A. Peters, "Product yields and kinetics from the vapor phase cracking of wood pyrolysis tars," *AIChE Journal,* vol. 35, no. 1, pp. 120-128, 1989.

References

[35] C.M. Kinoshita, and Y. Wang, "Kinetic Model of Biomass Gasification," *Solar Energy,* vol. 51, no. 1, pp. 19-25, 1993.

[36] C. S. CHEE, The Air Gasification of Wood Chips in a Downdraft Gasifier, MSc Thesis, Cansas, Manhattan: Department of Chemical Engineering, Kansas State University, 1987.

[37] A. K. Senelwa, Air gasification of woody biomass from short rotation forests : opportunities for small scale biomass-electricity systems, PhD Thesis, Massey University, New Zealand, 1997.

[38] T.H. Jayah, L. Aye, R.J. Fuller, and D.F. Stewart, "Computer simulation of a downdraft wood gasifier for tea drying," *Biomass Bioenergy,* vol. 25, pp. 459-469, 2003.

[39] C.A. Koufopanosi, G. Maschio, and A. Lucchesit, "Kinetic Modelling of the Pyrolysis of Biomass and Biomass Components," *The Canadian Journal of Chemical Engineering,* vol. 67, pp. 75-84, Feb, 1989.

[40] B.V. Babu, and A.S. Chaurasia., "Modeling, simulation and estimation of optimum parameters in pyrolysis of biomass," *Energy Conversion and Management 44,* p. 2135–2158, 2003.

[41] E. D. Gordillo, and A. Belghit, "A downdraft high temperature steam-only solar gasifier of biomass char: A modelling study," *Biomass and Bioenergy,* vol. 35, no. 5, pp. 2034-2043, 2011.

[42] C. Di Blasi, and C. Branca, "Modeling a stratified downdraft wood gasifier with primary and secondary air entry," *Fuel,* vol. 104, pp. 847-860, 2013.

[43] M. Barrio J.E. Hustad M. Fossum, "Operational characteristics of a small-scale stratified downdraft gasifier," in *Technologies and Combustion for a Clean Environment Sixth International Conference*, 2001.

[44] M. Barrio J.E. Hustad M. Fossum, "A Small-Scale Stratified Downdraft Gasifier Coupled to a Gas Engine for Combined Heat and Power Production," *Prog Thermo chem Biomass Convers,* p. 426–240, 2001.

[45] M. Simone, C. Nicolella, and L. Tognotti, "Numerical and experimental investigation of downdraft gasification of woody residues," *Bioresource Technology,* vol. 133, pp. 92-101, 2013.

References

[46] A. Dutta, and S. Jarungthammachote, "Thermodynamic equilibrium model and second law analysis of a downdraft waste gasifier," *Energy,* vol. 32, pp. 1660-1669, 2007.

[47] C. Koroneos, and S. Lykidou, "Equilibrium modeling for a downdraft biomass gasifier for cotton stalks biomass in comparison with experimental data," *Journal of Chemical Engineering and Materials Science,* vol. 2, no. 4, pp. 61-68, April 2011.

[48] T. A. Milne, R. J. Evans, and N. Abatzoglou, "Biomass gasifier "tars": their nature, formation, and conversion," NREL TP-570-25357, Golden, Colorado, Colorado, USA, 1998.

[49] A. M. A Ahmed, A. Salmiaton, T. S. YChoong, and W. A. Wan Azlina, "Review of kinetic and equilibrium concepts for biomass tar modeling by using Aspen Plus," *Renewable and Sustainable Energy Reviews,* vol. 52, p. 1623–1644, 2015.

[50] K. Maniatis, and A. Beenackers, "Introduction: tar protocols. IEA gasification," *Biomass Bioenergy,* vol. 18, pp. 1-4, 2000.

[51] C.F. Palma, "Model for Biomass Gasification Including Tar Formation and Evolution," *Energy Fuels,* vol. 27, no. 5, pp. 2693-2702, 2013.

[52] A. Dufour, L. Abdelouahed, O. Authier, G. Mauviel, J. P. Corriou, and G. Verdier, "Detailed Modeling of Biomass Gasification in Dual Fluidized Bed Reactors under Aspen Plus," *Energy and Fuels,* vol. 26, pp. 3840-3855, 2012.

[53] C. Chen, M. Horio, and T. Kojima, "Numerical simulation of entrained flow coal gasifers. Part I: modeling of coal gasifcation in an entrained flow gasifer," *Chemical Engineering Science,* vol. 55, pp. 3861-3874, 2000.

[54] P. Morf, P. Hasler, and T. Nussbaumer, "Mechanisms and kinetics of homogeneous secondary reactions of tar from continuous pyrolysis of wood chips," *Fuel,* vol. 81, pp. 843-853, 2002.

[55] C. Li, and K. Suzuki, "Tar property, analysis, reforming mechanism and model for biomass gasification—An overview," *Renewable and Sustainable Energy Reviews,* vol. 13, pp. 594-604, 2009.

[56] D. Swierczynski, S. Libs, C. Courson, and A. Kiennemann, "Steam reforming of tar from a biomass gasification process over Ni/olivine catalyst using toluene as a model compound," *Appl Catal B: Environ,* vol. 74, pp. 211-222, 2007.

References

[57] S. Liu, D. Mei, L. Wang, and X. Tu , "Steam reforming of toluene as biomass tar model compound in a gliding arc discharge reactor," *Chemical Engineering Journal,* vol. 307, p. 793–802, 2017.

[58] B. Zhao, X. Zhang, L. Chen, R. Qu, G. Meng, X. Yi, and L. Sun, "Steam reforming of toluene as model compound of biomass," *Biomass and Bioenergy,* vol. 34, pp. 140-144, 2010.

[59] P. Ji, W. Feng, and B. Chen, "Production of ultrapure hydrogen from biomass gasification with air," *Chemical Engineering Science,* vol. 64, no. 3, pp. 582-592, Feb, 2009.

[60] A. Jess, "Mechanisms and kinetics of thermal reactions of aromatic hydrocarbons from pyrolysis of solid fuels," *Fuel,* vol. 75, no. 12, pp. 1441-1448, 1996.

[61] P. Ji, W. Feng, and B. Chen, "Production of ultrapure hydrogen from biomass gasification with air," *Chem Eng Sci,* vol. 64, pp. 582-592, 2009.

[62] J. F. Bilodeau, N. Thérien, P. Proulx, S. Czernik, and E. Chornet, "A mathematical model of fluidized bed biomass gasification," *The Canadian Journal of Chemical Engineering ,* vol. 71, pp. 549-557, 1993.

[63] I. Narváez, A. Orío, M. P. Aznar, and J. Corella, "Biomass Gasification with Air in an Atmospheric Bubbling Fluidized Bed. Effect of Six Operational Variables on the Quality of the Produced Raw Gas," *Industrial & Engineering Chemistry Research,* vol. 35, p. 2110–2120, 1996.

[64] K. Norinaga, Y. Sakurai, R. Sato, and J Hayashi, "Numerical simulation of thermal conversion of aromatic hydrocarbons in the presence of hydrogen and steam using a detailed chemical kinetic model," *Chem Eng J,* vol. 178, pp. 282-290, 2011.

[65] J. Corella, M. A. Caballero, M. P. Aznar, and C. Brage, "Two advanced models for the kinetics of the variation of the tar composition in its catalytic elimination in biomass gasification," *Ind Eng Chem Res,* vol. 42, pp. 3001-3011, 2003.

[66] D. Fuentes-Cano, A. Gómez-Barea, S. Nilsson, and P. Ollero, "Kinetic Modeling of Tar and Light Hydrocarbons during the Thermal Conversion of Biomass," *Energy Fuels ,* vol. 30, pp. 377-385, 2016.

[67] A. Dufour, E. Masson, P. Girods, Y. Rogaume, and A. Zoulalian, "Evolution of Aromatic Tar Composition in Relation to Methane and Ethylene from Biomass Pyrolysis-Gasification," *Energy Fuels ,* vol. 25, p. 4182–4189, 2011.

References

[68] A. Fourcault, F. Marias, and U. Michon, “Modelling of thermal removal of tars in a high temperature stage fed by a plasma torch,” *biomass and bioenergy,* vol. 34, pp. 1363-1374, 2010.

[69] A. Veksha, A. Giannis, G. Yuan, J. Tng, W. Chan, V. Chang, G. Liszak, and T. Lim, “Distribution and modeling of tar compounds produced during downdraft gasification of municipal solid waste,” *Renewable Energy,* no. https://doi.org/10.1016/j.renene.2018.09.104, pp. 1-10, 2018.

[70] E.B. Ledesma, A.A. Mullery, J.V. Vu, and J.N. Hoang, “Lumped kinetics for biomass tar cracking using 4-propylguaiacol as a model compound,” *Ind. Eng. Chem. Res.,* vol. 54, pp. 5613-5623, 2015.

[71] Q. Li, Q. Wang, A. Kayamori, and J. Zhang, “Experimental study and modeling of heavy tar steam reforming,” *Fuel Processing Technology,* vol. 178, pp. 180-188, 2018.

[72] H. Richter, and J.B. Howard, “Formation and consumption of single-ring aromatic hydrocarbons and their precursors in premixed acetylene, ethylene and benzene flames,” *Phys. Chem. Chem. Phys,* vol. 4, no. 11, pp. 2038-2055, 2002.

[73] A. Dufour, E. Masson, P. Girods, Y. Rogaume, and A. Zoulalian, “Synthesis gas production by biomass pyrolysis: Effect of reactor temperature on product distribution,” *International journal of hydrogen energy,* vol. 43, p. 1726 – 1734, 2009.

[74] T. Phuphuakrat, N. Nipattummakul, T. Namioka, S. Kerdsuwan, and K. Yoshikawa , “Characterization of tar content in the syngas produced in a downdraft type fixed bed gasification system from dried sewage sludge,” *Fuel,* vol. 89, p. 2278–2284, 2010.

[75] F.O. González, E.E.S. Lora, H.F.V. Nova, L.J.M. Neto, A.M. Reyes, A. Ratner, and M. Ghamari, “CFD modeling of combustion of sugarcane bagasse in an industrial boiler,” *Fuel,* pp. 31-38, 2017.

[76] A. Gomez. Barea, and B. Leckner , “Modeling of biomass gasification in fluidized bed,” *Progress in Energy and Combustion Science,* vol. 36, pp. 444-509, 2010.

[77] U. Kumar, and M. C. Paul, “Sensitivity analysis of homogeneous reactions for thermochemical conversion of biomass in a downdraft gasifier,” *Renewable Energy,* no. https://doi.org/10.1016/j.renene.2019.11.025, 2019.

References

[78] D.F. Fletcher, B.S. Haynes, F.C. Christo, and S.D. Joseph, "A CFD based combustion model of an entrained flow biomass gasifier," *Appl Math Model,* vol. 24, pp. 165-182, 2000.

[79] L. Yu, J. Lu, X. Zhang, and S. Zhang, "Numerical simulation of the bubbling fluidized bed coal gasification by the kinetic theory of granular flow (KTGF)," *Fuel,* vol. 86, pp. 722-734, 2007.

[80] A. Rogel and J. Aguillón, "The 2D Eulerian Approach of Entrained Flow and Temperature in a Biomass Stratified Downdraft Gasifier," *American Journal of Applied Sciences,* vol. 3, no. 10, pp. 2068-2075, 2006.

[81] Y. Wu, Q. Zhang, W. Yang, and W. Blasiak, "Two-Dimensional Computational Fluid Dynamics Simulation of Biomass Gasification in a Downdraft Fixed-Bed Gasifier with Highly Preheated Air and Steam," *Energy Fuels,* vol. 27, no. 6, pp. 3274-3282, 2013.

[82] P.C. Murugan and S. Joseph Sekhar, "Numerical Simulation of Imbert Biomass Gasifier toSelect the Feedstock Available in Remote Areas," *Environmental Progress & Sustainable Energy,* vol. 36, no. 3, pp. 708-716, 2017.

[83] R. Gupta, P. Jain, and S. Vyas, "CFD Modeling and Simulation of 10KWE Biomass Downdraft Gasifier," *International Journal of Current Engineering and Technology,* vol. 7, no. 4, pp. 1446-1452, 2017.

[84] Z. A. Zainal, R. Ali, C. H. Lean and K. N. Seetharamu, "Prediction of performance of a downdraft gasifier using equilibrium modeling for different biomass materials," *Energy Conversion and Management, vol. 42,* pp. 1499-1515, 2001.

[85] P.C. Roy, A. Datta, and N. Chakraborty, "Modelling of a downdraft biomass gasifier with finite rate kinetics in the reduction zone," *Int J Energy Res,* vol. 33, pp. 833-851, 2009.

[86] R. Bridgewater, and A. Shand, "Fuel gas from biomass: Status and new modeling approaches," *Thermochemical Processing of Biomass,* pp. 229-254, 1984.

[87] P. N. Sheth. and B. V. Babu, "Modeling and simulation of reduction zone of downdraft biomass gasifier: Effect of char reactivity factor," *Energy Conversion and Management,* vol. 47, pp. 2602-2611, 2006.

[88] N.S. Rathore, N. L. Panwar, and Y. V. Chiplunkar, "Design and techno economic evaluation of biomass gasifier for industrial thermal applications," *African Journal of Environmental Science and Technology.,* vol. 3, no. 1, pp. 6-12, 2009.

References

[89] T. B. Reed, and A. Das, Handbook of Biomass Downdraft Gasifier Engine Systems., Solar Energy Research Institute, USA, 1988.

[90] S. Sivakumar, N. Ranjithkumar, and S. Ragunathan, "Design and Development of Down Draft Wood Gasifier," *International Journal of Mechanical Engineering,* vol. 2, no. 2, pp. 1-10, 2013.

[91] S. Sivakumar, K. Pitchandi, and E. Natarajan, "Modelling and simulation of down draft wood gasifier," *Journal of Applied Sciences.,* vol. 8, no. 1, pp. 271-279, 2008.

[92] R. C. Aiello, and D.T. Pedroso, "Biomass gasification on a new really tar free downdraft gasifier," *Rev. ciênc. exatas, Taubaté,* pp. 59-62, 2005.

[93] S.J. Yoon, Y. I. Son, Y. K. Kim, and J. Lee, "Gasification and power generation characteristics of rice husk and rice husk pellet using a downdraft fixed-bed gasifier," *Renewable Energy,* vol. 42, pp. 163-167, 2012.

[94] Y. Qin, A. Campena, T. Wiltowski, J. Feng, and W. Li, "The influence of different chemical compositions in biomass on gasification tar formation," *Biomass and Bioenergy,* vol. 83, pp. 77-84, 2015.

[95] S. J. Orisaleye,and J. I. Ojolo, "Design and Development of a Laboratory Scale Biomass Gasifier," *Journal of Energy and Power Engineering,* vol. 4, no. 8, pp. 16-23, 2010.

[96] SGSUnited Kingdom Limited, [Online]. Available: https://www.sgs.co.uk/?utm_source=googlemybusiness&utm_medium=Referral_GMB&utm_campaign=SGS+United+Kingdom+Ltd+7.

[97] C. Gai, and Y. Dong, "Experimental study on non-woody biomass gasification in a downdraft gasifier," *international journal of hydrogen energy* , vol. 37, pp. 4935-4944, 2012.

[98] P. Prasertcharoensuk, D. A. Hernandez, S. J. Bulla, Ana A. N. Phan, "Optimisation of a throat downdraft gasifier for hydrogen production," *Biomass and Bioenergy,* vol. 116, pp. 216-226, 2018.

[99] N. Bianco , M.C. Paul, G.P. Brownbridge , D. Nurkowski, A.M. Salem, U. Kumar, A.N. Bhave, and M. Kraft, "Automated Advanced Calibration and Optimization of Thermochemical Models Applied to Biomass Gasification and Pyrolysis," *Energy and Fuels,* vol. 32, no. 10, pp. 144-153, 2018.

References

[100] J. Yu, Experimental and Numerical Investigation on Tar Production and Recycling in Fixed Bed Biomass Gasifiers, Missouri University of Science and Technology, USA: ISBN: 9780438114807, 2018, PhD thesis.

[101] Swedish Cleantech, "Belab AB," [Online]. Available: https://swedishcleantech.com/companies/1089/belab-ab/. [Accessed 2019].

[102] Verdant Chemical Technologies, 2018. [Online]. Available: http://www.verdchem.se/technology/spa-off-line-tar-analysis/.

[103] F.Marias, A. Fourcault, and U.Michon, "Modelling ofthermalremovaloftarsinahightemperature stage fedbyaplasmatorch," *Biomass and Bioenergy,* vol. 34, pp. 1363-1374, 2010.

[104] M. Dogru, C.R. Howarth, G. Akay, B. Keskinler, and A. A. Malik, "Gasification of hazelnut shells in a downdraft gasifier," *Energy 27,* vol. 27, pp. 415-427, 2002.

[105] P. Hasler, and T. Nussbaumer, "Gas cleaning for IC engine applications from fixed bed biomass gasification," *Biomass Bioenergy,* vol. 16, pp. 385-395, 1999.

[106] ANSYS Inc, ANSYS 15 Fluent Theory Guide, Canonsburg, PA 15317, 2013.

[107] J. Xie, W. Zhong, B. Jin, Y. Shao, and H. Liu, "Simulation on gasification of forestry residues in fluidized beds by Eulerian Lagrangian approach," *Bioresource Technology,* vol. 121, pp. 36-46, 2012.

[108] J. Tomeczek, Z. Jastrzçab, and B. Gradoń, "Lateral diffusion of solids in a fluidized bed with submerged vertical tubes," *Powder Technology,* vol. 72, no. 1, pp. 17-22, 1992.

[109] P. Nakod, "Modeling and validation of oxy-fired and air-fired entrained flow gasifiers," *International journal of Chemical and Physical Science,* vol. 2, no. 6, pp. 2074-2091, 2013.

[110] A. Al-Akaishi, A. Valera-Medina, C. T. Chong, and R. Marsh, "CFD Analysis of the Fluidised Bed Hydrodynamic Behaviour inside an Isothermal Gasifier with different Perforated Plate Distributors," *Energy Procedia,* vol. 142, pp. 835-840, 2017.

[111] S.P . Shi, S. E. Zitney, M. Shahnam, M. Syamlal, and W. A. Rogers, "Modelling coal gasification with CFD and discrete phase method," *Journal of Energy Institute,* vol. 79, no. 4, pp. 217-221, 2016.

References

[112] A. Slezak, J. M. Kuhlman, L. J. Shadle, J. Spenik, and S. Shi, “CFD simulation of entrained-flow coal gasification: Coal particle density/sizefraction effects,” *Powder Technology,* vol. 203, no. 1, pp. 98-108, 2010.